Characterisation of scFv A7 reactivity and development of a novel bispecific antibody for targeted therapies in Rheumatoid Arthritis

Author

Mathieu Ferrari

A thesis submitted for the degree of
Doctor of Philosophy in the University of London

Queen Mary University of London,
Barts and the London School of Medicine and dentistry,
William Harvey Research Institute

2014

ACKNOWLEDGEMENTS

I would like to thank Professor Costantino Pitzalis for giving me the opportunity of moving to a new country and undertake my PhD with an exciting project in the centre of Experimental Medicine and Rheumatology. I thank also Dr Tahereh Kamalati for providing excellent guidance and supervision during my first years as a PhD student and for always being available for a chat when needed. A thank also goes to Professor Daniele Sblattero for giving me the opportunity of working in his laboratory for two months and establishing a collaboration that really helped the project to move forward.

These years have been a long journey which started with moving to a new country, leaving friends and family, working late nights and early mornings and although I've been happy to work in the ever exciting scientific world, let's face it, frustration was a big part of it. But I could have never done it without all the people that I met during the last 4 years. A great deal of gratitude goes to my flat mates, the old and the new, Florian, Charlotte, Cristina and Giulia, that made my "living outside the lab" so enjoyable. A nice work environment was vital in order to keep me sane and enjoy all the time spent in the laboratory. For that I have to thank my colleagues, the ones that left and the ones that stayed, in particular Elisa, Yvonne, Cristina, Davide, Beth, Giovanna, Jo, Sue, Elisa, Will, Emanuela, Botan, Chiara, Elena, Sofia, Vidi, Sudeh, Mattia and Ale. Special thanks also to Rita, Becki and Janice for always being a great source of help and support. But if in the last year I managed to take the project this far I have to give credit to Shimobi, with whom I finally managed to form a strong team and share the heavy burden of A7.

But I also have to thank Donata, who has been the biggest change in my life in the past year. She managed to stand by me despite the stressing months passed working late and writing during weekends, it has not been an easy task.

And finally I have to thank my family; they have supported me without fail throughout the long academic journey. For this I will always be grateful.

DECLARATION

I declare that the entire source presented in this thesis is less than 100000 words and the material presented has not been used in any other submission for an academic award. All the sources of investigation have been duly acknowledged.

The studies presented in this thesis were conducted in the centre of Experimental Medicine and Rheumatology at the William Harvey Research Institute, Queen Mary University of London.

The work described in this thesis is the product of original research performed and analysed by the candidate, with the following contributions:

Professor Costantino Pitzalis, Dr Tahereh Kamalati and Professor Daniele Sblattero have actively supervised the project, providing scientific support and guidance during the experimental design and result interpretation.

Dr Tahereh Kamalati performed the IE7 de-glycosylation experiment.

Professor Daniele Sblattero provided technical expertise and support for scFv-Fc antibody and bispecific scFv-Fc antibody development.

Dr Cecilia Deantonio and Miss Eleonora Rizzato contributed to protein expression library phage display screening.

Dr Shimobi Onuoha contributed to immuno-precipitation experiments and provided expertise for Biacore kinetic studies.

Candidate	First supervisor	Second supervisor
Mathieu Ferrari	Professor Costantino Pitzalis	Professor Daniele Sblattero

ABSTRACT

Despite the success of current biological agents, achievement of broader efficacy and improved safety profile remains an unmet need in rheumatoid arthritis therapy. Neovasculogenesis plays a vital role in the progression and perpetuation of rheumatoid arthritis and significant evidence has demonstrated molecular heterogeneity within the endothelium (MVE) of different tissues. The heterogeneity of the synovial MVE can be exploited for the development of organ-specific therapeutic and diagnostic reagents. A novel recombinant antibody fragment, scFv A7, with specificity for human arthritic synovium, was isolated in our laboratory following *in vivo* phage display. The aim of the project described in this thesis is to characterise the antibody reactivity and develop a novel tissue specific therapeutic.

The scFv A7 antibody proved to specifically target the microvasculature of human arthritic synovium with no detectable reactivity in a comprehensive range of normal tissues. Furthermore, the detected reactivity was not a common feature of chronic inflammatory conditions. Hence, the A7 antibody represents a unique and versatile tool with great potential for the development of diagnostic and/or therapeutic agents.

The unique properties of A7 were combined with the anti-TNF Adalimumab, forming a bispecific antibody with neutralising activity and synovial homing properties. The new construct was able to retain the synovial specificity and showed comparable TNF binding kinetics and biological activity to the parent Adalimumab antibody *in vitro*.

In conclusion, these results demonstrate that scFv A7 reactivity is specific to the microvasculature of human arthritic synovium, suggesting that the target molecule may have potential as a biomarker in arthritis and applications as an immunotherapeutic target. The bispecific antibody format developed showed unaltered TNF blocking capacity and synovial specificity that may allow reduction in the dosage and/or administration frequency, with the ultimate goal to reduce the systemic exposure, achieve a better therapeutic index and decreasing health care costs.

TABLE OF CONTENT

LIST OF FIGURES

LIST OF TABLES

LIST OF ABBREVIATIONS

2DE	Two dimensional gel electrophoresis
ABC-HRP	Avidin-biotin complex HRP conjugated
ACPA	Anti-citrullinated protein antibody
ACR	American college of rheumatology
ADA	Anti-drug antibody
ADCC	Antibody-dependent cellular cytotoxicity
AID	Activation-induced cytidine deaminase
bFGF	Basic fibroblast growth factor
BsAb	Bispecific antibody
CAM	Cell adhesion molecule
CDR	Complementarity determining region
CH	Constant domain of the heavy antibody chain
CHO	Chinese hamster ovary
CIA	Collagen induced arthritis
CL	Constant domain of the light antibody chain
CMC	Complement-mediated cytotoxicity
CMV	Cytomegalovirus
CNBr	Cyanogen Bromide
CRC	Colorectal cancer
CRT	Calreticulin
DAS	Disease activity score
DC	Dendritic cell
DMARD	Disease modifying anti-rheumatic drugs
DMEM	Dulbecco's modified Eagle medium
DPP6	Dipeptidyl aminopeptidase-like protein 6
DTT	Dithiothreitol
DVD	Dual variable domain
EBV	Epstain-Barr virus
EC	Endothelial cell
EC50	Half maximal effective concentration
ECM	Extra cellular matrix
ED	Extra domain
ELISA	Enzyme-Linked Immunosorbent Assay
ELS	Ectopic lymphoid structure
EULAR	European league against rheumatism
FBS	Foetal bovine serum
Fc	Antibody constant region

FCS	Foetal calf serum
FDA	Food and drug administration
FDc	Follicular dendritic cell
FLS	Fibroblast-like synoviocyte
FPLC	Fast protein liquid chromatography
Fv	Antibody variable fragment
GABARAPL	GABA (A) receptor-associated protein like
GALT	Gut associated lymphoid tissues
GC	Germinal centre
G-CSF	Granulocyte colony-stimulating factor
GM-CSF	Granulocyte-macrophage colony-stimulating factor
GMP	Good manufacturing practice
GSH	Glutathione
GST	Glutathione *S*-transferase
HEL	Hen egg lysozyme
HEV	High endothelial venule
HIER	Heat-induced epitope retrieval
HIF	Hypoxia-inducible-factors
His	Histidine
HLA	Human leucocyte antigen
HPLC	High-performance liquid chromatography
HRP	Horseradish peroxydase
HUVEC	Human umbilical vein endothelial cell
IBD	Inflammatory bowel disease
IC50	Half maximal inhibitory concentration
ICAM	intercellular adhesion molecule
IFN	Interferon
Ig	Immunoglobulin
IGF	Insulin-like growth factor
IHC	Immunohistochemistry
IL	Interleukine
IP	Immuno-precipitation
LTBP	Latent-transforming growth factor beta-binding protein
M-CSF	Macrophage colony-stimulating factor
MHC	Major histocompatibility complex
MLF	Myeloid leukemia factor
MLS	Macrophage-like synoviocyte
MMP	Matrix metalloproteinase
MVE	Microvascular endothelium
MW	Molecular weight
MWCO	Molecular weight cut-off

NK	Natural killer
ns	Non-significant
OA	Osteoarthritis
OCT	Optimal cutting temperature
OD	Optical density
ORF	Open reading frame
OTG	n-Octyl-β-D-thioglucopyranoside
PAD	Peptidylarginine deaminase
PAGE	Polyacrylamide gel electrophoresis
PCR	Polimerase chain reaction
PDGF	Platelet-derived growth factor
PDGFR	Platelet derived growth factor receptor
PECAM	Platelet endothelial cell adhesion molecule
pI	Isoelectric point
PIER	Proteolytic-induced epitope retrieval
PLN	Peripheral lymph node
PNAd	Peripheral lymph node addressin
PsA	Psoriatic arthritis
RA	Rheumatoid arthritis
RADF	RA dermal fibroblast
RASF	RA synovial fibroblast
RF	Rheumatoid factor
scFv	Single-chain Fv
SCID	Severe combined immunodeficiency
SD	Standard deviation
SDS	Sodium dodecyl sulfate
SpA	Spondyloarthritis
SV5	Symian-virus 5
TGF	Transforming growth factor
Th	T-helper cell
TIMP	Tissue inhibitor of metalloproteinases
TLS	Tertiary lymphoid structure
tmTNF	Trans membrane TNF
TNF	Tumour necrosis factor
TNFR	TNF receptor
VCAM	Vascular cell adhesion molecule
VEGF	Vascular endothelium growth factor
VH	Variable domain of the heavy antibody chain
VL	Variable domain of the light antibody chain
vWF	Von Willebrand factor

LIST OF PUBLICATIONS ARISING FROM THIS WORK

Kamperidis P, Kamalati T, **Ferrari M**, Jones M, Garrood T, Smith M, Diez-Posada S, Hughes C, Finucane C, Mather S, Nissim A, George AJT and Pitzalis C. Development of a novel recombinant biotherapeutic with applications in targeted therapy of human arthritis. Arthritis and rheumatism. 2011;63:3758-825. (included in supplementary material)

[Patent] Pitzalis C, inventor. Antibody specifically binding synovial microvasculature of arthritis patients. (WO/2012/042270) United Kingdom 2012 05.04.2012. (included in supplementary material)

Chapter 1
Introduction

1.1 Joint pathophysiology in health and disease

1.1.1 Normal synovial joint environment

In the normal human body, bones are connected in structures called joints that provide mechanical support and specific functional properties. The joints are classified structurally and functionally in three main groups: Fibrous joints (Synchondroses), Cartilaginous joints (Syndesmoses) and Synovial joints (Diarthrosis). Synovial joints are highly mobile articular structures composed of two bones linked by a fibrous capsule with a deeper synovium membrane, which lines the joints until the areas of articular cartilage, surrounding a synovial cavity (Figure 1.1 A).

The synovial membrane is characterised by two separate layers: the lining layer, called intima, consisting of condensed cells one- to four-cells thick and a sublining layer, sub-intima, formed by extracellular matrix, dispersed fibroblasts and macrophages, blood and lymphatic vessels. The presence of limited cell numbers embedded in the extracellular matrix makes the sublining an amorphous structure, consisting mainly of loose connective tissue that serves as a base for the lining layer. The lining, unlike regular epithelial layers, lacks a real basement membrane and the cells form an intricate network of compacted cells with regions of cell-to-cell contact where the cells and their processes are separated by wide intracellular spaces (1, 2). In the absence of a basal membrane, this function is provided by the matrix and the interdigitating cells of the lining themselves. The sublining allows for the transfer of protein, small molecules and cellular elements from the circulating blood to the lining layer where the reticular organisation of the cellular components and the extracellular matrix form a physical and chemical barrier respectively, influencing the passage of serum components into the joint cavity and provide nutrients to the avascular articular cartilage (1). In healthy conditions, the synovial lining layer contains two distinct cell types: macrophage-like synoviocytes (MLS) and fibroblast-like synoviocytes (FLS). MLS present similar features to other tissue resident macrophages, they derive from a common bone marrow precursor and show active phagocytic ability, supporting their role in

clearance of debris from the synovial cavity and acting as sentinels for microbial encounters (3). FLSs are mesenchymal cells expressing common fibroblast markers e.g. collagen, vimentin, CD90, while additional markers such as CD55 (decay-accelerating factor), CD106 (vascular cell adhesion molecule 1 VCAM-1), uridine disphosphoglucose dehydrogenase and lubricin have been detected only in the lining FLS, suggesting functional differences in the FLS subpopulations (4). FLSs play a critical role in normal joint homeostasis, maintaining the synovial extracellular matrix by producing matrix components (laminin, tenascin, fibronectin, collagen, elastin and proteoglycans), and by influencing matrix assembly via expression of integrins such as α5β1 and αVβ3 (5, 6).

Synovial fluid levels and composition are also influenced by FLS. The synovial fluid derives from dialysed plasma filtered by the extracellular matrix in the sublining and lining layer and is influenced by the cellular components of the synovial membrane. Mature intimal FLS secret the glycoprotein lubricin in the joint cavity, contributing to synovial fluid viscosity, and hyaluronan, a long-chain glycosaminoglycan, involved in the control of synovial fluid levels. High hyaluronan concentrations cause an increase in the oncotic pressure in the joint, restoring the reduced synovial fluid levels. Via a negative feedback loop, the expanded synovial fluid volumes increases the mechanical stress on intimal FLS, causing a down-regulation of hyaluronan production (7).

In the internal cavity of the synovial joint, the articular cartilage protects the subchondral bone, providing stiffness to compression and the ability to distribute loads, minimising the peak stresses on the bone. The articular cartilage appears as a firm inert tissue composed primarily of extracellular matrix with a sparse population of cells and absence of blood vessels, lymphatic vessels or nerves (8). The chondrocytes are the only cell type present within normal articular cartilage, embedded in a hydrated extracellular matrix. Water is the principal component of the cartilage matrix, contributing up to 80% of the wet weight, whereas the chondrocytes represent only 1% of the total volume. However, chondrocytes are essential to maintain the structural integrity and function of the matrix, synthesising collagen, proteoglycans and other non-collagenous proteins. Collagens

are a family of secreted matrix proteins characterised by a triple-helical peptide structure, important for their tensile strength, and represent the most abundant macromolecule in the cartilage (9). Among the 14 types of collagen, type II, IX and XI are responsible for the cross-banded fibrils in the articular cartilage. Proteoglycans are large, negatively charged macromolecules, consisting of a protein core and one or more glycosaminoglycan side chains. The chondrocytes maintain a tight interaction with the matrix, with the latter protecting the cells from mechanical damage, maintaining their shape and phenotype, filtering and storing nutrients, substrates for matrix synthesis, metabolic waste products and stimulatory molecules. On the other hand, chondrocytes are responsible for matrix turnover. The mechanisms that control the balance between anabolic and catabolic activity are not fully understood, but aggrecan content of the matrix and cytokines appear to have an important role (10, 11). Zinc-dependent matrix metalloproteinases (MMP) are primarily responsible for matrix degradation. Stimuli such as interleukin (IL)-1 and tumour necrosis factor (TNF)-α induce the expression of MMPs, reducing synthesis and increasing catabolic activity, while growth factors such as transforming growth factor-beta (TGF-β) and insulin-like growth factor-1 (IGF-1), promote cartilage synthesis (11).

1.1.2 Rheumatoid arthritis

Rheumatoid arthritis (RA) is a chronic, systemic autoimmune disease affecting joints and extra-articular structures and is considered one of the most common and severe forms of inflammatory arthritis with significant associated morbidity and mortality (12, 13). The disease primarily affects the small diarthrodial joints of hands and feet in a symmetrical manner, causing a chronic inflammation of the synovium membrane characterised by hyperplasia and hypertrophy (14, 15). The major clinical symptoms associated with RA are swelling of the joints, stiffness and pain and can develop into profound disability caused by bone erosion and cartilage destruction. Systemic features of rheumatoid arthritis include cardiovascular alterations, with pericardial inflammation and vasculitis, pulmonary, psychological and skeletal disorders, generally associated with increased disability and shortened life expectancy (13, 14, 16, 17). RA is a relatively common disease, affecting approximately 1% of the adult population in Western Europe with an average age of onset of 40 years and an increase in incidence with rising age (18). Disease occurrence is generally higher in women than in men with a ratio of 3 to 1 (18, 19). The burden caused by RA is not only confined to the affected patients, this severe chronic disease is also characterised by direct and indirect costs associated with primary medical costs, socio-economical costs such as sick leave and loss of productivity, and psychological costs represented by the deterioration of the quality of life of patients. The annual NHS cost is estimated to be around £560 million, with an average of £3500 per patient, and indirect costs amounting to £1.8 billion a year have been estimated (20-22).

RA has a wide clinical spectrum ranging from mild joint symptoms to severe inflammation and joint erosion. Clinical symptoms, serological and radiological data are taken into consideration when RA diagnosis needs to be assessed. The first classification criteria was proposed by the American College of Rheumatology (ACR) in 1956 and then revised in 1958 and 1987, and more recently a new classification criteria has been developed by the ACR and the European League Against Rheumatism (EULAR) in 2010 (23). Patients that show at least one joint with

definite clinical synovitis (swelling) not better explained by another disease can be considered eligible for the scoring system.

	Score
Joint involvement	
1 large joint	0
2-10 large joints	1
1-3 small joints (with or without involvement of large joints)	2
4-10 small joints (with or without involvement of large joints)	3
>10 joints (at least 1 small joint)	5
Serology (at least 1 test result is needed for classification)	
Negative rheumatoid factor (RF) *and* anti citrullinated protein antibody (ACPA)	0
Low-positive RF *or* low-positive ACPA	2
High-positive RF *or* High-positive ACPA	3
Acute-phase reactants (at least 1 test result is needed for classification)	
Normal CRP *and* normal ESR	0
Abnormal CRP *or* abnormal ESR	1
Duration of symptoms	
<6 weeks	0
≥6 weeks	1

Table 1.1 2010 ACR/EULAR classification criteria for rheumatoid arthritis

For classification purposes, a patient with a score ≥6 is indicative of the presence of definite RA. A patient with a score <6 cannot be classified as having definite RA, but might still fulfil the criteria at a later time point. This classification, compared to the earlier ACR 1987, includes also autoantibody status and acute phase response, showing a higher sensitivity but also a lower specificity, especially in patients aged ≥60 years (24).

1.1.2.1 Aetiology

The leading cause for rheumatoid arthritis remains elusive, however there is strong evidence linking genetic and environmental factors towards the development and progression of the disease.

Genetic factors

Hereditability seems to have an important impact on the risk of developing RA, several genetic regions have been associated with the disease using genomewide analyses. Twin studies have shown a concordance rate of 15-30% among monozygotic twins as opposed to 5% in dizygotic twins (25, 26). The region of the genome of greatest importance in all studies on RA is the major histocompatibility complex (MHC) locus which can account for 30-50% of the genetic susceptibility depending on the ethnic group. Human Leucocyte Antigen (HLA) class II is involved in antigen presentation to T-helper (Th) cells, which is in accordance with the hypothesis of a T-cell repertoire selection and/or antigen presentation in the onset of the autoimmune response in RA. In particular the HLA subclass HLA-DR1 and HLA-DR4 have shown higher frequency in RA patients who are positive for rheumatoid factor or ACPA than in the general population. The theory behind this genetic association is the presence of a shared epitope in the third hyper-variable region of the β chain. In particular, the HLA-DRβ1 molecules in RA share a sequence in position 70-74 (QRRAA or KRRAA or RRRAA) that constitute an α helical domain forming one side of the antigen binding site, likely affecting antigen presentation (27-29). In different ethnic groups the predominant RA-associated alleles vary considerably with the alleles DRB1*0101, *0401 and *0404 being more expressed in Caucasian population and *0405 and *0901 in Asia (27, 30). Recently it has been demonstrated that the shared epitope is able to specifically interact with cell surface calreticulin (CRT), a protein important for cellular stress response in the innate immune system triggering increased levels of cellular reactive oxygen species. Interaction between the HLA alleles and CRT may aberrantly activate an innate immune system signal transduction pathway (31). Additionally, the shared epitope was able to trigger murine dendritic cells (DC) to

enhance Th17 differentiation and inhibit the generation of Treg cells (32). Other gene polymorphisms involved in RA susceptibility have a minor impact. The polymorphism R620W on *PTPN22*, a gene encoding a tyrosine phosphatase essential in signal transduction of the T cell antigen receptor (TCR), causes a reduced binding activity of the enzyme for the target protein leading to a reduced down-regulation of activated T cells (33). However, a more recent study proposed an alternative mechanism in which the mutation causes a gain of function resulting in an increased threshold level of stimulation for T cells activation, due to a decreased TCR mediated calcium mobilisation, leading to thymocyte hyporesponsiveness and failure to delete autoreactive T cells during thymic selection (34).

Environmental factors

Population studies have shown that hereditability can account only for a proportion of disease risk factors and genetically similar groups can exhibit marked differences in disease prevalence (35). Environmental factors may act as triggers rather than being directly involved in the disease process or may act as initiators of the disease in susceptible hosts. Smoking represents a key risk factor for RA. Heavy smokers (more than 40 pack a year) have a 2-fold increase in the risk of RA compared to non-smokers which persists after cessation (30, 36). The exact mechanism of action is still unknown, however smoking has been associated with an increased level of peptidylarginine deaminase 2 (PAD2) and citrullinated proteins in pulmonary cells (37).

The presence of high levels of citrullinated proteins might trigger loss of tolerance towards these neoepitopes and elicit ACPA response, contributing to initiate the inflammatory response especially in those who carry the HLA-DRβ1 shared epitope. Interestingly, alcohol consumption has been found to offer lower risk of developing ACPA-positive RA and a dose dependent effect was demonstrated in a study of two Swedish cohorts, EIRA and CACORA, and in a more recent English study, with heavy drinkers showing a decreased risk compared to non-drinkers of up to 50% (38, 39). In addition, carriers of the shared epitope were

found to have a more pronounced risk reduction. Infectious agents such as Epstein-Barr virus (EBV), cytomegalovirus, Escherichia coli, have long been linked with rheumatoid arthritis. Molecular mimicry has been proposed as a possible mechanism of action (40). According to this model, a systemic infection with a microorganism bearing an antigen with enough similarity for a host antigen may trigger an immune response and break of tolerance towards the self-antigen, resulting in auto-antibodies production and autoimmune response (41). Viral infections may also influence and promote autoimmunity through a more direct mechanism. EBV is able to infect naïve B cells and allow them to enter the germinal centre (GC) in the tonsil where the cells will switch to the viral program called latency II and express EBNA-1, LMP-1 and LMP-2a, helping EBV to gain access to the memory B cell pool and enter the latent state. LMP-1 has been demonstrated to serve as a CD40 transduction signal initiated by CD4+ T cells (42), whereas LMP-2a mimics a constitutively activated B cell receptor (43). With these signals, an autoreactive EBV infected naïve B cell may be driven into latently infected memory B cells, escape apoptosis and ultimately migrate and persist in the target organ independently of T cell help.

1.1.2.2 Pathophysiology

As mentioned earlier, the aetiology of rheumatoid arthritis is poorly understood and although many possible mechanisms have been suggested none has proved to be determinant. However, the pathogenesis and the role of the immune system in the disease progression are much better understood. This disease can be considered as a syndrome spanning several disease subsets that can lead to a common outcome: chronic inflammation of the synovium. Clinically RA development consists in several stages beginning with swelling and pain in a limited number of joints, slowly spreading to unaffected joints and finally leading to destruction of the articular cartilage and subchondral bone caused by the hyperplastic and hypertrophic synovium (Figure 1.1 B). A local hypoxic condition due to increased metabolic demand of the hypertrophic synovium and extensive infiltration, combined to cytokines presence, stimulates local angiogenesis fuelling and exacerbating the pathological condition. At the cartilage-bone interface, the inflamed synovium forms an aggressive pannus lesion formed mainly of macrophages, osteoclasts and fibroblasts, which infiltrate the adjoining articular cartilage promoting joint destruction. The mechanism for cartilage destruction is related to the expression of a variety of degrading enzymes, including MMPs, collagenases, serine and cysteine proteases and cathepsins, that together with pro inflammatory cytokines and down-regulation of physiological tissue inhibitor of metalloproteinases (TIMP) causes increased cartilage and bone resorption (44).

The preclinical phase of the disease doesn't involve joint alterations, however ACPAs and rheumatoid factors can be detected more than 10 years before RA clinical onset (45) and are usually associated with a more rapid radiographic progression and worse outcome of the disease (46). This indicates that immunological abnormalities can precede the appearance of clinical features of RA. As described in section 1.1.2.2, environmental factors such as smoking can trigger the formation of citrullinated peptides and the loss of tolerance resulting in ACPA production especially in patients carrying the HLA shared epitope. A second event in the synovium, caused by viral infection or trauma, could induce citrullination in the joint causing an immune response on the ground of a pre-existing

immunisation. When the disease clinically manifests, the synovium shows a thickening of the intimal layer with increased numbers of MLS and FLS, the sublining layer becomes infiltrated by leukocyte migrating through the synovial microvessels causing increased expression of adhesion molecules and chemokines. Levels of infiltrate can vary greatly between patients, ranging from low infiltrate levels, diffuse distribution across the synovium, to the presence of follicular structures that may appear only as lymphoid aggregates or may present features of secondary lymphoid structures with high-endothelial venules (HEV), segregation of T- and B-cells with a follicular dendritic cell network, acquiring the structure and function of ectopic lymphoid structure (ELS) also known as tertiary lymphoid structures (TLS) (47, 48) (Figure 1.2).

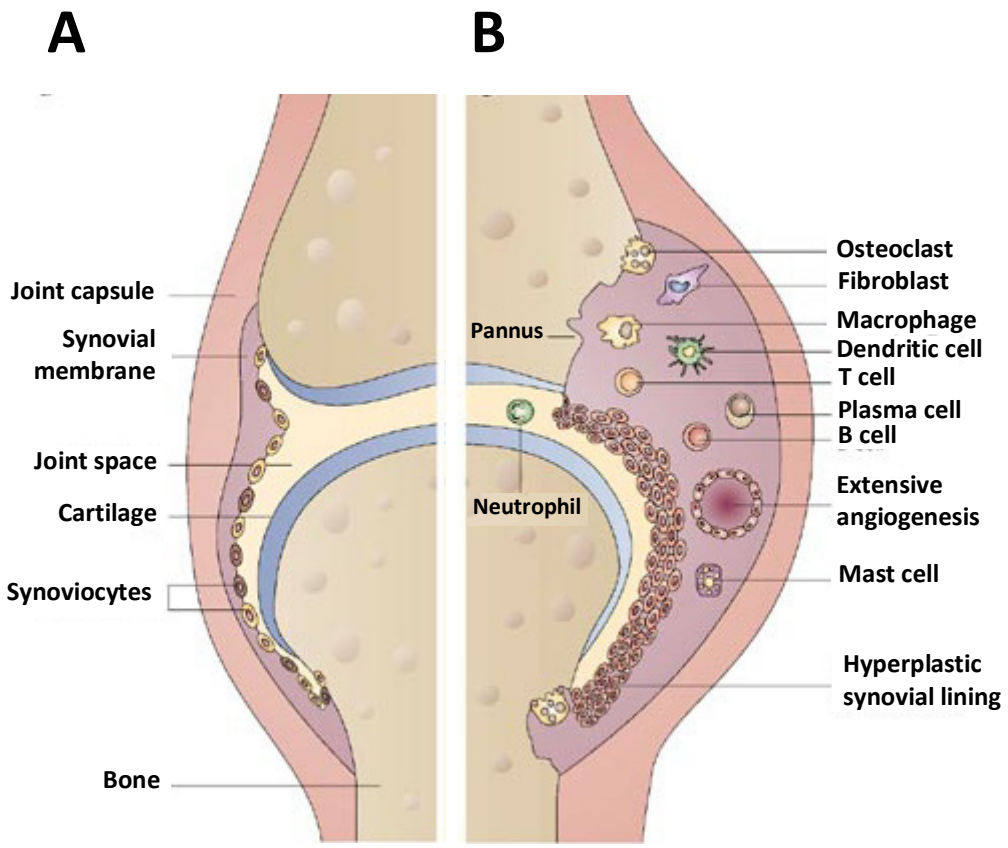

Figure 1.1 Healthy versus rheumatic joint

Healthy diarthrodial joint with thin synovial membrane lining the non-weight bearing parts of the joint enclosing the joint cavity (A). Rheumatoid joint characterised by hyperplastic synovial membrane forming an aggressive and invasive pannus with joint cartilage and bone erosion. Local infiltration with immune cells contribute to the formation of an hypoxic environment stimulating angiogenesis and exacerbating the inflammatory condition (B) (Image adapted from Strand et al, 2007) (49).

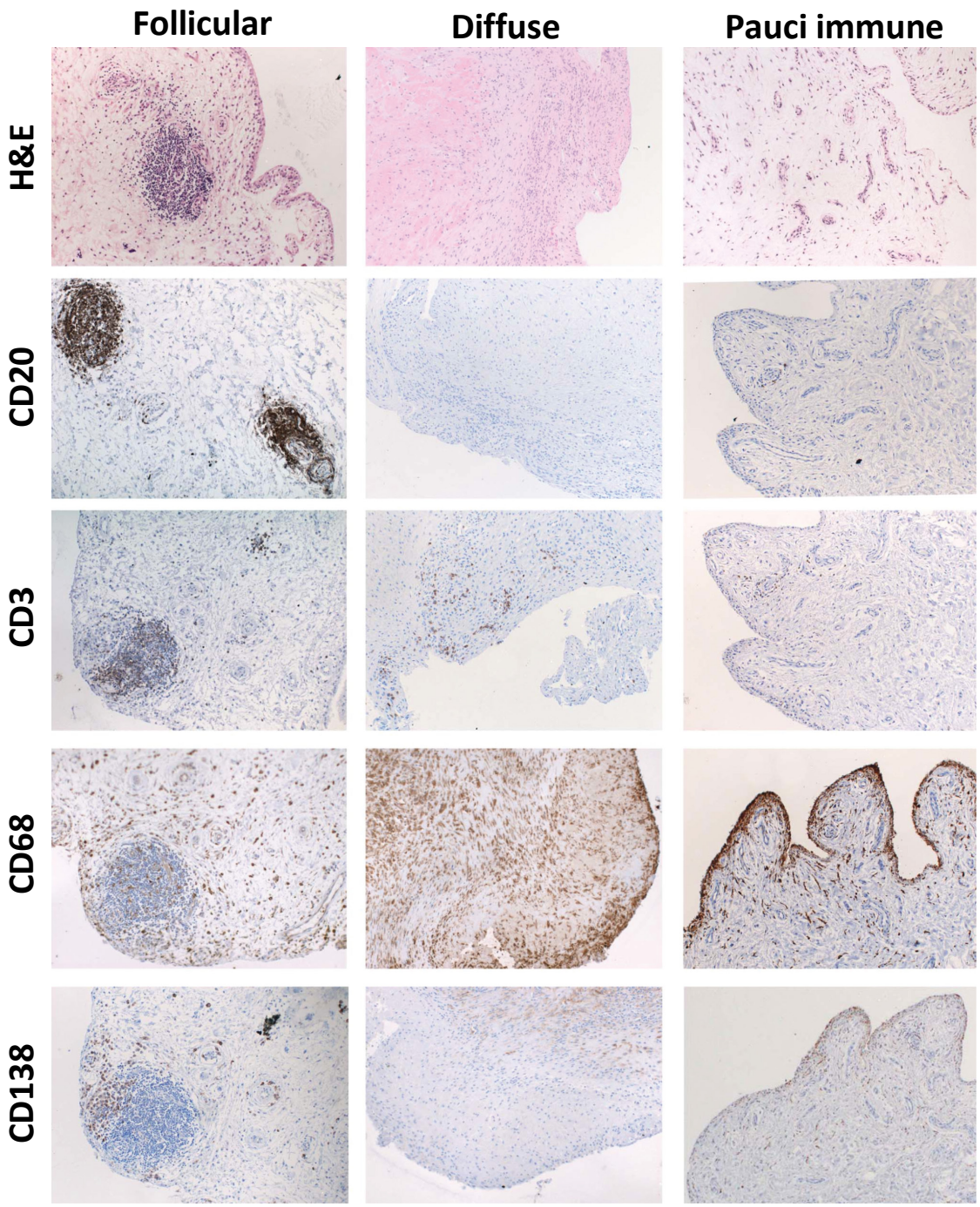

Figure 1.2 Histomorphological features of RA synovium

Diverse immune cell infiltrates in RA synovial tissue, showing pauci immune synovitis, diffuse and follicular distribution. Presence of B-cells (CD20), T-cells (CD3), macrophages (CD68) and plasma cells (CD138) showed via immunohistochemistry staining (figure taken from Pitzalis *et al*, 2013) (50).

FLS are the most abundant cell type in the synovium, accounting for up to two thirds of the total cell population, and characterised by an elongated phenotype and a prominent endoplasmic reticulum and Golgi apparatus, indicating a strong protein synthesis capacity (7). In disease conditions, this cell population undergoes hyperproliferation, possibly due to growth factors presence such as platelet-derived growth factor (PDGF), basic fibroblast growth factor (bFGF) and TGF-β (51, 52). However, increased mitotic rates of FLS in RA synovium have not been definitively documented. On the other hand however, a decrease of the apoptotic rate has been reported despite the toxic environment of the rheumatoid synovium. A possible role of p53 mutations (53), Bcl-2 overexpression (54) and Fas ligand disregulation (55) have been suggested. The presence of FLS at the cartilage/pannus junction suggests an active role in cartilage degradation and invasion. Indeed, secretion of MMP-1,3,8,9,10,11 and 13 induced by IL-1, TNF and growth factors has been reported in the literature (7, 56). Recently, FLS have been recognised as functional inflammatory cells with direct interactions with T- and B-cells. FLS are the principal source of IL-6 in the synovial intima and could promote Th17 differentiation and proliferation (57). In addition, FLS can directly promote B-cell survival and activity via production of BAFF and APRIL and stimulating class-switch recombination and IgG/IgA production (58).

The adaptive immune system has a pivotal role in development and perpetuation of the disease. Historically RA has been considered a disease mediated by T-cells, specifically $CD4^+$ type 1 helper T-cells (Th1), due to the relationship with the increased susceptibility in patients bearing the HLA shared epitope that could be responsible for antigen presentation of arthritogenic peptides to T-cells via antigen presenting cells (APC) interaction. T-cells are abundant in RA synovium, often found in close proximity to B-cells, follicular dendritic cells (FDc) and fibroblasts. Synovial T-cells show a highly differentiated phenotype $CD45RO^+$ (memory), display markers of activation such as CD69, CD28 and CD40L and are characterised by a marked shift towards the Th1 phenotype with production of interferon (IFN) γ and inadequate production of Th2 cytokines such as IL-4. However, only a limited amount of synovial T-cell cytokine appears to be secreted,

probably impaired by a chronic exposure to TNF-α in the synovium that mediates a down-regulation of the TCRζ chain causing limited proliferation and effector responses (59-62). The paradigm of Th1/Th2 imbalance is not sufficient to explain the mechanisms of synovitis and in an animal model of arthritis where the Th1 *Ifng* and *Ifngr* genes are knocked out, collagen induced arthritis (CIA) results in a faster progression (63). Recently more attention has been focused around the role of Th17 cells as potential crucial effector cells in RA and the paradigm has now shifted from Th1/Th2 to Th17/Treg imbalance. Th17 are a subset of $CD4^+$ T helper cells producing mainly IL-17, which differentiate from naïve T-cells upon stimulation with IL-6 and TGF-β. In a CIA mouse model of arthritis, onset of the disease in IL-17 deficient mice was suppressed, while the administration of anti-IL-17 antibodies could reduce joint inflammation and damage after the onset of arthritis (64, 65). The role of Th17 in the RA pathogenesis could be related to the IL-17 induced expression of IL-1, IL-6, TNF-α, metalloproteinases and chemokines by stromal cells, in particular fibroblasts. Tregs are an additional T-cell subset that plays an important role in maintenance of immune tolerance. They exhibit the $CD4^+CD25^{+high}$ phenotype and are characterised by the expression of the transcription factor Foxp3. Tregs have been described *in vitro* as able to suppress proliferation and cytokine production of $CD4^+$ $CD25^-$ T cells (66) and suppression of macrophages (67), B-cells (68) and dendritic cells (69). Secretion of cytokines such as IL-10, IL-35 and TGF-β and of cytotoxic factors such as perforin and granzyme B are at the basis of the suppressive activity of this cell population. In rheumatoid arthritis, the Treg function appears impaired, being unable to suppress pro-inflammatory cytokine release by T-cell and macrophages despite the inherent enhanced suppressive capacity of Tregs found in RA synovial fluid (70). This deficiency has been linked to a defective expression of cytotoxic T lymphocyte-associated protein (CTLA)-4 (71). Additionally, the elevated cytokine levels in the RA synovium, in particular TNF-α, IL-1 and IL-6, despite promoting an increased recruitment of Tregs at the site of inflammation, act as suppressor of their immune modulatory activity (70, 72).

As mentioned above and shown in Figure 1.2, immune cells aggregates can occur in the synovium of patients with rheumatoid arthritis, with B cells mainly

localised in the T-cell/B-cell aggregates (47, 48). These structures can be functional and present typical secondary lymphoid characteristics such as follicular dendritic cell (FDC) network, HEV, peripheral lymph node addressin (PNAd), important for lymphocyte homing, and CCL21 expression which is usually produced by lymph node myofibroblasts. In addition, these structures have been demonstrated to be able to promote B cell survival and proliferation, stimulate class switch recombination via activation-induced cytidine deaminase (AID) expression, and promote active expression of human IgG ACPA and therefore contribute to the pathogenesis of rheumatoid arthritis (73).

The synovial fluid and synovial tissue house a large number of innate effector cells, amongst which macrophages and neutrophils are the predominant cell type. Macrophages are found in the synovial membrane and represent, along with fibroblasts, the cellular constituent of the synovial lining layer in normal conditions (3). During RA, macrophages act as central effectors in synovitis development with a high efflux from the bone marrow directed to the synovium, following stimulation with macrophage colony-stimulating factor (M-CSF), granulocyte colony-stimulating factor (G-CSF) and granulocyte-macrophage colony-stimulating factor (GM-CSF) (74). Their role in the pathogenesis of RA is further supported by the fact that conventional therapies act to reduce the levels of cytokines produced by macrophages (75). Macrophages are an important source of pro-inflammatory cytokines in the synovium, including TNF-α, IL-1, IL-6, IL-15, IL-18, IL-23 which suggests a predominant M1 phenotype (14), and produce short half-life mediators of inflammation, matrix-metalloproteinases, nitrogen intermediates and growth factors that promote cell survival in the rheumatoid synovium. Activated macrophages can be found at the cartilage-pannus junction and are important contributors in joint erosion. The second innate effector population is neutrophils, which is the most abundant cell type in synovial fluid. This cell type is known for producing a wide range of inflammatory mediators such as TNF-α, IL-1, IL-6, IL-15, IL-18 and BAFF, promoting synovial inflammation and joint destruction and contribute to synovitis by synthesis of prostaglandins, proteases and reactive oxygen intermediates (76).

1.1.3 Synovitis in Osteoarthritis

Osteoarthritis is the most common articular disorder worldwide consisting in a chronic disease resulting from biomechanical damage to the articular cartilage. Although initially considered as a simple disease arising from joint cartilage degradation due to advanced age, now it is considered a complex disorder with a substantial involvement of immunological factors in the synovium. This disease shows a similar prevalence in males and females during reproductive life, although post-menopausal women are subjected to an increased predisposition suggesting a role of sex hormones in disease modulation (77). Obesity is currently considered the strongest risk factor for OA development (78, 79), however, mechanical factors are considered the leading cause of the disease in which injury to the joint may cause disruption of joint biomechanics, accentuating pathological damage and increasing the risk of OA development (77). The OA synovium is often characterised by a thickened lining layer and the presence of perivascular and diffuse lymphocyte infiltrates (80). Macrophages are among the most abundant cells present in the OA inflamed synovium and are responsible for the expression of the two major pro-inflammatory cytokines IL-1β and TNFα (81). IL-1β is overexpressed during OA and has been shown to up-regulate the expression of MMP catabolic enzymes 1, 3 and 13, the aggrecanases ADAMTS-4 and 5 in human chondrocytes (82, 83) and inhibit the expression of type II collagen and proteoglycans (84, 85). TNFα acts in synergy with IL-1β stimulating cartilage resorption and inhibiting proteoglycan synthesis (86). The OA synovium is also characterised by the presence of T-cell infiltrates both $CD8^+$ and $CD4^+$, with a predominant Th1 phenotype (87). In addition, analysis of the α/β gene repertoire suggested an undergoing clonal expansion in response to synovial antigens (88). Oligoclonal expansion was also reported for activated B-cells and several groups described the presence of antibodies targeting cartilage components (89).

1.2 Neoangiogenesis

During organ development, growth and tissue remodelling, the vascular compartment undergoes reorganisation, characterised by vasculogenesis, defined as recruitment of endothelial progenitor cells and formation of new vessels, or angiogenesis, formation of new capillaries from pre-existing vessels. A subpopulation of $CD34^+$ cells expressing the vascular endothelium growth factor (VEGF) receptor 2 has been identified as endothelial cell progenitors and is responsible for vasculogenesis following recruitment via stimulation of the CXCR4 receptor with the chemokine SDF-1/CXCL12. Several factors can stimulate angiogenesis *in vivo*, including chemokines, matrix molecules, cell adhesion molecules, growth factors and cytokines. VEGF is one of the strongest stimulators of angiogenesis and can be upregulated in conditions of hypoxia, leading to enhanced blood vessel formation and the restoration of blood and oxygen supply to the affected tissues (90). In response to those stimuli, the vascular endothelial cells (EC) become activated and release proteases (such as MMPs) to digest the underlying basal membrane and allow the emigration of endothelial cells from the extracellular matrix in a mechanism called sprouting (91). The sprouting cells would then form a column of migrating and proliferating cells moving towards a VEGF gradient (92). When the destination is reached, the endothelial cells start forming the lumen of the newly formed vessel and secrete growth factors such as PDGFβ to attract pericytes that envelop the immature vessel, induce EC growth arrest and promote vessel maturation (93, 94) (Figure 1.3).

Pericytes are important components of the microvasculature and are ubiquitously present in blood microvessels, extending the cytoplasmic processes along the surface of endothelial cells. Pericytes and ECs are generally separated by the basal membrane in which the pericytes are embedded, with occasional contacts of peg-socket type. The reason for tissue specific density and distribution is unknown but it is modulated by blood pressure levels, inflammation and hypoxia (95). Pericytes are responsible for vasoconstriction and vasodilation of capillaries, regulating diameter and blood flow in response to specific adrenergic stimuli,

angiotensin II and endothelin-1 (96). In addition, oxygen levels have been proven to influence cellular contraction. Specifically, hyperoxia increases pericyte contraction, causing vasoconstriction and blood flow reduction, while hypoxia and high levels of carbon dioxide cause relaxation and vasodilation increasing blood flow (93). Organ specific functions have been reported in the literature, pericytes are important for structural integrity of the blood-brain barrier (97) and for the glomerular capillaries in the kidney (98).

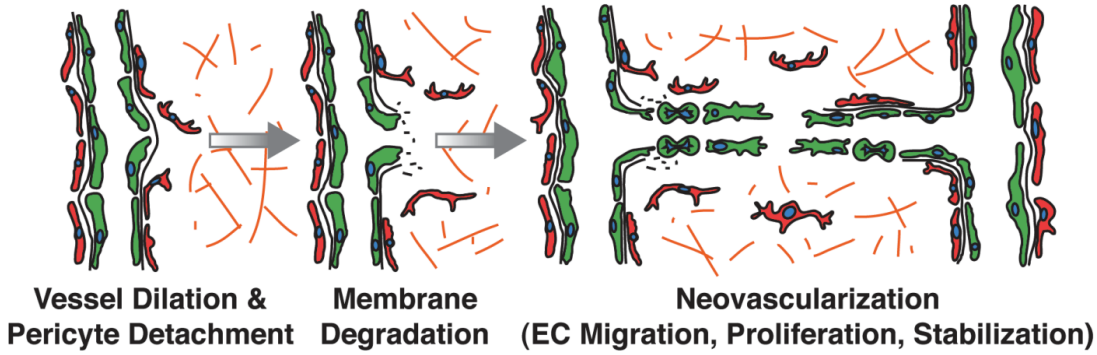

Figure 1.3 Angiogenesis

Hypoxia induced vessel sprout characterised by degradation of basal membrane and extracellular matrix (orange lines) and endothelial cell (green cells) migration following a VEGF gradient. Endothelial expression of PDGFβ attracts pericytes (red cells) that provide support to the newly formed vessel and promote maturation (figure adapted from Bergers et al, 2005) (93).

1.2.1 Role of angiogenesis in rheumatoid arthritis

As previously described, rheumatoid arthritis is characterised by inflammation and extensive angiogenesis. During disease onset and progression, the synovium undergoes expansion with hyperproliferation of synoviocytes and leukocytes infiltration from peripheral circulation. This change in synovial cellularity causes an increased metabolic demand and oxygen consumption, leading to hypoxia. The oxygen pressure in the synovium can then drop from 9-12% in normal individuals to 2-4% in RA patients (99). The regulators of the oxygen tension are called hypoxia-inducible-factors (HIF). HIF is a heterodimeric transcription factor, formed of subunits HIF-α and HIF-β, able to bind to hypoxia-response elements (HRE) on target genes and activate transcription. Two isoforms of HIF-α are expressed in human arthritic synovium (100). VEGF is one of the best characterised HRE-containing genes and increased levels of VEGF/VEGF receptor in RA synovium have been described in the literature as a consequence of hypoxia (99, 101). Up-regulation of SDF-1, proinflammatory cytokines (IL-6) and matrix metalloproteinases (MMP1 and MMP6) have also been associated with HIF activation in RA synovium (102, 103), suggesting a direct role of hypoxia in synovial angiogenesis, inflammation and cartilage degradation. Interestingly, proinflammatory cytokines such as IL-1β and TNFα are able to directly stimulate HIF expression in normoxia, further strengthening the relation between hypoxia and inflammation (104). However, despite the increased vascularisation, the synovial tissue remains hypoxic, which is possibly due to the formation of abnormal vessels and results in impaired perfusion and oxygenation (105).

During inflammation circulating immune cells are recruited in the affected tissue via interaction with the endothelial layer of blood vessels. This passage involves interaction of constitutive and inducible surface cell adhesion molecules (CAM) on endothelial cells and leukocytes and extravasation of the latter in the target tissue (Figure 1.4). In the first step, weak adhesion takes place between leukocyte and the vascular endothelium mediated by low affinity binding of selectins. In the presence of inflammation, the cells undergo activation/triggering induced by the presence of chemokines anchored to the EC via proteoglycans (106).

Following chemokine/chemokine receptor binding, the cells become activated, triggering the expression of integrins necessary for high affinity interaction with the endothelial layer (107). Finally, the adhered leukocytes initiate the extravasation process through the endothelium and the basal membrane. During this process the leukocytes engage specific immunoglobulin molecules, causing the opening of the endothelial barrier mediated by production of proteases, polarisation of chemokine receptors and migration towards the chemokine gradient (108-110).

General inflammation triggers the expression of E- and P-selectins on endothelial cells to facilitate the initial tethering phase, alongside ICAM-1 and VCAM-1 to induce firm adhesion with β2 integrins and stimulate trans-endothelial migration. Similarly, rheumatoid synovial endothelial cells express E- and P-selectins as well as ICAM-1 and VCAM-1 (111, 112). Notably, the integrin αVβ3 seems to play and important role in angiogenesis and disease progression (113) and blockade with αVβ3 antagonist provided reduction of angiogenesis and significant protection against cartilage erosion in animal models (114). However, very little efficacy was demonstrated in human RA trial (113). Chemokines and chemokine receptors have also been implicated in synovial inflammation and angiogenesis, where constitutively expressed chemokines important for homeostatic functions can drive and actively promote inflammation in the synovium. Hypoxia can stimulate the production of SDF-1/CXCL12 from synovial fibroblasts contributing to $CXCR4^{+}$ T-cell retention and stimulation of angiogenesis (115, 116). CXCL13 chemokine, mainly expressed by FDCs, interacting with the CXCR5 receptor has been implicated in the formation of tertiary lymphoid structures in RA synovium, where organisation of T- and B-cell aggregates can support and promote local inflammation (117). Among other chemokines important during phase two of leukocyte migration, CCL2, CXCL8/IL-8 and CCL5 (RANTES) are overexpressed in RA synovium. CCL2, mainly expressed by macrophages, contributes to attraction of macrophages, T- and natural killer (NK)-cells on site; CXCL8 is important for neutrophil and monocyte attraction and CCL5, mainly expressed by synovial fibroblasts acts as a chemoattractant for monocytes and T-cells (118).

1.2.2 Organ tropism

The vascular endothelium represents the first barrier encountered by circulating leukocytes before they migrate into the target tissue. Direct interaction between CAMs expressed on the endothelial layer and on the migrating leukocytes is the basis of general translocation mechanism. However, there is evidence supporting organ specific signals that can direct specific leukocyte subsets to the target tissue. The organ tropism is mediated by the expression of homing receptors on circulating leukocytes that interact with specific vascular addressins expressed on the microvascular endothelium of the target organ and facilitated by chemokine gradient (119, 120).

Peripheral lymphoid organ tropism has been described in the past, L-selectin expression on naïve T-cells interacts with PNAd expressed on HEV in secondary lymphoid organs, necessary for peripheral lymphoid tissue homing (121). L-selectin knockout mice showed reduced leukocyte adhesion to HEV and smaller peripheral lymph nodes (PLN) structures, related to reduced PLN lymphocyte numbers (122). A second homing signal is dictated by CCR7 chemokine receptor expressed by PLN naïve T cells, which interacts with CCL19 and CCL21 chemokines expressed in the lymph nodes (123).

Intergrin α4β7 expression in T-cell subsets is important for interaction with gut mucosal venular endothelium MAdCAM-1 and homing to gut associated lymphoid tissues (GALT) (124). Mice deficient for α4 or β7 subunits or treated with α4β7 antagonists are characterised by underdeveloped GALT (125). CCL25 expression further strengthens the homing capacity of CCR9 expressing $\alpha4\beta7^{+}$ T-cells to gut mucosal tissues (126).

Another well characterised organ tropism is T-cell skin homing mechanism, where CLA expressing T-cells are able to bind to E-selectin on skin MVE (127). In conditions characterised by skin inflammation and patients affected by T-cell lymphoma, infiltrating T-cells are confined to CLA expressing subsets (128, 129), aided by CCL17 chemokine stimulation of CCR4 receptor on T-cell surface (127).

There is thus evidence for molecular heterogeneity within the microvascular endothelium of different organs and tissues. In an attempt to identify such molecules, *Rajotte and colleagues* adopted intravenous *in vivo* phage display technology (described in section 1.4.1) to select several peptides able to selectively target lung, skin and pancreatic tissues among others, in murine models (130). For each organ different peptides were isolated, suggesting the presence of a variety of organ specific markers. Furthermore, they showed that specific peptide motifs preferentially recognised the vascular environment of different tissues. Similarly, *Arap and colleagues* used *in vivo* phage display in terminally ill human patients via intravenous administration of the phage library and recovery of bound phage clone from biopsies (131). More than 47000 motifs from 4716 phage clones were isolated showing specific organ localisation. More recently, the adaptation of the *in vivo* phage display assay using severe combined immunodeficient (SCID) mice grafted with human arthritic synovium allowed the isolation of peptides showing homing specificity for the synovial microvasculature (132).

This heterogeneity can be exploited for the identification of tissue and/or disease specific markers to be used for targeted delivery approaches. Towards this goal, it has been demonstrated that specific peptides can be exploited for targeted drug delivery in an attempt to lower systemic doses and increase effectiveness (133-136).

1.3 Treatment of rheumatoid arthritis

With 1% of incidence in the Western population, rheumatoid arthritis is considered a relatively common disease (18) with a high impact on national health systems (20-22). From a commercial point of view, rheumatoid arthritis is one of the most lucrative markets for pharmaceutical industries, mostly related to monoclonal antibody therapies which generated revenues for US$ 23 billion in 2011 and are expected to rise from US$ 11.5 billion in 2011 to US$ 15.7 billion in 2018 in US, Japan, Germany, France, Spain, Italy and UK markets (137). Despite the obvious success of the current therapeutic approaches in treatment of RA, clinical studies have shown that achievement of treatment-free remission, which is the ultimate goal for clinical practice, can be reached only by 9.4-15% of patients (138). Additionally, 20-40% of the patients do not respond to the available therapeutics (139, 140). To evaluate responsiveness to treatments and validate clinical outcome, the Disease Activity Score (DAS) in Europe and the ACR response criteria in North America have been adopted. The DAS28 is a composite outcome measure assessing how many joints in the hand, wrists, elbows, shoulders and knees are swollen or tender, the ESR and CRP in the blood to assess inflammation, and the patient's visual analogue score to assess the patient's feeling. A score below 2.6 indicates disease remission, while a score over 5.1 suggests high disease activity (141). For standard readout, the ACR score is set at three goal points, ACR20, ACR50 and ACR70, representing 20%, 50% and 70% improvement respectively, of the ACR criteria. These criteria involve number of swollen or tender joints, patient's global assessment, pain assessment and physical assessment, physician's global assessment, ESR and CRP values (142).

1.3.1 Synthetic DMARD

The clinical approach to RA has changed over the past 30 years. In the 1980s a pyramid strategy was adopted, following the "go low go slow" philosophy with a gradually build up therapeutic intervention starting with non-steroidal anti-inflammatory drugs (NSAIDs) and finishing with disease modifying anti-rheumatic drugs (DMARD) when erosion became evident. Often the therapy was maintained

unaltered for long periods of time. This approach has now been substituted by an inverted pyramid approach, characterised by the use of DMARDs early in the course of the disease with frequent therapy changes to tailor the therapy to the individual (143).

Methotrexate is now the first-line DMARD for most patients. This molecule acts as a folate antagonist, blocking purine synthesis with cytostatic properties at high dosage. At the therapeutic dosage however, extensive cytotoxicity does not occur (143). The reason behind the success of this compound lies on the relatively fast onset of action, a considerable success rate with 50-80% clinical response compared to baseline and acceptable adverse side effects that translates increased patient's tolerability (144). However, true remission has not been reported.

Leflunomide is an inhibitor of dihydroorotate dehydrogenase, an enzyme required for pyrimidine synthesis, primarily used as an alternative to methotrexate. The specific mechanism of action in rheumatoid arthritis is not known but it has been shown to affect lymphocyte function (145). Leflunomide produced similar clinical results to methotrexate, with approximately 50% of patients achieving ACR20 and 34% achieving ACR50 (144). Due to the similar mechanism of action, the adverse effects of Leflunomide were comparable to methotrexate, however, due to the teratogenic effect observed in animals it is not recommended for women in childbearing potential.

Sulfasalazine is a synthetic compound developed in the late 1940's with the specific purpose of RA inflammation treatment, showing efficacy in reducing radiological damage and alleviating symptoms (143).

Comparison of DMARD monotherapy in patients revealed an increased ACR20 success rate for methotrexate compared to leflunomide but a worse health-related quality of life (146, 147). Leflunomide however, resulted in a higher percentage of patients achieving ACR20 and 50 compared to sulfasalazine in a double-blind randomised trial (147, 148), while three trials showed similar ACR20 for methotrexate and sulfasalazine (147). Notably, triple combination of

methotrexate, sulfasalazine and hydroxychloroquine resulted more efficacious that single therapy or double therapy in randomised double blind trials (149, 150), stressing the importance of inhibiting different pathways to achieve better effectiveness. However, data are still insufficient to determine which combination outweighs another, especially when highly selected populations in different trials are compared, and a patient tailored therapeutic approach is still preferable.

1.3.2 Biologic agents

Since the mid 1970's production of rodent-derived monoclonal antibodies became accessible, opening the road for the magic-bullet dream and the beginning of the antibody therapy era (151). The new possibilities given by this technology radically changed the clinical management of RA with the raise of the biologic agents in the therapy or arthritis (Figure 1.4). Monoclonal antibodies developed for clinical purposes generally belong to the IgG class due to the effector functions exerted by the constant region of γ globulins (152). In particular, the IgG1 isotype is the most suited to trigger effector functions such as antibody-dependent cellular cytotoxicity (ADCC) and complement fixation (152). An IgG antibody is characterised by the presence of a heavy chain and a light chain. The heavy chain is composed of a variable region (V_H) linked to three constant domains (C_H) with a hinge region separating the C_H1 from the Fc region (C_H2 and C_H3 domains), responsible for homodimerisation through the formation of two disulphide bonds. The light chain is constituted of a variable (V_L) and a single constant domain (C_L) which forms a disulphide bond with the C_H1 domain, allowing heavy and light chain pairing (153). Two types of V_L, defined as κ and λ light chain, are available, with the former being the most represented amongst functional natural IgG antibodies. Schematic of an IgG antibody is shown in Figure 1.6.

By the mid 1980's TNF had been described as a pleiotropic cytokine with clear contribution to synovitis and bone resorption in rheumatoid arthritis (154, 155). $CD4^+$ T-cells and macrophages are the main producers of this cytokine and the expanded population in the synovium can lead to an overproduction with deleterious effects. In addition, TNF inhibition was able to reduce the production of

pro-inflammatory cytokines such as IL-1, IL-6 and IL-8 as well as growth factor G-CSF (156) and showed to efficiently prevent joint destruction in animal models of arthritis (157, 158). These findings led to the notion that TNF plays a dominant role in the inflammatory cascade. TNF-α is initially expressed as a trans-membrane protein of 26 kDa (tmTNF) in a homotrimeric format with a total molecular weight of 78 kDa. The soluble form of TNF is created by cleavage of the extracellular domain by the TNF-converting enzyme TACE (or ADAM17). The final molecular weight of the soluble TNF is 17 kDa, present in a 51 kDa homotrimer. Once in soluble format, the TNF maintains the biological activity of the tmTNF without the localisation constriction (159). Two receptors are available for TNF: p55 (TNFR1) and p75 (TNFR2). Interestingly, the two forms of TNF are able to elicit distinct effects, which is to be put in relation with the differential binding capacity for the two receptors. Indeed, tmTNF was shown to be superior in activating the TNFR2 compared to sTNF (160). In respect to rheumatoid arthritis, the p55 TNFR1 was shown to be more influential in disease onset and progression. Mice overexpressing TNF are characterised by the spontaneous development of inflammatory conditions such as erosive polyarthritis and bowel disease. Knockout of the p55 gene showed abrogation of arthritic condition and reduced gut involvement, while knockout of the p75 gene didn't provide the same protection (161). Possibly, the pathologic role of p55 is to be linked to the downstream activation pathway that leads to NFkB activation, stimulating cell survival (162).

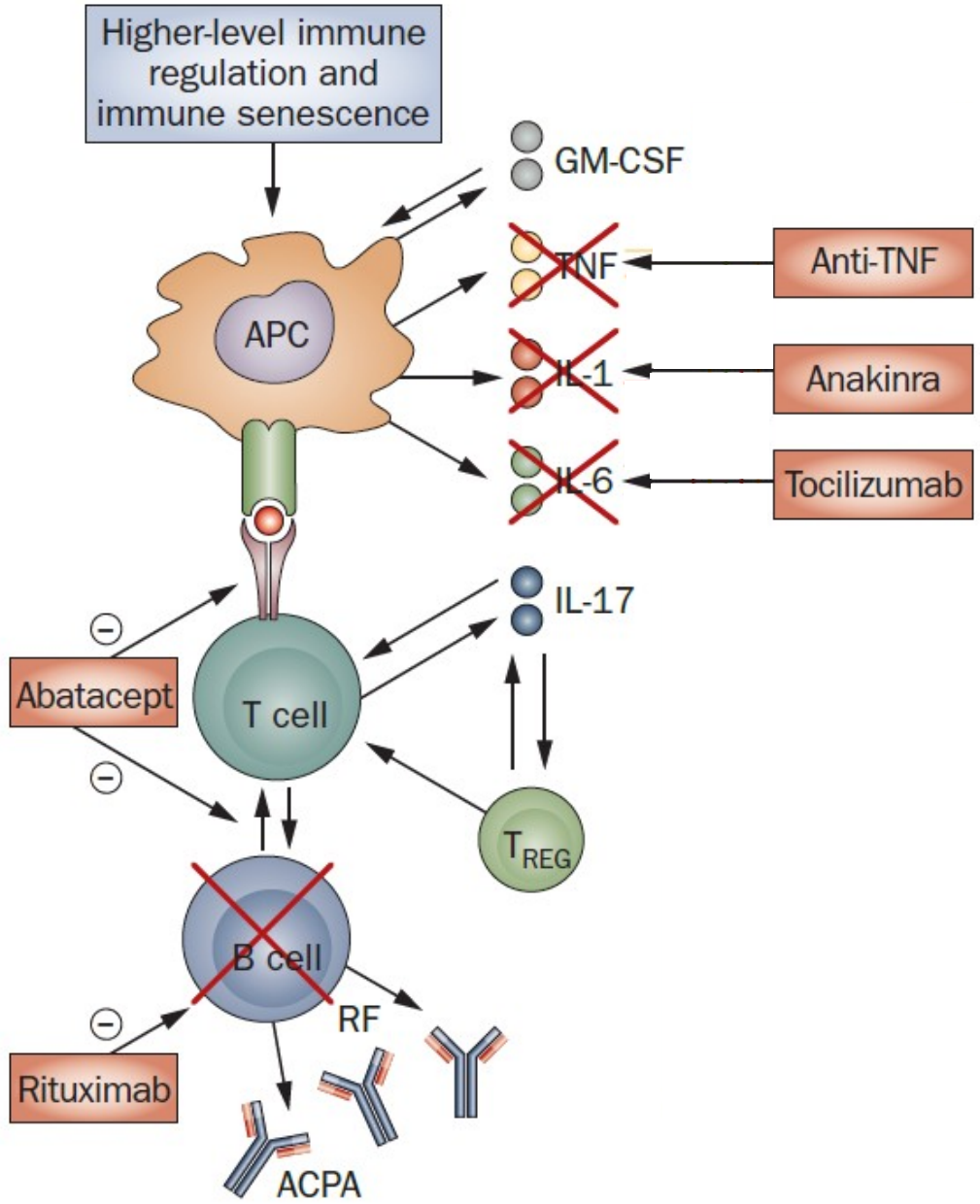

Figure 1.4 Biologics in rheumatoid arthritis

Schematic demonstration of current biologic therapeutic targets. Anti-TNF biologics, Anakinra and Tocilizumab act as cytokine inhibitors, blocking TNFα, IL-1 and IL-6 respectively. Abatacept, a CTLA-4 –Fc fusion protein, binds CD80/86 on APC, preventing co-stimulation of CD28 and T-cell activation. Rituximab is an anti-CD20 antibody able to induce B-cell depletion, preventing antibody production such as ACPA and RF (figure adapted from van Vollenhoven 2009) (143).

In 1999 two anti-TNF molecules were almost simultaneously registered for the treatment of RA, Etanercept and Infliximab. Etanercept is a fusion protein consisting in the human IgG1 Fc domain and the TNFR2 (163). Infliximab is a chimeric monoclonal antibody characterised by human IgG1 constant domains and murine derived variable regions (164). A few years later a fully human anti-TNF antibody was developed under the name of Adalimumab and commercialised as Humira (165). Interestingly, Adalimumab is the first FDA approved antibody to be derived from phage display technology. Since then, two more anti-TNF agent have been produced, Golimumab and Certolizumab pegol. Golimumab is a human monoclonal IgG1κ antibody (166), while Certolizumab pegol is a PEGylated Fab (fragment antigen binding) of a humanised anti-TNF monoclonal antibody (167). No randomised controlled clinical trials comparing Etanercept, Infliximab and Adalimumab are available. However, two cohort studies reported a faster response for Etanercept, compared to Infliximab, but with no clinically relevant differences in efficacy (168, 169). Indirect comparison of the three anti-TNF biologics showed no difference in terms of ACR20 and ACR50 rates (147, 170). Furthermore, a patient who has failed to respond to an anti-TNF agent, has a probability of responding to a second anti-TNF agent of approximately 50% (ACR20 criteria) (139). Infliximab and Adalimumab proved to be effective in Crohn's disease while Etanercept showed no efficacy (171-173). The reason behind this discrepancy may lie on the mode of administration and on the anti-TNF structure. Both Infliximab and Adalimumab are full IgG antibodies, while Etanercept contains only the Fc domain of an IgG. This might result in a differential ability to fix complement or induce ADCC. However, no real indication of complement or ADCC on Infliximab activity has yet been described (174). Most likely, the differential efficacy of anti-TNF agents derives from the interaction with TNF (Figure 1.5). Infliximab and Adalimumab are bivalent antibodies able to target two TNF monomers at the same time and potentially two TNF homotrimers as well (175, 176). Interestingly, the most thermodynamically stable complex was a 600 kDa macromolecule composed of three antibodies and three TNF homotrimers (Figure 1.5 B) (176). At the same time, Adalimumab and Infliximab are able to engage the tmTNF and act as a bridge, crosslinking two tmTNF trimers. In doing so, the tmTNF cytoplasmic domain is phosphorylated in a specific

serine residue, causing a reverse signalling transduction and inducing apoptosis (177, 178). Due to the monovalent format, Etanercept was not able to elicit the apoptotic signal through tmTNF, although the ability could be restored following crosslinking (178). However, the clinical importance of the apoptotic signal in RA therapy is still debated (159).

Among the adverse effects related to anti-TNF therapy, injection site reactions are the most common. However, the most severe adverse effects are related to the mechanism of action of the drug. Increased incidence of infectious complications, from common or opportunistic pathogens, has been reported in clinical practice and reactivation of latent tuberculosis was reported early in the development of Infliximab (179). Screening for at-risk patients substantially reduced tuberculosis occurrence (180).

Infliximab is a chimeric antibody, containing the murine variable domains and Etanercept is a fusion protein with a synthetic linker. Due to the exogenous amino acid sequences, immunogenicity is a concern. The production of anti-drug antibodies (ADA) against Infliximab, but also Adalimumab, has been described, with IgG1 and IgG4 subtypes as predominant ADA detected for the two biologics (181). Reduction of clinical efficacy might occur in some patients and increased frequency of minor and major clinical adverse effects has been linked to ADA levels (181). Difference in patients' reaction is related to variable levels of circulating ADA which if in low concentration are insufficient to bind and inhibit the entire pool of therapeutic antibody. The proposed mechanism of action of ADA is neutralisation of the antibody by steric hindrance, blocking the binding to its target and preventing biological activity, and formation of immune complexes, resulting in faster clearance and reduced half-life (181).

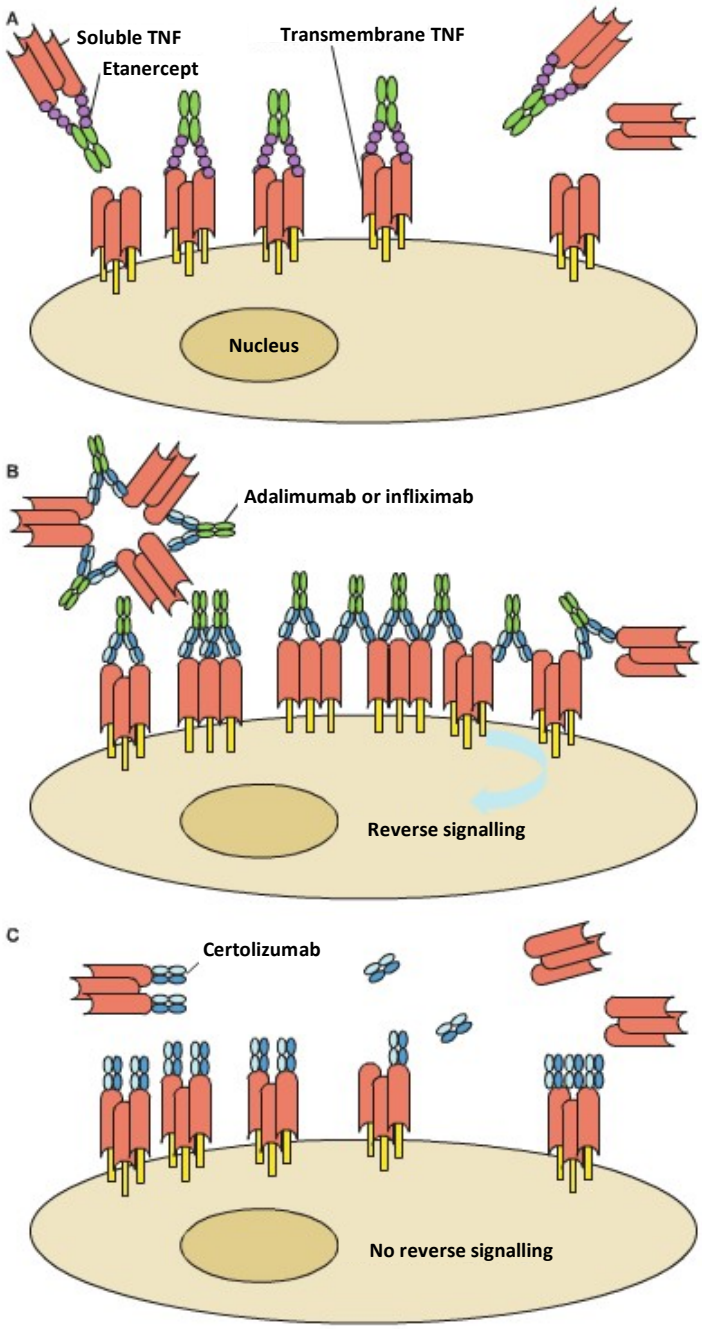

Figure 1.5 Mechanism of action of anti-TNF agents

Schematic representation of TNF neutralisation by anti-TNF biologics. The TNFR2-Fc fusion protein Etanercept is able to engage TNF in a monomeric fashion (A). Adalimumab and Infliximab IgG antibodies are able to bind two TNF monomer or trimers simultaneously. The stable soluble aggregate consists in three TNF trimers and three anti-TNF IgGs. Binding on trans-membrane TNF induces ligand cross-linking and reverse signalling through the cytoplasmic domain (B). Fab antibody fragment Certolizumab is able to bind TNFα only in a monomeric manner (C). (figure adapted from Rigby, 2007) (159).

Anakinra is an IL-1 receptor antagonist used in the treatment of moderate-severe rheumatoid arthritis in patients that did not respond to the initial DMARD therapy. Animal models overexpressing IL-1 are characterised by joint histopathologic changes similar to RA and increased osteoclast differentiation (182, 183). A double blind randomised clinical trial confirmed efficacy of Anakinra in comparison to placebo (184), although a lower efficacy and increased risk for injection-site reactions was observed when compared to anti-TNF biologics (ACR20 and ACR50 criteria) (170, 185).

A third strategy is the inhibition of IL-6 activity. Tocilizumab is a humanised monoclonal antibody, characterised by the backbone of the human IgG antibody with murine CDR regions, targeting the IL-6 receptor (IL-6R). During RA, IL-6 binds the soluble or membrane-bound form of IL-6R, inducing angiogenesis and activating osteoclasts, T- and B-cells (186). Tocilizumab showed comparable efficiency to the anti-TNF agents with similar adverse effects (187). Most common side effects were infections of the upper respiratory tract and gastro-intestinal tract. Patients previously treated with anti-TNF agents were more prone to develop severe side effects such as pneumonia, gastroenteritis and urinary-tract infections but also malignancies and haematological disturbances with significant alterations in plasma lipid concentrations (187).

Rituximab, a chimeric monoclonal antibody against the membrane protein CD20 found on naïve, mature and memory B-cells but not on pro-B-cells, plasmablasts and long-lived plasma cells (188). Although the exact mechanism of action remains unknown, Rituximab appears to act via induction of apoptosis, ADCC, and complement–dependent cytotoxicity (189). Generally one month after single treatment the B-cell compartment appears depleted, with the exception of B-cell precursors and long-lived plasma cells (190, 191). The depletion is reversible and peripheral B-cells start to repopulate to reach basal levels around 6-10 months post treatment (192). Interestingly, RF and ACPA serum titres were significantly decreased at 24 and 36 weeks respectively, while antibodies against common foreign antigens were not affected (192). Furthermore, clinical response was more pronounced in RF^+ and $ACPA^+$ patients, providing a biomarker for patients

stratification (193, 194). This suggests that Rituximab is able to selectively affect short-lived autoantibody secreting plasma cells. However, despite efficiently depleting B-cells in all the treated patients, a substantial percentage of patients do not respond to the treatment in clinical terms. Notably, synovial B-cells seem to be less affected by Rituximab treatment, probably due to environmental factors in the synovium, and patients with higher levels of clinical response are characterised by a more consistent B-cell depletion (195, 196). Following Rituximab treatment, many patients relapse when B-cell titres are still low, suggesting a more complex mechanism of action than the one described above (197). Genome-wide gene expression profiling revealed a clear distinction between responder and non-responder patients. In patients responding to the therapy, the INF response gene expression was increased, while limited or no expression could be detected in non-responding patients (197). Concern was raised for Rituximab therapy due to the prolonged B-cell depletion. Assessment of toxicity and impact of side effects in the long term are still preliminary but encouraging (198). Among the adverse effect described for Rituximab the most common are injection-site reaction and increased rate of infections (199).

The CD80/86 – CD28 interaction between antigen presenting cells and T-cells respectively, is the target of Abatacept. This biologic agent is a fusion protein between the extracellular domain of CTLA-4 and the Fc region of human IgG1 (200). The CTLA-4 domain is able to bind CD80 and CD86, preventing co-stimulation of CD28 on T-cells and promoting anergy (201). In phase III studies Abatacept proved to be efficient in patients showing inadequate methotrexate response and TNF blockade failure with an average of 50% improvement for the ACR20 criteria compared to placebo (199). As mentioned for the other biologics, the main adverse effects were related to infusion reactions and increased infections rates but generally the drug is well tolerated (202).

Although the biologics have substantial impact as monotherapy, combination with methotrexate showed a better clinical response than Adalimumab, Infliximab, Etanercept or Rituximab alone (147). However, due to the immunosuppressive properties of each biologic agent, combination therapies

between biologics showed increased incidence of severe adverse effects and did not provide evidences for higher efficiency compared to biologic + DMARD co-therapy (203, 204).

1.3.3 Bispecific antibodies

Recently, bispecific antibodies (BsAb) are gaining momentum with increasing clinical success. Bispecific antibodies are an emerging class of biological therapeutics characterised by binding capacity to two distinct epitopes. This can potentially lead to simultaneous inhibition of two cell surface receptor or soluble molecules, cross-linking of two receptors and recruitment of effector cells in the proximity of a target expressing cell. This last aspect has been the reason for the success of bispecific antibodies in cancer therapy. BsAbs directed against the CD3 antigen expressed on T-cells are able to redirect the T effector cells to the desired site when the second arm has the relevant specificity (205).

Engineering of standard IgG antibodies has led to the development of several bispecific antibody construct strategies, combining different properties and characterised by variable success rates (Figure 1.6). Bispecific antibodies can be distinguished based on the dimerisation strategy employed and are generally a result of development by pharmaceutical companies. Efficacy of this constructs was first demonstrated against tumours using chemically cross-linked antibodies and hybrid hybridomas (or quadromas) however with little clinical success (206-208). The limiting step in bispecific antibody design is the efficiency of heterodimerisation. Quadromas approach was characterised by fusion of two distinct hybridomas, providing a mixture of parent monoclonal antibodies, bispecific antibodies and inactive antibodies due to the random coupling of heavy and light chains belonging to the two original antibodies (209). The use of mouse IgG2a and rat IgG2b developed by Trion Pharma (Triomab) demonstrated a preferential species-restricted heavy/light chain pairing, increasing the rates of functional bispecific antibodies (210). The EpCAM/CD3 bispecific antibody Catumaxomab proved to be efficient in the treatment of ovarian cancer with

malignant ascites obtaining the first marketing approval for a bispecific antibody (205). Additional antibodies with the same framework are currently in clinical trials.

Several attempts to increase the heterodimerisation efficiencies have been reported in the literature. Of note is the "Knob-into-Holes" technology developed by Ridgway and colleagues at Genentech, based on the substitution of a small amino acid with a larger one in the C_H3 domain of the first Fc region, and the substitution of a large amino acid with a small one on the second Fc (211). This design would create a knob and a hole in the two heavy chains, allowing a preferential heterodimerisation in order to accommodate the protruding side chain. Up to 92% of efficient heterodimerisation was reported for this strategy (211). A second strategy is the SEED platform developed by EMD Serono, consisting in strand-exchange engineered C_H3 domains (212). This construct derives from dimerization of heavy chains carrying a chimeric IgG and IgA C_H3 domain that allows preferential heterodimerisation, with less than 1% of contaminant homodimers, and unaltered Fc effector functions (212).

The development of phage display (described in section 1.4.1) and scFv (single-chain variable-region antibody fragment), marked the advent of the recombinant antibody era. This antibody fragment, composed of the heavy and light chain variable domains linked with a small peptide linker, has been used as a building block for antibody engineering. Bispecific T-cell engagers (BiTE) are a simple form of tandem scFv antibodies showing bifunctional activity. Blinatumomab anti-CD3/CD19 was the first BiTE to be developed and is currently in clinical trials for lymphoma and leukaemia treatment. Additional non-standard bispecific antibodies have been reported in the literature, including among others the dual variable domain (DVD)-Ig developed by Abbott (213) and the mAB^2 developed by F-star (214).

As mentioned above, cancer therapy has been the pioneer in bispecific antibody development. None of the available bispecific antibodies has yet been approved for rheumatoid arthritis. However, increasing reports are being published regarding development of bispecific molecules tailored to the needs of

autoimmune diseases. Recently, a bispecific antibody targeting IL-1β and IL-17A in tandem scFv format was adopted in a collagen induced arthritis (CIA) mouse model. The BsAb proved to significantly ameliorate the pathological lesions when compared to anti-IL1β or IL-17A monotherapy (215). Kanakaraj and colleagues adopted a bispecific antibody to target TNFα and Angiopoietin 2 (Ang2), adding anti-angiogenic properties to the well-established anti-TNF Adalimumab. The bispecific antibody was shown to maintain unaltered the functionalities of Adalimumab but was significantly more effective in controlling the progression of arthritis in Tg197 TNF transgenic mice (216). Lastly, Veri and colleagues developed a scFv diabody (DART technology) targeting the inhibitory CD32B and the CD79B on B-cells, negatively regulating B-cell activation and IgG production, resulting in delayed onset of arthritis in CIA mice (217).

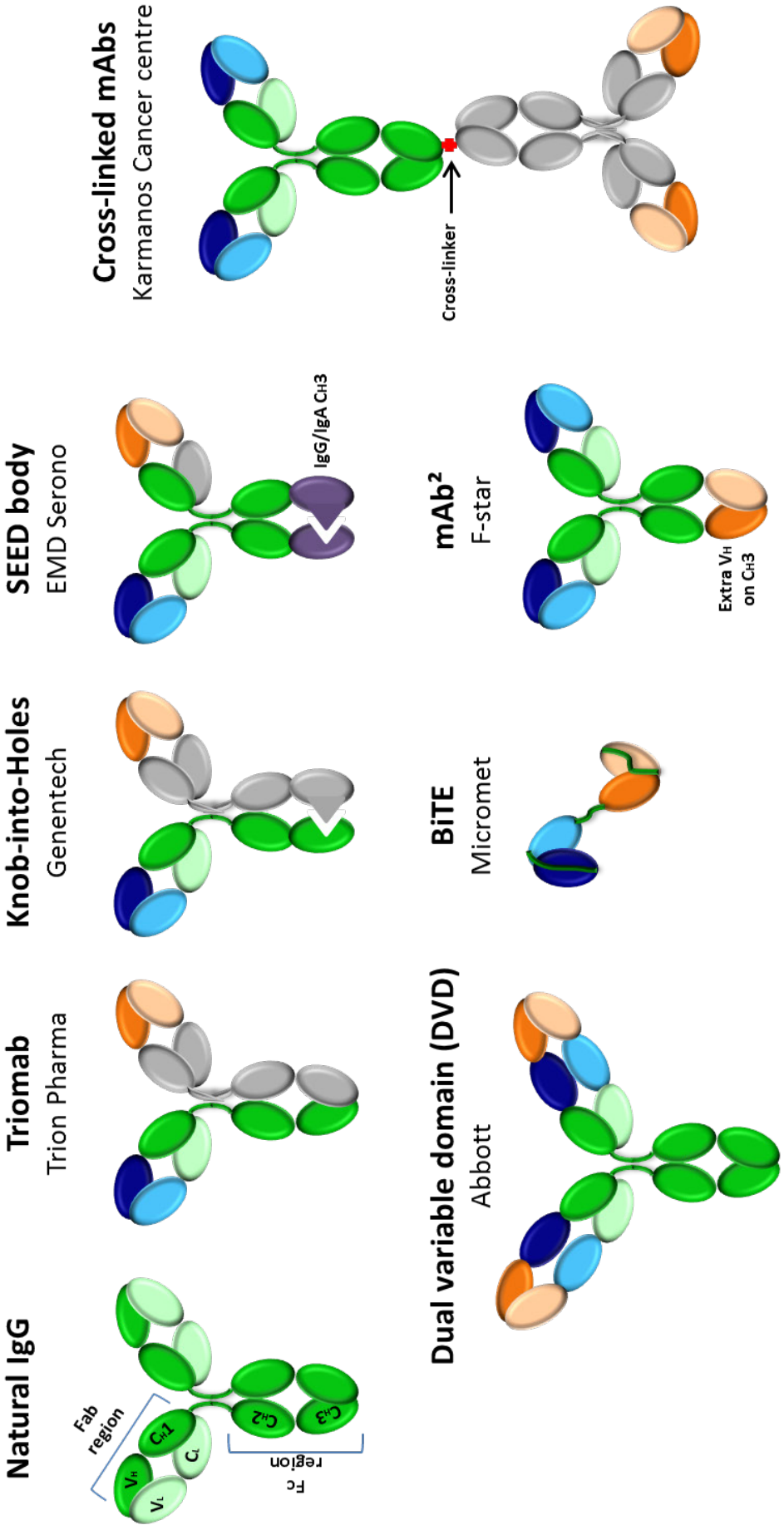
Natural IgG
Fab region
Fc region
Triomab
Trion Pharma
Knob-into-Holes
Genentech
SEED body
EMD Serono
IgG/IgA CH3
Cross-linked mAbs
Karmanos Cancer centre
Cross-linker
mAb²
F-star
Extra VH on CH3
BiTE
Micromet
Dual variable domain (DVD)
Abbott

Figure 1.6 Bispecific antibodies

Schematic representation of bispecific antibody constructs. Various bispecific antibody strategies have been employed; strategies include symmetric IgG-like molecules such as the cross-linked mAbs developed by Karmanos Cancer Centre showing two antibodies cross-linked at the Fc region, the mAB^2 structure developed by F-star characterised by engineered CH3 domains containing additional VH regions, and the DVD structure by Abbott, with two extra Fv regions in series to the original IgG Fv domains. Asymmetric antybodies are design with two independent binding arms, including Triomab design by Trion Pharma, exploiting mouse IgG2a and rat IgG2b species-restricted heavy/light chain pairing, the Knob-into-holes technology developed by Genentech, characterised by steric stabilisation of heterodimers, and SEED bodies, EMD Serono, with preferential heterodimerisation obtained through IgA/IgG chimeric CH3 domains.

1.4 Synovium as target organ

As described in section 1.2.2, the vascular compartment can be exploited for the identification and isolation of tissue specific homing receptors or vascular addressins. To date the identification of a synovial specific homing antigen is still lacking. Our group described in 2002 the isolation of a synthetic peptide with preferential homing specificity for the human arthritic synovium. This peptide was able to accumulate in the synovial microvasculature *in vivo*, in a SCID mouse model double grafted with human arthritic synovium and normal human skin as control (132). Recently, the peptide has been fused to IL-4, demonstrating efficient delivery of the cytokine to human RA synovium, using the same SCID mouse xenograft model, and provide proof of concept for peptide-targeted tissue specific immunotherapy in RA (136).

There is therefore evidence of synovial specific antigens that can be used for targeted drug delivery or as diagnostic tools. Peptide based screening using phage display has already been proven efficient in identifying such vascular determinants (130-132). Monoclonal antibodies lend themselves well to the development of ligand based therapeutic strategies, they are notoriously efficient in screening for specific antigens, are characterised by high affinity targeting of both linear and conformational epitopes and are characterised by long retention times *in vivo*, providing better therapeutic capacities (218). Since the first publication by Kohler and Milstein, the hybridoma technology has been an inestimable tool for recombinant antibody production (151). Clinical studies, however, have been disappointing due to the murine origin of the monoclonal antibodies and the related immunogenicity (218). As mentioned earlier, reduction of immunogenicity could be achieved by substituting the constant regions with human IgG counterparts. Such constructs were defined as chimeric antibodies, human constant regions and murine variable domains, or humanised antibodies, when the murine sequences are restricted to the CDR regions. However, this process is laborious and not necessarily successful with reported anti-humanised and anti-chimeric antibody response *in vivo* (219). The use of transgenic mice expressing human

immunoglobulin loci superseded the mouse hybridoma technology, providing a more natural immune response including direct affinity maturation (220). However, the shortcomings of these technologies for the intended application described above lie on the fact that the animals need to be challenged with the foreign antigen to elicit an immune response. This requires for the antigen to be known and possibly purified. Alternatively, the animals can be immunised with a mixture of proteins extracted from the target tissue, therefore extrapolated from their natural environment, which may result in isolation of antibodies targeting regions not exposed *in vivo* and impair clinical efficacy. In order to avoid this problem and identify specific vascular determinants directly *in vivo*, our group adopted the antibody phage display technology in a SCID mouse xenograft model (described below).

1.4.1 Phage display

The phage display technology developed in the late 80's (221) is based on the expression of a foreign antigen on the surface of filamentous bacteriophage particles, via fusion to the gene III (gIII) or VIII (gVIII). The exogenous protein was efficiently produced (limited to the bacterial expression machinery) and exposed on the particle surface, allowing fast screening with interacting molecules. The technology has been further developed in the early 1990's by Winter's group and adapted to antibody display (222).

The filamentous bacteriophage M13, and the relative fd bacteriophage, is the most commonly used vector for display purposes (223). This class of *E.coli* bacteriophage is characterised by a central cylindrical capsid containing the single-stranded circular DNA genome encoding for non-structural proteins and for the five coat proteins: pIII, pVI, pVII, pVIII and pIX (Figure 1.7 A). The pVIII protein is most abundant with 2700 copies expressed; pIII, pVI, pVII and pIX are present only in 5 copies each with apical distribution. The lifecycle of M13 starts with the infection of the *E.coli* host via interaction between the pIII coat protein and the bacterial F-pilus that retracts upon engagement, bringing the phage to the bacterial surface (224). Once in contact with the cell surface, the bacteriophage injects the DNA into the

host, disassembles and inserts the coat proteins in the bacterial membrane (225). At this point the phage takes control of the replicative machinery of the host and new phage particles are produced. The new phage are then released without cell lysis (223).

The phage life cycle depends therefore on the bacterial host for protein expression and assembly. This represents a limitation for the applications of phage display. Specifically, only small proteins that do not require post-translational modification can be efficiently expressed. All coat proteins have been exploited for display purposes, however, pIII and pVIII are the most commonly used (223). By logic the highly represented pVIII protein would be the optimal target for fusion protein display, allowing high density of target protein on the phage surface. Though, the resulting "avidity effect" may cause the selection of low-affinity binders and cause a less efficient screening. The pIII coat protein represents a valid alternative and many expression libraries are designed to express the foreign protein at the N-terminus of the pIII gene (gIII).

Full IgG antibodies are complex molecules that bacteria are not able to process, therefore for phage display antibody fragments are used instead. Both Fab and scFv have been successfully exposed on the surface of phage particles (226, 227). The protein to be displayed is fused to the N-terminus of the pIII in a vector (phagemid) containing the M13 origin of replication (ori), an *E.coli* ori (for episomal vector amplification), an inducible promoter (e.g. LacZ) and an antibiotic resistance gene to allow screening (Figure 1.7 B). This phagemid vector is able to replicate in the *E.coli* host but it doesn't produce phage particles due to the lack of the additional phage genes needed for virion packing. Transformed *E.coli* cells are then superinfected with a helper phage (227). This helper phage is a wild type filamentous phage engineered by disabling the packaging signal due to a defective M13 ori. This phage is therefore able to provide the necessary accessory genes to the phagemid carrying *E.coli* hosts, forming new phage particles preferentially containing the fusion pIII protein on the capsid. Helper phage pIII protein may still be incorporated, creating a mixed phage population. This is important to bear in mind because it could introduce a bias for wild type phage clones during *E.coli*

infection step and invalidate the system. In order to reduce this possible scenario, the helper phage used in the preliminary data for this thesis project was the KM13 mutant, characterised by a trypsin cleavable site between the D2 and D3 domain of the pIII protein (228). Trypsin treatment of phage particles would render inactive the wild type pIII protein, preventing wild type phage infection, while maintaining active the fusion pIII protein.

As a general protocol, a large repertoire of phage particles containing scFv or other peptides fused to the pIII are screened (panning) by affinity selection either *in vitro* against immobilised antigens, tissue samples, cell cultures or *in vivo* using animal models. Unbound non-specific clones are removed following extensive washes and bound phage are eluted using trypsin digestion. The trypsin step allows the removal of the fused scFv/peptide from the pIII protein, while at the same time inactivating the wild type pIII. The recovered phage particles are then used to infect *E.coli* bacteria in selective medium, allowing amplification of the phagemid vector containing the fusion protein gene. Phagemids are subsequently rescued via superinfection with helper phage and prepared for a second round of selection (228, 229). In libraries characterised by the presence of an amber codon between the peptide gene and the gIII gene, induced expression with IPTG in non-suppressive *E.coli* strains promotes the production of soluble protein (229).

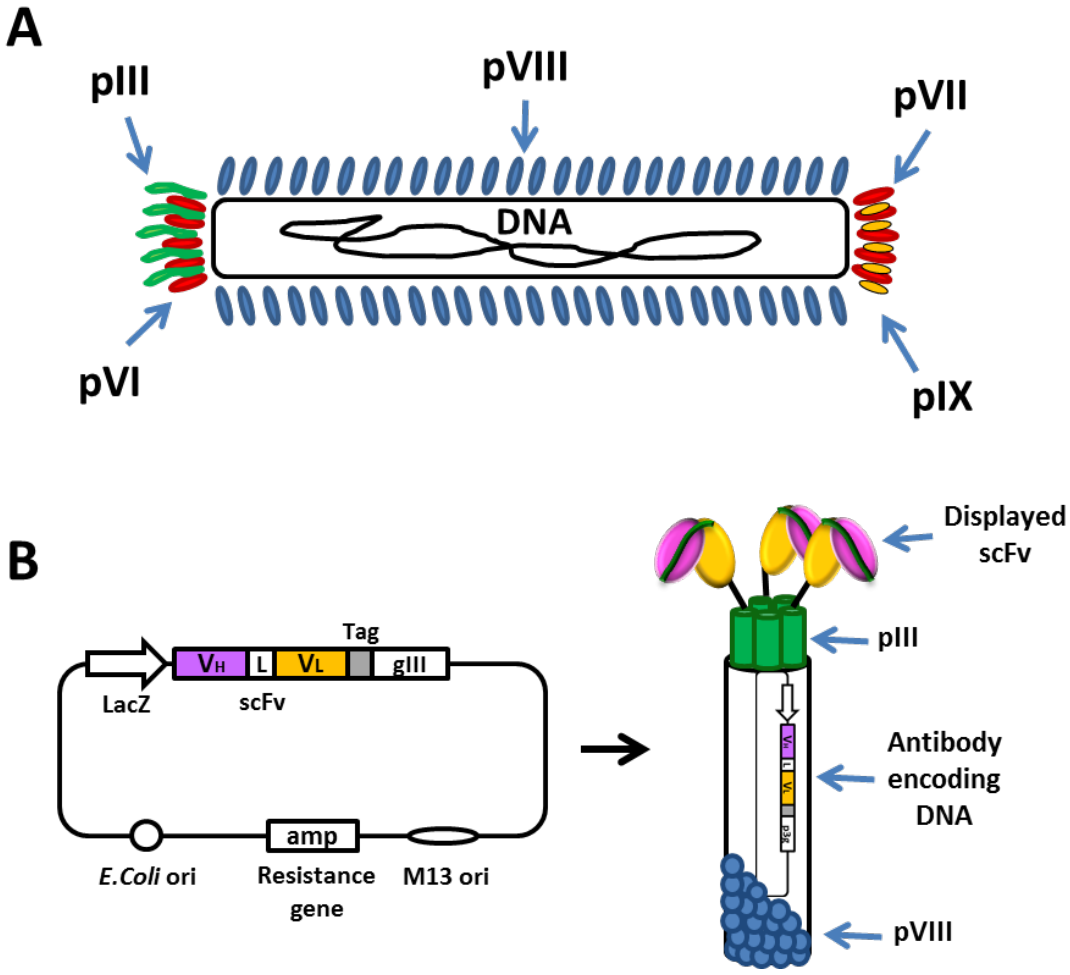

Figure 1.7 Phage display

Schematic structure of filamentous bacteriophage composed of a circular single strand DNA genome and 2700 copies of pVIII protein coating the phage particle. Minor proteins include pIII, pVI, pVII and pIX, each present in 5 copies (A). Structure of the phagemid vector carrying the LacZ inducible promoter to express the scFv fused to the gIII gene. scFv is then exposed on the phage surface anchored to the pIII coat protein (B).

1.4.2 scFv A7 antibody fragment

Antibody phage display technology represents a unique opportunity for rapid selection of high affinity antibody clones. This technique was therefore adopted in our group for the identification of specific scFv antibody fragments interacting with the microvasculature of human arthritic synovium, isolating among others the scFv clone A7 which represents the main focus of the work presented in this thesis (230).

As mentioned above, screening antigens *in vitro* or using cell lines may impair the chances to identify a scFv antibody with applications *in vivo*. Animal models are able to mimic the human pathology but are characterised by the expression of murine antigens that may not find counterpart in humans or with only low sequence homology and may therefore not be directly applicable to humans. In order to obviate this limitation, screening in humans would be the ideal solution. Ethical considerations, however, prohibit the use of humans in research unless in strictly regulated circumstances. The work carried out in our group provided an elegant solution to these boundaries, pioneering a chimeric mouse model using SCID mice grafted with human tissues (231, 232). In this human/mouse chimeric model the grafts are sustained by the murine vasculature via functional anastomoses with the resident human vessels (232). Furthermore, intragraft injection of TNF-α in synovium grafted SCID mice was able to upregulate ICAM-1 and VCAM-1 expression, causing intravenously injected human lymphocytes to migrate in the tissue (232). Additionally, in a PLN grafted SCID mouse model, stimulation with CXCL12 promoted human lymphocytes migration in the grafted tissue (231). These results confirm the validity of the model in which the grafted tissue is sustained by the murine host while maintaining the human vasculature environment and supporting the natural tissue specific response. This model has been previously adopted for the isolation of synovium specific antigens via phage display (132), providing proof of concept for the validity of this investigation.

The synthetic Tomlinson scFv library, developed in Greg Winter's group, was chosen for the presented screening (233). This library is based on the common V_H3

(1-3) and V_k (2-1-1) framework, with diversified CDR3 and CDR2 regions. SCID mice double grafted with human arthritic synovium and normal human skin as control, were injected with the unchallenged library via the tail vein and allowed to recirculate for 15 minutes in order to distribute across the mouse vasculature and the grafted tissues. Synovial grafts were then harvested and bound phage eluted to be used for a second round of selection. A total of 4 enrichment cycles were used for the screening (Figure 1.8 A). Randomly picked colonies from *E.coli* infected with phage clones from the last round of selection were screened for efficient scFv production. 24 clones showed high protein expression and were subsequently shown to encode for the same scFv sequence (scFv clone A7). The soluble scFv A7 was isolated in two independent screenings and was shown to retain synovium specificity *in vivo.* Xenograft SCID mice were injected with the scFv A7, scFv anti-hen egg lysozyme (scFv HEL) as negative control and anti-vWF/CD31 antibodies to stain the vasculature. The scFv A7 was able to target the synovial microvasculature with no cross-reactivity with the human skin tissue or mouse tongue tissue (Figure 1.8 B). Additionally, radiolabeled scFv A7 showed statistically significant differential reactivity between synovium and skin grafts up to 24h post-injection *in vivo* (Figure 1.8 C), further confirming the synovium-specific reactivity of the scFv A7 antibody (230) (Paper attached).

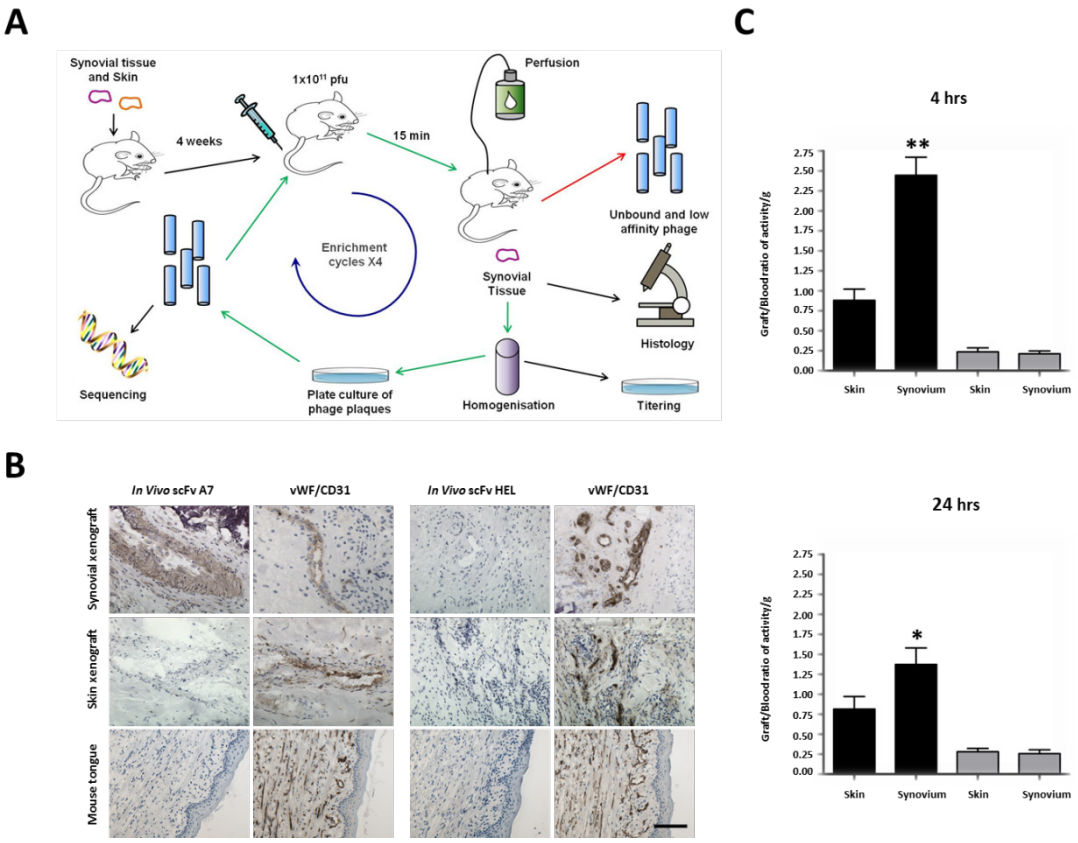

Figure 1.8 *in vivo* antibody phage display

A phage library was injected in double grafted SCID mice with human arthritic synovium and normal human skin. After 15 minutes of recirculation, synovium was harvested and phage eluted to use in a second round for a total of 4 enrichment cycles (A). *In vivo* recirculation of soluble scFv A7 describing specific reactivity with microvasculature of arthritic synovium as shown in HRP immunohistochemistry. No reactivity shown in skin sample of mouse tongue (B). *In vivo* retention of ^{125}I labelled scFv A7 showing significant accumulation in human synovium compared to skin graft up to 24h post injection (C). (figure B and C taken from Kamperidis, Kamalati *et al*, 2011)(230).

1.5 Rationale and aims of the project

Despite the obvious success of the biologic agents used in the treatment of rheumatoid arthritis, many patients fail to respond to the available therapies and although true remission is achieved only by a minority, a “cure”, that is treatment free remission still remains an unmet goal for most. The specific mechanism of action of the currently available biologic therapies in RA involves a systemic targeting of cytokines or immune effector cells, increasing the risk of developing or re-emergence of bacterial and viral infections. There is therefore room for the development of tissue specific agents able to circumvent or reduce systemic side effects, increase the potency and possibly decrease the cost inherent to disease management in patients.

Several lines of evidence suggest that neoangiogenesis plays a crucial role in the development and progression of rheumatoid arthritis, furthermore the presence of molecular heterogeneity in the microvascular environment of different tissues and/or disease conditions has been correlated with the capacity to target and direct circulating leucocytes subpopulation, contributing to local enrichment and selecting for specific response. The synovial microvasculature, with the presence of post-capillary vessels reminiscent of lymphoid HEV morphology, represents therefore a unique opportunity to identify synovium specific vascular addressins that may be used as tools for tissue specific drug delivery and disease tissue imaging.

However, to date the identification of such specific microvascular addressin in the joint still remains elusive. Our group has pioneered the development of a chimeric SCID mouse model able to sustain long-term survival of human tissue xenografts, maintaining the natural human environment and overcoming the problem of *in vitro* culturing dedifferentiation of the microvascular endothelium and loss of antigen expression. Combining this platform with the *in vivo* phage display technology, our group has successfully isolated several peptides showing preferential homing specificity for the arthritic human synovium. Additionally, the same strategy has been used to isolate scFv antibody fragments showing specificity

for the human arthritic synovium compared to the control normal human skin tissue. In particular, a scFv clone named A7 has shown a great homing specificity for the human arthritic synovium and represents the main focus of this thesis.

On the basis of the evidence reported above, the main aim of my project was to develop a reagent with selective synovial specificity to be used as a therapeutic tool for tissue specific drug delivery in the treatment of arthritic disease conditions. Specifically, the hypothesis that scFv A7 binds to a unique synovial microvascular antigen, or one preferentially expressed at high levels in this tissue, able to efficiently discriminate between disease and normal state will be tested in this thesis. This hypothesis will be addressed in detail in chapters 4 and 5. In addition, experiments in this thesis are designed to test the hypothesis that the scFv A7 antibody can be developed as a building block for the generation of bispecific antibodies for tissue specific drug delivery in the context of arthritis, to circumvent the adverse biological effects caused by systemic administration of the current biological therapies. This hypothesis will be specifically addressed in chapter 6.

Results organisation and experimental design of the work are summarised below.

- **Chapter 3** is focused on the optimisation of scFv A7 and the IgG-like A7 scFv-Fc fusion protein production, comparing purification systems, assessing the purity and quality of the obtained antibody and optimising the immunohistochemistry protocol necessary for the work presented in Chapter 4.

- **Chapter 4** describes the scFv A7 *in vitro* reactivity in human tissues, aiming at characterising the tissue, disease and species specificity of the antibody and defining the localisation of A7 binding capacity.

- **Chapter 5** is centred on the identification of A7 target antigen, involving identification of cell lines expressing the antigen, proteomic approaches

towards the isolation of the putative target protein and phage library screening.

- **Chapter 6** represents the translational application of the project with the development of a novel bispecific antibody combining the A7 synovial homing capacity to the anti-TNF properties of the Adalimumab antibody. In this chapter the strategy adopted for the bispecific antibody design is reported along with A7 quality assessment and characterisation and Adalimumab tissue reactivity and biological functions.

- In **Chapter 7** the significance of the findings will be analysed and discussed, including the implications and future work arising from this investigation.

Chapter 2
Materials and Methods

2.1 scFv production and purification

A single colony of *E.coli* strain HB2151 expressing the scFv clone of interest (vector map can be found in Figure 3.1) was picked from a 2TY agar plate and inoculated in 20 ml 2TY, 1% glucose, 100 µg/ml ampicillin and left at 37 ^{o}C overnight shaking at 200 rpm. On day 2, 2 ml of overnight subculture was diluted in 40 ml 2TY 0.1% glucose, 100 µg/ml ampicillin and grown at 37 ^{o}C 200 rpm shaking until an optical density (OD) of 0.8 was reached. The bacteria were then incubated with 1 mM IPTG to induce antibody expression and incubated overnight at 30 ^{o}C 200 rpm shaking. Following overnight induction of expression of scFv A7 from *E.coli* strain HB2151, the bacteria were pelleted by centrifugation at 5000 rpm for 30 minutes at 4 ^{o}C. The media containing secreted antibody was store at 4 ^{o}C as supernatant. The bacterial pellet was resuspended in 6.4 ml ice-cold TES buffer and added 13.6 ml dH2O (ice cold), mixed by inversion and incubated on ice for 30 minutes to release proteins from the periplasmic compartment. The bacterial cells were then spun to a pellet at 13000 rpm for 20 minutes at 4 ^{o}C and the supernatant containing scFv protein removed and stored at 4 ^{o}C as periplasmic extract. In order to remove bacterial particles from the protein extracts, supernatant and periplasmic extract were filtered separately, using a 0.22 µm filter unit. To remove salt contained in the medium, the filtered supernatant and periplasmic extract were dialysed using dialysis tubing with molecular weight cut off of 10000 Da against 10 litres of PBS for 2 hours at room temperature with stirring. To increase the efficiency of dialysis, the buffer was changed every 2 hours and finally left to dialyse at 4 ^{o}C overnight.

2.1.1 Purification of scFv by affinity chromatography

2.1.1.1 Protein A Sepharose

Following supernatant and periplasmic extract dialysis, the samples were retrieved from the tubing and placed in a sterile bottle and allowed to bind with 200 mg of rehydrated protein A Sepharose CL-48 beads (GE Healthcare, Amersham UK) for 30 minutes at room temperature with gentle mixing. The beads were then

loaded into Econo Column Chromatography columns and packed by gravity flow. The packed column was washed with 50 ml PBS, then with 50 ml PBS + 0.5 M NaCl and finally with 100 ml 0.2 M Glycine pH6. To elute the bound antibody protein, 20 ml of 0.2 M glycine pH 2.8 was added to the column and fractions to the volume of 1 ml collected. Low pH was neutralised with Tris 1 M pH 9 using 200 µl for 1 ml fractions. The protein concentration in each fraction was assessed by OD analysis via spectrophotometry at 280 nm. Protein fractions with similar OD were pooled and dialysed overnight at 4 °C against PBS for buffer exchange using 10000 Da Slyde-A-Lyser dialysis cassettes (Thermo Fisher scientific, Loughborough UK). Proteins were then aliquoted and stored at -80 ^{o}C.

Purification of periplasmic extract and supernatant from empty HB2151 host cells was processed as above. Since no detectable protein was present in the elution fraction, a concentration step was introduced. Fractions were incubated with 20 µl Strataclean resin (Agilent Technologies, Berkshire UK) to non-selectively bind proteins, and lysed in Laemmli lysis buffer (0.5 M DTT, 10% glycerol, 0.44 M Tris pH 6.8, 0.04% Bromophenol Blue, 10% SDS) for further analysis.

2.1.1.2 Talon® metal affinity resin

Periplasmic protein extract and bacterial supernatants were prepared as above. The samples were then retrieved from the tubing, placed in a sterile bottle and allowed to bind to 8 ml of pre equilibrated Talon® metal affinity resin (Clontec, Mountain View, CA USA) for 30 minutes at room temperature with gentle mixing. The resin was then packed by gravity flow into Econo Column Chromatography columns. Subsequently two serial washes with 20 bed volumes of dialysis buffer (50 mM NaH_2PO_4, 300 mM NaCl, pH 7) were performed. The antibody protein was eluted with 150 mM imidazole pH 7, collected in 1 ml fractions and the protein concentration assessed by spectrophotometry at 280 nm. Protein fractions with similar OD were pooled and dialysed overnight at 4 °C in PBS for buffer exchange using 10000 Da Slyde-A-Lyser dialysis cassettes (Thermo Fisher scientific, Loughborough UK). Proteins were then aliquoted and stored at -80 ^{o}C.

Purification of periplasmic extract and supernatant from empty HB2151 host cells was processed as above. Since no detectable protein was present in the elution fraction, a concentration step was introduced. Fractions were incubated with 20 µl Strataclean resin (Agilent Technologies, Berkshire UK) to non-selectively bind proteins, and lysed in Laemmli lysis buffer (0.5 M DTT, 10% glycerol, 0.44 M Tris pH 6.8, 0.04% Bromophenol Blue, 10% SDS) for further analysis.

2.1.2 FPLC

2 ml of concentrated Talon® purified protein was loaded on a Superdex 75 10x300 mm Sepharose column with a size exclusion limit of 200 kDa and a resolution power between 3 kDa and 70 kDa. 1 ml fractions were collected at a flow rate of 0.5 ml/min in PBS and the protein concentration assessed by OD 280 nm measurements. The relative molecular masses of fragments present in the sample were compared to standard proteins used to calibrate the machine. Specifically, thyroglobulin (MW 670 kDa), bovine-globulin (MW 158 kDa), chicken ovalbumin (MW 44 kDa) equine myoglobin (MW 17 kDa) and vitamin B12 (MW 1.35 kDa). Protein fractions were aliquoted and stored at -80 ^{o}C.

2.1.3 HPLC

100 µg of Talon® purified protein in 100 µl final volume was loaded on Phenomenex silica-based size exclusion column BIOSEP-SEC-S-2000 300x7.8 mm, in an automated chromatograph, using a 0.5 ml/minute flow rate. The relative molecular masses of fragments present in the sample were compared to standard proteins used to calibrate the machine. Specifically, thyroglobulin (MW 670 kDa), bovine-globulin (MW 158 kDa), chicken ovalbumin (MW 44 kDa) equine myoglobin (MW 17 kDa) and vitamin B12 (MW 1.35 kDa). scFv antibody monomer generally eluted between 18 and 19 minutes.

2.2 scFv-Fc production and purification

2.2.1 pHygro scFv-Fc vector cloning

A modified version of pCDNA3.1/Hygro(+) from Invitrogen, carrying a XbaI restriction site instead of NheI and HindIII in the place of PmeI, was provided by Professor D. Sblattero, University of Eastern Piedmont, Novara, Italy, and was used as base vector (referred as pHygro vector). This vector also contained the human IgG1 CH2 and CH3 domains gene amplified from lymphocyte cDNA and the SV5 tag at the 3' end (234). scFv A7 VH and VL sequences were obtained from the clone isolated by phage display. Codon usage was optimised for CHO expression and synthesised using GeneArt gene synthesis service (Life Technologies, Paisley UK). The original V_H-L-V_L structure was maintained unaltered (vector map for pHygro A7 scFv-Fc can be found in Figure 3.11). Adalimumab sequence for V_H and V_L domains was obtained from the original patent (165). V regions in V_H-V_L orientation were linked using the scFv A7 15 amino acids linker and codon optimised for CHO expression using GeneArt gene synthesis service (Life Technologies, Paisley UK). NheI and BssHII restriction sites were included at the 3' and 5' respectively of both sequences, to facilitate insertion in pHygro vector (vector map for pHygro Adalimumab scFv-Fc can be found in Figure 6.1).

1 µg of scFv A7 or scFv Adalimumab optimised insert and pHygro vector were digested using NheI restriction endonuclease (New England BioLabs, Herts UK) at 37 °C for 1 h in NEB buffer 2, followed by incubation with BssHII restriction enzyme (New England BioLabs, Herts UK) at 50 °C in NEB buffer 2 for 1 h. Reaction was then resolved in 0.8% agarose gel and purified following gel extraction of the relevant bands using PCR clean-up Gel extraction kit (Macherey-nagel, Düren Germany) following manufacturer recommendations. Briefly, bands were excised from the gel and dissolved in buffer NT at 50 °C. Sample was then loaded in Nucleospin columns, washed in buffer NT3 and eluted in buffer NE. Digested insert and vector were ligated to reconstitute the expression plasmid using T4 DNA ligase (New England BioLabs, Herts UK). A 3:1 molar ratio between insert and vector was used and incubated at 16 °C overnight. The ligase reaction was transformed in

competent DH5α *E. coli* bacteria, leaving the reaction for 15 minutes in ice to allow optimal plasmid distribution, incubating 30 seconds at 42 °C and finally 2 minutes in ice. Bacteria were left recovering in 2TY culture medium with 1% glucose at 37 °C at 200 rpm for 1 h. Finally, bacteria were plated in 2TY agar plates containing 100 µg/ml ampicillin and left overnight at 37 °C. Grown colonies represented efficiently transformed cells. Single colonies were screened for presence of the correct plasmid via polymerase chain reaction (PCR) using pHygro SEQ sense (5'-CTGCTTACTGGCTTATCG-3') and pHygro SEQ antisense (5'-CAGATGGCTGGCAACTAG-3') and sequenced to confirm protein identity.

2.2.2 Transfection in cell line

2.2.2.1 CHO-S transfection

Vector showing correct nucleotide sequence was used to transfect CHO-S cell line. Cells were grown in serum free medium OptiPRO SFM (Life Technologies, Paisley UK) without selective agents and transfected using FreeStyleTM Max Reagent (Life Technologies, Paisley UK) according to manufacturer's conditions. 37.5 µg of plasmid DNA were mixed with 37.5 µl of FreeStyle Max Reagent in a final volume of 1.2 ml OptiPRO SFM and incubated 15 minutes at room temperature to allow DNA-lipid complex to form. The DNA-lipid complex was slowly added to CHO-S cells at a density of $1x10^6$ cells/ml in 30 ml of medium in T175 flasks and incubated at 37°C in humid environment with 5% CO_2. In order to select for efficiently transfected cells, cells were re-suspended in serum free ProCHO 5 medium (Lonza, Slough UK) supplemented with 100 U/ml penicillin, 100 µg/ml streptomycin and the selective agent hygromycin B at 200 µg/ml and cultured at 37 °C in humid environment with 5% CO_2. The selective agent will allow survival only of the cells expressing the hygomycin resistance gene present in the pHygro vector.

In order to achieve a monoclonal cell population, transfected cells were diluted to limiting dilution obtaining single cell suspension in selective medium. Cells were grown in 96 well plates in 100 µl of medium and cell growth rate was monitored via cell count. Protein production was assessed via Enzyme-Linked Immunosorbent Assay (ELISA), coating with cell culture supernatant and probing for

the SV5 tag. Cell clones showing highest growth rate and protein production were selected for antibody expression.

2.2.2.2 HEK-293T transfection

Vector showing correct nucleotide sequence was used to transfect HEK-293T cell line. Cells were grown in Dulbecco's modified Eagle medium (DMEM) (Life Technologies, Paisley UK) supplemented with 10% foetal calf serum (FCS), 100 U/ml penicillin and 100 µg/ml streptomycin. Cells at 60-70% confluence were transfected with JetPRIME reagent (Polyplus, Illkirch France) according to the manufacturer's protocol. $6x10^6$ cells were grown in 20 ml of complete medium in 15 cm petri dishes, with overnight incubation at 37 °C in humid environment with 5% CO_2. 20 µg of plasmid DNA were mixed with 40 µl JetPRIME reagent in 1 ml JetPRIME buffer and incubated at room temperature (RT) for 10 minutes before adding the mixture to the cells. After 4 h incubation the medium was replaced with serum free DMEM supplemented with 100 U/ml penicillin, 100 µg/ml streptomycin and Nutridoma-SP (Roche, Indianapolis USA) and incubated for 48 h to allow protein production. Media containing the antibody was then collected and cells incubated with fresh media for 48 h for a second harvest.

2.2.3 scFv-Fc protein purification

2.2.3.1 Protein A Sepharose

Supernatant from transfected cells was filtered using 0.22 µm filter units to remove remaining cells and cell components. The suspension was then dialysed overnight at 4 °C against 2 L of PBS using dialysis tubing with 10000 Da molecular weight cut-off (MWCO) to remove contaminant low molecular weight proteins and remove detergent present in the CHO-S medium. Dialysed supernatant was incubated with protein A Sepharose CL-4B (GE Healthcare, Amersham UK) for 2 hours at 4 °C with gentle rotation. Beads were then loaded in Econo Column Chromatography columns and packed by gravity flow. Columns were washed twice with 20 bed volumes of PBS or dialysis buffer, eluted with IgG Elution Buffer (Thermo Fisher Scientific, Loughborough UK) and buffered with 1 M Tris pH 9 using

50 µl for 400 µl fraction, to obtain a final solution at pH 7. The protein concentration in each fraction was assessed by OD analysis via spectrophotometry at 280 nm. Protein fractions with similar OD were pooled and dialysed overnight at 4 °C in PBS for buffer exchange using 10000 Da Slyde-A-Lyser dialysis cassettes (Thermo Fisher Scientific, Loughborough UK). Proteins were then aliquoted and stored at -80 ^{o}C.

2.2.3.2 Supernatant concentration

Supernatant from transfected cells was filtered using 0.22 µm filter units to remove remaining cells and cell components. The suspension was then dialysed overnight at 4 °C against 2 L of PBS using dialysis tubings with 10000 Da MWCO to remove contaminant low molecular weight proteins and remove detergent present in the CHO-S medium. Antibody content was assessed via ELISA assay coating with cell culture supernatant and probing with anti-Human Fc HRP conjugated antibody (Jackson ImmunoResearch, Pennsylvania USA). Concentration was determined via comparison with standard curve of human IgG1 antibody. Dialysed supernatant was concentrated using Millipore Centricon system 10000 Da MWCO (Millipore, Massachusetts USA). Centricon filter units were spun at 4000 g to remove excess medium and low molecular weight protein. Suspension volume was reduced in order to achieve a 1 mg/ml antibody concentration. Concentrated supernatant was dialysed again overnight at 4 °C against 2 L of PBS using dialysis tubings with 10000 Da MWCO for buffer exchange.

2.3 Bispecific antibody production

The pHygro plasmid described in section 2.2.1 was used as a base expression vector. CH2 and CH3 domains were amplified from the pHygro CD59-CD20 bispecific plasmid (kindly provided by Professor D. Sblattero, University of Eastern Piedmont, Novara Italy) in two steps (for schematic refer to Figure 6.8 and 6.9).

To generate the pHygro 407 human vector (pHygro 407 opt), the starting Fc region was amplified using the forward primer NheI 407 senso (5'-AGCTGCTAGCGACAAGACCCACACCTGT-3') and reverse primer AgeI-HindIII 407 anti

(5’- ACGTAAGCTTTCACACCGGTGCCCTCTTGGCTCT-3’). The 769 bp amplified fragment consisted in the CH2-CH3 domain (with Y407T mutation) containing the NheI restriction site at 5’ end, the SV5 tag and the first fraction of the 2A peptide and the AgeI and HindIII at the 3’ end. In addition, the sequence contained the stop codon TGA before the HindIII restriction site. The amplified region was then cloned inside a pHygro vector containing the Adalimumab scFv sequence, using NheI and HindIII restriction sites.

Similarly, the pHygro 366 human vector was obtained amplifying the starting vector with primer forward NheI 366 sense (5’-AGCTGCTAGCGATAAGACACATACCTGC-3’) and primer reverse pHygro SEQ antisense (5’-CAGATGGCTGGCAACTAG-3’). The 751 bp fragment amplified consisted in the CH2-CH3 domain (with the T366Y mutation) containing the NheI site at 5’, the 6-His tag and the HindIII site at 3’. The amplified region was then cloned inside a pHygro vector containing the A7 scFv or E2 scFv sequence, using NheI and HindIII restriction sites. A sequential PCR was used to introduce the second portion of the 2A peptide. First the primer forward XbaI-AgeI 366 1 senso (5’-TGCTGAAGCTGGCCGGCGACGTGGAATCCAACCCTGGCCCTATGGGCTGGAGCCTGATC-3’) and the primer reverse CH2 Human anti (5’-CGGTCCCCCCAGGAGTTCAGGTGC-3’) were used to introduce the first part before the leader sequence and then the primer forward XbaI-AgeI 366 2 senso (5’-AGCTTCTAGAGCACCGGTGAAGCAGACCCTGAACTTCGACCTGCTGAAGCTGGCCGGCG-3’) and primer reverse CH2 Human anti (5’-CGGTCCCCCCAGGAGTTCAGGTGC-3’) were used to complete the second part of the 2A peptide. The newly amplified XbaI-AgeI-2A-scFv sequence was cloned in the pHygro vector before the CH2-CH3 (T366Y)-HIS region to complete the pHygro 366 human vector (pHygro 366 opt).

Finally, the bispecific antibody vector was obtained by cloning the XbaI-AgeI region from pHygro 407 opt into the pHygro 366 opt in order to introduce the first scFv-Fc molecule and reconstitute the full 2A peptide linking the second scFv-Fc sequence. The bispecific vector obtained is referred as pDuo-opt.

Protein production from CHO was carried out as described in Section 2.2.2.1 and protein purified using Talon® metal affinity chromatography as described in Section 2.1.1.2 using CHO supernatant and 2 ml of Talon® resin.

2.3.1 Bispecific scFv-Fc truncated for heterodimerisation assessment

Truncated bispecific antibody showing single Adalimumab scFv domain was obtained from A7/Adalimumab pDuo-opt vector following PCR removal of A7 scFv region. The A7 scFv-Fc region was first amplified using primer forward pHygro AgeI sense (5'-TTAGATACCGGTGAAGCAGACCCTG-3') and primer reverse pHygro SEQ antisense (5'-CAGATGGCTGGCAACTAG-3'). The PCR product was the purified using the PCR clean-up Gel extraction kit (Macherey-nagel, Düren Germany) and used for a second round of amplification. The PCR template was used to amplify the 2A-leader-intron region using the forward primer pHygro AgeI sense and the reverse primer pHygro BssHII mini-intron antisense (5'-GGCATGCGCGCCACCTGT-3'). At the same time hinge-CH2-CH3-6His region was amplified using forward primer pHygro BSSHII mini-intron/Hinge overlapping sense (5'-ACAGGTGGCGCGCATGCCGATAAGACACATACCTGCCCC-3'), characterised by a complementary region to the pHygro BssHII mini-intron antisense at 5', and the reverse primer pHygro SEQ sense. The resulting PCR products were then used for an overlapping PCR exploiting the complementary portions at 3' for PCR 1 and at 5' for PCR 2, using the forward primer pHygro AgeI sense and reverse primer pHygro SEQ sense. The resulting PCR product consisted in the 2A-Leader-Hinge-CH2-CH3-6His region that was cloned in the pHygro 407 opt using the AgeI and HindIII restriction sites (for vector map refer to Figure 6.13).

The truncated bispecific antibody was produced by transiently transfected HEK-293T cells (as described in Section 2.2.2.2) and purified from supernatant using protein A (as described in Section 2.2.3.1) followed by Talon® metal affinity chromatography (as described in Section 2.1.1.2 using 2 ml of resin).

2.4 Antibody biotinylation

Biotinylated scFv or scFv-Fc proteins were generated using the Pierce EZ-link® Sulfo-NHS-SS-Biotinylation kit (Thermo Fisher scientific, Loughborough UK). Protein at the desired concentration was diluted in 0.5-2 ml PBS. Immediately before use, a 10 mM Sulfo-NHS-SS-Biotin dilution was prepared in filtered ultrapure water. The protein was mixed with a 10 fold molar excess of biotin reagent and the reaction incubated for 1 hour at 4 °C. Unincorporated free biotin in the reaction mixture is removed by a desalting column or by dialysis using a MWCO 10 kDa cassette. Desalting columns were pre-equilibrated via 3 washes in PBS intercalated by 2 minutes 1000 g centrifugation. Sample was applied directly to the resin bed and recovered via centrifugation at 1000 g for 2 minutes. Dialysis cassettes were pre-equilibrated in dialysis buffer (50 mM NaH_2PO_4, 300 mM NaCl, pH 7) or PBS for 2 minutes and sample loaded in the inner chamber. Sample was recovered following 2 hours dialysis against 2 L of dialysis buffer or PBS. Biotin incorporation was estimated using HABA (4'-hydroxyazobenzene-2-carboxylic acid) assay, following manufacturer specifications. Briefly, HABA/avidin complex is dissociated by biotin causing a proportional decrease in 500 nm absorbance, allowing quantitation of protein conjugated biotin. 100 µl of solution containing the biotinylated scFv was added to 900 µl HABA/Avidin solution and change in OD measured at 500 nm. Biotin/protein ratio was calculated using the HABA calculator (www.piercenet.com/haba/habacalccuv.cfm).

2.5 SDS-PAGE

Polyacrylamide gel electrophoresis was performed on Novex Tris-Glycin precast polyacrylamide-based gel at 10% or in gradient 8-16% (Life Technologies, Paisley UK). The gels were characterised by a stacking (4%) and resolving (10% or 8-16%) acrylamide concentration and comprised Tris, HCl, acrylamide, bisacrylamide, Ammonium persulfate (APS) and ultrapure water. Occasionally, homemade gels were employed. In this case, resolving gel at 10% was made with 250 mM Tris pH 8.8, 10% Protogel (National Diagnostics, Hessle UK), 0.05% APS and 0.2% N,N,N´,N´-

tetramethylethylenediamine (TEMED) in ultrapure water. Stacking gel was made with 250mM Tris pH 6.8, 4% Protogel, 0.05% APS and 0.2% TEMED.

For reduced conditions, samples were diluted at the desired concentration in 5x Laemmli lysis buffer (0.5 M DTT, 10% glycerol, 0.44 M Tris pH 6.8, 0.04% Bromophenol Blue, 10% SDS), to achieve a 1x solution, and boiled at 95 °C for 5 minutes on heating block to obtain complete denaturation and reduction of the proteins. For non-reduced conditions, samples were diluted at the desired concentration in non-reducing LDS Sample Buffer (Thermo Fisher scientific, Loughborough UK) without boiling.

Samples were then loaded onto SDS-PAGE gels and run immersed in running buffer (25 mM Tris, 192 mM glycine 0.1% SDS) at a constant rate of 50 mA. A standard molecular weight ladder was included in each run. The gel was then washed in dH_2O for 10 minutes to remove excess SDS and soaked in Coomassie Brilliant Blue (Coomassie Blue R250 0.25%, methanol 42%, acetic acid 16% and dH_2O 42%) for 2 h at RT or overnight at RT with gentle rocking. Excess of dye was removed via multiple washings in de-stain solution (isopropanol 12.5%, glacial acetic acid 10% dH_2O 77.5%) until optimal staining was achieved. Alternatively, the gel was soaked in colloidal Coomassie Blue EZ-Blue reagent (Sigma, Dorset UK) for 1 h at RT with gentle rocking and de-stained in dH_2O until optimal staining was reached. Stained gels were then washed in dH_2O and soaked in gel drying solution (20% ethanol, 4% glycerol in water) for 15 minutes or 5 minutes for colloidal stain. The gel was subsequently included in two cellophane sheets and left to air dry. Once dry the gel could be stored at RT.

Alternatively, the gel was soaked twice in 100 ml of fix solution (50% methanol, 7% acetic acid) for 30 minutes, and then stained with 60 ml of SYPRO® Ruby protein gel stain (Life Technologies, Paisley UK) overnight with gentle rocking in a dark chamber. Gel was then washed in 100 ml of wash solution (10% Methanol, 7% Acetic acid) for 30 minutes at RT followed by wash in dH_2O in dark chamber. Presence of protein bands was then assessed when exited under UV light in a standard bench top transilluminator (UV 300 nm). Occasionally the ruby stained gel

was post-stained with Coomassie Brilliant Blue as described above. Molecular weight markers were always present in Commassie Brilliant Blue and Sypro® ruby protein gel stained gels but cropped from the figures presented in this thesis.

2.5.1 Analysis of SDS-PAGE gels

Gels stained with Ruby protein gel stain were exited with UV light (300 nm) and scan of the gel acquired using UVItec gel station (Uvitec, Cambridge UK). Jpeg pictures of exited gels were analysed with the image analysis tool ImageJ 1.44 (NIH, Maryland USA) (235). First, the gel pictures were colour inverted and specific lanes to be analysed were highlighted and the plot profile created using the gel analysis plugin. Relative proportion of peaks was measured by the program with Label peaks function.

2.5.2 Western Blot

Subsequent to protein separation, the gel was soaked in tris-glycine transfer buffer (25 mM Tris, 192 mM glycine and 20% methanol) for 10 minutes at room temperature. Protein transfer was performed at 400 mA for 1 hour at room temperature (236) using a nitrocellulose membrane (GE Healthcare, Amersham UK). For detection of proteins of interest the blotted nitrocellulose membrane was blocked with 5% dried milk powder (Marvell, Dublin Ireland) in PBS at 4 ^{o}C overnight with constant shaking. The membrane was then washed 3 times with PBS for 5 minutes and incubated with the appropriate primary antibody for 1 h at room temperature with shaking. The membrane was subsequently washed 3 times for 10 minutes in PBS 0.05% Tween 20 and incubated with a secondary antibody HRP conjugated for 1 h at room temperature with shaking. The membrane was then further washed 3 times for 10 minutes in PBS 0.05% Tween, followed by 5 minutes in dH_2O. To detect the Horse Radish Peroxidase (HRP) activity, the membrane was incubated with ECL reagent (GE Healthcare, Amersham UK) for 1 minute at room temperature and developed by exposure on X-ray film (GE Healthcare, Amersham UK).

For scFv detection:

Primary antibody mouse anti-HIS (clone HIS-1, Sigma, Dorset UK) diluted 1:3000 in PBS 0.5% BSA or mouse anti-cMyc (clone 9E10 Sigma, Dorset UK) diluted 1:3000 in PBS 0.5% BSA.

Secondary antibody goat anti-mouse HRP (SantaCruz, California USA) diluted 1:2000 in PBS 0.5% BSA.

For scFv-Fc detection:

Primary antibody mouse anti-SV5 (kindly provided by Professor D.Sblattero University of Eastern Piedmont, Novara Italy) diluted 1:5000 in PBS 0.5% BSA.

Secondary antibody goat anti-mouse HRP (SantaCruz, California USA) diluted 1:2000 in PBS 0.5% BSA or anti-mouse AP conjugated antibody.

For bispecific scFv-Fc:

Primary antibody mouse anti-SV5 (kindly provided by Professor D.Sblattero University of Eastern Piedmont, Novara Italy) diluted 1:5000 in PBS 0.5% BSA, or mouse anti-HIS (clone HIS-1, Sigma, Dorset UK) diluted 1:3000 in PBS 0.5% BSA.

Secondary antibody goat anti-mouse HRP (SantaCruz, California USA) diluted 1:2000 in PBS 0.5% BSA or anti-mouse AP conjugated antibody.

For E-cadherin detection:

Primary antibody mouse anti-E-cadherin (clone 36/E-Cadherin, Becton Dickinson, Oxford, UK) 1µg/ml in PBS 0.5% BSA.

Secondary antibody goat anti-mouse HRP (SantaCruz, California USA) diluted 1:2000 in PBS 0.5% BSA or anti-mouse AP conjugated antibody.

For α-tubulin detection:

Primary antibody mouse anti-α-tubulin (clone 236-10501, Life technologies, Paisley UK) at 1µg/ml in PBS 0.5% BSA.

Secondary antibody goat anti-mouse HRP (SantaCruz, California USA) diluted 1:2000 in PBS 0.5% BSA or anti-mouse AP conjugated antibody.

For ICAM1 detection:

Primary antibody rabbit anti-ICAM1 (clone EP1442Y, Abcam, Cambridge UK) at 1:2000 dilution in PBS 0.5% BSA.

Secondary antibody goat anti-rabbit IgG H+L (Jackson ImmunoResearch, Pennsylvania USA) at 1µg/ml in PBS 0.5% BSA.

2.6 Staining on tissue sections

Synovial tissues were obtained from patients with RA and OA that attended the Royal London Hospital/Barts & The London NHS Trust, Mile End Hospital/Barts NHS Trust and St Bartholomews Hospital/Barts & The London NHS Trust after informed consent, either by ultrasound-guided joint biopsy, total joint replacement or following synovectomy (NRes No 07/Q0605/29).

Non-arthritic synovial tissues were kindly provided by M.D. Smith (Repatriation General Hospital, Adelaide Australia).

Skin tissues were obtained from healthy individuals or RA/OA patients that attended the Guys & St Thomas Hospital, NHS Foundation Trust after informed consent (NRes No 07/Q0605/29).

Tonsil tissues were obtained from patients undergoing tonsillectomy at the St Bartholomews Hospital/Barts & The London NHS Trust after informed consent (NRes No 07/Q0605/29).

AccuMax normal tissue array was purchased from Isu Abxis (Isu Abxis, Seoul Korea).

Crohn's disease, ulcerative colitis and colon cancer tissues were kindly provided by Dr P. Biancheri (Queen Mary University of London, London UK).

Malignant melanoma tissue sections were kindly provided by Professor R. Cerio (Queen Mary University of London, London UK).

2.6.1 Preparation of formalin fixed paraffin embedded tissues

Tissue samples were fixed with 4% paraformaldehyde (PFA) in PBS for 1 hour with rocking at room temperature. The fixed samples were then processed in a LEICA TP1050 tissue processor overnight before being embedded in wax and stored at room temperature until use. The samples were cut at 3 µm thickness using a microtome and mounted on Superfrost-Plus glass slides (VWR, Leicestershire UK), dried for 2 hours at room temperature and baked at 55-60 ^{o}C for 2 hours. Slides were then stored at RT until needed.

2.6.2 Preparation of frozen tissue samples

Tissue samples were snap frozen in liquid nitrogen cold iso-pentane and then embedded in Optimal cutting temperature compound (OCT) (Miles, California USA) supported on 1 cm^3 cork disk, frozen in liquid nitrogen and stored at -80 ^{o}C. Frozen tissue sections were then cut at 3 µm thickness using a cryostat and mounted on Superfrost-Plus glass slides (VWR, Leicestershire UK) and stored at -80 °C until needed.

2.6.3 Immunohistochemistry

2.6.3.1 Paraffin embedded sections

Slides were de-waxed by immersion in xylene twice for 7.5 minutes followed by two washes in 96% ethanol for 7.5 minutes. The slides were then rehydrated in dH_2O for 3 minutes at room temperature. Antigen retrieval was carried out according to the specification of each individual antibody (see below). The endogenous peroxidase activity was blocked by adding 3% H_2O_2 in methanol for 20 minutes at RT. The sections were then washed in dH_2O and soaked in PBS for 5 minutes. Sections were blocked with Avidin-Biotin block (Vector, Peterborough UK) to block endogenous avidin or biotin reactivity. Serum free protein block (Dako, Cambridgeshire UK) was added to the sections for 30 minutes at RT in order to

prevent unspecific antibody binding and then washed 3 times in PBS for 3 minutes with gentle rocking. The sections were incubated with 100 µl of the primary antibody at the desired concentration (2 hours for scFv and 1 hour for commercial antibodies), with matching concentrations of the isotype control antibody, at room temperature in humid environment. Unbound antibodies were removed by 3 washes in PBS for 3 minutes with gentle rocking. The sections were then incubated with 100 µl of the appropriate secondary antibody for 1 h at RT in humid chamber, washed 3 times in PBS for 3 minutes and followed by incubation with avidin-HRP conjugate (Vector, Peterborough UK or Dako, Cambridgeshire UK) for 30 minutes at room temperature and washed 3 times in PBS for 3 minutes to remove excess of reagent. Diaminobenzidine (DAB) chromogenic substrate was used to reveal HRP activity. Reaction was stopped by immersion in dH_2O when optimal intensity was reached. To reveal nuclei presence, the sections were counterstained in haematoxylin for 2 minutes and washed in dH_2O, followed by tap water. The sections were then dehydrated in ethanol twice for 3 minutes followed by xylene twice for 3 minutes, mounted in DPX and covered using glass coverslips. The stained sections were stored at RT.

Antigen retrieval procedures varied according to the primary antibody used. For scFv A7 the preferred retrieval procedure was proteinase K proteolytic-induced epitope retrieval (PIER). Tissue sections following de-waxing and rehydration were incubated with 100 µl of proteinase K (Dako, Cambridgeshire UK) pre-warmed 10 minutes at 37 °C, for 4 minutes at room temperature followed by serial washes in PBS. Digest-All^3 retrieval (Life technologies, Paisley UK) required 10 minutes incubation with 100 µl of the solution at 37 °C, followed by serial washes in PBS. When in combination with Proteinase K, the latter was performed as first procedure, followed by Digest-All^3 digestion. Chondrotinase ABC (Sigma, Dorset UK) was used at 1 U incubating 100 µl over the tissue section for 1 h at 37 °C, followed by serial washes in PBS. When in combination with proteinase K, it was performed as last retrieval. EDTA Heat-induced epitope retrieval (HIER) was performed at pH 9. Buffer was heated to boiling point and sections immersed in the solution for 3 or 20 minutes and allowed to cool in water bath for 20 minutes. Sections were then

washed in dH_2O and PBS. Trisodium citrate HEIR procedure was conducted using 0.01% trisodium-citrate buffer at pH 6. Buffer was heated to boiling point and sections immersed in the solution for 3 or 20 minutes and allowed to cool in water bath for 20 minutes. The 3 minutes incubation protocol was used as standard retrieval procedure for anti-vWF, anti-CD31, anti-CD34 and anti-α actin stainings. Finally, HCl retrieval was performed with 2 M HCl with 100 µl of buffer per tissue section for 10 minutes at RT, followed by serial washes in PBS.

Concentration of biotinylated scFv and biotinylated scFv-Fc antibody was assay dependent. When not specified, a concentration of 10 µg/ml was used. As detecting agent was used avidin-HRP complex (Vector, Peterborough UK) via mixing 1:1 volumes of reagent A and reagent B in PBS and allowed to form HRP-biotin-Avidin complexes with a 30 minutes incubation. 100 µl of the avidin-HRP complex was added to each section for 30 minutes at RT in humid chamber. Commercial antibodies anti-vWF (clone F8/86 - Dako, Cambridgeshire UK), anti-CD31 (clone 1D2-1A5 - Sigma, Dorset UK), anti-CD34 (clone QBEnd-10 - Dako, Cambridgeshire UK) and anti-α actin (clone 1A4 - Sigma, Dorset UK) were used at 1 µg/ml with 1h incubation at RT in humid environment. Sections were then treated with biotinylated anti rat/mouse antibody (Dako, Cambridgeshire UK) and followed by incubation with avidin-HRP complex (Vector, Peterborough UK) as described above.

2.6.3.2 Frozen sections

Slides were defrosted at RT for 30 minutes, fixed in ice-cold acetone for 10 minutes and air dried for 30 minutes at RT. The slides were then rehydrated in PBS for 10 minutes at RT. The endogenous peroxidase activity was blocked by adding 0.3% H_2O_2 in methanol for 20 minutes at RT and the sections processed as described above. No antigen retrieval was required for frozen tissue section.

2.6.4 Immunofluorescence

Frozen tissue slides were defrosted at RT for 30 minutes, fixed in ice-cold acetone for 10 minutes and air dried for 30 minutes at RT. Serum free protein block (Dako, Cambridgeshire UK) was added to the sections for 30 minutes at RT in order

to prevent non-specific antibody binding and then washed 3 times in PBS for 3 minutes. 100 µl of primary antibody was applied to the sections and incubated at room temperature before washing 3 times with PBS for 3 minutes to remove unbound antibody. The primary antibody was detected with 100 µl of fluorochrome conjugated secondary antibody upon incubation for 1 h at RT in dark chamber and humid environment. The sections were washed as above and incubated with 100 µl DAPI 1:1000 solution in PBS for 10 minutes at RT in humid chamber away from the light. Slides were then washed once in PBS, mounted with 20 µl Mowiol (Sigma, Dorset UK) per section and closed with glass coverslips. In order to prevent mounting medium evaporation or diffusion, the sections were sealed with nail varnish and stored at 4 °C or -20 °C for longer storage.

Concentration of scFv or scFv-Fc biotinylated and non-biotinylated antibodies was assay dependent. When not specified a concentration of 10 µg/ml was used. As detecting agent for biotinylated antibodies was used avidin-Texas red conjugated molecule (Life technologies, Paisley UK) diluted 1:1000 in PBS 0.5% BSA. Anti-vWF (clone F8/86 - Dako, Cambridgeshire UK), anti-CD31 (clone 1D2-1A5 - Sigma, Dorset UK), anti-α actin (clone 1A4 - Sigma, Dorset UK), anti-NG2 (Millipore, Massachusetts USA), anti-CD248 (clone B1/35 – Millipore, Massachusets USA) and anti-CD31 biotinylated (clone MEM-05 – Abcam, Cambridge UK) were used at 1 µg/ml in PBS 0.5% BSA. Bound antibodies were detected with anti-mouse IgG (Isotype specific) antibody directly conjugated to Alexa Fluor 488 (green) or 594 (red) (Life Technologies, Paisley UK) at a concentration of 1 µg/ml or avidin-Texas red (for biotinylated antibodies) in PBS 0.5% BSA. When in dual fluorescence staining the antibody were chosen with different IgG subclass and detected with the relevant isotype specific conjugated antibody.

2.6.5 Image analysis

Pictures from DAB staining were acquired using Cell-P imaging software (Soft *Imaging* System, Münster, Germany) in bright field with Olympus microscope unit. UV fluorescent pictures were acquired using Cell-P imaging software using UV-light at the required excitation wavelength with Olympus microscope unit. Alexa

Fluor 488 was excited at 488 nm and emission detected at 519 nm, Alexa Fluor 594 was excited at 591 nm at emission detected at 618 nm, Texas red was excited at 589 nm and emission detected at 615 nm.

Quantification of HRP/DAB staining intensity was performed on digitally captured colour images, saved as tiff files and analysed using ImageJ 1.44 (NIH, Maryland USA) after using the colour deconvolution algorithm as described previously (237). DAB layer was thresholded using ImageJ 1.44, for consistency samples included in the same analysis were thresholded to a fixed value. Thresholded pictures were converted in grey scale and the mean grey value, which is the sum of the grey values of all the pixels in the selection divided by the number of pixels, was calculated for vascular regions (positive staining region) and comparable size areas in a non-relevant portion of the tissue (background value) using ImageJ 1.44 analysis tool. A total of 5 regions per sample or category were calculated and expressed as mean ± standard deviation (SD) and compared using unpaired non parametric statistical analysis.

ImageJ 1.44 (NIH, Maryland USA) colocalization indices plugin was used to perform thresholded Pearson's Correlation Co-efficient analysis of images in order to accurately quantify and correlate overlap of image pixels from 2 different channels (238, 239). A value of +1 indicates complete pixel-to-pixel overlap between the two chosen channels. A value of 0 indicates no overlap or correlation of pixels from two different channels, and −1 indicates complete disparity/exclusion of pixels from the two channels that have been compared.

2.7 *In vitro* cell culture

Cell cultures were grown in plastic tissue-culture flasks (Corning, Massachusetts USA) in Binder CO_2 incubators (Binder, Tuttlingen Germany) at 37 °C with 5% CO_2 and humid environment.

2.7.1 Cell line culture

Prostate cancer cell line (PC3), Epithelial cancer cell line JU77 and human embryonic kidney cell line (HEK-293) were cultured in Dulbecco's Modified Eagle Medium (DMEM) (Life Technologies, Paisley UK) supplemented with 10% foetal calf serum (FCS), 100 U/ml penicillin, 100 µg/ml streptomycin and 2 mM L-glutamine. HEK-293 SV40 transformed (HEK-293T) cell line was cultured in DMEM supplemented with 10% FCS, 100 U/ml penicillin, 100 µg/ml streptomycin, 0.5 mg/ml geneticin and 2 mM L-glutamine. IE7 cell line was cultured in M200 medium (Life Technologies, Paisley UK) supplemented with Low Serum Growth Supplement (LSGS) (foetal bovine serum, 2% v/v; hydrocortisone, 1 mg/ml; human epidermal growth factor, 10 ng/ml; basic fibroblast growth factor, 3 ng/ml; and heparin, 10 mg/ml), 100 U/ml penicillin and 100 µg/ml streptomycin and 2 mM L-glutamine. Monocyte cell line U937 was cultured in RPMI medium (Life Technologies, Paisley UK) supplemented with 10% FCS, 100 U/ml penicillin, 100 µg/ml streptomycin and 2mM L-glutamine.

2.7.2 Primary fibroblast culture

Rheumatoid arthritis synovial fibroblasts (RASF) kindly provided by Dr Ngar-woon Kam (Queen Mary University of London, London UK), were derived and maintained as previously described (58). Briefly, after discarding fat and dense fibrous tissues, synovium was minced, mashed under a 70 µm nylon mesh cell strainer (Becton Dickinson, Oxford, UK) and digested overnight at 37 °C with 1.5 mg/ml dispase II in DMEM supplemented with 10% FCS, 50 U/ml penicillin-streptomycin and 10 mM HEPES buffer (Life technologies, Paisley UK). The resulting suspension was passed through a cell strainer, centrifuged and the cell pellet was re-suspended in culture medium and incubated in T75 tissue-culture flasks. When 90% confluent, fibroblasts were passaged at a ratio of 1:3 using 0.25% trypsin/EDTA (Sigma, Dorset UK). Synoviocytes were used between passages 4 and 8 (240).

2.7.3 Immunocytochemistry

$3x10^4$ cells were seeded in 13 mm round autoclaved coverslips (VWR, Leicestershire UK), in 24 well plates with 1ml of appropriate medium and incubated overnight at 37 °C. 500 µl of medium were then removed and 500 µl of 1% formaldehyde in PBS added and incubated at RT for 5 minutes with gentle rocking. The medium was then completely removed from the wells via aspiration and replaced with 1ml of 1% formaldehyde and left for 10 minutes at RT with gentle rocking. The wells were then washed extensively in PBS to remove excess of fixing agent. 0.1 M glycine was used for 10 minutes at RT to quench the reactive aldehyde groups. When permeabilisation of the cells was required, 1 ml of 0.1% Triton X-100 in PBS was used for 5 minutes followed by extensive washes with PBS. Primary antibody was then applied to coverslips and incubated for 2 hours at 37 °C in a humidified chamber. 100 µl of antibody was used when applied directly on the coverslip surface and 500 µl if the incubation was performed in 24 well plates. Three washings with PBS were performed to remove unbound antibody. The primary antibody was detected with a fluorochrome conjugated secondary antibody in a dark chamber. The cells were washed as above and incubated with 100 µl DAPI 1:1000 solution in PBS for 10 minutes at RT in humid chamber away from the light. Slides were then washed once in PBS, mounted with 20 µl Mowiol (Sigma, Dorset UK) per section and closed with glass coverslips. In order to prevent mounting medium evaporation or diffusion, the sections were sealed with nail varnish and stored at 4 °C or -20 °C for longer storage.

Concentration of scFv biotinylated and non-biotinylated antibodies was 20 µg/ml. As detecting agent for biotinylated antibodies, anti-c-Myc antibody (clone 9E10 – Sigma, Dorset UK) was used at 1 µg/ml concentration in PBS 0.5% BSA, followed by anti-mouse IgG Alex Fluor 488 (green) conjugated antibody at a concentration of 1 µg/ml. Biotinylated antibodies were detected with streptavidin Alexa Fluor 488 conjugated molecule (Life technologies, Paisley UK) at a concentration of 1 µg/ml. Anti-ICAM1 antibody (clone EP1442Y - Abcam, Cambridge UK) was detected with anti-Rabbit IgG Alexa Fluor 488 (Green) conjugated antibody (Life Technologies, Paisley UK).

2.7.4 Image analysis

Image acquisition was performed as described in section 2.5.5. Additionally, image acquisition was also performed using Leica confocal microscope (Leica, Wetzlar Germany) using Leica Application Suite Advanced Fluorescence (LAS AF) software platform (Leica, Wetzlar Germany).

2.7.5 Cellular ELISA

Cells were seeded at a concentration of $5x10^3$ cells/well in 100 µl of complete medium in 96 well plates and incubated overnight at 37 °C. If needed cells were stimulated with 10 ng/ml TNFα for 24 hours. Culture medium was aspirated and cells washed in PBS (pre-warmed at 37 °C). Cells were then fixed in 2% PFA in PBS for 12 minutes at 37 °C. Cells were washed twice in PBS 0.1% BSA, ensuring that the cells were not dislodged. 1% BSA in PBS was used to block reactive aldehyde groups for 30 minutes at 37 °C. Blocking solution was aspirated and 100 µl of primary antibody was added to the wells and incubated for 1 h at 37 °C. 50 µg/ml was used as first scFv concentration with serial 1:2 dilutions in duplicate in PBS 0.1% BSA. Unbound antibodies were removed by three washes in 0.1% BSA in PBS. Anti-cMyc secondary antibody (clone 9E10, Sigma, Dorset UK) was incubated for 1 h at 37 °C. Three washes were performed as described above to remove antibody excess. Anti-mouse IgG HRP conjugated antibody (SantaCruz, California USA) was used as detection agent and incubated for 1 h at 37 °C. Cells were washed as previously described and incubated with 70 µl of TMB substrate according to manufacturer's conditions (Becton Dickinson, Oxford UK) for 5 minutes at room temperature. Reaction was stopped with 35 µl 1N H_2SO_4 and absorbance read at 450nm in Genios Tecan plate reader (Tecan, Mannedorf Switzerland).

2.8 Protein extracts

Cells were seeded at a density of $3x10^6$ in 10 cm petri-dishes and incubated overnight at 37 °C. Alternatively, 90% confluent T75 flasks were lysate in 1 ml buffer.

RIPA buffer (150 mM NaCl, 10 mM Sodium Phosphate pH 7.2, 1% Na deoxycholate, 1% Triton X-100, 0.1% SDS, 5.2 mM 4-(2-Aminoethyl)benzenesulfonyl fluoride hydrochloride (AEBSF), 4 µM Aprotinin, 200 µM bestatin, 70 µM E-64, 100 µM leupeptin, 75 µM pepstatin) extraction was performed as follows: cells were washed twice in ice cold PBS, 1 ml of RIPA buffer was added and cells scraped from the plate. The lysed cells were then left to incubate on ice for 30 minutes with gentle mixing and centrifuged at 10000 rpm using a table top centrifuge for 10 minutes at 4 °C. The supernatant was collected and stored at -80 °C.

For extraction in OTG buffer (1% w/v octylglucopyranoside in Tris-buffered saline pH 7.4, 2 mM EDTA, 5.2 mM AEBSF, 4 µM aprotinin, 200 µM bestatin, 70 µM E-64, 100 µM leupeptin, 75 µM pepstatin) cells were washed as above and 1ml of OTG buffer added and the cells scraped from the plate. The lysed cells were then left to incubate on ice for 1 hour with gentle mixing and centrifuged at 10000 rpm in a table top centrifuge for 10 minutes at 4 °C. The supernatant was collected and stored at -80 °C.

To prepare cell lysates using saponin (0.2% saponin in PBS, 5.2 mM AEBSF, 4 µM aprotinin, 200 µM bestatin, 70 µM E-64, 100 µM leupeptin, 75 µM pepstatin) the cells were washed as above, 1 ml of saponin added and the cells incubated on ice for 30 minutes with gentle rocking. The saponin buffer was then gently removed and stored at -80 °C. The cells were then lysed by scraping into 1ml Triton X-100 (1% v/v Triton X-100, 20 mM Tris pH 8, 150 mM NaCl, 5.2 mM AEBSF, 4 µM aprotinin, 200 µM bestatin, 70 µM E-64, 100 µM leupeptin, 75 µM pepstatin). The lysed cells were incubated on ice for 30 minutes with frequent gentle agitation and then centrifuged at 10000 rpm for 10 minutes in a table top centrifuge at 4 °C. The supernatant was collected and stored at -80 °C.

Triton X-114 (1.5% v/v Triton X-114, 50 mM Tris pH 7.4, 150 mM NaCl, 1 mM $MgCl_2$, 1 mM $CaCl_2$, 5 mM EDTA, 5.2 mM AEBSF, 4 µM aprotinin, 200 µM bestatin, 70 µM E-64, 100 µM leupeptin, 75 µM pepstatin) extraction was performed by washing the cells as above. 1ml of Triton X-114 buffer was then added and cells scraped from the plate. The lysed cells were left to incubate on ice for 1 hour with

frequent vortexing and then centrifuged at 10000 rpm in a table top centrifuge for 10 minutes at 4 °C to pellet unbroken cells and nuclei. The supernatant was transferred in a clean tube and incubated at 37 °C for 3 minutes. The solution was then centrifuged at 3000 rpm for 10 minutes and the two phases (detergent phase [bottom] and aqueous phase [top]) separated and stored at -80 °C.

To prepare cell lysates using hypotonic shock buffer (10 mM Tris pH 7.5, 200 µM $MgCl_2$, 5.2 mM AEBSF, 4 µM aprotinin, 200 µM bestatin, 70 µM E-64, 100 µM leupeptin, 75 µM pepstatin) the cells were washed twice in ice cold hypotonic buffer, incubated with 1 ml ice cold hypotonic buffer for 10 minutes on ice. The cells were then scraped from the dishes and mechanically disrupted in a Dounce homogeniser (50 strokes). The lysed cells were transferred to a clean tube, centrifuged at 500 g for 5 minutes at 4 °C and the supernatant transferred to a new tube and centrifuged at 20000 g for 30 minutes at 4 °C. The supernatant containing the cytoplasmic fraction was stored at -80 °C.

Lysate buffer for cell lysate ELISA (100 mM Tris pH 7.4, 150 mM NaCl, 1 mM EGTA, 1 mM EDTA, 1% IGEPAL, 5.2 mM AEBSF, 4 µM aprotinin, 200 µM bestatin, 70 µM E-64, 100 µM leupeptin, 75 µM pepstatin) extraction was performed as follows: cells were washed once in ice cold PBS, 1 ml of lysis buffer was added and cells scraped from the flask and collected in pre-chilled tubes. The lysate was agitated on vortex briefly, incubated on ice for 30 minutes and centrifuged at 13000 rpm for 10 minutes in bench top centrifuge at 4 °C to pellet insoluble content. The supernatant was collected and stored at -80 °C.

Cell extracts were analyse in Western blot (as described in section 2.4.2), in cell lysate ELISA (as described in section 2.7.1) and in Immunoprecipitation assays (as described in section 2.8).

2.8.1 Cell lysate ELISA

A 96 well plate was coated with cell lysate diluted in equal volume of PBS and incubated overnight at 4 °C. Plate was then emptied, washed once in PBS and blot dry. 200 µl of PBS 4% milk was added as blocking solution for 1 h at 30 °C.

Blocking solution was removed after the incubation, washed once in PBS and blot dry. 100 µl of primary antibody in 0.5% BSA in PBS was added to each well and incubated for 1 h at 30 °C. For biotinylated scFv was used a concentration of 10 µg/ml or 20 µg/ml, while for mouse anti-αtubulin (clone 236-10501 Life Technologies, Paisley UK) a concentration of 1 µg/ml was used. Plate was then washed three times in PBS 0.05% Tween 20 and PBS, blot dry and incubated with 100 µl/well of secondary antibody. For biotinylated scFv, avidin-HRP conjugate (Vector, Peterborough UK) was used with 15 minutes incubation at 30 °C. For mouse antibodies, anti-mouse IgG HRP conjugate (SantaCruz, California USA) was incubated for 1h at 30 °C. Plate was then washed as described above and incubated with 70 µl of TMB substrate according to manufacturer's conditions (Becton Dickinson, Oxford UK) for 5 minutes at room temperature. Reaction was stopped with 35 µl 1 N H_2SO_4 and absorbance read at 450 nm in Genios Tecan plate reader (Tecan, Mannedorf Switzerland).

2.9 Immunoprecipitation

2.9.1 scFv, scFv-Fc and IgG IP using protein A/G agarose beads

50 µl of protein A/G agarose beads (Sigma, Dorset UK) were resuspended in PBS and centrifuged at 2500 g for 1 minute to remove suspension buffer. The washing step was repeated twice to equilibrate the buffer. 500 µl of protein extract (RIPA or Lysate ELISA lysis buffer) were incubated with the protein A resin for 10 minutes at 4 °C to pre-clear the lysate and reduce non-specific binding of the proteins to the agarose beads. Pre-cleared lysate was recovered by centrifugation at 13000 rpm on bench top centrifuge for 5 minutes. The lysate was then incubated with 10 µg of scFv (Figure 5.11) or 5 µg of scFv, scFv-Fc and IgG antibody (Figure 5.12 and 5.14 B) for 2 h at room temperature with rotation. Antibody-lysate complex was then incubated with the resin overnight at 4 °C with tilting rotation to allow antibody binding to the resin. The resin was washed twice in 1 ml of PBS with 2500 g centrifugation for 1 minute. Bound antibody-antigen complex was recovered via elution in 50 µl of Laemmli lysis buffer boiled at 95 °C for 5 minutes. Samples

were resolved in SDS-PAGE as described in section 2.4 and processed for Western blot (section 2.4.2) or stained with Ruby protein gel stain (section 2.4).

2.9.2 scFv IP with CNBr activated agarose beads

To prepare the covalently coupled scFv-cyanogen bromide (CNBr) activated Sepharose beads, 0.05 g of lyophilised Sepharose beads (GE Healthcare, Amersham UK) were resuspended in 1 mM HCl and washed for 15 minutes in a 2 ml disposable gravity column with 20 ml of 1 mM HCl dispensed in several aliquots. 1 mg of scFv antibody was concentrated to 100 µl using Ultracel YM3000 MWCO (Millipore, Massachusetts USA) and re-diluted in coupling buffer (0.1 M $NaHCO_3$ pH 8.3 and 0.5 M NaCl) to a final concentration of 1 mg/ml. Concentration of antibody was measured after buffer exchange to evaluate effective protein content and protein loss, using a spectrophotometer at 280 nm. The antibody solution was added to the medium suspension in a stoppered vessel and incubated overnight at 4 °C with end over end rotation. Following incubation, the unbound antibody suspension was aspirated and beads were washed with 5 bed volumes of coupling buffer. Unbound antibody solution was measured to determine quantity of unbound antibody and determine coupling efficiency. Remaining active groups of the resin were blocked in 0.1 M Tris-HCl buffer pH 8 for 2 h. Resin was then washed with three cycles of alternating pH, consisting in 5 bed volumes of 0.1 M acetic acid/sodium acetate pH 4 containing 0.5 M NaCl, followed by wash with 0.1 M Tris-HCl pH 8 containing 0.5 M NaCl.

500 µl of cell lysate was incubated with 10 µl of scFv coupled Sepharose beads for 2 h at 4 °C with end over end rotation. The suspension was centrifuged at 3000 rpm on a bench top centrifuge for 2 minutes and the unbound lysate was discarded. Aliquot of unbound lysate, or flowthrough, was kept for analysis. Beads pellet was resuspended in 500 µl of PBS to wash and remove remaining lysate proteins. The suspension was spun a second time at 3000 rpm for 2 minutes and resuspended in 10 µl of Laemmli lysis buffer (0.5 M DTT, 10% glycerol, 0.44 M Tris pH 6.8, 0.04% Bromophenol Blue, 10% SDS) and boiled at 95 °C for 5 minutes. Similarly, flowthrough and wash samples were prepared in Laemmli lysis buffer for

further analysis. Samples were run on 8-16% polyacrylamide gels and stained with Ruby protein gel stain as described in section 2.4.

2.9.3 IgG and scFv-Fc IP using protein A Dynabeads

To prepare protein A Dynabeads resin (Life Technologies, Paisley UK), 50µl of the resin (1.5 mg beads) were transferred to a 1.5 ml tube and placed on a magnet. The magnetic field would retain the Dynabeads allowing the removal of the suspension buffer without resin loss. The tube was then removed from the magnet support and beads resuspended in 200 µl of PBS 0.05% Tween 20 containing 5 µg of scFv-Fc antibody and incubated at RT for 10 minutes with tilting rotation. After the coupling step, the tube was placed on the magnet and the supernatant containing unbound antibodies was discarded. Aliquot of the flowthrough was kept for further analysis. Beads were washed by resuspention in 200 µl of PBS 0.05% Tween 20. 400 µl of PC3 cell lysate or 500 µl of RASF protein extract were added to the beads - scFv-Fc complex and gently resuspended by pipetting. Cell lysate was allowed to interact with the beads for 25 minutes at RT with tilting rotation. The tube was placed on the magnet to remove the supernatant containing unbound lysate proteins and resuspended in 200 µl of PBS for a total of 3 washes. Resuspended beads were then transferred to a clean tube to reduce carry-over of lysate and washing buffer, and supernatant removed. Dynabeads were then gently resuspended in 20 µl of Laemmli lysis buffer to elute the bound antigens and incubated at 85 °C for 10 minutes. Elution fraction, flowthrough and total cell lysate were resolved in SDS-PAGE with 8-16% polyacrylamide gels and stained with Ruby protein gel stain as described in section 2.4.

2.9.3 scFv-Fc IP using cross-linked protein A Dynabeads

50 µl of protein A dynabeads suspension (1.5 mg resin) was transferred to a tube and placed under magnetic field to remove supernatant as described in section 2.8.2. The beads were then removed from the magnetic support and resuspended in 200 µl of PBS 0.05% Tween 20 containing 4.2 µg of scFv-Fc antibody and incubated for 10 minutes at RT with tilting rotation. Unbound antibodies were removed and the beads washed with 200 µl of PBS 0.05% Tween 20.

In order to chemically cross-link the antibodies to the protein A Dynabeads, bis-sulfosuccinimdyl-suberate (BS3) was prepared by making a 100mM solution in conjugation buffer (20 mM sodium phosphate, 0.15 M NaCl at pH 7-9) and diluting to a final 5 mM concentration. scFv-Fc coupled protein A Dynabeads were washed twice in 200 µl of conjugation buffer, placed on a magnet and removed supernatant. The beads were then resuspended in 250 µl of 5 mM BS3 and incubated at room temperature for 30 minutes with tilt rotation. Cross-linking reaction was quenched by adding 12.5 µl of quenching buffer (1 M Tris-HCl pH 7.4) with 15 minutes incubation at RT with tilting rotation. Cross-linked beads were washed three times with 200 µl PBS 0.05% Tween 20 and IP performed as described in section 2.8.2.

2.10 TNF cytotoxicity assay

The TNF cytotoxicity test was conducted on mouse fibroblast cell line L929. The L929 cells ($1.5 \cdot 10^4$) were placed in each well of 96 well plates (Corning, Massachusetts USA) in 100 µl of DMEM medium supplemented with 10% FCS in the presence of 100 U/ml penicillin, 100 µg/ml streptomycin, 2 mM L-glutamine and incubated for 18 h at 37 °C 5% CO_2. The medium was then removed and 100 µl of complete medium with 1µg/ml actinomycin D, 0.45 ng/ml TNFα or TNFα and the antibody of interest, were added to the cell monolayer and incubated 24 h at 37 °C in a CO_2 incubator. Test antibody was used at a starting concentration of 18.8 nM with 1:2 serial dilutions. 10 µl of 5 mg/ml thiazolyl blue tetrazolium bromide in PBS (Sigma, Dorset UK) was added to the wells and incubated for 3 h at 37 °C. The medium was then removed and the cells resuspended in 100 µl 90% isopropanol 10% DMSO for 15 minutes. Optical absorption was measured at 560 nm or 595 nm with a TECAN GENios plate reader (Tecan, Mannedorf Switzerland).

2.11 TNF ELISA

Nunc 96 well immunosorbent plates (Thermo Fisher Scientific, Loughborough UK) were coated overnight at 4 °C with 100 ng/ml TNFα in PBS. Medium was then discarded, wells washed once in PBS and incubated with 200 µl

2% BSA in PBS to block non-specific reactive sites for 1 h at RT. Blocking solution was discarded after incubation and wells rinsed in PBS. 100 µl of primary antibody diluted in PBS 0.5% BSA was added per well and incubated for 2 h at RT. Test antibody was used at a starting concentration 6.8 nM with 1:3 serial dilutions. Unbound antibodies were removed via three repeated washes in PBS 0.05% Tween 20. Secondary goat anti-Human IgG (Jackson ImmunoResearch, Pennsylvania USA) was used at 1:3000 dilution in PBS 0.5% BSA and incubated for 1 h at RT. Washes were repeated as described above and plate incubated with 70 µl per well of TMB substrate (GE Healthcare, Amersham UK) for 5 minutes and reaction stopped with 35 µl 1 N H_2SO_4. Optical absorption was measured at 450 nm with a TECAN GENios plate reader (Tecan, Mannedorf Switzerland).

2.12 DPP6 ELISA

DPP6 ELISA assay was performed as described in section 2.11 with the following difference: Nunc 96 well immunosorbent plates were coated with 100 ng/ml of recombinant DPP6, kindly provided by Professor D. Sblattero (University of Eastern Piedmont, Novara Italy), overnight at 4 °C.

2.13 Biacore

Set up of the Biacore T200 instrument was carried out according to Biacore procedure manual. A CM5 chip (GE healthcare, Amersham UK) carrying a carboxymethylated dextran matrix covalently attached to the gold sensor surface was used to covalently bind the capture mouse anti-human Fc antibody (GE healthcare, Amersham UK). The carboxyl groups were activated with a mixture of 0.4 M 1-ethyl-3-(3-dimethylaminopropyl)carbodiimide (EDC) and 0.1 M N-hydroxysuccinimide (NHS) (flow rate 10 µl/min for 7 minutes) to form succinimide esters. The capture antibody at a concentration of 25 µg/ml in immobilisation buffer (GE Healthcare, Amersham UK) was applied to the chip at a flow rate of 10 µl/min for 7 minutes, in order to allow the exposed succinimide ester groups to react spontaneously with the amine groups of the capture antibody. Immobilisation of the antibody resulted in 2000 response units (RU). 1 M Ethanolamine-HCl pH 8.5

was used to deactivate excess reactive groups in the chip (flow rate 10 µl/min for 7 minutes). To measure kinetic interactions of the test antibodies with TNF-α, the antibodies were injected at a concentration of 1 µg/ml with a flow rate of 30 µl/min for a contact time of 60 seconds. TNF-α was then injected at different concentrations starting at 20 nM with 1:2.5 serial dilutions at a flow rate of 30 µl/min for a total contact time of 180 seconds, followed by 700 seconds of dissociation time. The chip was then regenerated via two injections of 3 M $MgCl_2$ (30 µl/min 60 seconds), removing all trace amounts of captured ligand and TNF-α from the chip surface. After successful regeneration, the capture and kinetic studies were repeated as described above.

2.14 Phage library screening

The cDNA phage expression library obtained from mRNA of human colon carcinoma, human lung fibroblasts and human pancreatic islets was kindly provided by Professor D. Sblattero (University of Eastern Piedmont, Novara Italy). The library was characterised by 18000 genes present in multiple copies with fragments varying from 200 to 700 bp (241). Phage library in DH5αF' was rescued from glycerol stock and grown in 2TYAG bacterial medium (for 1 L 16 g bactotryptone, 10 g bacto-yeast, 5 g NaCl, 100 µg/ml ampicillin, 2% glucose in dH_2O pH 7) at 250 rpm for 1.5-2 h at 37 °C until reached an OD 600 nm of 0.5. At this OD the bacterial cells should have reached a concentration of $3x10^8$ cells/ml. 20 fold excess of helper phage was used to trigger phage expression for 45 minutes incubation at 37 °C with occasional agitation. Bacterial culture was spun at 4000 g for 10 minutes to pellet the infected cells. The pellet was then resuspended in a volume 5 times greater than the initial culture volume in 2TYAK (for 1 L 16 g bactotryptone, 10 g bacto-yeast, 5 g NaCl, 100 µg/ml ampicillin, 25 µg/ml kanamycin in dH_2O pH 7), grown at 30 °C with 250 rpm agitation overnight. The following day the bacteria were centrifuged at 7000 rpm for 25 minutes at 4 °C to pellet the cells, and the supernatant was collected and subjected to PEG precipitation.

1/5 volumes of PEG/NaCl solution was added to the cleared phage supernatant and incubated for 30-60 minutes on ice. The solution was centrifuged

at 4000 g for 15 minutes at 4 °C and the phage pellet resuspended in 1/10 of the original volume with PBS. The solution was then spun in a microcentrifuge to remove remaining bacterial cells and the supernatant was transferred to a new tube.

1 ml of scFv or scFv-Fc antibody at a concentration of 5-10 µg/ml was used to coat Nunc immunotubes (Thermo Fisher scientific, Loughborough UK) and left overnight at 4 °C in rotation to allow antibody binding to the plastic surface. The following day the immunotubes were washed twice in PBS to remove unbound antibodies and blocked with 2% milk in PBS for 45 minutes at RT with rotation. The blocking step was necessary to block non-specific reactive sites of the plastic tubes. At the same time, the PEG precipitated phage pool was blocked with 2% milk in PBS in a final volume of 1 ml. After the blocking step the immunotubes were washed twice with PBS 0.05% Tween 20 and twice in PBS and incubated with the phage mix for 30 minutes at room temperature. Tubes were then washed 20 times in PBS 0.05% Tween 20 and 20 times in PBS by pouring buffer in and out of the tubes. Bound phage clones were then eluted by adding 1ml of DH5αF' at OD 600 nm of 0.5 and left for 45 minutes at 37 °C. Infected bacteria were plated on 2TY agar plates with 100 µg/ml ampicillin as selective agent and incubated at 30 °C overnight. This plate represents the phage output of the first selection. Titration of the phage output was performed by colony count on 2TY agar plates.

Following rounds of selection were performed as described above with doubled washing steps to increase stringency. The inverted third round of selection was performed as above by using the output of scFv selection as input for scFv-Fc selection and vice versa.

2.14.1 Phage ELISA

Individual colonies were picked from the phage selection. 100 µl of 2TYAG medium was added to each well of a 96 well plate and single colony was inoculated in each well. The bacteria were allowed to grow at 30 °C with 250 rpm agitation overnight. The following day 2 µl of each well was transferred in 120 µl of 2TYAG medium in a new 96 well plate with round bottom and grown at 37 °C with 250 rpm

agitation until reached OD 600 nm of 0.5. To each well was added 50 µl of 2TYAG medium containing $1x10^9$ pfu helper phage (ratio of 20:1 phage to bacteria) and incubated for 30 minutes at 37 °C. Plate was then spun at 1700 rpm for 10 minutes to pellet the bacterial cells and the supernatant was discarded. Pellet was resuspended in 150 µl of 2TYAK and grown overnight at 28 °C with agitation.

Immunosorbent 96 well plates were coated with 100 µl of 10 µg/ml scFv or scFv-Fc antibody in PBS overnight at 4 °C. Antibody solution was discarded and plate washed once in PBS and incubated with 120 µl of 2% milk in PBS for 45 minutes at RT to block remaining reactive sites of the plate. Plate was then washed twice in PBS. 50 µl of 4% milk in PBS and 50 µl of culture supernatant containing the phage clones were added to each well and incubated 1 h at RT with gentle agitation. Solution was discarded and plate washed three times in PBS 0.05% Tween 20 and PBS. 100 µl of HRP conjugated mouse anti-M13 antibody was added to each well and incubated for 1h at RT. Plate was washed as described above and 70 µl of TMB substrate solution (Becton Dickinson, Oxford UK) was added in each well. The reaction was left for 5-20 minutes or until a suitable signal was detected, and quenched with 35 µl of 1 N H_2SO_4. Absorbance was read at 450 nm in a Genios Tecan plate reader (Tecan, Mannedorf Switzerland).

2.14.2 Soluble protein expression from phage clone

Single infected DH5αF' colonies were inoculated in 100 µl of 2TY medium supplemented with 100 µg/ml ampicillin and 2% glucose in each well of a 96 well plate and allowed to grow overnight at 30 °C with 250 rpm shaking. The following day, 2 µl from each well was transferred in a new 96 well plate with 100 µl 2TY with 100 µg/ml of ampicillin and 0.1% glucose per well. Cells were grown at 37 °C until OD 600 nm was 0.6. 50 µl of 2TY with 100 µg/ml ampicillin and 1.5 mM IPTG (final concentration 0.5 mM IPTG) was added in each well and incubated at 28 °C overnight with 250 rpm shaking. The following day the plate was spun at 1700 rpm for 10 minutes and the supernatant containing the soluble protein was collected for ELISA screening. In addition, the bacterial pellet was resuspended in PPB solution (200 mg/ml sucrose, 1 mM EDTA, 30 mM Tris-HCl pH 8) and incubated for 45

minutes on ice. The solution was then centrifuged at 13000 rpm at 4 °C for 20 minutes and the periplasmic extract collected for ELISA screening.

2.15 Target antigen validation

2.15.1 LTBP2 soluble protein expression

In collaboration with the University of Eastern Piedmont in Novara, the vector coding for LTBP2 cDNA fragment was amplified and digested using NheI restriction endonuclease (New England BioLabs, Herts UK) at 37 °C for 1 h in NEB buffer 2, followed by incubation with BssHII restriction enzyme (New England BioLabs, Herts UK) at 50 °C in NEB buffer 2 for 1 h. Reaction was then resolved in 1% agarose gel and purified following gel extraction of the relevant band using PCR clean-up Gel extraction kit (Macherey-nagel, Düren Germany) as described in section 2.2.1. A modified version of the pGEX 4T-1 vector (GE Healthcare, Amersham UK), containing the NheI and BssHII restriction sites and the glutathione S-transferase (GST), was used as expression plasmid and digested as described above to accommodate the insert. Digested insert and vector were ligated to reconstitute the expression plasmid using T4 DNA ligase (New England BioLabs, Herts UK). A 3:1 molar ratio between insert and vector was used and incubated at 16 °C overnight. Ligase reaction was transformed in competent DH5αF' *E. coli* bacteria, leaving the reaction for 15 minutes in ice to allow optimal plasmid distribution, incubating 30 seconds at 42 °C and finally 2 minutes in ice. Bacteria were left recovering in 2TY culture medium with 1% glucose at 37 °C at 200 rpm for 1h. Finally, bacteria were plated in 2TY agar plates containing 100 µg/ml ampicillin and left overnight at 37 °C. Grown colonies represented efficiently transformed cells. Single colonies were screened for presence of the correct plasmid via polymerase chain reaction (PCR) using primer sense (5'-GGGCTGGCAAGCCACGTTTGGT-3') and primer antisense (5'-GGTGAAAACCTCTGACACATGCAGCTCCCGG -3') and sequenced to confirm correct gene insertion.

Transformed bacteria were grown in 2TY medium with 100 µg/ml ampicillin with agitation at 37 °C until OD 600 nm reached 0.6. Bacteria were then induced with 0.5mM IPTG with overnight incubation at 30 °C to stimulate protein expression. Bacteria were collected following centrifugation at 4000 rpm for 20 minutes and resuspended in 1% Triton X-100 in PBS at 4 °C with agitation until solution appeared clarified, in the presence of 200 µg/ml of lysozyme and 20-50 µg/ml DNAase. Clarified lysates were centrifuged at 8500 rpm for 20 minutes at 4 °C and supernatant purified by affinity chromatography with 25 µl of settled GSH agarose resin (Sigma, Dorset UK). The suspension was incubated with gentle mixing for 30 minutes at 4 °C, loaded on filter column and allowed to settle by gravity flow. Resin was washed three times in 0.05% Tween 20 in PBS and once in PBS and eluted with 100 µl of elution buffer (50 mM GSH reduced, 100 mM NaCl, PBS pH 8). Protein fractions were dialysed overnight against PBS for buffer exchange at 4 °C, recovered and stored at -80 °C.

2.15.2 C19 ORF 10 soluble protein expression

pCMV6 plasmid containing the C19 ORF 10 519 bp gene, cloned with SgfI-MluI restriction sites, was purchased from OriGene (OriGene, Washington D.C. USA). HEK-293T cells were grown on the surface of glass coverslips, previously degreased and autoclaved, in 24 well plates at a concentration of $5x10^4$ cells/ml for 24 h at 37 °C in 1 ml of complete medium. Cells were then transfected with the pCMV6-C19 ORF 10 plasmid using the JetPrime reagent (Polyplus, Illkirch France) following manufacturer's recommendations. Briefly, a mixture of 50 µl JetPrime buffer with 0.5 µg of plasmid DNA and 1 µl JetPrime reagent was left to incubate for 10 minutes and applied drop-wise to the cells. Transfection was protracted for 4 h at 37 °C before medium was replaced and incubated for 24 h. The supernatant was then collected, centrifuged at 1500 rpm and filtered to remove cells and cellular debris.

2.15.3 ELISA on soluble proteins

Nunc immunosorbent 96 well plates (Thermo Fisher Scientific, Loughborough UK), were coated with 100 µl 10 µg/ml of soluble protein in PBS or

100 µl of C19 ORF 10 transfected or non-transfected HEK-293T supernatant overnight at 4 °C. Coating solution was discarded and plate washed once in PBS and incubated with 200 µl of 4% milk in PBS for 1 h at RT to block remaining reactive sites of the plate. Plate was then washed once in PBS and wells incubated with 100 µl of primary antibody at 10 µg/ml (or 1 µg/ml for commercial antibodies) in PBS 0.5% BSA for 1 h at RT with agitation. Solution was discarded and plate washed three times in PBS 0.05% Tween 20 and once in PBS. 100 µl of secondary antibody HRP conjugated was added per well and incubated for 1 h at RT. For scFv antibodies, a mouse anti-cMyc antibody followed by anti-mouse IgG HRP conjugated antibody was used. For scFv-Fc it was used an anti-SV5 antibody followed by anti-mouse IgG HRP conjugated antibody. Plate was washed as described above and 70 µl of TMB substrate solution (Becton Dickinson, Oxford UK) was added in each well. The reaction was left for 5-20 minutes or until a suitable signal was detected, and quenched with 35 µl of 1 N H_2SO_4. Absorbance was read at 450 nm in a Genios Tecan plate reader (Tecan, Mannedorf Switzerland).

2.15.4 PDGFR fusion protein

The LTBP2 gene fragment was amplified from the phagemid plasmid using PCR using the primer LTBP2 BglII Display sense (5'-AGCTAGATCTGGCGCGCCTGGCTTCGT-3') and primer LTBP PstI Display anti (5'-CGACCTGCAGCCGCTCGTCAATATCCA-3') and including the restriction sites BglII and PstI to allow cloning in the pDisplay vector (Life Technologies, Paisley UK). Similarly, the C19 ORF 10 gene sequence was amplified from pCMV6-C19 ORF 10 plasmid, described in section 2.10.2, following PCR using the primer ORF BglII Display (5'-AGCTAGATCTATGGCGGCGCCCAGCGG-3') and antisense ORF PstI Display anti (5'-CGACCTGCAGCAGCTCAGTGCGCGATGA-3'). 1 µg of pDisplay vector and PCR products were digested with restriction enzymes BglII and PstI at 37 °C for 1 h in NEB buffer 3 (New England BioLabs, Herts UK). Digestion products were resolved in 0.8% agarose gel and purified following gel extraction of the relevant band using PCR clean-up Gel extraction kit (Macherey-nagel, Düren Germany) as described in section 2.2.1. Digested insert and vector were ligated to reconstitute the expression

plasmid using T4 DNA ligase (New England BioLabs, Herts UK) and transformed in competent DH5α as described in section 2.10.1.

Plasmid coding for PDGFR-LTBP2 or PDGFR-C19 ORF 10 were transfected in HEK-293T cells grown on glass coverslips on 24 well plates as described in section 2.10.2. Transformed cells were stained in immunofluorescence as described in section 2.6.3. Biotinylated scFv antibodies were used at 50 µg/ml concentration in PBS 0.5% BSA and detected with streptavidin-Alexa 488 conjugated molecule (Life Technologies, Paisley UK). Mouse anti-HA (clone HA-7 Sigma, Dorset UK) and mouse anti-cMyc (clone 9E10 Sigma, Dorset UK) were used at 1µg/ml in PBS 0.5% BSA and detected with anti-mouse IgG Alexa 594 conjugate antibody (Life Technologies, Paisley UK) at 1 µg/ml.

2.16 Polymerase chain reaction

Polymerase chain reaction (PCR) was generally performed with Herculase II Fusion DNA polymerase (Agilent Technologies, Berkshire UK) using 10 ng DNA template, 0.5 µl DNA polymerase, 5% DMSO, 0.25 µM of each primer and 250 µM of each dNTP, in a total volume of 50 µl. Reaction was performed in GeneAmp PCR system 9700 (Life Technologies, Paisley UK). PCR cycle was performed as follows: 95 °C 2 minutes; 2 cycles of 95 °C 10 seconds, 62 °C 30 seconds and 72°C 2 minutes; 2 cycles of 95 °C 10 seconds, 60 °C 30 seconds and 72 °C 2 minutes; 2 cycles of 95 °C 10 seconds, 58 °C 30 seconds and 72 °C 2 minutes; 15 cycles of 95 °C 10 seconds, 56 °C 30 seconds and 72 °C 2 minutes; final extension at 72 °C for 10 minutes.

2.17 Statistical analysis

Statistical analysis was performed using GraphPad Prism version 5 for Windows OS (GraphPad, California USA). Specifically, Mann-Whitney test was used for unpaired non-parametric quantitative variables when comparing two groups; Kruskal-Wallis test was used when comparing more than two groups of unpaired non-parametric quantitative variables; Paired or unpaired T-test was used to compare paired or unpaired quantitative variables respectively; 2 way ANOVA with Bonferroni's post-test to compare more than two groups of unpaired quantitative

variables. A p value <0.05 was considered statistically significant. # or *= p value <0.05, **= p value <0.01, ***= p value <0.001.

Chapter 3

Optimisation of scFv A7 and A7 scFv-Fc production and quality control

3.1 Introduction

Phage display library screening *in vivo* using a SCID mouse model double transplanted with human arthritic synovium and normal human skin as control tissue, has allowed the isolation of the phage clone A7, as described in section 1.4.2, showing high homing specificity for the arthritic synovium. In order to express a soluble scFv antibody, the HB2151 non suppressor *E.coli* strain was infected with phages carrying the scFv gene of interest. The HB2151 strain, as opposed to the TG1 strain, is able to recognise the Amber (TAG) codon present in the sequence between the scFv and the pIII phage protein. This step is crucial to allow the scFv antibody fragment to be expressed as an independent protein and evaluate its binding capacity and tissue reactivity. However, the production efficiency of a heterologous protein in a bacterial host is highly variable, mainly being a direct consequence of the primary sequence and the propensity to form insoluble aggregates during the folding process, leading to low yields (242). Despite yield being an important aspect when it comes to large scale antibody preparation, protein sequence can also influence the stability and determine the propensity to aggregate during storage conditions. For the past 20 years periplasmic expression in *E. coli* has been the standard approach to functional antibody fragments production (243), ensuring good yields and correct protein folding. In particular three different types of folding modulators with chaperone activity have been discovered in the periplasmic compartment of *E.coli* and may have a role in the correct folding and expression of foreign proteins. Such folding modulators include the disulphide-bond-forming machinery (244), periplasmic proteins with peptidyl prolyl *cis/trans* isomerase (245) and the protease DegP that shows chaperone activity at low temperatures (246).

Due to the variability observed among different antibodies and expression systems, it is important to thoroughly evaluate the protein production efficiency and reactivity of each antibody. In this chapter it will firstly be described the production method adopted for scFv expression, comparing different strategies for protein purification and assessing protein purity and quality. Subsequently the

development of biotinylated reagents and the evaluation tissue reactivity *in vitro* will be presented. In the second part of the chapter the development of a scFv-Fc fusion protein, characterising production efficiency, quality assessment and tissue reactivity *in vitro* will be described.

3.2 scFv A7 protein production

Achieving a successful protein production with correct expression, high purity and optimal reactivity, is the critical limiting step towards the characterisation of a potential therapeutic molecule. As described in detail in section 2.1, the expression of the scFv antibody of interest from the HB2151 *E.coli* strain can be triggered by IPTG induced Lac promoter activation in the pIT2 plasmid. A schematic of the expression vector used for scFv expression is shown in Figure 3.1. The pelB leader sequence provides the necessary signal for bacterial periplasmic expression from which the protein can then be isolated and purified in a more efficient way compared to whole cell lysate (247). However, the purification strategy adopted for protein isolation can determine the yield of recovered protein. Two purification systems, specifically protein A Sepharose purification procedure and Talon® metal affinity resin purification, were compared in order to determine which was the most efficient.

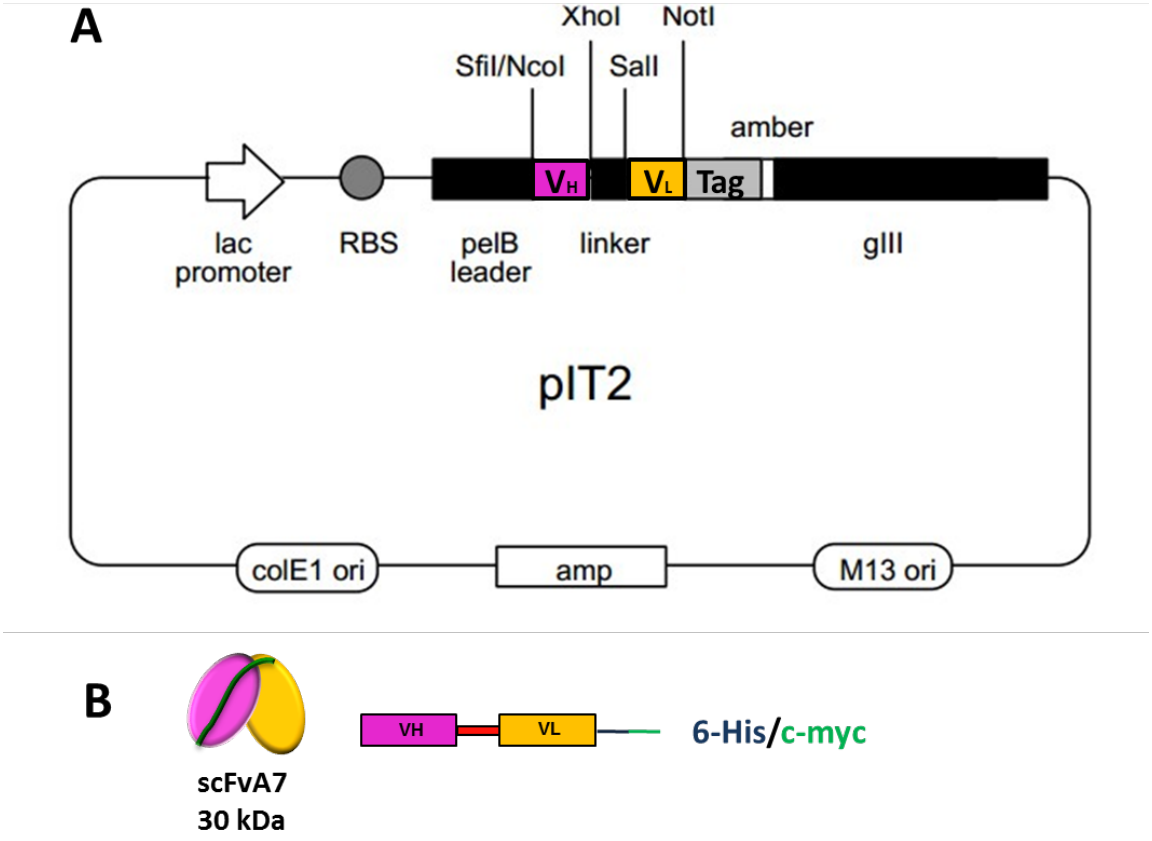

Figure 3.1 pIT2 vector and scFv A7 protein structure

Schematic of pIT2 vector encoding the scFv gene with the pelB leader sequence under the control of the inducible lac promoter (A). Schematic of the expressed scFv protein showing the V_H and V_L domains linked by a serine-glycine linker and carrying the 6-His and c-myc tags (B).

3.2.1 Optimisation of scFv protein purification

The *Staphylococcus aureus* protein A is a protein able to interact with the Fc portion of IgG1 and IgG2 and therefore is the method of choice for isolation of IgG isoforms from complex medium. Additionally, protein A has been proven to interact with the variable region of the VHIII subgroup (248). Since the Tomlinson library, used for the phage display scFv isolation, is based on the VHIII gene frame work (V_HIII 1-3), antibody clones derived from this library can be purified using this method. Further, antibody clones derived from the Tomlinson library carry a c-myc and a 6-Histidine (6-His) tag (Figure 3.1). The presence of a 6-Histidine tag can be exploited with use of an immobilised metal affinity resin. Specifically, the metal affinity resin Talon® is composed of Sepharose beads bearing a tetradentate chelator for the metal ion Cobalt that, under conditions of physiological pH, allows the binding of histidine to the resin that can then be released by competition with free imidazole (249, 250). Both resins are loaded in chromatography columns following incubation with the medium containing the scFv protein to be purified.

Direct comparison of the two purification strategies using the same bacterial culture divided in equal measure, showed Talon® purification to be more efficient than protein A, generating a 1.8 fold increase in protein yield and was able to purify up to 3 mg scFv A7 from 100 ml culture (Table 3.1).

Purification system	Supernatant	Periplasmic extract	Total protein	Culture volume
Protein A	0.34 (±0.001) mg	1.30 (± 0.05) mg	1.65 mg	100 ml
Talon®	0.83 (± 0.01) mg	2.17 (± 0.23) mg	3 mg	100 ml

Table 3.1 scFv A7 protein yields

Protein yields obtained through Protein A and Talon® metal affinity purification of 100ml bacterial culture. Supernatant purification and periplasmic extract are shown as separate values as a mean of 3 independent purifications (± SD), quantified using spectrophotometry at OD 280 nm and densitometry analysis of Coomassie stained SDS-PAGE. Total protein obtained from 100 ml bacterial culture has been calculated by sum of supernatant and periplasmic mean yield.

SDS-PAGE and Western blot analysis of the purified scFv A7 showed no difference in terms of purity between the two methods compared. A specific band at 30 kDa could be detected with both purification systems and the scFv identity was confirmed in a Western blot targeting the 6-His tag (Figure 3.2). The presence of a lower molecular weight band was detected in the Talon® purification which represents a breakdown product of the purified protein at the linker region. This breakdown product is most likely the V_L carrying the 6-His tag which can thus be pulled down using the metal affinity chromatography. In the same way, the V_H region could be pulled down using protein A and the fact that it is not detectable in the Coomassie stained SDS-PAGE in Figure 3.2 is ascribed to lower protein content in the protein A purified fractions below the coomassie sensitivity limit. In order to further confirm the specificity of both Talon® and protein A resins for the scFv protein, parent (empty) HB2151 bacteria were grown and processed using the above techniques. The results obtained, showed that no detectable protein could be measured by spectrophotometry (OD_{280nm}), SDS-PAGE and Western blot analysis even after concentrating the material 10 fold (Figure 3.3).

Talon® purification appeared to be more efficient in scFv purification. The optimised purification procedure was used to purify a second scFv targeting hen egg lysozyme (scFv HEL), kindly provided by Dr. Ahuva Nissim. The scFv HEL was isolated from the Tomlinson phage library and therefore shares the same framework of scFv A7, representing an ideal control antibody. Figure 3.4 shows the efficient purification of scFv HEL using Talon® metal affinity resin.

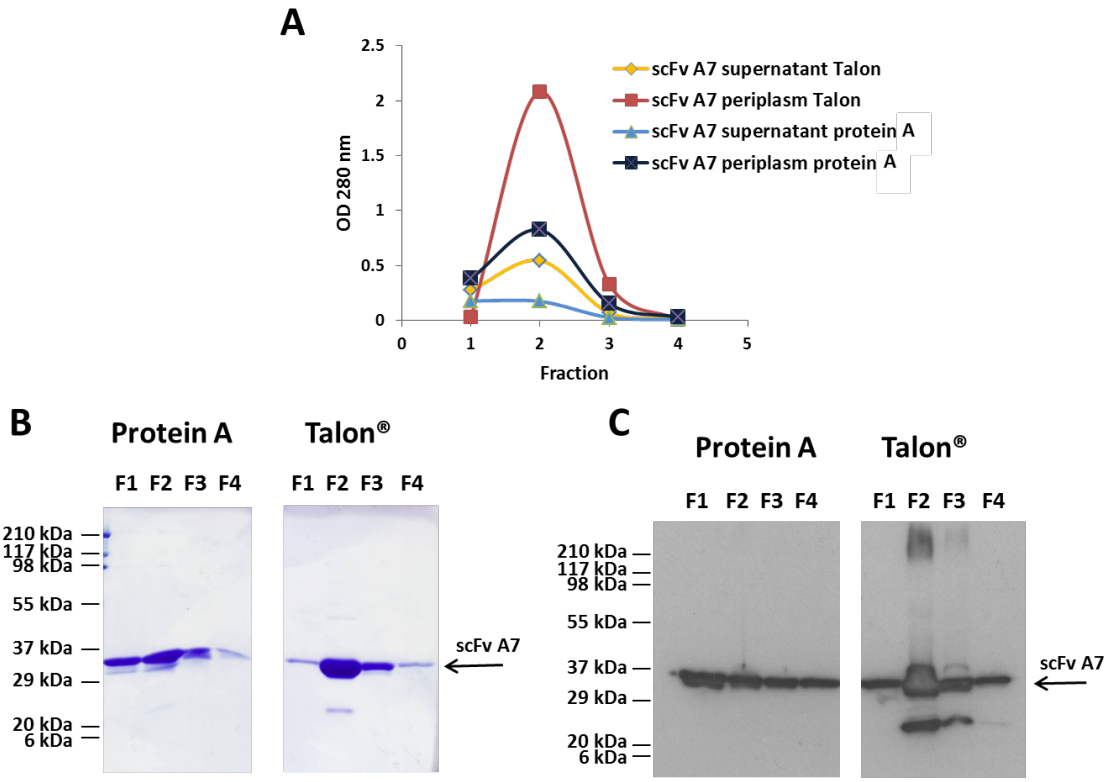

Figure 3.2 scFv A7 production and purification

Optical density analysis of scFv A7 eluted fractions from supernatant and periplasmic extracts using protein A or Talon® purification systems (A). SDS-PAGE resolved scFv A7 fractions from protein A or Talon® stained with Coomassie brilliant blue (B) or probed with anti 6-HIS and anti-mouse HRP conjugated antibody (Western blotting) (B).

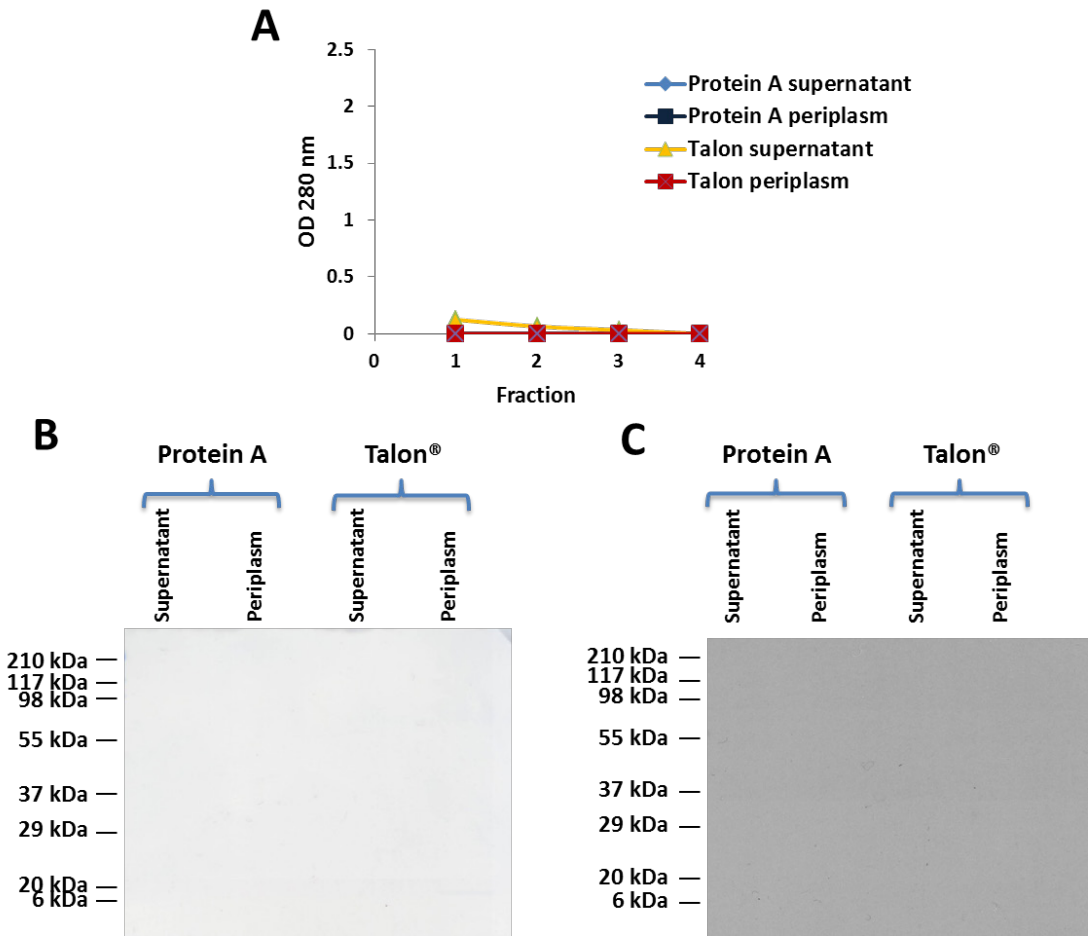

Figure 3.3 Purification control on empty HB2151 host

Optical density analysis of eluted fractions from supernatant and periplasmic extracts using protein A or Talon® purification system (A). SDS-PAGE resolved protein from 10 times concentrated fractions eluted from protein A or Talon® stained with Coomassie brilliant blue (B) or probed with anti 6-HIS and anti-mouse HRP conjugated antibody (Western blotting) (B).

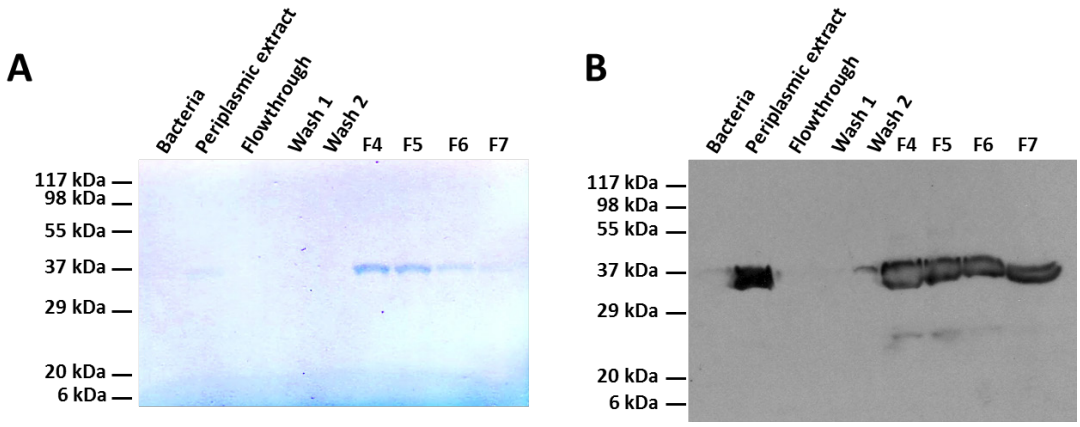

Figure 3.4 scFv HEL production and purification

SDS-PAGE resolved scFv HEL fractions from Talon® metal affinity purification stained with Coomassie brilliant blue (A) or probed with anti 6-HIS and anti-mouse HRP conjugated antibody (Western blotting) (B).

3.2.2 Quality assessment of scFv A7 protein production

As described in the previous section, analysis of the purified scFv A7 antibody protein by Coomassie blue staining of SDS-PAGE gels and Western blots, shows the presence of a main band at approximately 30 kDa corresponding to the intact scFv antibody, and a minor band at approximately 20 kDa corresponding to a breakdown product of the protein (Figure 3.2). Staining of the gel using a high sensitive colloidal Coomassie brilliant blue reagent (EZBlue), shows the presence of several minor bands appearing at 60 kDa and above that did not appear in 6-His targeted Western blots (Figure 3.5). These high molecular weight bands most likely correspond to bacterial chaperone proteins, like the hsp60 GroEL, that are retained during the purification steps (251).

Since achieving good quality, highly pure protein production is essential to characterise the antibody reactivity, an additional analysis step was performed to clearly define the protein constituents of the HB2151 purified periplasmic extracts. Specifically, HPLC size exclusion chromatography was performed on a freshly Talon® purified scFv A7 batch. The UV detection plot showed the predominant protein to be the monomeric form of the scFv A7, eluting between 18 and 19 minutes and corresponding to a putative molecular weight of 30 kDa, a small portion of dimers, eluting between 16 and 17 minutes (60 kDa), and no detectable contaminant proteins within the resolution power of the column (Figure 3.6 A). FPLC size exclusion chromatography performed on freshly Talon® purified scFv A7 confirmed the result obtained in HPLC, showing the monomeric form of scFv A7 as the predominant protein and only a limited amount of dimers and contaminant proteins (Figure 3.6 B).

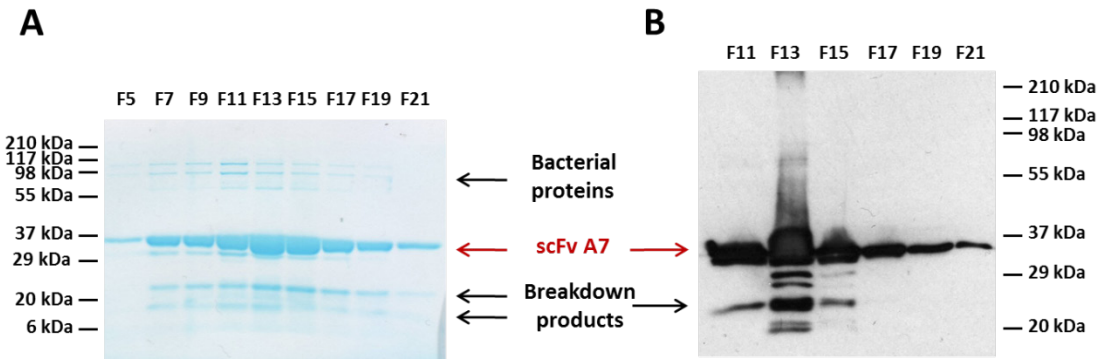

Figure 3.5 Analysis of scFv A7 protein purity

Talon® purified scFv A7 protein fractions resolved in SDS-PAGE gel and stained with colloidal Coomassie brilliant blue (EZBlue) (A) or probed with anti 6-His and anti-mouse HRP conjugated antibody following Western blotting (B). The gels show the presence of a predominant band at 30 kDa corresponding to scFv A7 and breakdown products of lower molecular weight. The presence of high molecular weight contaminant proteins in the Coomassie stained gel probably correspond to bacterial contaminants as they do not show His reactivity in Western blot.

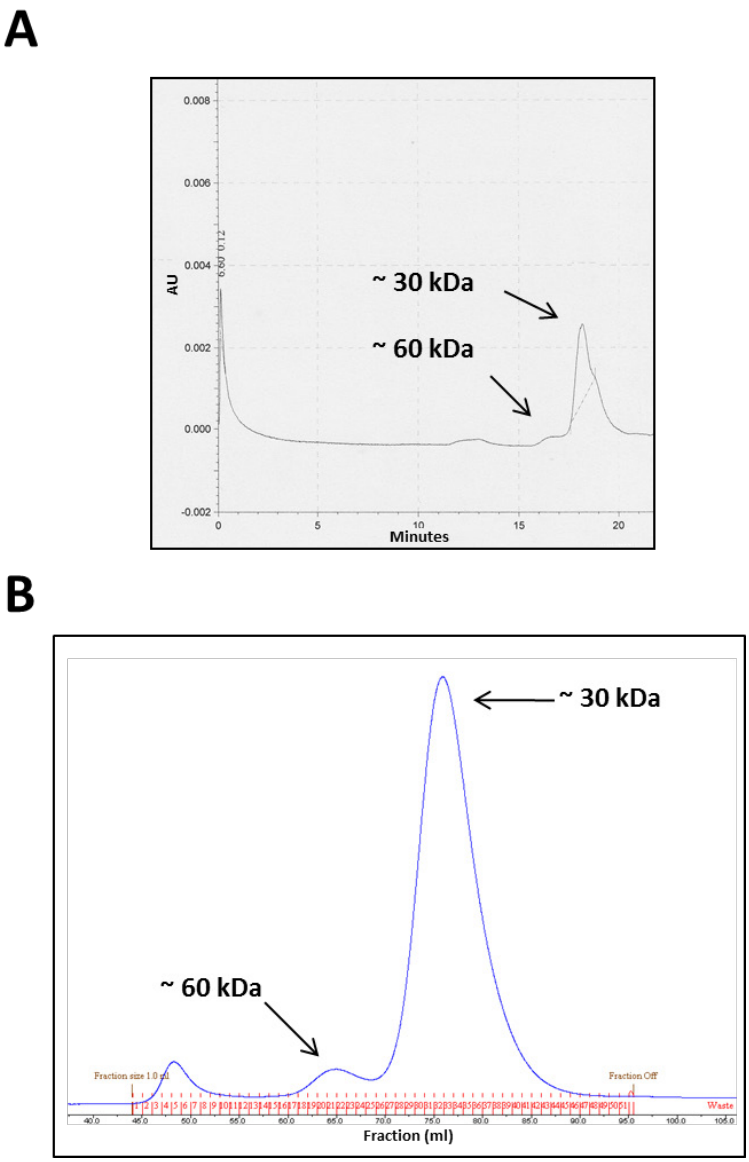

Figure 3.6 HPLC and FPLC analysis of scFv A7

HPLC analysis of scFv A7 Talon® purified using phenomenex silica-based size exclusion column biosep-sec-S-2000. The elution plot shows the presence of a predominant peak at 18-19 minutes corresponding to a predicted molecular weight of 30 kDa, consistent with the size of the monomeric form of scFv A7. A small amount of contaminant proteins can be detected at 16-17 minutes corresponding to 60 kDa (putative scFv A7 dimers) and 12-13 minutes corresponding to proteins over 200 kDa (A). FPLC analysis of scFv A7 Talon® purified using Superdex 75 size exclusion column. The elution plot shows the presence of a predominant peak corresponding to the monomer format of scFv A7 at 30 kDa with small amount of scFv dimers at 60 kDa and contaminant proteins.

3.2.3 Optimisation of immunohistochemistry and assessment of synovial reactivity

Immunohistochemistry (IHC) is a method used to demonstrate the distribution of proteins in tissue sections. This technique is less sensitive than conventional immunoassays, such as Western blot and ELISA, however, IHC combined with optical microscopy allows the assessment of the binding capacity of the test antibody in the context of an intact tissue and provides information on antibody reactivity such as tissue distribution and cellular localisation. Despite a relatively straightforward experimental method, many variables can influence the outcome and the best possible protocol conditions need to be determined for each antibody tested. In particular, the fixation step of fresh tissue was performed using 4% formaldehyde, preserving tissue morphology by protein crosslinking and preventing autolysis and necrosis of the tissue. This step may cause a masking of the target antigen that needs to be retrieved prior to staining procedure. The optimisation of IHC conditions are discussed in this section.

3.2.3.1 Biotinylation of scFv antibody

After purity and quality assessment of the soluble scFv antibody produced, the proteins were conjugated to biotin according to the protocol described in section 2.4. The coupling with biotin allows an amplification of the signal, due to a high molar ratio of biotin to scFv, to be detected using avidin conjugated HRP reagent. The pre- and post-biotinylation scFv antibodies were resolved on coomassie stained SDS-PAGE gel and analysed by HPLC where no loss in protein purity or quality could be detected (Figure 3.7)

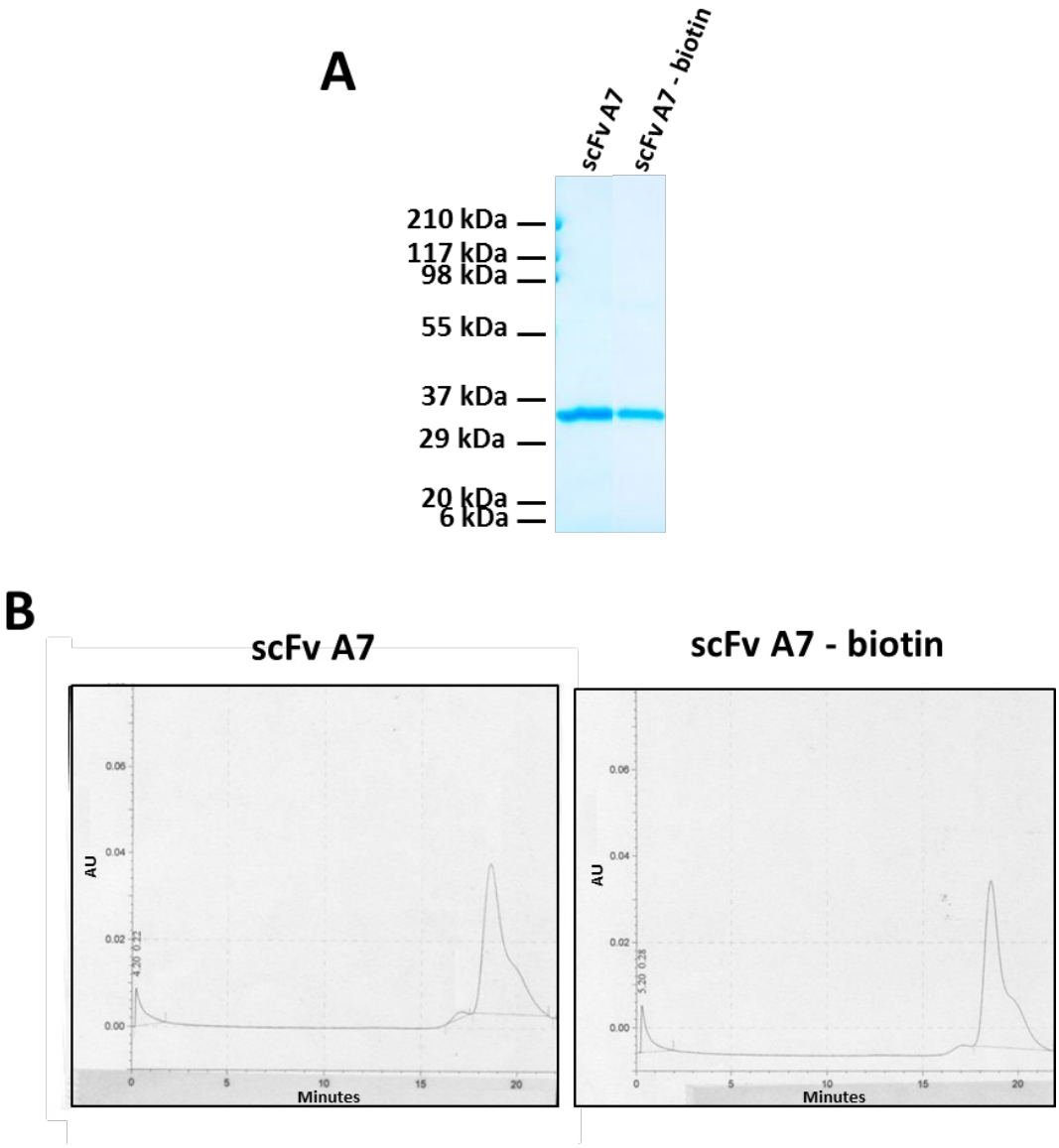

Figure 3.7 Analysis of scFv A7 biotinylation

SDS-PAGE resolved scFv A7 pre- and post-biotinylation stained with colloidal Coomassie brilliant blue (EZBlue) (A) and HPLC analysis (B) show no loss of protein purity or increased aggregation due to the biotinylation procedure.

3.2.3.2 Antigen retrieval procedures in paraffin embedded tissue sections

The process of sample fixation can lead to protein crosslinking that can cause masking of the target antigen, reducing or completely blocking the binding to the specific antibody. In order to remove this artificial alteration of the tissue and restore antigen availability, two different approaches can be used: Proteolytic-induced Epitope Retrieval (PIER) or Heat-induced Epitope Retrieval (HIER). The PIER approach uses the proteolytic activity of an enzyme to partially digest the tissue and unmask the target antigen. The HIER approach utilises heated buffers with different composition and pH to unmask epitopes. Table 3.2 describes a list of PIER and HEIR buffers used to test scFv A7 activity in synovial tissue sections.

The most suitable retrieval procedure to reveal scFv A7 reactivity in human arthritic synovium was assessed via IHC staining in formalin fixed paraffin embedded tissue sections as described in section 2.6.3.1. Briefly, paraffin was removed from the sections via a xylene – ethanol exchange buffer and rehydrated in PBS. Subsequently the sections were incubated with a spectrum of antigen retrieval buffers as listed in Table 3.2. Varying degrees of background noise could be detected between the different buffers. In general proteolytic retrieval appeared to be more efficient while procedures involving heat inactivation showed increased tissue degradation especially at long incubation times (Figure 3.8). Proteinase K retrieval was more convenient due to a combination of a short incubation time (4 minutes) and efficient retrieval of the scFv A7 target antigen with a good signal to noise ratio that did not improve when used in conjunction with other proteolytic enzymes.

PIER	Incubation time
Proteinase K	4 minutes 37 °C
Digest-All^3 (pepsin)	10 minutes 37 °C
Digest-All^3 (pepsin) + proteinase K	10 minutes 37 °C + 4 minutes 37 °C
Chondrotinase	1 hour 37 °C
Chondrotinase + proteinase K	1 hour 37 °C + 4 minutes 37 °C
HIER	
EDTA pH 9	3 minutes boiling in water bath
EDTA pH 9	20 minutes boiling in water bath
0.01% trisodium-citrate pH 6	3 minutes boiling in water bath
0.01% trisodium-citrate pH 6	20 minutes boiling in water bath
Additional procedure	
HCl 2 M	10 minutes room temperature

Table 3.2 Antigen retrievals

List of buffers tested in antigen retrieval procedure for scFv A7 staining in arthritic synovium tissue sections.

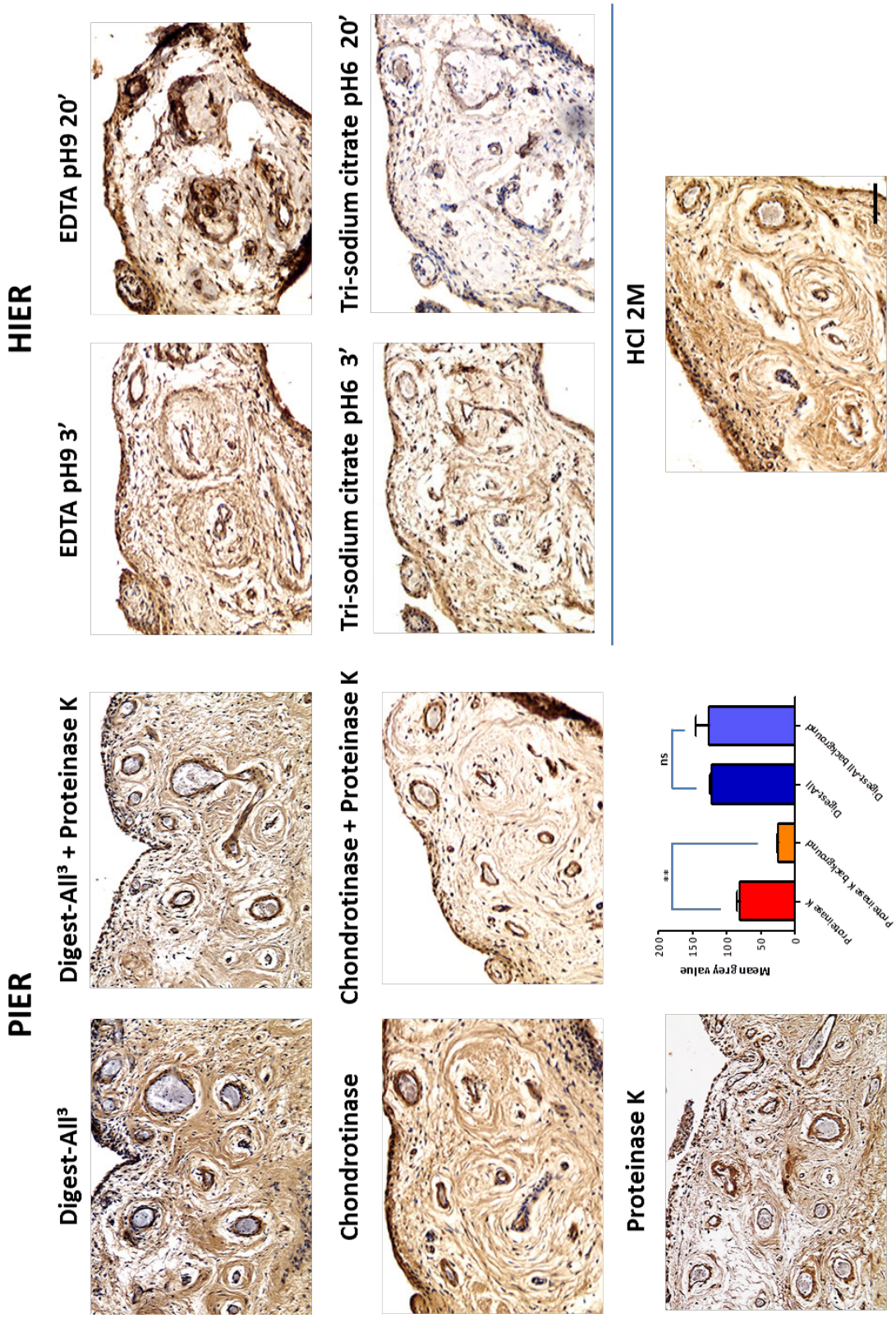
HIER
EDTA pH9 20'
Tri-sodium citrate pH6 20'
EDTA pH9 3'
Tri-sodium citrate pH6 3'
HCl 2M
PIER
Digest-All³ + Proteinase K
Chondrotinase + Proteinase K
Digest-All³
Chondrotinase
Proteinase K
Mean grey value
200
150
100
50
0
**
ns
Proteinase k
Proteinase k background
Digest-All
Digest-All background

Figure 3.8 Comparison of retrieval procedures in arthritic synovium

RA synovial tissue sections treated with PIER, HIER or HCl retrieval procedures. Staining obtained with biotinylated scFv A7 and detected with ABC-HRP. Various degrees of signal to noise ratio were detected among the different procedures tested. Proteinase K showed a significant difference between positive staining and background signal when mean grey value was compared between vessel area and a comparable region in a non-relevant portion of the tissue. A total of 5 vessels and 5 non-vascular areas were counted per sample, values expressed as mean ± SD. (Mann-Whitney test ** = p value <0.01, ns = not significant). Scale bar = 100 µm.

3.2.3.3 Analysis of scFv monomer reactivity in human arthritic synovium

FPLC was performed as an additional purification step in order to increase the purity of the protein and isolate the monomeric form of scFv A7. To do this, 1 mg of purified antibody protein was loaded on a Superdex 75 size exclusion column, eluted and single fractions collected, obtaining a separation of the total protein content of purified periplasmic extract (Figure 3.9 A). The protein fractions were pooled together in groups and analysed by SDS-PAGE and Western blot analysis in reducing conditions (Figure 3.9 B and C). In order to characterise the role of the monomeric form of scFv A7 in the reactivity observed in arthritic synovium, the fractions comprising the main peak and corresponding to the monomer were pooled so as to generate three fractions. Each fraction pool was then biotinylated according to the protocol described in section 2.4, reaching comparable protein to biotin ratio (generally 2 biotin molecules per protein). Their reactivity was assessed by immunohistochemistry on OA samples and compared to that of the protein before FPLC purification. The reactivity and signal to noise ratio observed in the monomeric peak proved to be significantly different between the central fraction (yellow) and the third fraction (red) but no statistically significant difference was shown between the central fraction (yellow) and the scFv pre-FPLC (Figure 3.10). These results therefore demonstrate that the bacterial protein contaminants and the breakdown products present in scFv A7 preparations (Figure 3.5) do not contribute or substantially interfere with the specific interaction between this antibody and its antigen in IHC.

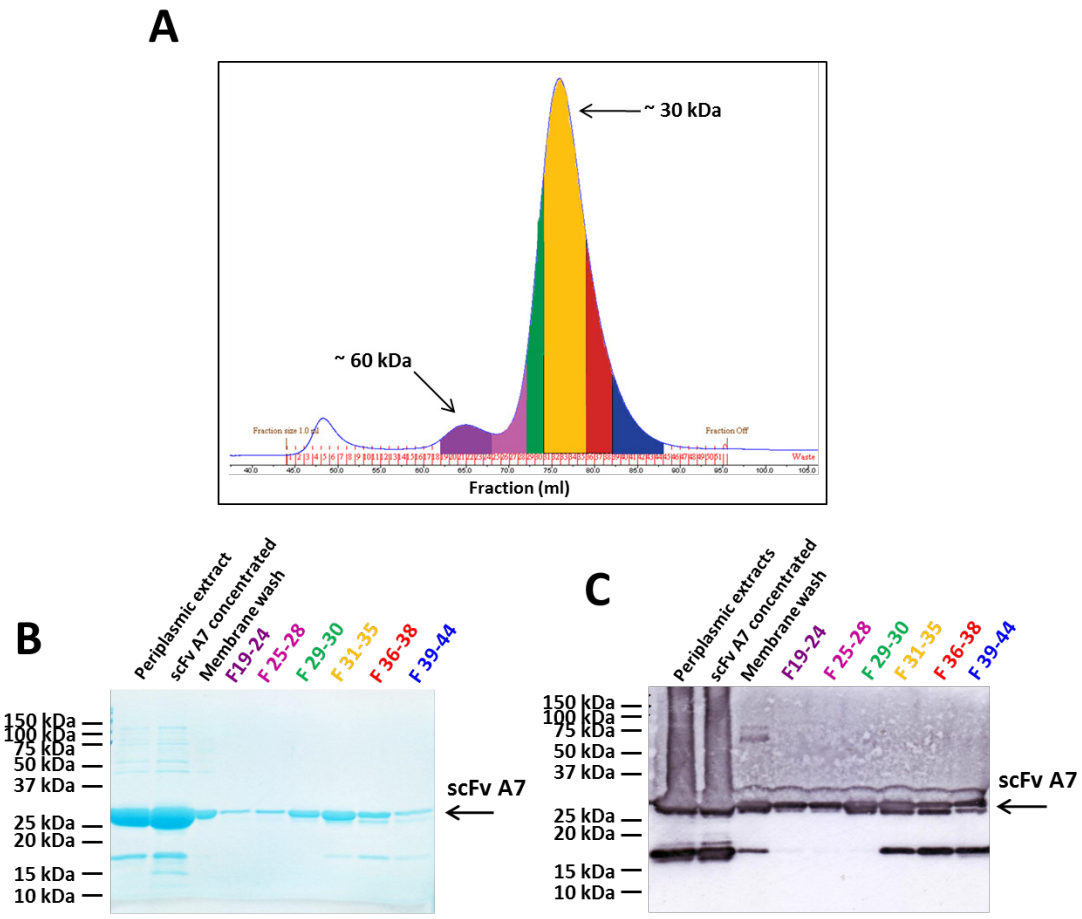

Figure 3.9 Analysis of scFv A7 protein fractions from FPLC

Pooled fractions from FPLC purification of scFv A7 depicted by colour visualisation (**A**). SDS-PAGE analysis of FPLC purified fractions of scFv A7 stained with colloidal Coomassie brilliant blue (EZBlue) (**B**) or probed with anti 6-His and anti-mouse HRP conjugated antibody (Western blotting) (**C**).

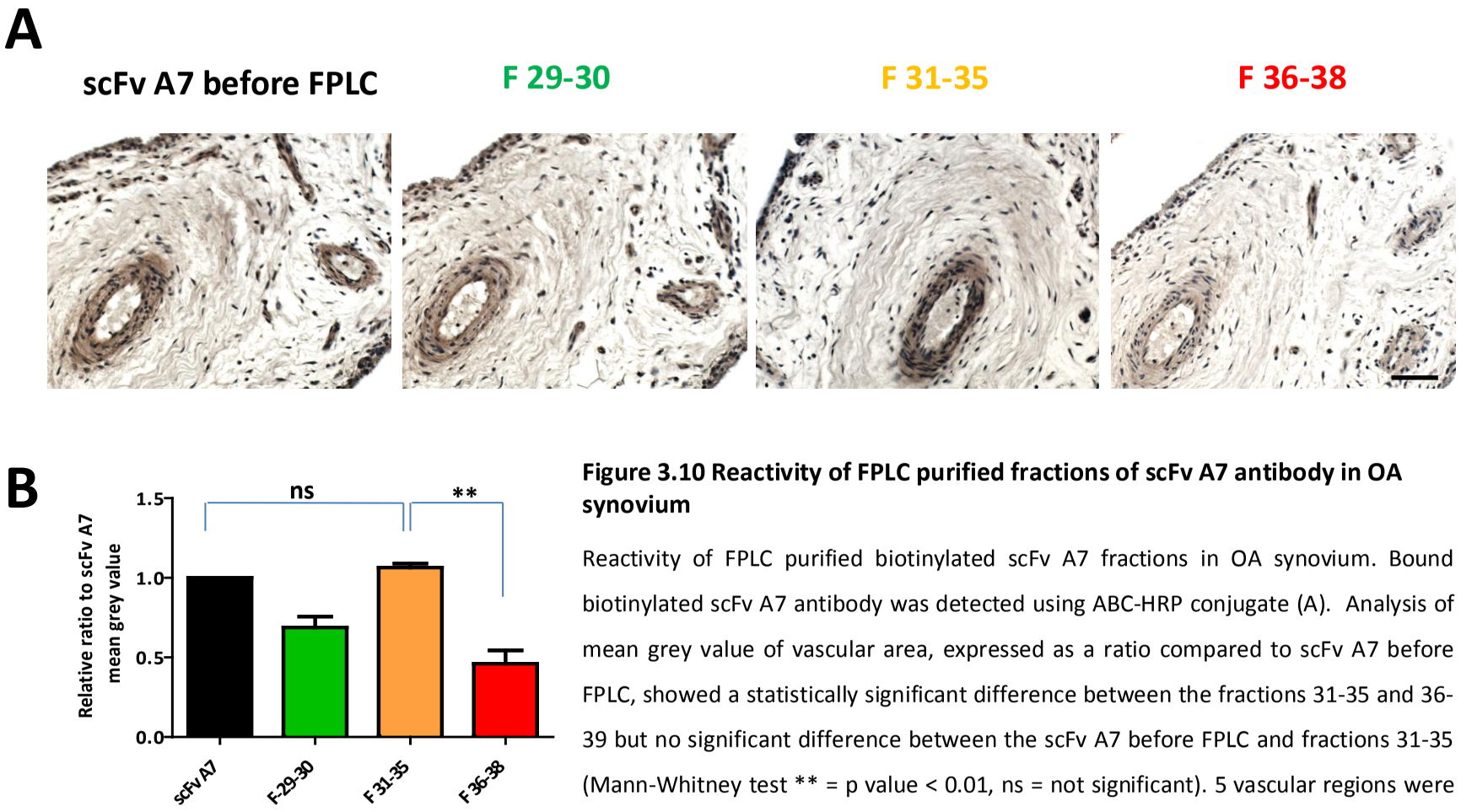

Figure 3.10 Reactivity of FPLC purified fractions of scFv A7 antibody in OA synovium

Reactivity of FPLC purified biotinylated scFv A7 fractions in OA synovium. Bound biotinylated scFv A7 antibody was detected using ABC-HRP conjugate (A). Analysis of mean grey value of vascular area, expressed as a ratio compared to scFv A7 before FPLC, showed a statistically significant difference between the fractions 31-35 and 36-39 but no significant difference between the scFv A7 before FPLC and fractions 31-35 (Mann-Whitney test ** = p value < 0.01, ns = not significant). 5 vascular regions were counted per sample, values expressed as mean ± SD. Scale bar = 50 µm.

3.3 A7 scFv-Fc protein production

In collaboration with the University of Eastern Piedmont in Novara, Italy, the scFv A7 antibody was fused with the C_H2 and C_H3 domain of a human IgG, as described in detail in section 2.2, to form a mini antibody defined as scFv-Fc (234). As a scFv-Fc fusion protein, this IgG-like structure differs from the conventional IgG1 form due to the missing C_H1 and C_L domains. The natural IgG1 format is characterised by the expression of a separate light and a heavy chain, linked by a disulphide bond at the C_H1-C_L interface, and by the presence of a hinge region connecting two heavy chains in a homodimer fashion through the formation of two disulphide bonds (153, 252). However, the role of the missing C1 domain of both heavy and light chain in the scFv-Fc construct is played by the small peptide linker between the V_H and V_L domains. Using this strategy, the heavy and light chains are expressed as a single chain, and the presence of the IgG1 hinge region allows the formation of disulphide bonds linking the two chains forming a homodimeric structure. In addition, the presence of the C_H2 and C_H3 domains allows N-glycosylation, promoting and stabilising the Fc dimerisation (252-254). The vector map used to produce the molecule and a schematic of the scFv-Fc structure is described in Figure 3.11. The nucleotide sequence encoding for the scFv A7 has been optimised for mammalian expression systems prior to cloning in the Fc containing vector.

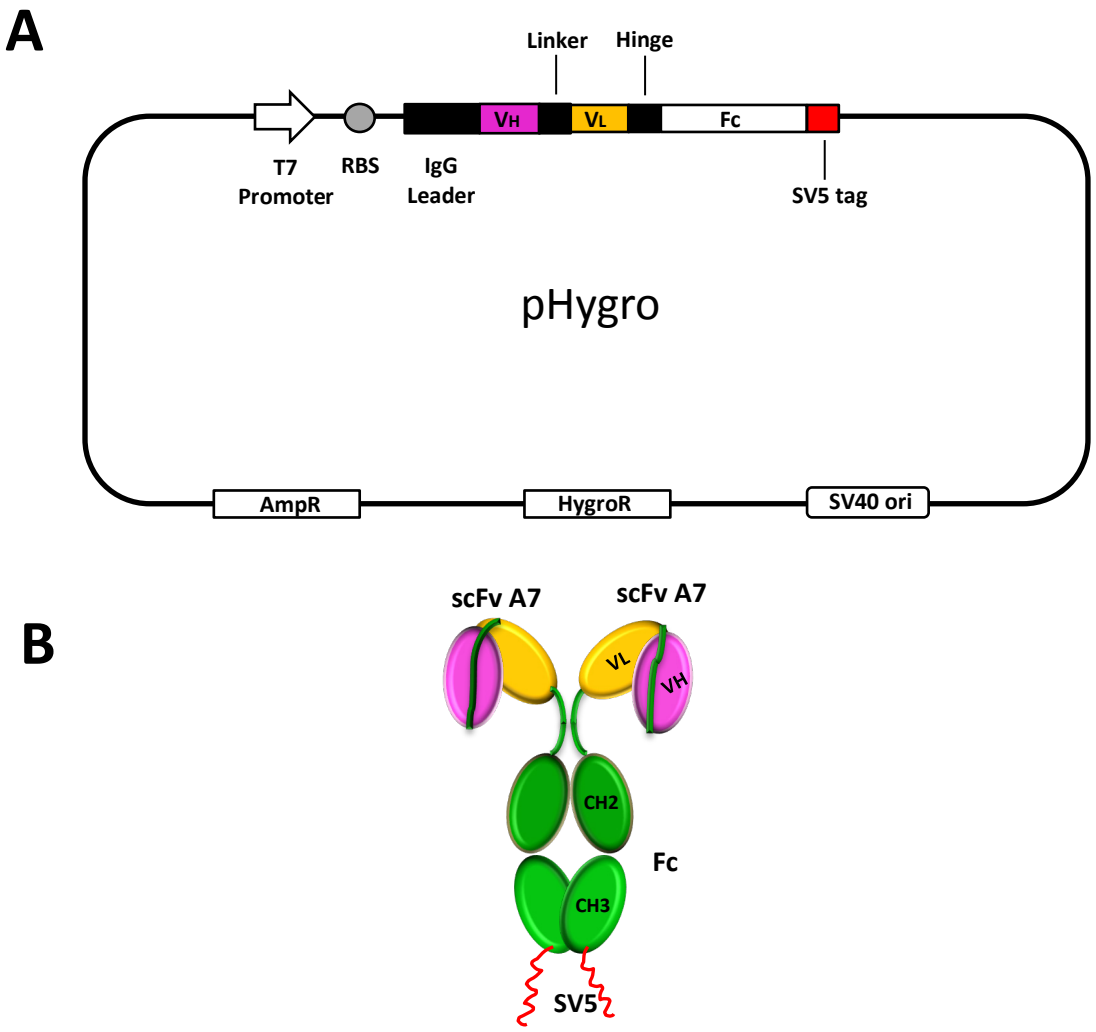

Figure 3.11 pHygro vector and A7 scFv-Fc protein structure

Schematic of pHygro vector encoding the scFv-Fc gene with the IgG leader sequence containing a mini intron (A). Schematic of the expressed A7 scFv-Fc protein showing the scFv domain linked to the IgG1 Fc domain and carrying the SV5 tag (B).

In order to ensure the correct dimerization of the A7 scFv-Fc protein and a correct Fc effector function, it is of pivotal importance to promote efficient glycosylation of the Fc domain (254). The bacterial expression system used for the scFv antibody fragment is extremely efficient, allowing the production of large protein quantities. However, bacteria are not able to perform post-translational modifications on the produced proteins. This shortcoming would not allow glycosylation of the Fc region potentially resulting in protein mis-folding and low yields (255). In order to overcome this limitation, a mammalian expression system was adopted for efficient scFv-Fc protein production. Specifically, a Chinese Hamster Ovary (CHO) derived cell line able to grow in suspension in serum free medium (CHO-s) was used as a primary expression system. The absence of serum in the culture medium eliminates the possibility of contaminant bovine immunoglobulins during antibody purification. CHO-s cells were transfected with the scFv-Fc pHygro vector, as described in section 2.2.2.1, in a culture medium containing the selective agent Hygromycin B to select for efficiently transfected cells. The surviving cell population was then diluted to a single cell suspension in order to monitor growth and protein production of a single clone and select the most efficient (Figure 3.12). The presence of the A7 scFv-Fc antibody in the culture medium was confirmed by Coomassie stained SDS-PAGE and Western blot (Figure 3.13).

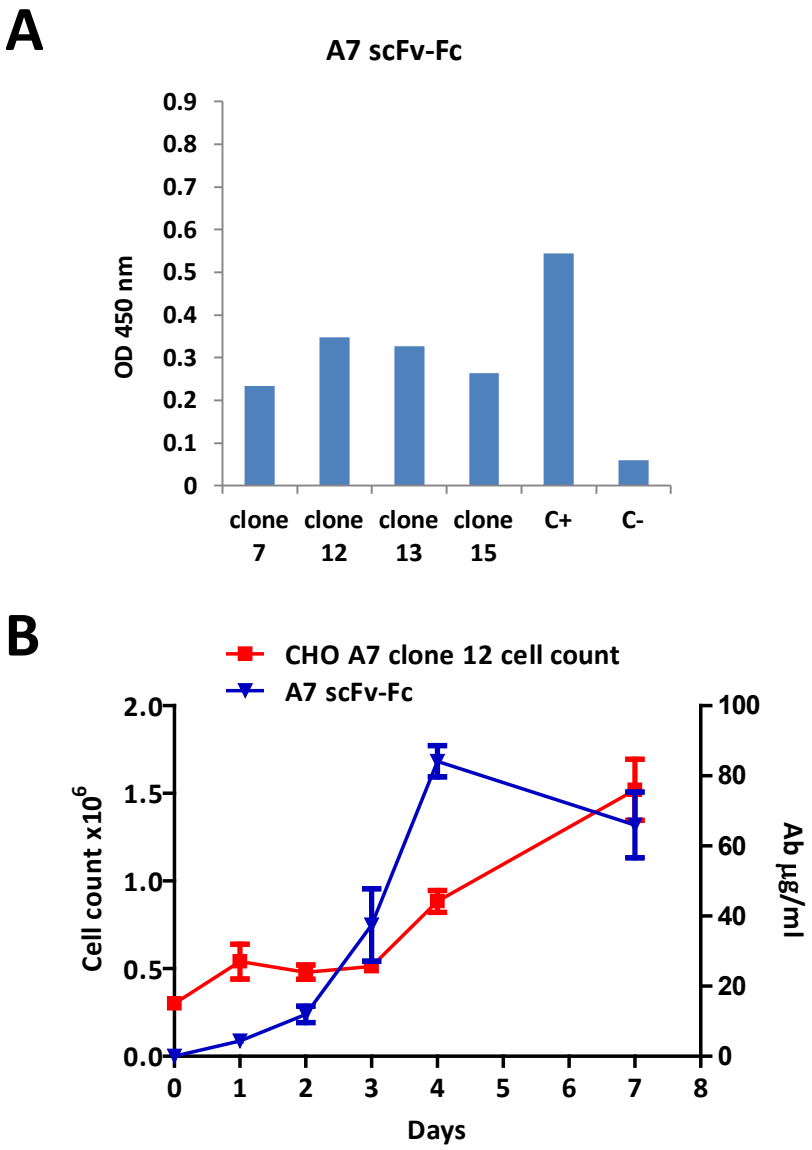

Figure 3.12 Selection of A7 scFv-Fc CHO-s expressing clone

ELISA assay on culture supernatant of transfected CHO-s clones carrying the A7 scFv-Fc construct. ELISA performed on anti-Human Fc coated plates and presence of scFv-Fc antibody detected using anti-SV5 and anti-mouse HRP conjugated antibody. Positive clone (C+) and negative clone (C-) included as control (A). Comparison of correlation between cell number and scFv-Fc protein content in the supernatant of CHO-s clone 12 detected at different time points (B).

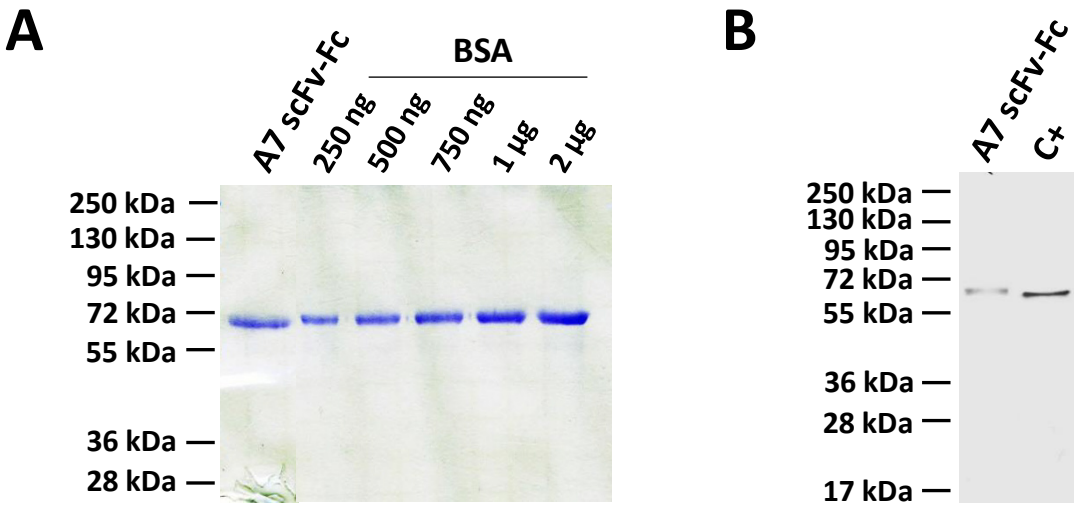

Figure 3.13 A7 scFv-Fc production from CHO-s

SDS-PAGE resolved A7 scFv-Fc from CHO-s clone 12 stained with Coomassie brilliant blue (A) or probed with anti-SV5 and anti-mouse AP conjugated antibody following Western blotting (B). Positive clone (C+) included as control.

3.3.1 Optimisation of A7 scFv-Fc purification

The high efficiency observed in Talon® purification of scFv antibodies cannot be applied to the purification of the scFv-Fc fusion protein due to the absence of a 6-His tag. However, protein A purification is an established method for IgG purification (256) and was used as primary purification system in this context. Culture supernatant from stably transfected CHO-s cells bearing the A7 scFv-Fc encoding vector, was collected, incubated with protein A Sepharose beads, as described in detail in section 2.2.3.1, and the purification was carried out with the same principle as applied for scFv protein A purification in section 3.2.1. Analysis of the eluted fractions with a spectrophotometer at 280 nm showed high readings in the first elution fractions (Figure 3.14 A). Fractions showing similar readings were pooled and dialysed overnight in PBS for buffer exchange. Presence of the A7 scFv-Fc protein was assessed through Coomassie stained SDS-PAGE and Western blot probing with an anti-SV5 tag antibody, showing the prevalence of a single band at 60 kDa corresponding to the size of the scFv-C_H2-C_H3 chain under reducing conditions without detectable contaminant proteins and with only minor protein loss in the flowthrough and washing steps (Figure 3.14 B and C). This purification protocol was able to purify up to 20 mg/L.

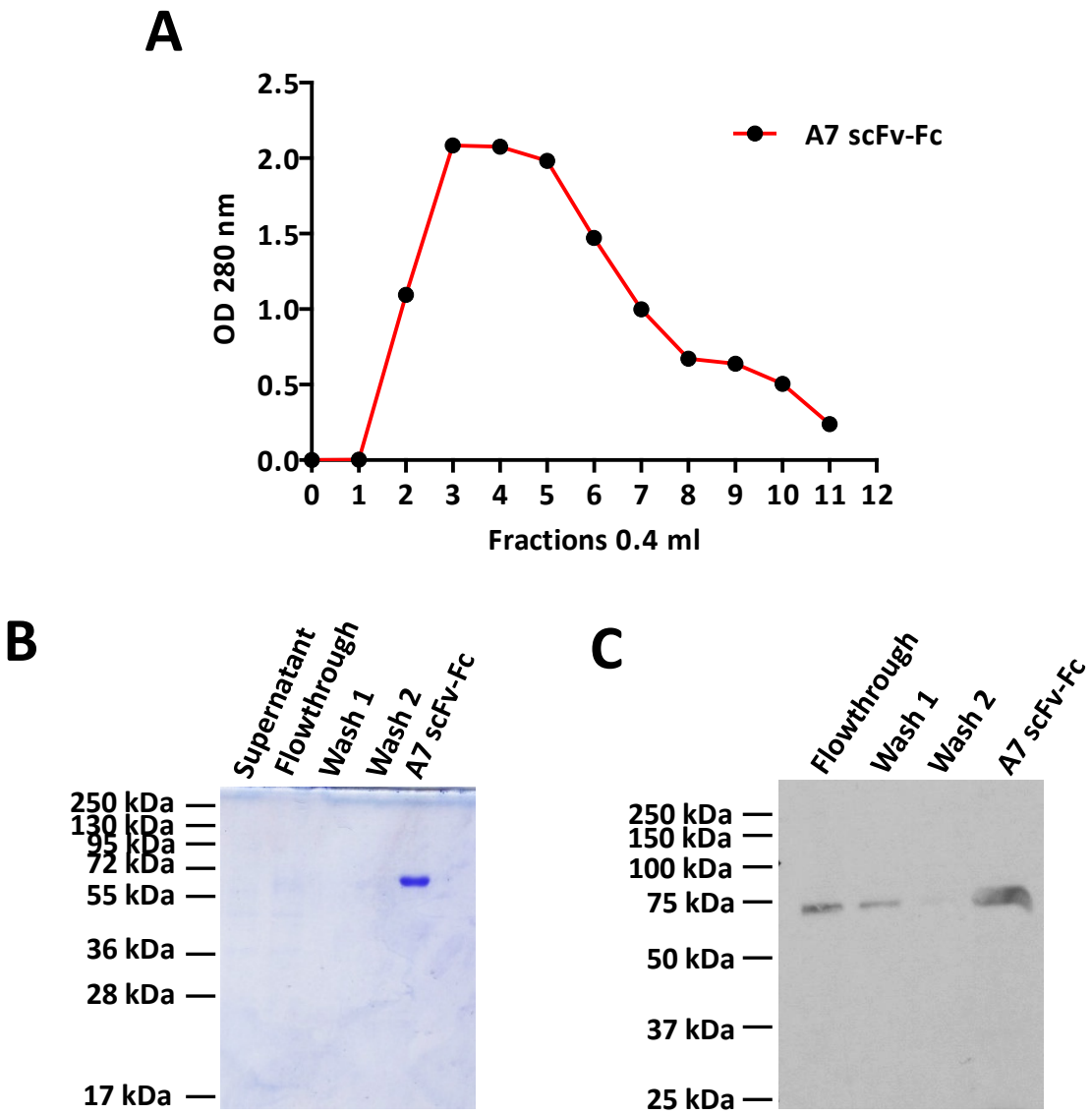

Figure 3.14 A7 scFv-Fc production and purification via CHO-s

Optical density analysis of A7 scFv-Fc eluted fractions from CHO-s supernatant using protein A purification system (A). SDS-PAGE resolved purified A7 scFv-Fc fractions from CHO-s stained with Coomassie brilliant blue (B) or probed with anti-SV5 and anti-mouse HRP antibody following Western blotting (B).

Protein A purification requires an acidic elution step at pH 2.8 that may not be well tolerated by some antibodies, leading to conformational changes and often causing degradation and formation of insoluble aggregates (257). To overcome this possible scenario, a simple culture supernatant concentration step was adopted as an alternative purification procedure as described in section 2.2.3.2. In this case, to reduce the carryover of detergents contained in the culture medium, the supernatant was dialysed in PBS before and after concentration. Analysis in Coomassie stained SDS-PAGE and Western blot in Figure 3.15, show the presence of the predominant band at 60 kDa, confirming the presence of A7 scFv-Fc with little detectable contaminant proteins.

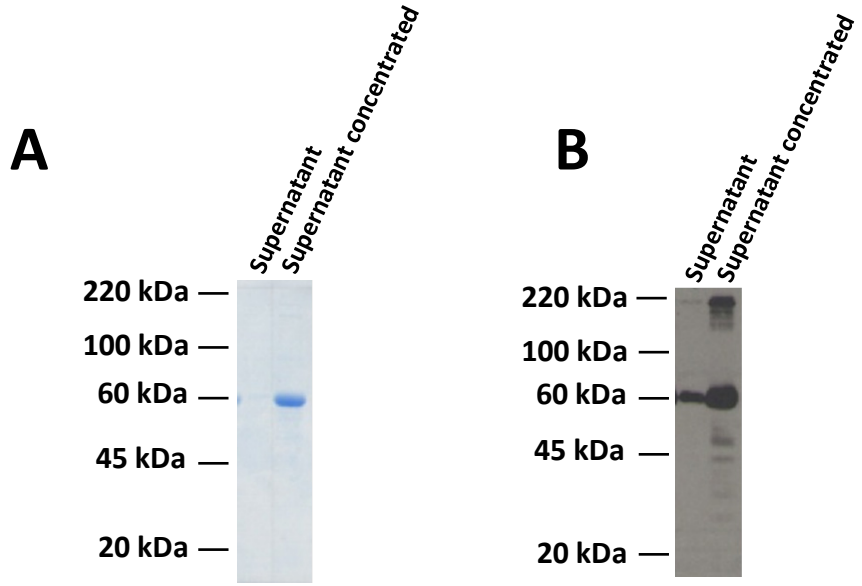

Figure 3.15 Concentration of CHO-s culture medium

300 ml of CHO-s stably transfected with A7 scFv-Fc concentrated using Millipore centricon filter unit (MWCO 10 kDa). 3 µl of supernatant and concentrated supernatant resolved in 10% SDS-PAGE and stained with Coomassie brilliant blue, showing a single band at 60 kDa corresponding to the A7 scFv-Fc protein (A). 1 µl of supernatant and concentrated supernatant resolved in 10% SDS-PAGE and detected with anti-SV5 and anti-mouse HRP conjugated antibody, showing the presence of a predominant band at 60 kDa corresponding to the A7 scFv-Fc antibody and several breakdown products at lower molecular weight (B).

3.3.2 Quality assessment of A7 scFv-Fc protein production

Protein A purified A7 scFv-Fc from CHO-s cells showed the presence of a marked band at 60 kDa with no detectable contaminant proteins (Figure 3.14). In order to further investigate the protein composition of the purified batch from CHO cell line, SDS-PAGE resolved protein batch was stained with Sypro® Ruby protein gel stain, as described in section 2.5, characterised by a limit of detection of 0.25 ng. The plot profile of A7 scFv-Fc purified from CHO-s cells analysed with ImageJ, showed the presence of a single peak at 60 kDa accounting for 87% of signal above background (Figure 3.16 A and B).

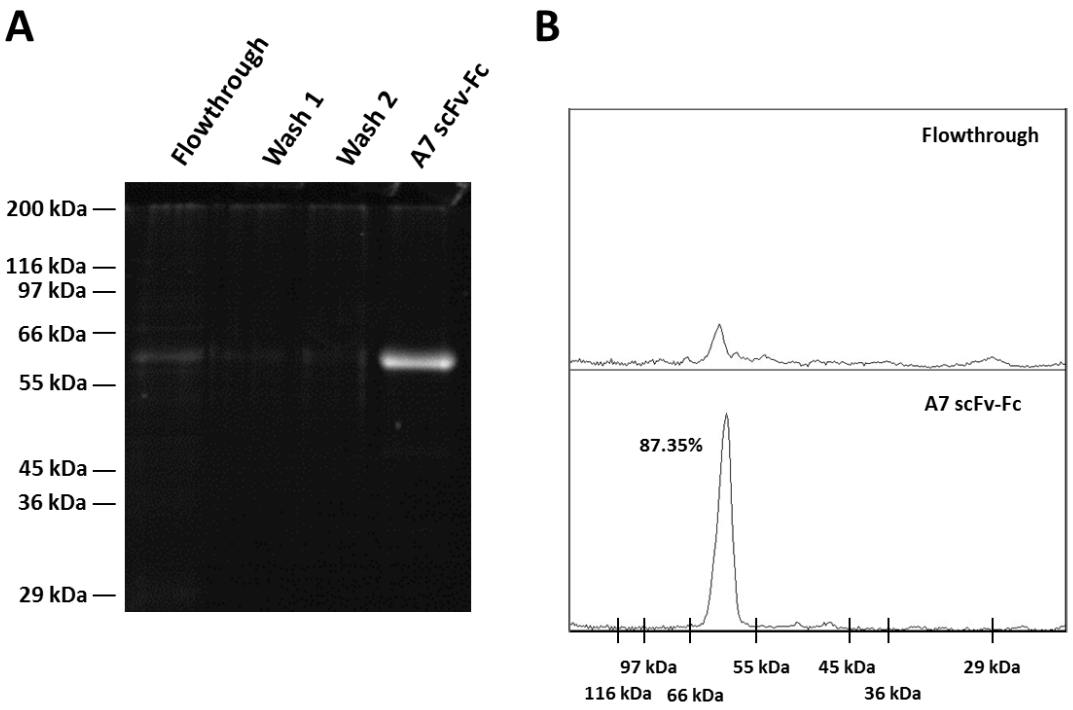

Figure 3.16 Quality assessment of CHO-s produced A7 scFv-Fc

SDS-PAGE resolved A7 scFv-Fc produced in CHO-s (A) stained with Sypro® ruby protein gel stain. Analysis of plot profile from the purified A7 scFv-Fc lane produced in CHO-s (B) reveals a high purity of produced antibody with little detectable contaminant proteins.

3.3.3 Assessment of A7 scFv-Fc reactivity in human arthritic synovium

Prior to IHC staining on human arthritic synovium, the A7 scFv-Fc antibody was biotinylated with the same procedure that was applied to the scFv antibody and described in section 2.4. SDS-PAGE resolved protein pre- and post-biotinylation showed no loss of purity and protein quality (Figure 3.17) with a biotin to protein molar ratio over 2.

A critical point to the development of an IgG-like version of the scFv A7 is the retention of A7 specific synovium reactivity. The ability of the scFv-Fc fusion protein to target the human arthritic synovial tissue was assessed using the optimised protocol adopted for scFv staining and described in section 2.6.3.1. The pictures presented in Figure 3.18 show a similar staining pattern between the scFv and the scFv-Fc antibodies. This result confirms the retention of the scFv A7 reactivity in the new antibody format. In addition, since the acidic elution step included in the protein A purification procedure may cause conformational changes in the protein leading to loss of activity (257), the reactivity of the protein A purified A7 scFv-Fc protein was compared to the reactivity of the A7 scFv-Fc obtained through supernatant concentration. The results in Figure 3.19 show a stronger reactivity of the concentrated protein. However, an increased background level could be detected at high antibody concentrations, probably due to the presence of contaminant proteins in the pool that can be processed during the non-selective biotinylation step contributing to background noise.

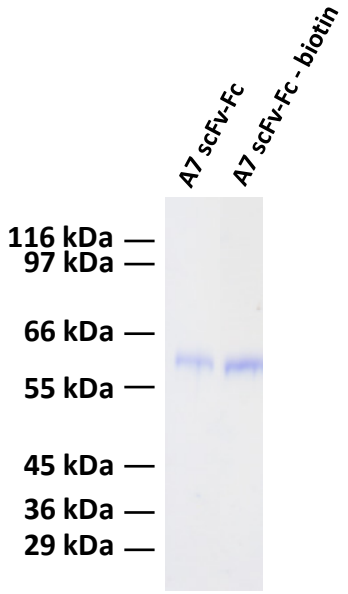

Figure 3.17 Biotinylation of A7 scFv-Fc antibody

Coomassie stained SDS-PAGE of A7 scFv-Fc pre- and post-biotinylation, resolved in 10% polyacrylamide gel. No increase in breakdown products could be detected after biotinylation process.

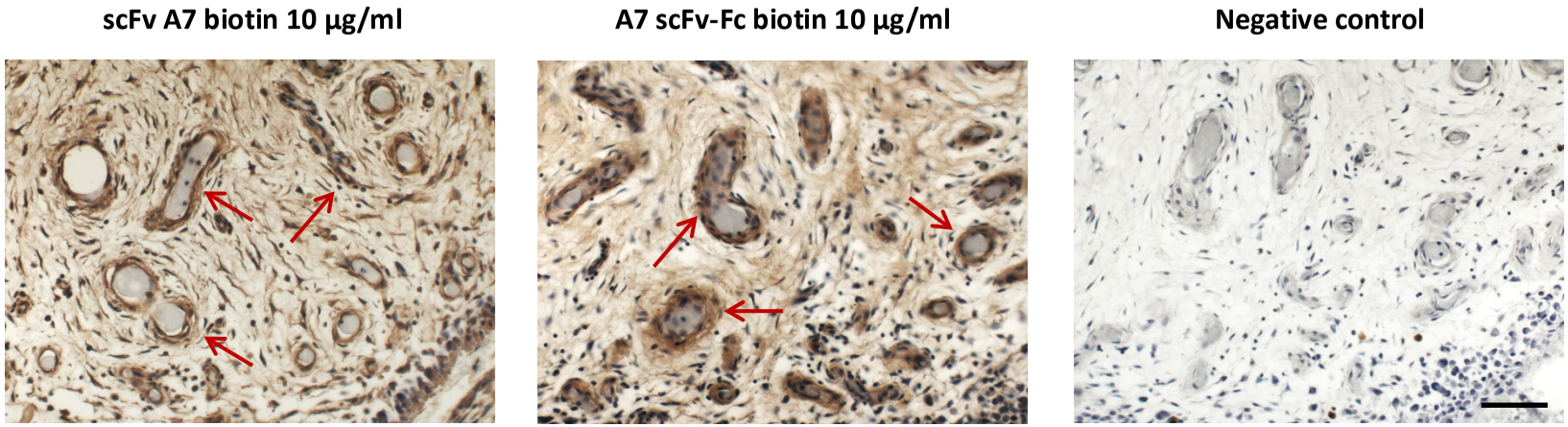

Figure 3.18 Reactivity of A7 scFv-Fc

IHC on OA synovium stained with biotinylated scFv A7 at 10 µg/ml, biotinylated A7 scFv-Fc at 10 µg/ml and control section without primary antibody. Binding of antibody to the tissue section detected with ABC-HRP. Both scFv A7 and A7 scFv-Fc were reactive in arthritic synovium showing a similar staining pattern as depicted by the red arrows. Scale bar = 50 µm.

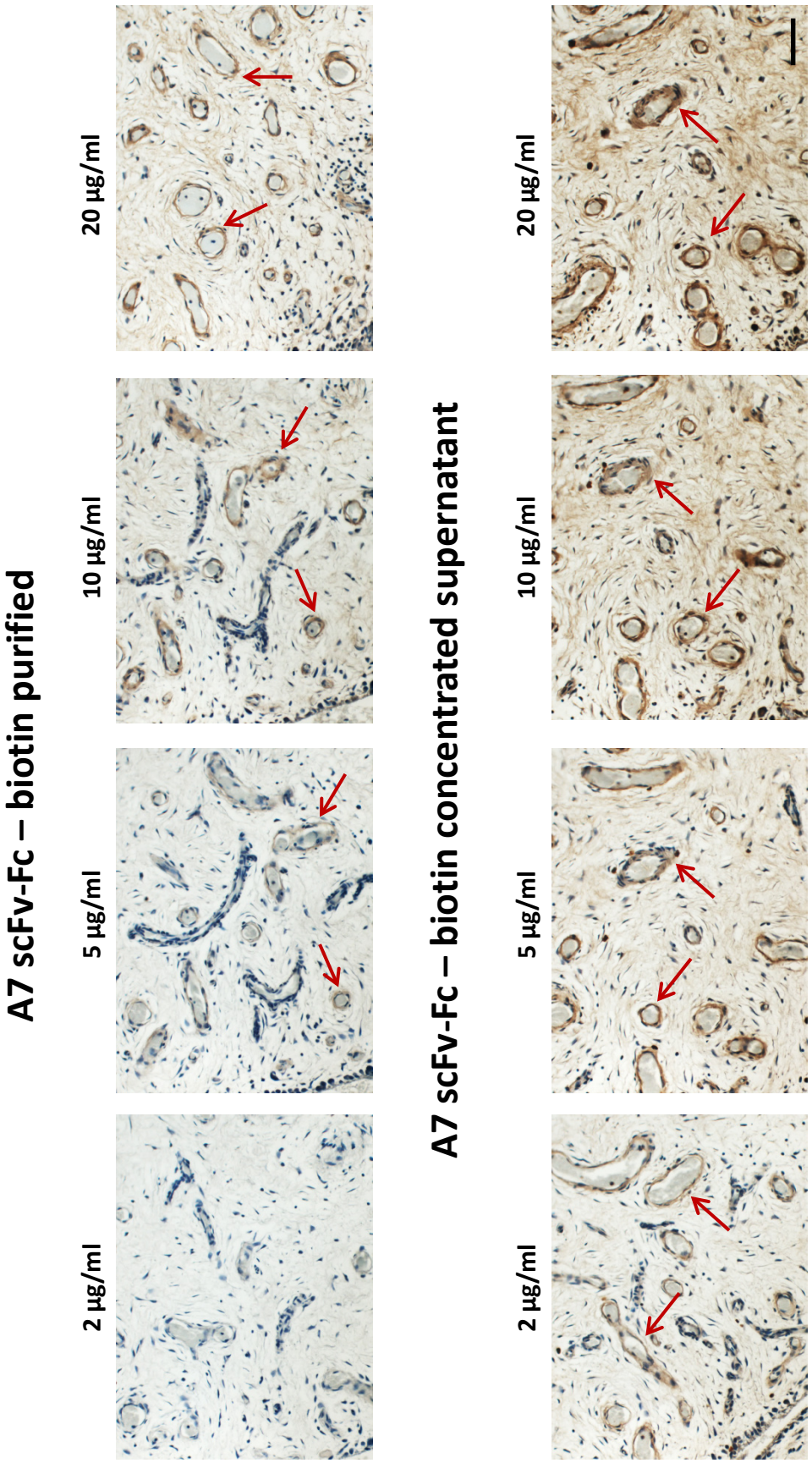
A7 scFv-Fc – biotin purified
20 µg/ml
10 µg/ml
5 µg/ml
2 µg/ml
A7 scFv-Fc – biotin concentrated supernatant
20 µg/ml
10 µg/ml
5 µg/ml
2 µg/ml

Figure 3.19 Comparison of protein A purified and supernatant concentrated A7 scFv-Fc

IHC on OA synovium stained with protein A purified A7 scFv-Fc – biotin and supernatant concentrated A7 scFv-Fc – biotin. Both antibodies were able to target the synovium with a similar pattern (red arrows). The supernatant concentrated A7 scFv-Fc showed stronger reactivity compared to the protein A purified protein but showing also showed a higher background at high concentrations. Scale bar = 50 µm.

3.4 Discussion

The aims of the experiments presented in this chapter were to characterise the production efficiency of the scFv A7 and the A7 scFv-Fc fusion protein in terms of protein yield and quality. In addition, an effort was made towards the optimisation of the procedures for immunohistochemistry to be used for assessment of tissue, disease and species specificity of A7 described in the next chapter.

The first important step when working with antibody fragments isolated through phage display is to verify the ability of the clone to produce a soluble protein. The Tomlinson library adopted for the scFv A7 isolation consists of a vector carrying the scFv gene fused to the gIII phage gene by the presence of the Amber stop codon. Phages are produced via transformation of a permissive *E.coli* strain that will translate the amber codon, allowing the formation of the scFv-pIII fusion protein. In order to produce the soluble scFv protein, phages carrying the clone of interest are used to infect a non-permissive host that will recognise the stop codon and produce only the scFv protein. However, due to the nature of the high diversity of the library which guarantees the production of a high number of different scFv with different specificities, it is possible that the amber stop codon would be present in the scFv sequence itself, impeding the production of a soluble scFv protein. This possible scenario, together with the unpredictability of protein properties due to the primary antibody sequence itself, requires a careful characterisation of production efficiency and protein reactivity. The scFv A7 clone was readily produced by the HB2151 *E.coli* strain upon IPTG stimulation. The protein recovered from culture supernatant or from the periplasmic compartment was purified using two approaches: protein A purification, exploiting the ability of protein A to bind the V_H3 framework, and the Talon® metal affinity purification, exploiting the 6-His tag. Both resins were used in gravity flow column chromatography. The use of a column system is important because it ensures a more efficient washing step and the retention of bead particles. In addition, column based chromatography guarantees a better separation of the protein mixture

present in the starting medium, due to the Theoretical Plate Model. This plate model supposes that the chromatographic column contains a large number of separate layers, called *theoretical plates*. Separate equilibrations of the sample between the stationary and mobile phase occur in these "plates", moving the analyte down the column by transfer of equilibrated mobile phase from one plate to the next. The resolution between two peaks, in this case two proteins with similar molecular weights, depends on the number of theoretical plates, with this number varying according to the length of the column and the tightness of the packed bead volume. A higher number of theoretical plates increases the resolution power of the column (258). Talon® proved to efficiently purify the scFv A7 with higher yield compared to protein A. Analysis of protein purity and quality in SDS-PAGE, HPLC and FPLC showed the monomer of scFv A7 as the predominant protein following Talon® purification, with little detectable contaminants. Purification with Talon® metal affinity resin has been therefore chosen as the primary purification strategy for scFv A7.

In order to optimise the conditions to be used in IHC for tissue staining, a comprehensive panel of retrieval procedures was used to identify the best candidate. Proteinase K was able to provide a good signal to background noise ratio and was selected as standard protocol for IHC. Furthermore, an in-depth analysis was made on the reactivity of the components of the scFv A7 purified protein content. Specifically, the main peak corresponding to scFv A7 monomer was divided in 3 groups following FPLC purification and the reactivity in human arthritic synovium was determined for each of them in comparison to the full scFv A7 pool. Despite a significant difference in the reactivity of the central fraction and the one showing a lower molecular weight, compared to the total scFv A7 pool the reactivity was not significantly different, meaning that the presence of contaminant proteins and background products do not inhibit or impair the scFv A7 reactivity and therefore it can be safely used following Talon® purification without need of further purification steps.

The increasing interest that has been focused on scFv development in recent years is to be attributed mainly to the extreme efficiency of phage display

technology in isolating *in vivo* specific peptides and antibody fragments allowing the characterisation of new organ specific antigens (130, 259, 260). Another key characteristic of this class of antibody fragments, is the high versatility of these molecules, allowing a large spectrum of functionalisation strategies with effector moieties including conjugation with cytokines, therapeutic radionuclides, photosensitisers and established therapeutic molecules (261). This high versatility can also be exploited to convert the scFv fragment into an IgG-like molecule by fusing the IgG Fc domain to the protein (234). By fusing the scFv to the C_H2 and C_H3 domain of an IgG1, the protein acquired the structural and functional characteristics of a native IgG molecule. In particular, this format allows having a bivalent molecule with increased avidity, higher molecular weight, determining higher serum half-life, and introduction of Fc effector functions (153, 252, 262). Since bacteria are not equipped for post-translational modifications and glycosylation exerts a pivotal role in IgG structural integrity and functions (254), the mammalian CHO expression system was chosen as the primary production platform. The use of mammalian expression systems for biopharmaceutical molecules is well accepted (263), furthermore, CHO cells have been demonstrated as safe hosts for the past two decades, with several FDA approved derived products, and are capable of efficient post-translational modifications that are compatible and bioactive in humans, making them the cell line of choice in biopharmaceutical production (264).

CHO demonstrated an efficient production of the scFv-Fc fusion protein at high yield and with high purity levels following protein A purification. The staining pattern of the scFv-Fc molecule was comparable to the one observed with the parent scFv antibody fragment. However, the acidic elution step necessary for antibody recovery in protein A purification, seemed to partially impair the reactivity of the A7 scFv-Fc. When compared to a concentrated supernatant preparation of the antibody showing very low contaminant proteins, the protein A purified protein needed a concentration 5 times higher to obtain a detectable signal. The use of concentrated supernatant may be acceptable for *in vitro* testing of the antibody reactivity but a purified antibody preparation will be necessary for *in vivo* testing.

Although the reactivity of the protein A purified antibody does not seem to be inhibited but only partially impaired and can therefore be used as standard approach for protein production, testing alternative elution buffers requiring less stringent pH conditions remains an important aspect to investigate (257).

In summary, this chapter provides the ground base conditions for functional characterisation of both the scFv A7 and the A7 scFv-Fc antibodies described in the following chapters.

Chapter 4

Characterisation of scFv A7 reactivity

4.1 Introduction

Phage display has proven a potent tool to select and identify new vascular determinants showing organ specificity *in vivo* that may have an impact in the field of targeted drug delivery (130, 259). The scFv A7 antibody fragment isolated via *in vivo* phage display in SCID mouse model double transplanted with human arthritic synovium and normal human skin (described in section 1.4.2), showed a preferential homing specificity for the synovium compared to the control human skin tissue. The 4 enrichment cycles employed, have guaranteed the bias towards clones showing high specificity for the synovium compared to the skin control tissue, confirmed by the *in vivo* recirculation experiment using the soluble scFv fragment (described in section 1.4.2 introduction). The preferential homing capacity of this clone for the human synovium may suggest the targeting of a synovium specific molecule or a molecule subjected to overexpression in arthritic conditions. However, the presence of the target antigen in other human tissues or disease conditions still remains to be assessed. In order to develop the scFv A7 antibody into a therapeutic tool for the treatment of rheumatoid arthritis and related arthritic conditions, it is crucial to investigate the two main aspects that may have an impact on the antibody efficacy: tissue specificity and disease specificity. Towards the first aspect, it is important to thoroughly investigate the tissue distribution of the target antigen and evaluate the scFv A7 reactivity in normal human tissues. As a therapeutic tool for arthritic conditions, the disease specificity of the antibody plays a pivotal role. The inflammatory condition underlying rheumatoid arthritis can influence the expression of selective cell adhesion molecules in the microvasculature to direct circulating lymphocytes (265). However, the expression of such molecules in the inflamed synovial tissue may be due to the inflammatory condition rather than being a disease specific feature and therefore it is important to verify the antibody reactivity in diseases that show similar characteristics.

In the previous chapter the purification of a soluble scFv A7 and optimisation of conditions for IHC were optimised, showing specific reactivity of the

antibody for the human arthritic synovium. In this chapter characterisation of the disease, tissue and species specificity of the scFv A7 antibody will be assessed through immunohistochemistry on tissue sections. In addition, the localisation of the antibody binding, defining the target cell population and distribution, will be discussed.

4.2 Disease specificity of scFv A7 reactivity

As mentioned above, characterisation of the disease specificity of scFv A7 is a crucial aspect for this project. In this section the reactivity of the scFv A7 will be characterised in the target tissue, the arthritic synovium, and compared to other inflammatory disease conditions such as inflammatory bowel disease, colorectal cancer, psoriasis and melanoma skin cancer.

4.2.1 Reactivity in RA and OA synovium

Analysis of the staining pattern in grafted synovial tissue following an *in vivo* recirculation assay in SCID mice, showed a vascular reactivity of the scFv A7 antibody (Figure 1.8 B). The specificity of reactivity of scFv A7 within synovial tissue was further characterised using immunohistological analysis on a considerable number of synovial samples from osteoarthritic patients (n=16) and patients suffering from rheumatoid arthritis (n=8), including normal human skin tissue (n=5) as a negative control. In Figure 4.1 is shown a representative staining pattern. scFv A7 was able to specifically target both the RA and OA synovium but no reactivity could be detected in the control skin tissue. Staining of sequential tissue sections with a control scFv (scFv HEL) and sections with no primary antibody (Negative control) confirmed the specificity of the staining observed with scFv A7. In addition, staining with an antibody targeting the vascular marker von Willbrand Factor (vWF), showed a similar staining distribution, confirming the vascular targeting of scFv A7. Since the original phage clone was isolated using *in vivo* phage display in which the phage library was injected into the tail vein of SCID mice and thus selected against vascular determinants, this result further confirms the specificity of the scFv A7 reactivity. The image analysis software ImageJ was used to quantify the intensity of staining and evaluate whether the scFv A7 antibody reactivity was specific and significantly above background. The data presented in Figure 4.2 demonstrate that as measured by the Mean Gray Value, scFv A7 antibody had substantial reactivity in the blood vessels of RA and OA tissue and significantly above background (p value <0.01). Further, the reactivity of control scFv antibody (scFv HEL) was minimal and very close in value to the corresponding tissue background and negative control. As

expected, in all tissues examined vWF antibody showed substantial reactivity with blood vessels that was significantly above background, reflecting the specificity of reactivity of this antibody with the endothelial layer in the blood vessels.

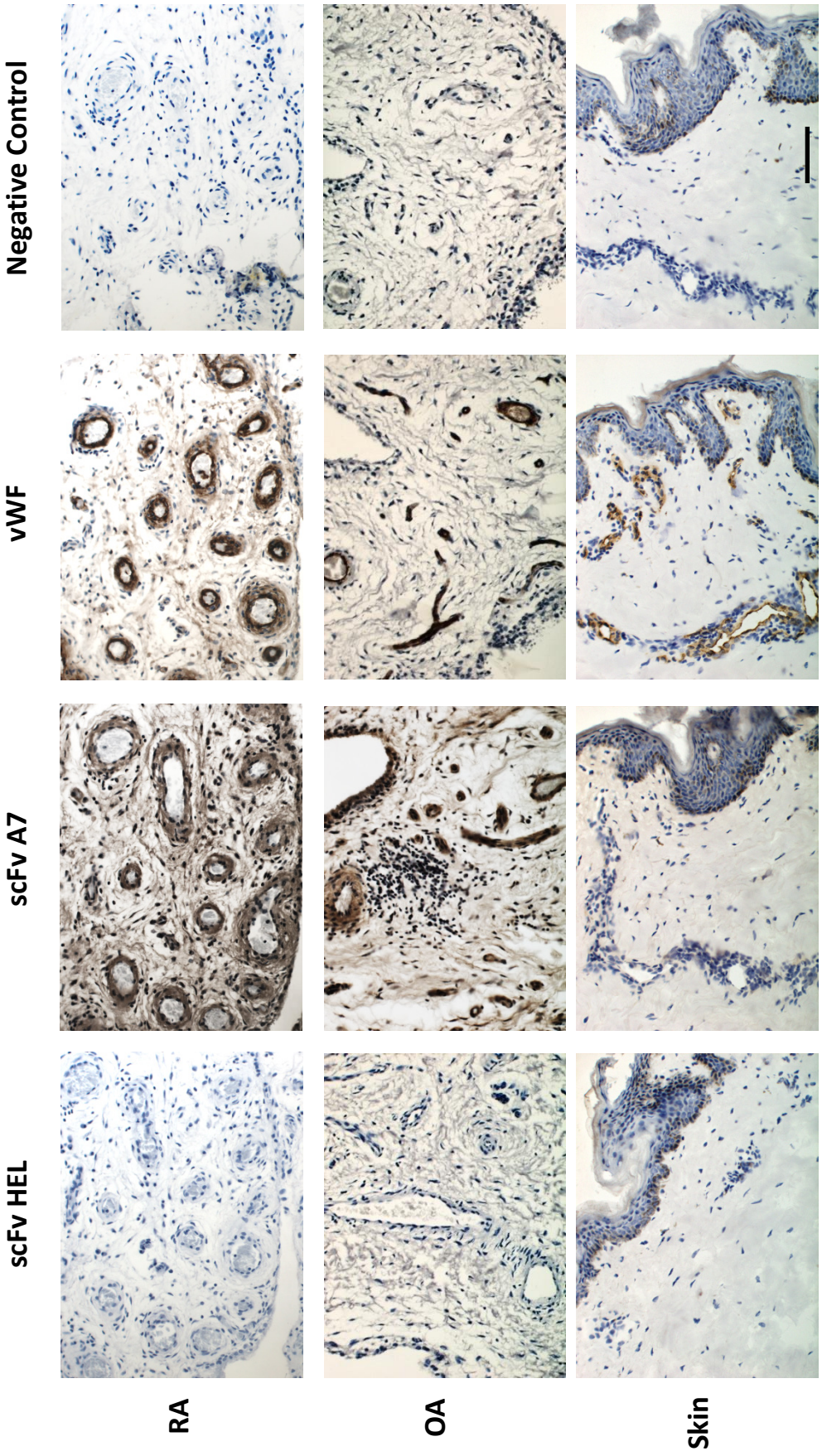
Negative Control
vWF
scFv A7
scFv HEL
RA
OA
Skin

Figure 4.1 Immunohistochemical analysis of scFv A7 antibody reactivity with human arthritic synovial tissue

The reactivity of scFv A7 with sections of human arthritic synovial and skin tissue was examined using biotinylated scFv A7. Biotinylated scFv HEL was used as antibody negative control. The presence of blood vessels in tissue samples was visualised with anti-human vWF antibody. Biotinylated scFv antibodies were detected with avidin-biotin complex HRP conjugated (ABC-HRP) application whilst vWF antibody reactivity was detected using an HRP labeled antibody. Scale bar = 100 μm.

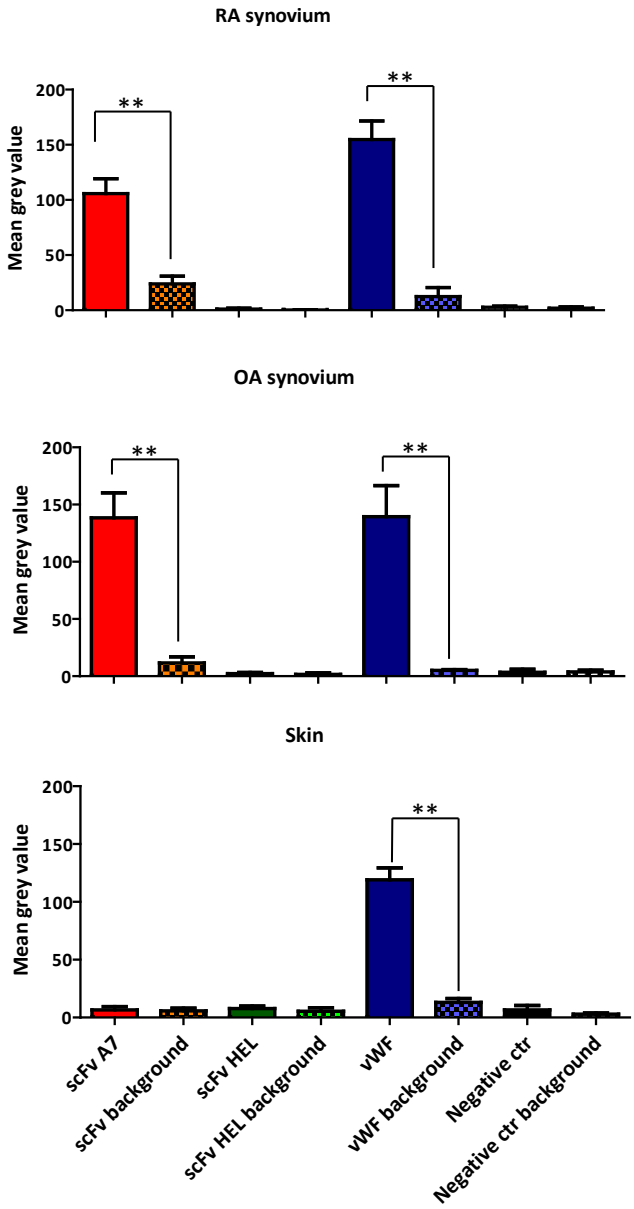

Figure 4.2 Quantification of intensity of immunohistochemical staining

Immunoreactivity of scFv A7, scFv HEL and vWF found in the vessels presented in Figure 4.1 was quantified using the image analysis tool ImageJ (plain) and compared to a matched area size in a non-relevant tissue area representing the background (checked). Intensity of staining is represented by the mean grey value (mean ± SD) of 5 vessels and 5 non-vascular areas per sample. Mann Whitney test ** = p value < 0.01.

Other than synovial lining layer hypertrophy and neo-angiogenesis, a third characteristic feature of RA/OA synovitis is infiltration of immune cells of both innate and adaptive immune system. The spatial distribution of these cells can vary greatly among different patients. The immune cells infiltrating the synovium can display from a disperse distribution with no clear organisation, to a highly organised aggregated structure reminiscent of secondary lymphoid organ follicles (50). The functional implication of such structures in the progression of the disease or therapeutic response is still unclear (48, 266). However, cell type distribution and specific cytokine/chemokine expression have been shown to vary depending on the presence or absence of the follicular structures (267). To investigate the role that different degrees of cell infiltrate within the synovium may exert on the A7 target antigen expression, tissues ranging from non-infiltrated (OA n=7), diffuse infiltrate (OA n=5), 1 to 5 cells thick perivascular aggregates (grade 1) (OA n=2), 5 to 10 cells thick perivascular aggregates (grade 2) (OA n=2) and more than 10 cells thick perivascular aggregates (grade 3) (OA n=3 and RA n=5) were screened for scFv A7 reactivity. The results presented in Figure 4.3 demonstrate that scFv A7 is able to target the arthritic synovium independently of the degree and organisation of immune infiltrates within the tissue (Figure 4.4). Furthermore, scFv A7 recognises the microvasculature of both OA and RA synovium with no significant difference in reactivity when comparing the two diseases (Figure 4.4).

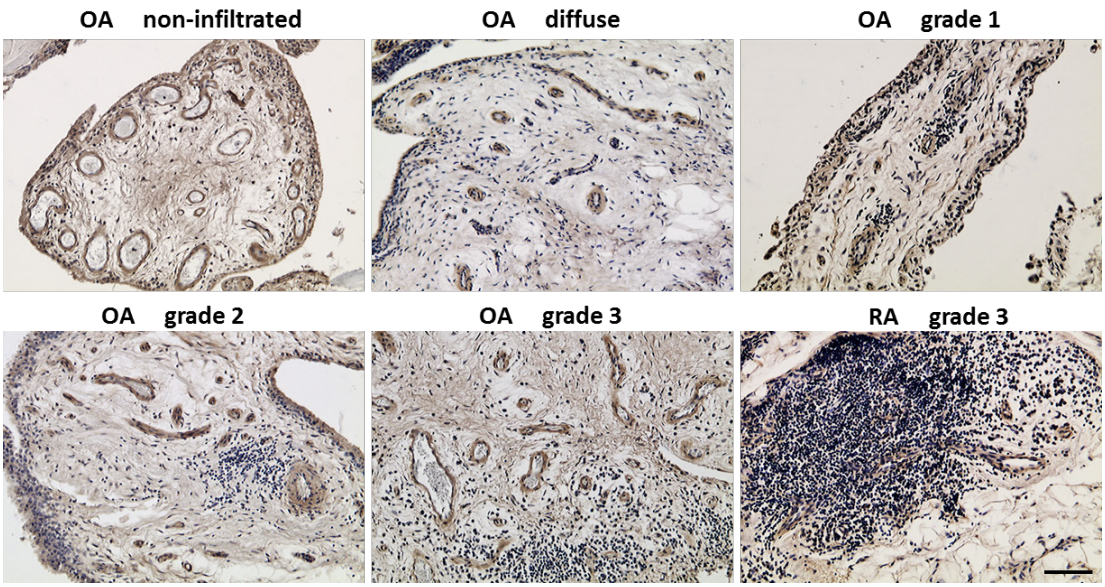

Figure 4.3 Immunohistochemical analysis of scFv A7 antibody reactivity with OA and RA synovium

10 µg/ml biotinylated scFv A7 IHC staining in inflamed OA and RA sections with varying degrees of infiltrate. Bound biotinylated scFv A7 antibody was detected using ABC-HRP conjugate. Scale bar = 100 µm.

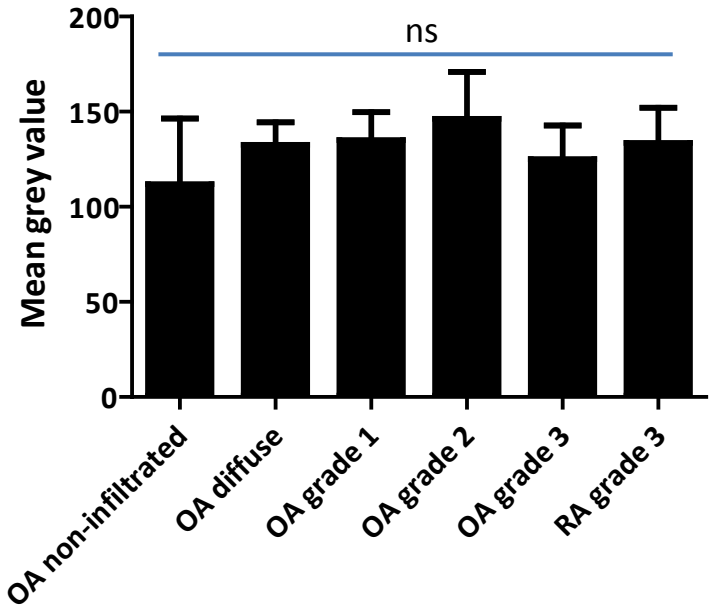

Figure 4.4 Quantification of intensity of immunohistochemical staining

Immunoreactivity of scFv A7 found in the vessels presented in Figure 4.3 was quantified using the image analysis tool ImageJ. Intensity of staining is represented by the Mean grey value (mean ± SD). 5 comparable vascular regions were counted spanning the tested tissues of each category. Kruskal-Wallis test ns = p value > 0.05.

4.2.2 Reactivity in inflammatory bowel disease

Inflammatory bowel disease (IBD) is a group of inflammatory conditions of the colon and small intestine with unknown etiology, associated to an increase risk of developing colorectal cancer (CRC). The two major types of IBD are Crohn's disease and ulcerative colitis. The first is generally absent from the upper gastrointestinal tract and affects mainly the terminal ileum and the proximal colon, the lesions are generally separated by uninvolved "skip areas" and characterised by the presence of granulomas, mucosal lesions and a transmural inflammation causing a thickened bowel wall involving submucosa and muscularis propria. The second starts from the rectum and spreads proximally involving a variable length of the colon, is characterised by an inflammatory reaction with special distribution and structural abnormalities of the mucosa (268). Both of these diseases are associated with an initial physiological angiogenesis to supply nutrients and oxygen to the regenerating bowel mucosa and remove waste products. However, this physiological remodelling is soon turned into a pathological process due to aberrant expression of angiogenic molecules (269).

Among the 12 Crohn's disease sample tested, 9 showed no reactivity with scFv A7 while 3 showed a minor reactivity confined to the muscular layer. The ulcerative colitis sample tested proved to be non-reactive with scFv A7 while the 2 CRC samples showed staining in the muscular layer. Five healthy control samples were included in the experiment and none of them showed detectable reactivity with scFv A7 at any concentration tested (Figure 4.6).

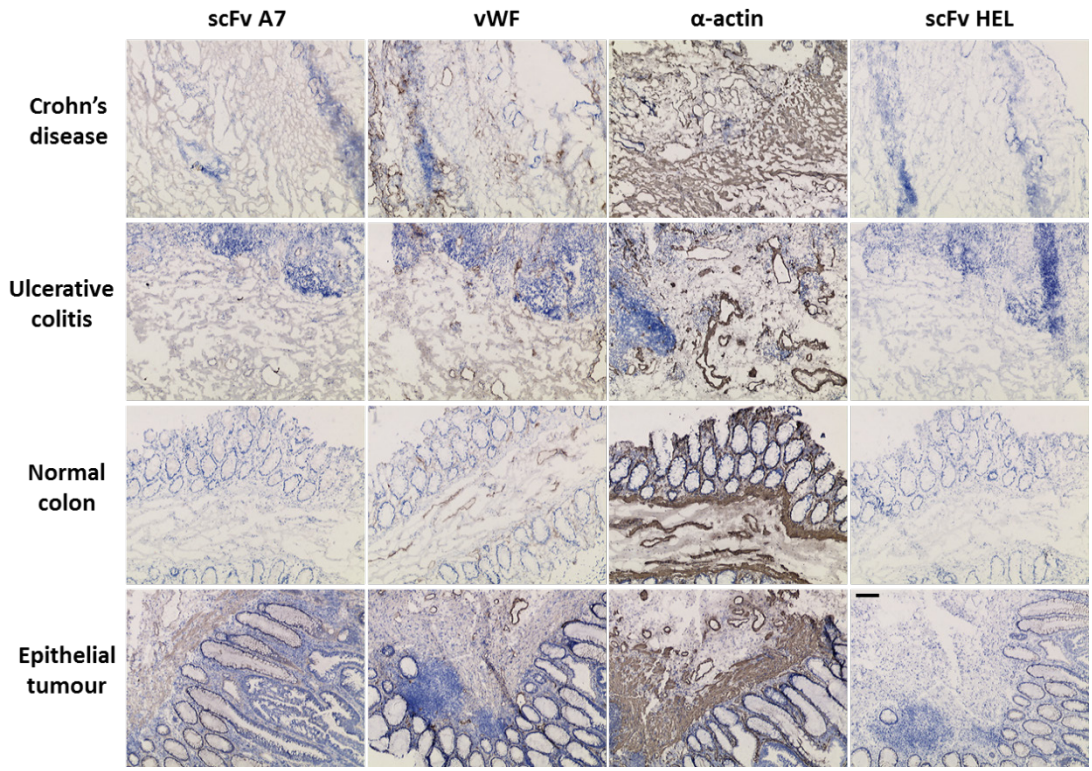

Figure 4.5 Reactivity of scFv A7 antibody with the microvasculature of inflammatory bowel disease

The reactivity of scFv A7 with normal colon, Crohn's colon, ulcerative colitis and epithelial tumour was assessed. The presence of microvasculature was visualised using anti-human vWF antibody and α-actin for the stromal compartment. Biotinylated scFv A7 was detected with ABC-HRP. vWF and α-actin antibody reactivity were detected using an HRP labeled secondary antibody. The images shown are representative of the 9 negative Crohn's disease samples, 1 ulcerative colitis, 5 healthy colon and 2 CRC samples. Scale bar = 200 µm.

4.2.3 Reactivity in psoriatic skin

Psoriasis is a chronic, autoimmune disease that appears in the skin and is characterised by overgrowth of skin cells with rapid accumulation. There are five main forms of psoriasis: plaque, guttate, inverse, pustular and erythrodermic. This disorder can also cause inflammation of the joints, a condition which is known as psoriatic arthritis (270). Due to its correlation with the arthritic diseases subject of this study, the reactivity of scFv A7 was tested in 3 psoriatic skin tissue samples. The results presented in Figure 4.6 show that scFv A7 had no detectable reactivity with this tissue.

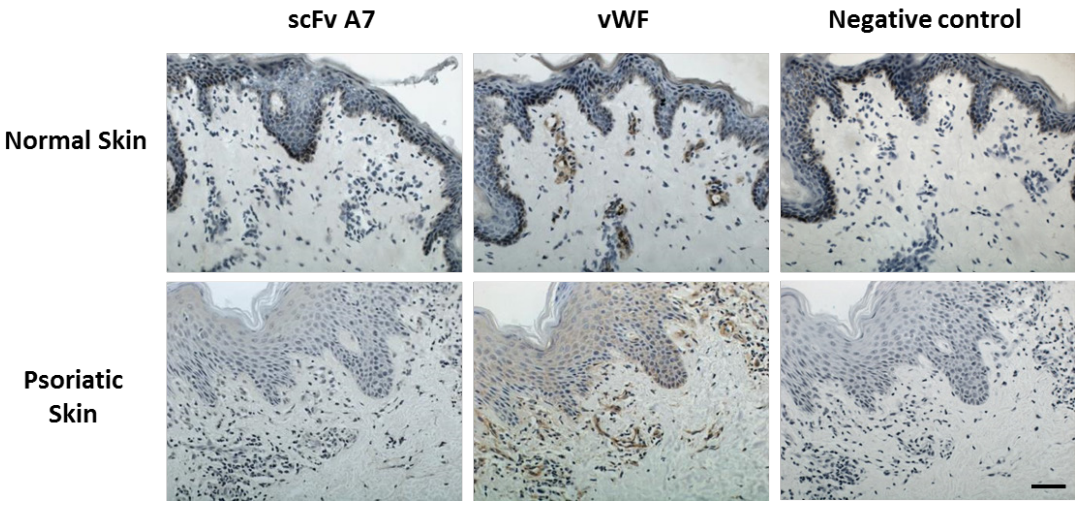

Figure 4.6 Reactivity of scFv A7 antibody with the microvasculature of psoriatic skin

The reactivity of scFv A7 with normal skin and psoriatic skin was assessed. The presence of microvasculature was visualised using anti-human vWF antibody. Biotinylated scFv was detected with ABC-HRP conjugate. vWF antibody reactivity was detected using an HRP labeled secondary antibody. The images shown are representative of the 5 skin samples and 3 psoriatic skin tissues examined. Scale bar = 100 µm.

4.2.4 Reactivity in melanoma skin cancer

Melanoma is the most serious type of skin cancer, with a good chance of regression only if surgically removed at an early stage. If not treated, metastasis may be found mainly at lymph node sites, lungs, liver, brain and bones. Three tissues from one patient with melanoma skin cancer, presenting metastasis in sigmoid colon and axillary lymph nodes, were tested for reactivity with scFv A7. The results presented in figure 4.7 show that scFv A7 had no detectable reactivity with this tissue despite the presence of vasculature as depicted by anti-vWF staining. Clearly larger numbers of samples need to be examined before firm conclusions can be derived.

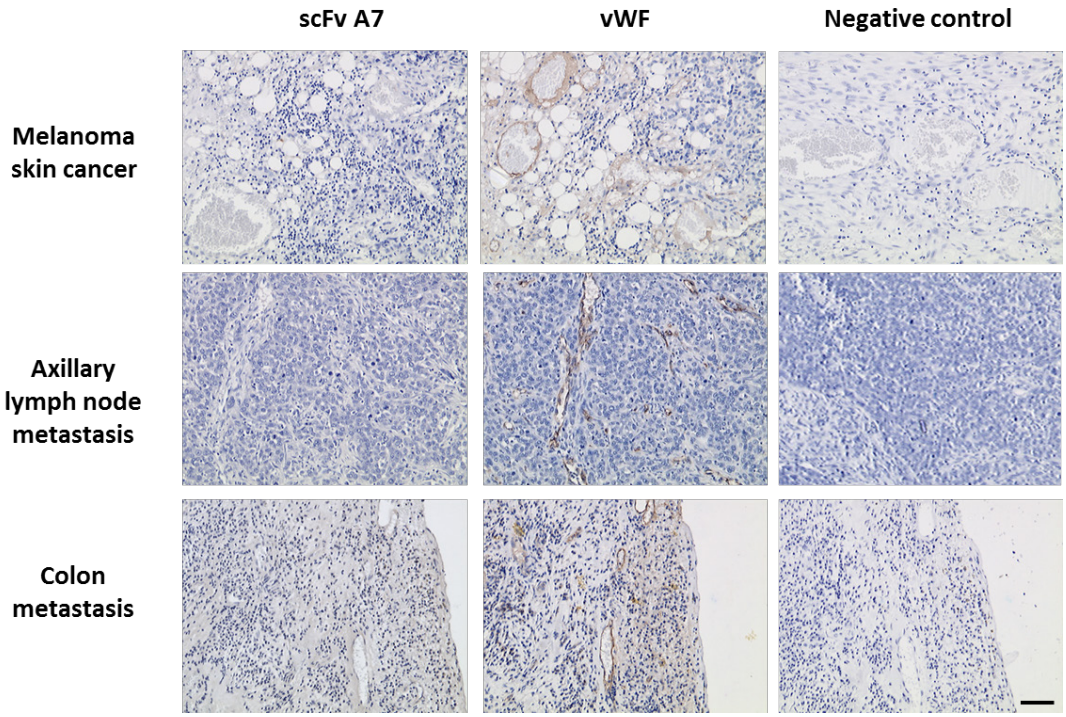

Figure 4.7 Reactivity of scFv A7 antibody with the microvasculature of melanoma skin cancer

The reactivity of scFv A7 melanoma skin cancer, lymph node and colon metastasis was assessed. The presence of microvasculature was visualised using anti-human vWF antibody. Biotinylated scFv were detected with ABC-HRP conjugate. vWF antibody reactivity was detected using an HRP labeled secondary antibody. Scale bar = 100 µm.

4.3 Tissue specificity of scFv A7 reactivity

The overall aim of this project is the development of a therapeutic tool for arthritic disease, able to selectively target the synovium and reduce possible systemic adverse effect. In order to achieve these goals, the ideal candidate antibody should not exhibit reactivity with normal healthy tissues.

As shown in Figures 4.1, 4.5 and 4.6, the scFv A7 antibody does not show reactivity with normal skin and healthy colon. However, a more comprehensive analysis on normal human tissues derived from various organs is required to clearly define the tissue distribution of the target antigen. In order to do so, a whole-body tissue microarray was screened for scFv A7 reactivity. As shown in Figure 4.8, scFv A7 did not exhibit reactivity with the vasculature or cellular components of the tissues represented in the array despite the presence of microvasculature detected using anti-vWF antibody.

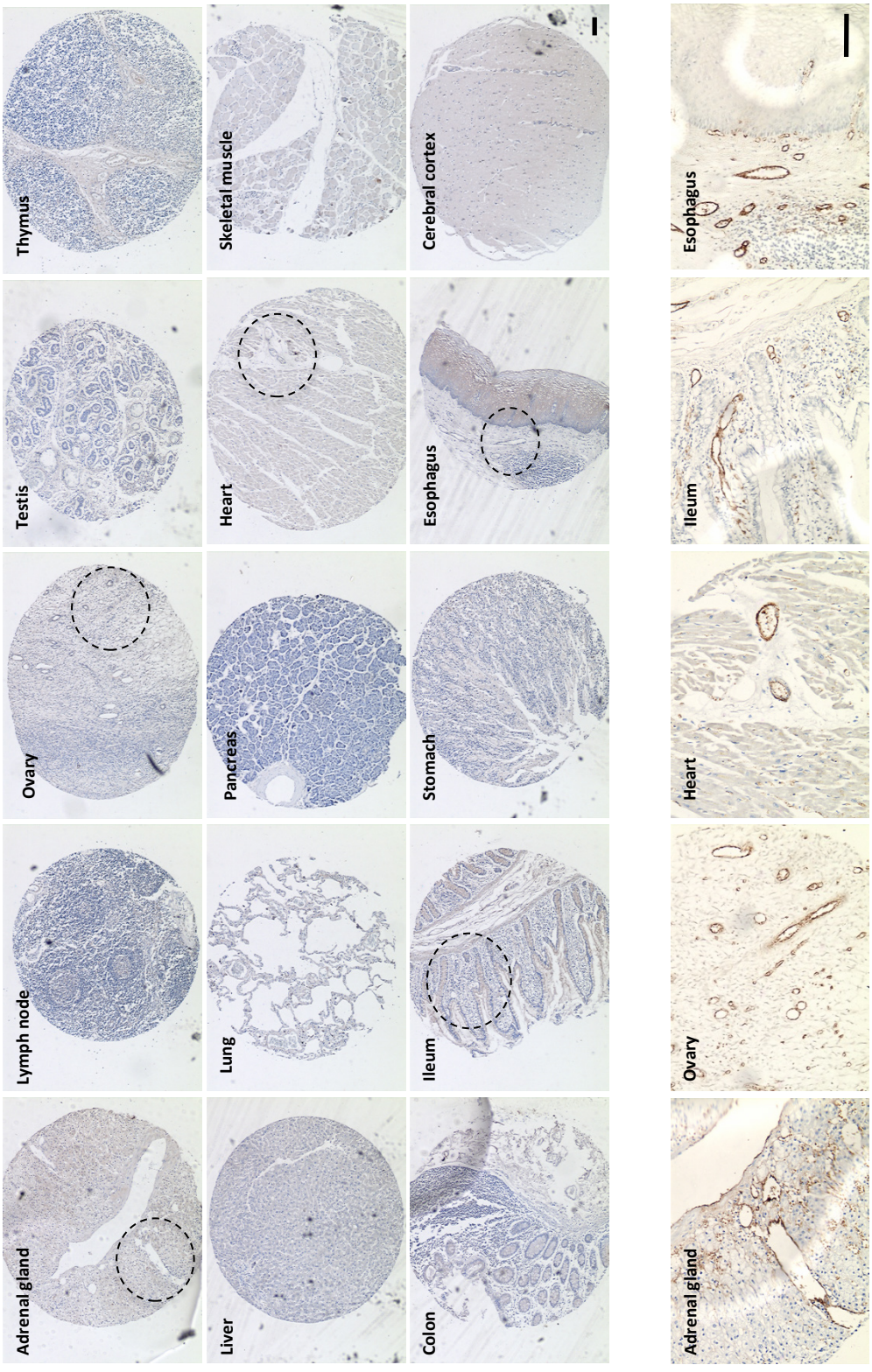
scFv A7
vWF
Thymus
Skeletal muscle
Cerebral cortex
Esophagus
Testis
Heart
Esophagus
Ileum
Ovary
Pancreas
Stomach
Heart
Lymph node
Lung
Ileum
Ovary
Adrenal gland
Liver
Colon
Adrenal gland

Figure 4.8 Immunohistochemistry of scFv A7 in normal human tissues

The reactivity of scFv A7 antibody with normal human tissues was assessed using paraffin embedded whole body survey tissue microarray. Bound biotinylated scFv A7 antibody was detected using avidin HRP conjugate. The presence of blood vessels in tissue samples was visualised with anti-human vWF antibody and an HRP labeled secondary antibody. Representative areas in selected samples (**---**) are presented at higher magnification for clarity. Scale bar = 100 µm.

From the data presented in section 4.2, it is clear that the scFv A7 target antigen is expressed by both RA and OA synovium and may represent a common feature of arthritic conditions in the synovium. To confirm the disease specificity of this antibody fragment, it is important to verify whether the normal synovium tissue retains the same antigen expression and scFv A7 reactivity as the arthritic tissue. Because of obvious ethical implications, it is very difficult to obtain normal synovium from healthy patients. One way to overcome this limitation is to collect tissues post-mortem or from limb amputations of patients with osteosarcoma or injuries. The samples used in this project were obtained using arthroscopy from patients with prolonged unexplained knee pain that did not develop arthritic conditions in a 5 years follow up survey (271). IHC staining with scFv A7 antibody, showed no significant reactivity with the microvasculature in 11 samples of normal (non-arthritic) human synovium (Figure 4.9). The intensity of staining in the OA sample run at the same time as a positive control was comparable to what was seen in the previous experiments.

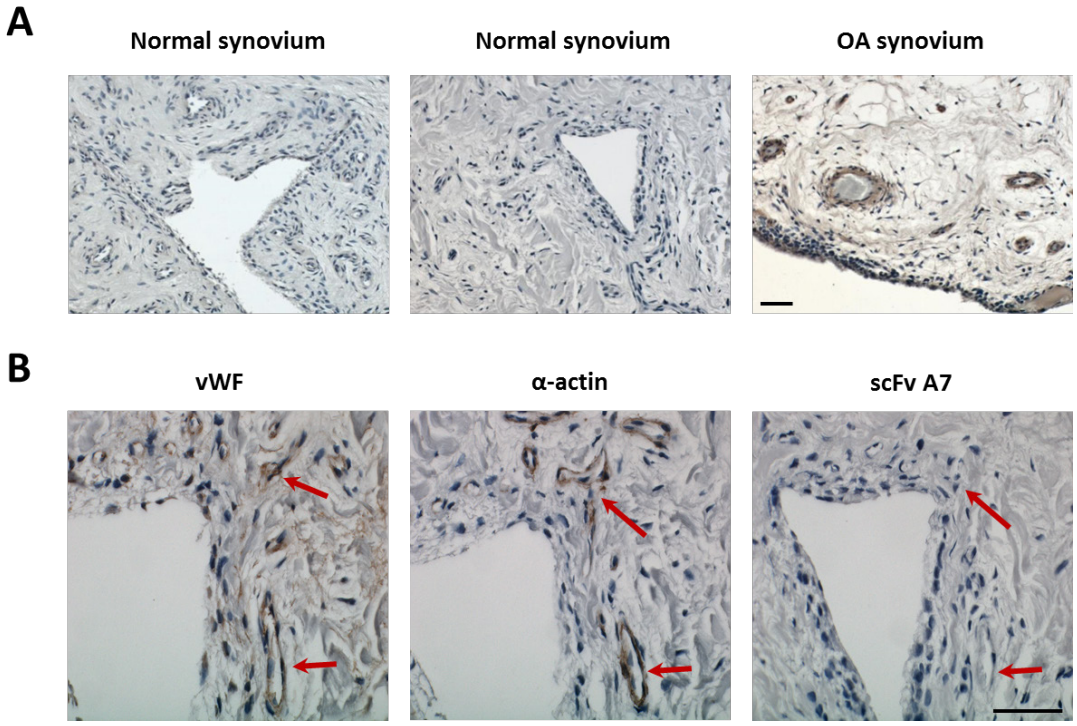

Figure 4.9 Reactivity of scFv A7 antibody with the microvasculature of normal synovium

The reactivity of scFv A7 with normal synovium was assessed. Biotinylated scFv A7 reactivity was detected with ABC-HRP conjugate. The images shown are representative of 11 normal synovium tissues (A). Higher magnification of normal synovium showing vasculature (red arrows) depicted by anti-vWF and anti-smooth muscle α-Actin (B). Scale bar = 50 µm.

4.4 Species specificity of scFv A7 reactivity

One important aspect to be considered is that the expression of the antigen may not be restricted to human tissue. Therefore, the reactivity of scFv A7 with mouse tissues was tested using paw and knee sections of CIA mice. This mouse model is an extensively studied animal model sharing both immunological and pathological features of human RA. In this model, injection of type II collagen in susceptible mice strains, such as DBA/1, elicits a T- and B-cell response causing proliferative synovitis, cartilage degradation and bone erosion (272). The data presented in Figure 4.10, demonstrate that despite the presence of prominent lymphoid infiltrates and neo-vasculogenesis in the CIA mouse synovium (assessed by CD34 staining), no detectable scFv A7 staining was observed in the arthritic mouse joint or in the blood vessels of the neighbouring joint tissues. In addition, no scFv A7 reactivity was detected in normal non inflamed DBA/1 knee.

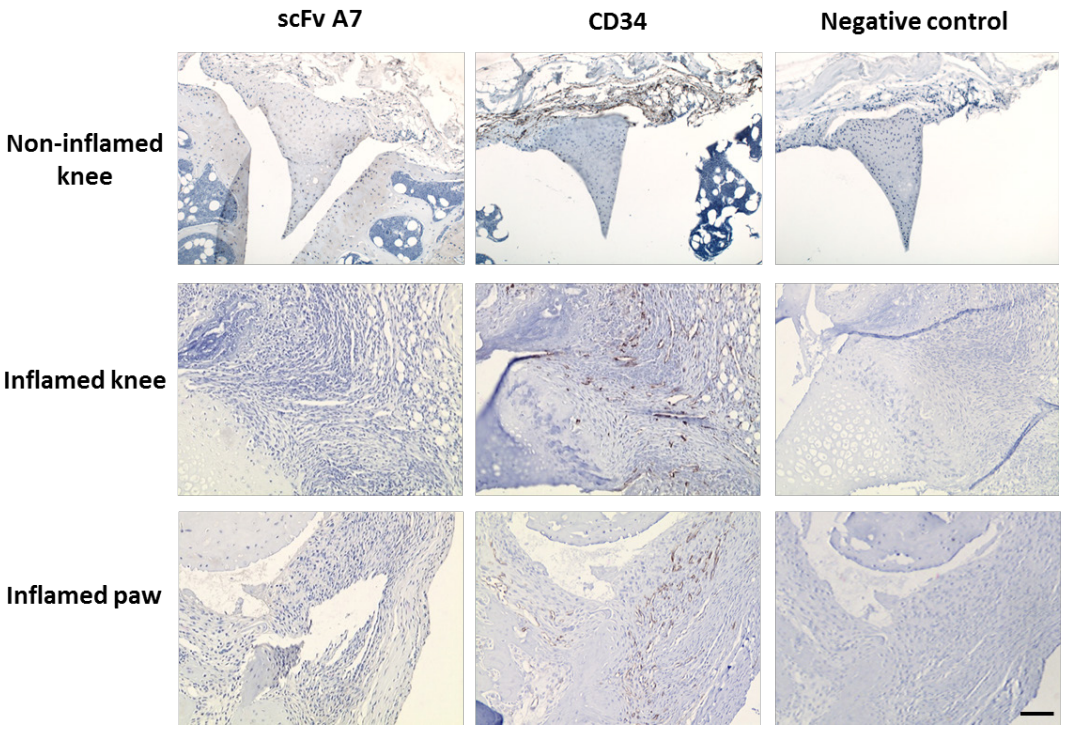

Figure 4.10 Reactivity of scFv A7 antibody with the microvasculature of CIA mice joints

10 µg/ml biotinylated scFv A7 IHC staining in normal DBA/1 knee and CIA inflamed knee and paw. CD34 staining included to highlight joint microvasculature. Biotinylated scFv A7 was detected with ABC-HRP. CD34 antibody reactivity was detected using an HRP labeled secondary antibody. The images shown are representative of 4 CIA mice joints analyzed. Scale bar = 100 µm.

4.5 Comparison between scFv A7 and current vascular markers

The immunohistochemistry performed with scFv A7 in Figures 4.1 and 4.3, shows a vascular staining in the human arthritic synovium. However, arteries and veins are characterised by the presence of three layers: the tunica intima characterised by the presence of endothelial cells forming the internal wall of the vessel; the tunica media, characterised by smooth muscle cells with varying degrees of thickness depending on the type and calibre of the vessel; and the tunica adventitia made of connective tissue which may present nerves and capillaries in the larger vessels. The main cell types constituting the vessels are therefore endothelial cells and smooth muscle cells. In the small blood vessels there is also the presence of a cell population called pericyte, generally one cell thick, surrounding and providing structural stability to the vessels (273, 274). In order to determine which cell type within the microvasculature was able to react with scFv A7, a dual immunofluorescent staining using scFv A7 and the endothelial markers vWF and CD31 was performed. The data presented in Figure 4.11 shows no overlap between the scFv A7 staining and the endothelial cell layer. However, when stained in combination with NG2, a pericyte specific marker, and smooth muscle α-Actin, a marker for the smooth muscle layer, a complete overlap in the pattern of cellular staining was observed (Figure 4.11). In order to quantify the degree of co-localisation, the Pearson's correlation coefficient was used to provide a numerical and non-subjective analysis (275). The Pearson correlation ranges from +1 to −1, whereby a correlation of +1 indicates complete overlap of pixels from two different channels. A value of 0 indicates no overlap and, a correlation of −1 indicates complete pixel disparity/exclusion between the two channels being compared. The Pearson's co-localisation analysis of scFv A7 reactivity (red pixels) and vWF-CD31 (green pixels) resulted in a correlation (r) of 0.09, demonstrating no co-localisation of scFv A7 and the endothelial layer. Similarly, Pearson's co-localisation analysis of NG2 or α-actin (red pixels) with vWF-CD31 (green pixels) resulted in a correlation of 0.05 and 0.03 respectively, demonstrating no colocalisation. However, staining with scFv A7 (red pixels) in combination with NG2 or α-actin (green pixels) showed a co-localisation index of 0.7 and 0.74 respectively, demonstrating that the reactivity of

scFv A7 is specific for the stromal component of the microvasculature in the synovium.

Further, staining of a broad spectrum of normal human tissues and inflammatory disease tissue samples with scFv A7 showed that the reactivity of this antibody is specific for the microvasculature of arthritic synovium only and therefore doesn't represent a universal marker for the stromal compartment (Figure 4.1, 4.5, 4.6, 4.7 and 4.8). In order to further confirm the specificity of scFv A7, a dual immunofluorescent staining of human tonsil was performed using scFv A7 and NG2. The data presented in Figure 4.12 shows the presence of NG2 positive cells in the stromal compartment of the vessels while no scFv A7 reactivity could be detected. This result clearly demonstrates that scFv A7 is not merely a new common marker of pericytes.

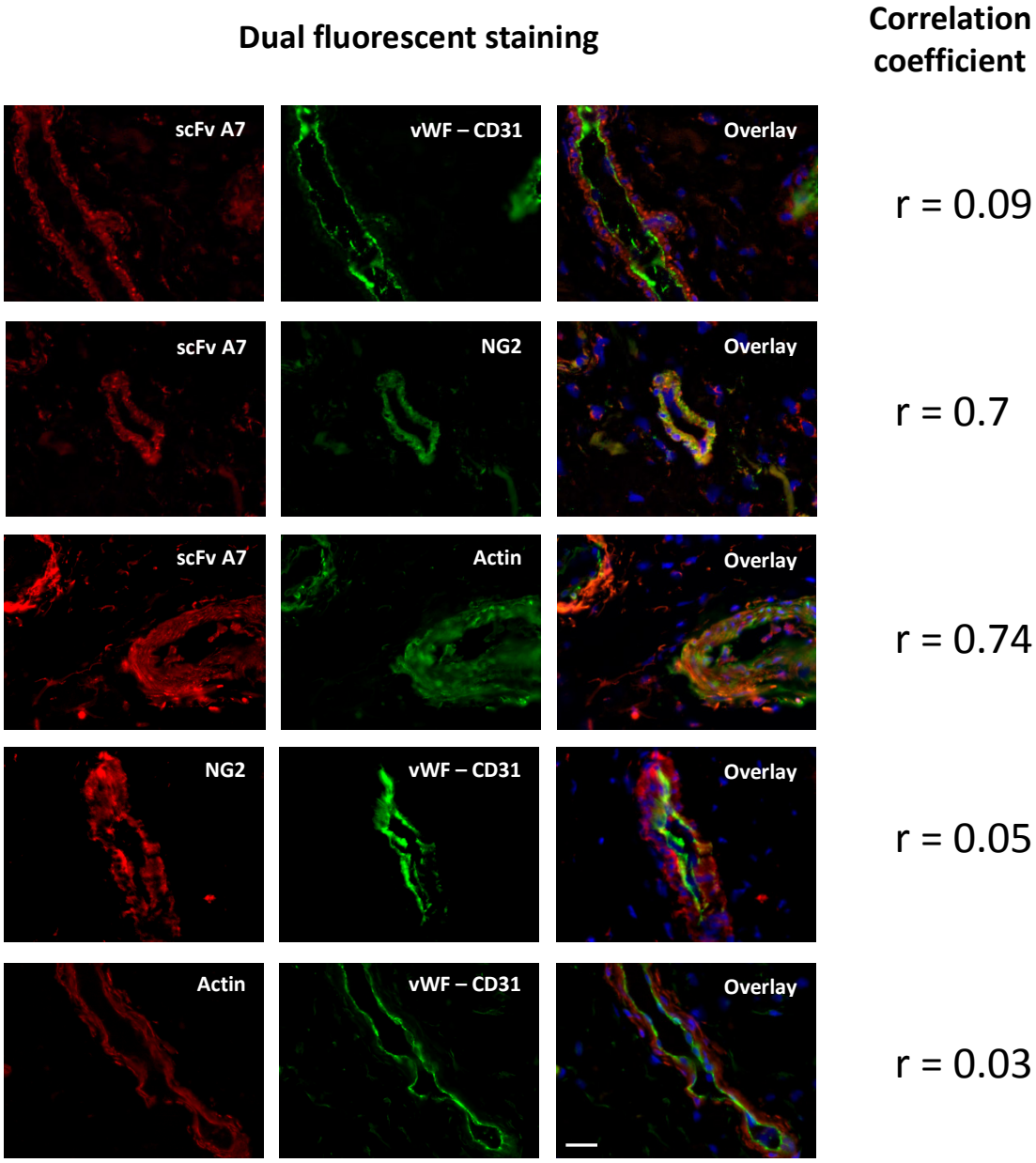
Dual fluorescent staining
Correlation coefficient
scFv A7
vWF – CD31
Overlay
r = 0.09
scFv A7
NG2
Overlay
r = 0.7
scFv A7
Actin
Overlay
r = 0.74
NG2
vWF – CD31
Overlay
r = 0.05
Actin
vWF – CD31
Overlay
r = 0.03

Figure 4.11 Characterisation of cellular reactivity of scFv A7 within synovial microvasculature

The reactivity of biotinylated scFv A7 with cellular components of synovial microvasculature was examined by dual staining of frozen human synovial tissue from RA patients and compared with staining for the endothelial markers vWF and CD31, the pericyte specific marker NG2 and the smooth muscle marker α-actin. Bound scFv A7 was detected using Texas Red – Avidin conjugate. vWF, CD31, NG2 and α-actin binding were detected using Alexa 488 (green) or Alexa 594 (red) labelled secondary antibodies. Sections were counter stained with DAPI to depict nuclei (blue). Correlation coefficient (r) calculated using Pearson's correlation coefficient in the image analysis tool ImageJ. Scale bar = 100 μm.

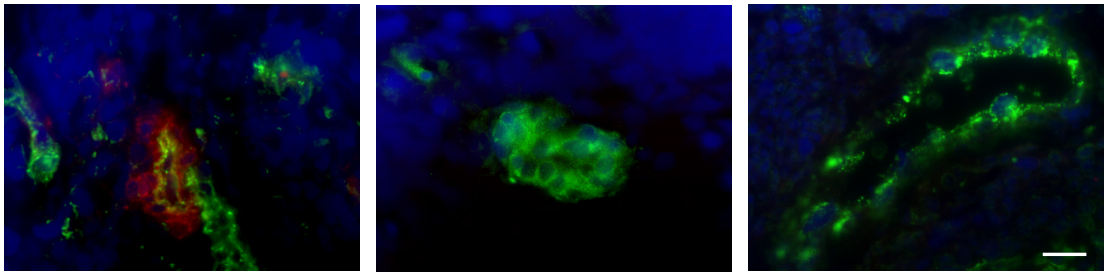

NG2 + CD31 NG2 + scFv A7 CD31 + scFv A7

Figure 4.12 Co-staining of human tonsil tissue

The reactivity of scFv A7 antibody with cellular components of human tonsil microvasculature was examined by co-staining of frozen human tonsil tissue with the pericyte specific marker NG2 and endothelial marker CD31. scFv A7 antibody binding was detected using Texas Red – Avidin conjugate. CD31 and NG2 binding were detected using Alexa Fluor 488 (green) or Alexa Fluor 594 (red). Sections were counter stained with DAPI to depict nuclei (blue). Scale bar = 100 µm.

More recently, endosialin (CD248), a transmembrane glycoprotein with a C-type lectin-like domain, has been implicated as a marker of mural (pericyte/smooth muscle) cells and fibroblasts associated with tumour blood vessels (276, 277). Further, expression of endosialin has been observed in rheumatoid fibroblast-like synoviocytes and in a subset of fibroblasts involved in the remodelling of lymphoid tissues (276, 278). In order to investigate the potential correlation between CD248 and scFv A7 staining in RA and OA synovial tissues, dual immunofluorescent stainings were performed comparing CD248, smooth muscle α-actin, CD31, NG2 and scFv A7 reactivity. The data presented in Figure 4.13 show that in both RA and OA synovial tissue, CD248 could be detected in the fibroblast-like synoviocytes surrounding the microvasculature but not in the pericytes nor in the smooth muscle compartment of these blood vessels as demonstrated by the lack of overlap in the staining of CD248 with that of NG2 and smooth muscle α-actin, respectively. Similarly no co-localisation was observed between scFv A7 staining and that of CD248. CD248 pattern of staining was comparable between the RA and the OA synovial tissue samples (Figure 4.13). Further comparison between scFv A7 and markers of pericytes will not be pursued in this project since the primary aim of this study is identification of the target molecule for this antibody.

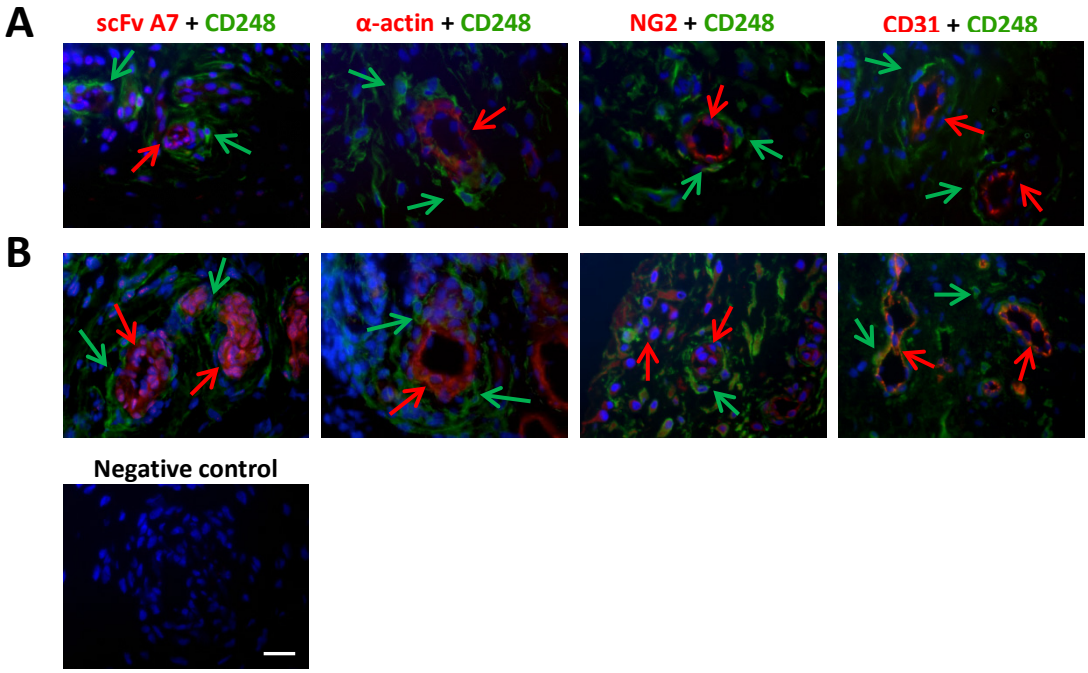

Figure 4.13 Comparison between scFv A7 reactivity and CD248

Characterisation of CD248 (Alexxa 488 green) cellular reactivity in OA synovium (A) and RA synovium (B), in a dual immunofluorescent staining with biotinylated scFv A7 (Avidin - Texas red), α-actin (Alexxa 594 red), NG2 (Alexxa 594 red) and CD31 (Avidin – Texas red) respectively. Scale bar = 100 µm

4.6 Discussion

The chimeric SCID mouse model adopted for the isolation of the scFv A7 using *in vivo* phage display, has the advantage of overcoming the limitations of a mouse environment allowing the selection of phage with homing specificity for human tissue determinants. The scFv A7 showed preferential homing specificity for human arthritic synovium compared to normal human skin both as a phage and as a soluble antibody fragment in *in vivo* recirculation assays. However, the characterisation of the reactivity in terms of tissue specificity and cellular localisation, disease specificity and species specificity is important to clearly define the potential of the molecule as a diagnostic or therapeutic tool. To answer this question and define the possible applications of the antibody fragment, a comprehensive screening was carried out in human arthritic tissues, normal tissues, disease tissues and in an animal model of arthritis.

The evaluation of synovial reactivity was assessed using immunohistochemistry on synovial tissue sections. The scFv A7 was able to specifically target the microvasculature of both OA and RA synovium but not the normal human skin tissue included as a control (Figure 4.1). Although phage display screening was performed in SCID mice transplanted with human OA synovium, the capacity to target both OA and RA is not unheard of. A previous project within our group showed that peptides isolated through phage display from RA synovium grafted SCID mice had the ability to target also OA synovium both *in vivo* and *in vitro* (279). This may be due to the targeting of synovium specific antigens expressed on the vascular compartment of the tissue or may be due to the presence of antigens that are expressed or up-regulated in arthritic conditions. The possibility of shared antigens driven by the arthritic disease condition in OA and RA is in line with recent findings showing an overlap in synovitis and inflammatory processes between the two conditions (86). In addition, the targeting of the microvasculature within the synovium is consistent with the isolation of a scFv from a phage library injected through the blood stream and confirms the specificity of the reactivity observed. Further, scFv A7 did not show reactivity with other

inflammatory disease conditions such as inflammatory bowel disease and psoriatic skin (Figure 4.5 and 4.6) both characterised by neo-angiogensis and inflammation, and with a melanoma skin cancer tissue with related metastasis characterised by extensive neo-angiogenesis, strengthening the disease specificity of the scFv A7 molecule.

Analysis of reactivity in a large panel of normal human tissues from various organs showed no reactivity with the vasculature or other cellular components of the tissues tested (Figure 4.8). Most importantly no reactivity could be detected in normal human synovium (Figure 4.9), further strengthening the disease specificity of this antibody. However, it may be argued that the normal synovium tissues used in this study were from patients with knee pain and therefore not entirely normal. Nonetheless, since the donors of these samples did not develop arthritis in a follow up survey of 5 years (271), it can be concluded that the expression of the target antigen for scFv A7 is absent in non-arthritic synovial tissues or up regulated in arthritic conditions.

The collagen induced arthritis model is one of the most commonly studied models of arthritis and has been intensively researched for its immunological and pathological features. CIA is primarily an autoimmune disease involving both T- and B-cells in susceptible mice strains. This model is based on injection of heterologous type II collagen in the joint eliciting a break of tolerance, developing a Th1 response and production of autoantibodies. The reactivity of scFv A7 for CIA mice joints proved to be negative despite the presence of large lymphoid infiltrates and the presence of extensive neo-vasculogenesis (Figure 4.10). This result may be dependent on a masking of the antigen not retrieved with the proteinase K but may also suggest the identification of a human specific synovial antigen not shared by other species. Although this finding may represent a limitation for the preclinical assessment of a potential therapeutic activity of the antibody, the identification of a human specific synovial antigen over-expressed in arthritic conditions would have a great impact in the understanding of pathological processes during disease onset and progression. However, the fact that CIA mice do not share the antigen expression is not conclusive to rule out the possibility of homologous protein

expression in other mice strains or other species. Different animal models of arthritis are currently used in research and due to the fact that none of them perfectly duplicates the pathological condition and implications of human RA, it is possible that different stimuli and pathways could lead to different protein expression profiles. There is therefore the need to screen additional animal models of arthritis for scFv A7 reactivity.

Using double immunofluorescent staining combining scFv A7 with known vascular markers such as vWF, CD31, α-Actin and NG2, allowed the identification of the target cell population for scFv A7. Von Willebrand Factor is a glycoprotein constitutively produced by the endothelium and megakaryocytes (280) and is used as a marker for endothelial cells in mature vessels. CD31 or Platelet endothelial cell adhesion molecule (PECAM)-1 is a protein normally found on the surface of platelets, neutrophils, monocytes and is responsible for endothelial cells intercellular junctions (281, 282). NG2 is a chondroitin sulphate proteoglycan that is expressed by pericytes but not shared by the smooth muscle cells, allowing a clear discrimination between the two populations (283). Smooth muscle α-Actin is important for muscle cell architecture and therefore is a shared feature of smooth muscle cells and pericytes (284, 285). Analysis of co-localisation showed no correlation between scFv A7 and vWF ($r < 0.1$) and a significant correlation ($r > 0.6$) with NG2 and α-Actin. scFv A7 specifically targets the microvasculature of arthritic synovium and localises to the stromal compartment rather than the endothelial layer as demonstrated by the dual immunofluorescent staining with NG2, CD31/vWF and α-Actin (Figure 4.11), showing reactivity to both pericytes and smooth muscle cells. Since it is well established that pericytes are multipotent cells and retain the capacity to differentiate into vascular smooth muscle cells (286) our data could suggest that scFv A7 may represent a marker for pericytes. In this context, staining of a broad spectrum of normal human tissues and inflammatory disease tissue samples with scFv A7 showed that the reactivity of this antibody is specific for the microvasculature of arthritic synovium only and therefore doesn't represent a universal marker for pericytes (Figure 4.1, 4.5, 4.6, 4.7, 4.8, 4.9 and

4.12). Further, since NG2 shows no reactivity with the smooth muscle cells of the microvasculature, it is unlikely that NG2 represents the scFv A7 target molecule.

The stromal targeting may seem in contrast with the design of an *in vivo* bio-panning of a phage library in which the most obvious target compartment would be the endothelial layer (130, 259, 279). However, the mechanism of phage selection *in vivo* requires the antigen to be accessible at the moment of bio-panning to a probe much larger than the scFv i.e. the phage carrying multiple copies of the scFv. The xenograft SCID mouse model adopted in this project allows the graft to remain viable, maintaining human vasculature and expression of related protein (287). In this context, the inflammatory environment of the grafted arthritic synovium may allow the extravasation of large molecules through permeable vessels and promote the targeting of stromal antigens (118).

In conclusion, the scFv A7 displays all the properties of an arthritic synovium specific antibody and is the ideal candidate for a targeted therapeutic tool to be used in the treatment of rheumatoid arthritis.

Chapter 5

Towards the identification of scFv A7 target antigen

5.1 Introduction

The scFv A7 isolated from *in vivo* phage display has demonstrated a synovial specific reactivity (section 4.2). Most importantly, the antibody was also able to discriminate between healthy and arthritic synovium (section 4.3). All the information provided in chapter 4 points towards the targeting of a synovium specific antigen or an antigen undergoing up-regulation in arthritic conditions. In both cases, the A7 target antigen displays potential as diagnostic tool. Furthermore, the accessibility of this antigen, demonstrated by the *in vivo* phage display and recirculation assay of soluble scFv A7, makes it an ideal candidate for targeted drug delivery. The isolation and characterisation of the target antigen remains a primary goal of this project and is vital for further development of the antibody and translation in clinical practice. Two main approaches can be used to determine the nature and identity of the target antigen: a standard proteomic approach and a peptide library based screening.

The classical proteomic approach consists of the identification of a suitable source of the target protein such as cell lines, tissues or body fluids, to be used as a bulk protein producer from which the antigen of interest can be extracted for subsequent analysis. A well characterised and commonly adopted method of analysis is antigen solubilisation from the original source using detergents. Protein extracts are then resolved in two dimensional gel electrophoresis (2DE) and probed with the relevant antibody to identify the candidate target antigen (288-290). Alternatively, the protein mixture can be incubated with the antibody of interest, forming antibody-antigen complexes that can be pulled down using standard immuno-precipitation (IP) procedures and resolved in 2DE gels (291). The 2DE allows the separation of the proteins based on molecular weight and isoelectric point (pI), providing resolution of proteins within a mixture. Mass spectrometry analysis of the individual reactive spots will then provide information on the molecular weight and amino acid composition of the protein and determine protein identity by comparison with comprehensive protein databases (292, 293). Efficient protein solubilisation vastly depends on the detergent adopted and on the

biophysical properties of the protein itself. It is rare that a protein profile representative of the entire proteome can be obtained. Highly hydrophobic proteins and high molecular weight proteins for example tend to precipitate especially during isoelectric focusing and can be poorly resolved in 2DE (292). Extensive optimisation of the solubilisation buffer conditions are therefore required when looking for an unknown antigen.

The second approach involves the use of cDNA peptide libraries for antigen screening. Recently, the increased knowledge of the human genome and proteome has allowed the development of cDNA peptide libraries encoding virtually all putative human proteins. Screening of these libraries against the tested antibody will allow the isolation of the relative DNA sequence and identification of the target antigen. Several efficient methods have been described in the recent years for cDNA library screening, such as phage display, ribosome display and yeast two hybrids. Phage display, already described in section 1.4.2 for scFv isolation, can be applied to peptide library screening against a known antibody, selecting specific reactive phage clones and rapidly identifying the protein encoding DNA sequence (294). In ribosome display technology, the open reading frame (ORF) sequences contained in the library are transcribed and translated by the ribosomal machinery. However, due to the absence of a stop codon, the complex mRNA-ribosome-protein remains stable. Panning of these ribosome complexes against the test molecule allows the isolation of the protein and the coding mRNA at the same time. The mRNA isolated can then be reverse transcribed and sequenced for gene identification (295, 296). In contrast to phage display, which requires bacterial protein expression, and ribosome display, which is characterised by *in vitro* protein expression, the yeast two-hybrid technology allows post-translational modifications on the coded proteins. In this system, the antibody (bait) is used to screen expressed proteins (prey) from the library. Antibody antigen complexes can then reconstitute a transcription activator and promote the expression of a reporter gene. This method has been successfully used in the past to identify the targets for several scFv antibodies (297, 298). However, cDNA library expression is inherently limited by the translation efficiency of the host organism. Despite high titre of

putative ORF in the library, proteins can be expressed at different levels, introducing a bias for antigen copy number in the screening procedure. Furthermore, expression in a heterologous environment can cause protein precipitation or altered protein folding, inhibiting or impairing antibody-antigen binding (292).

More recently, synthetic protein microarrays have been successfully used for antibody profiling in autoimmune diseases (299, 300). In this technique, immobilised proteins synthesised or extracted from various sources can be rapidly screened for antibody interaction. This technique however, despite allowing high-throughput screening, is subjected to protein expression efficiency, relatively low antigen representation and is characterised by generation of false positive and false negative results.

In this chapter the strategies adopted towards A7 target antigen isolation and validation of target candidates will be presented.

5.2 Proteomic approach

Conceptually, the most suitable source of A7 target antigen would be the arthritic human synovium. However, low availability of fresh synovium represents a limiting factor for this approach. In addition, the staining observed with scFv A7 in human synovium is confined in the perivascular region (Figure 4.1 and 4.3) and therefore can account only for a minor fraction of the total tissue. Protein extracts obtained from total tissue digest would therefore provide only low concentration of the antigen and may not be detected in a conventional proteomic approach. Identification of an antigen expressing cell line would provide a significant amount of protein and represent a more stable antigen source.

5.2.1 Identification of cells expressing the target antigen

Several available cell lines were screened in order to identify one showing reactivity to A7 antibody. This resulted in two cell lines with reactivity to scFv A7 being identified. Specifically, PC3 cells (prostate cancer cell line) and IE7 cells (SV40 transformed primary, human umbilical cord vein endothelial cell line) appeared to express the target molecule. Immunofluorescent staining was performed on non-permeabilised conditions to detect cell surface signals as described in detail in section 2.7.3. Two additional cell lines, human embryonic kidney (HEK)-293 and the human monocytic cell line u937, were screened. As shown in Figure 5.1, both PC3 and IE7 expressed the target antigen for scFv A7 on the cell surface, however only a minor percentage of the cell population was positive. Among the HEK-293 and u937, no reactivity with scFv A7 was detected. Confocal imaging on positive cells confirmed the presence of the staining on the cellular membrane as shown in Z-stack imaging in Figure 5.2. In order to evaluate the presence of the target antigen in the intracellular compartment, cells were permeabilised with Triton X-100 (as described in section 2.7.3) prior to the standard staining procedure. The data shown in Figure 5.1, demonstrate that PC3, IE7 and HEK-293 cells displayed strong intracellular reactivity with scFv A7 in 100% of the cells examined, while staining remained undetectable on the u937 cell line. Confocal imaging on permeabilised

PC3 cell line showed indeed a distinct staining pattern compared to the non-permeabilised condition (Figure 5.2).

These data indicate that the above mentioned cell lines may serve as a good protein source for characterisation of the target molecule for scFv A7.

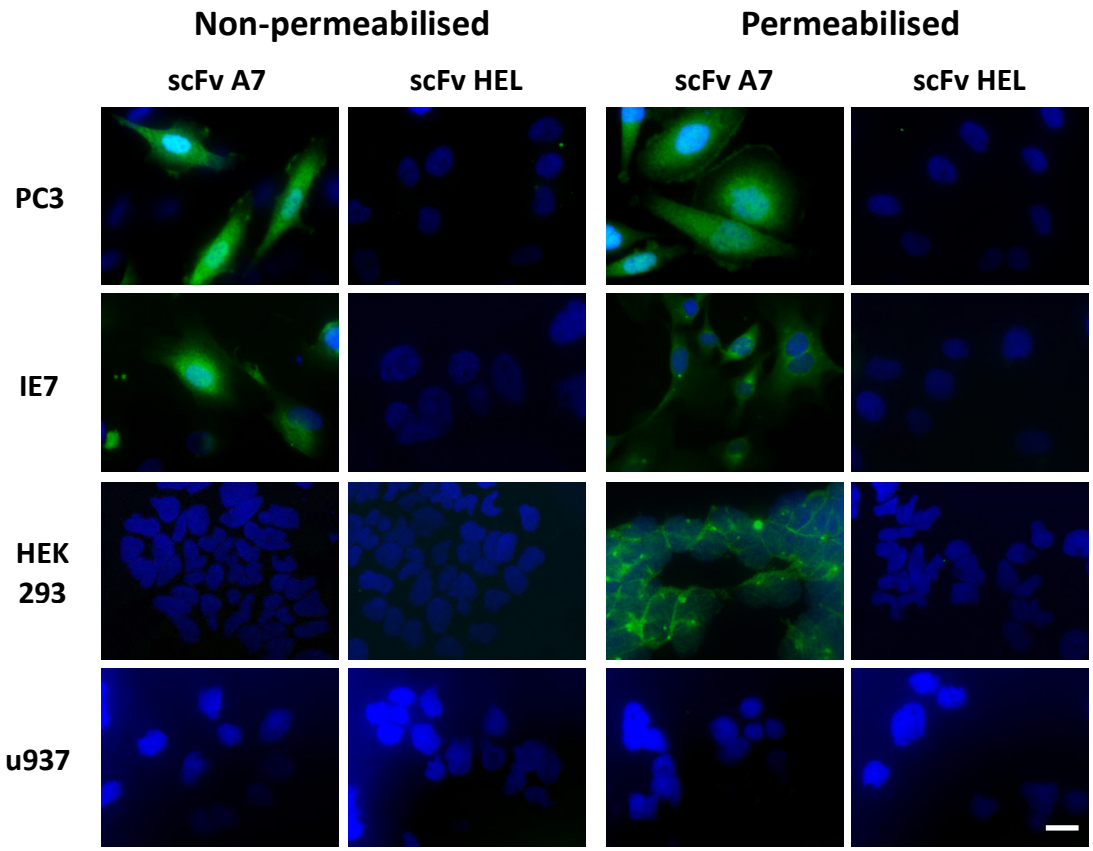

Figure 5.1 scFv A7 reactivity in cell lines

Immunofluorescent staining in PC3, IE7, HEK 293 and u937 cell lines with biotinylated scFv A7 and biotinylated scFv HEL as control, detected by α-myc antibody (Alexa 488 green). Cells were stained in non permeabilised condition as well as in permeabilised condition after treatment with Triton X-100. Scale Bar = 20 µm.

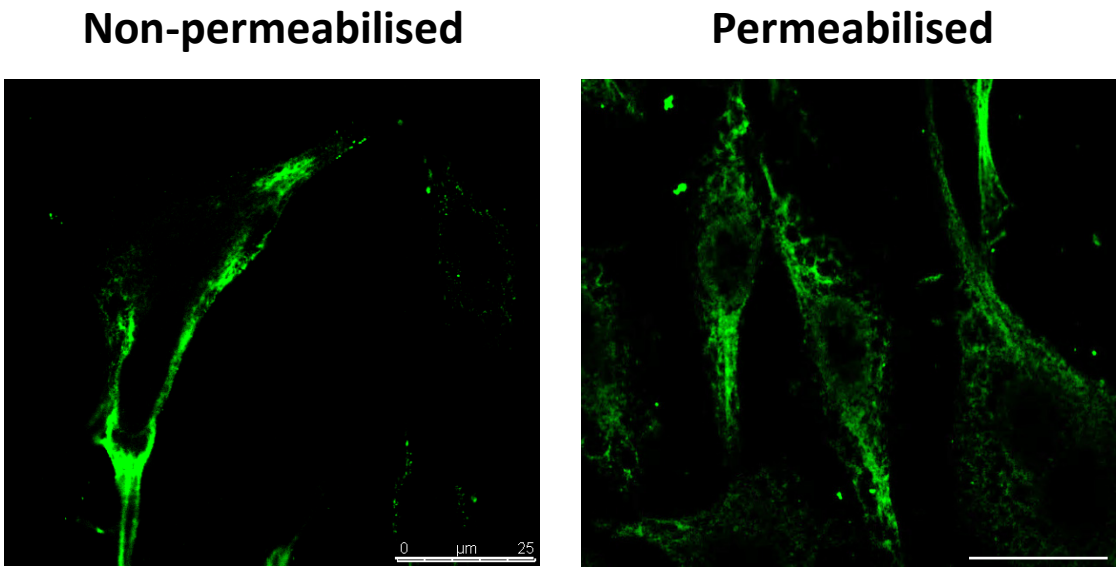

Figure 5.2 scFv A7 reactivity in PC3 cell line

Immunofluorescent staining in PC3 cell line with biotinylated scFv A7 detected by α-myc antibody (Alexa 488 green). Cells were stained in non permeabilised condition as well as in permeabilised condition after treatment with Triton X-100. Pictures show confocal imaging Z-stack of positive cells. Scale Bar = 25 µm.

The staining observed in the endothelial cell line IE7 is in contrast with the data presented in Figure 4.11, in which the staining pattern showed stromal rather than endothelial involvement. However, it is now well established that the expression of cell type specific markers is disregulated once cells are removed from the three dimensional context of tissue (301, 302). This may reflect in loss of differentiation specific antigens but also acquired expression of previously silenced genes. Since the IE7 cell line is derived from endothelial cells of the umbilical cord vein, the endothelial layer of fresh human umbilical cord veins were examined to determine whether they exhibited reactivity with scFv A7. Using IHC and immunofluorescence analysis, three umbilical cord samples were tested for reactivity with scFv A7. The results presented in Figure 5.3 A, demonstrate that scFv A7 exhibits reactivity with the stromal components of the vessels found in the umbilical cord. Specifically, dual immunofluorescent staining using vWF and scFv A7, further confirmed that the reactivity of scFv A7 localises in the stromal compartment with no detectable signal in the endothelial cell layer (Figure 5.3B).

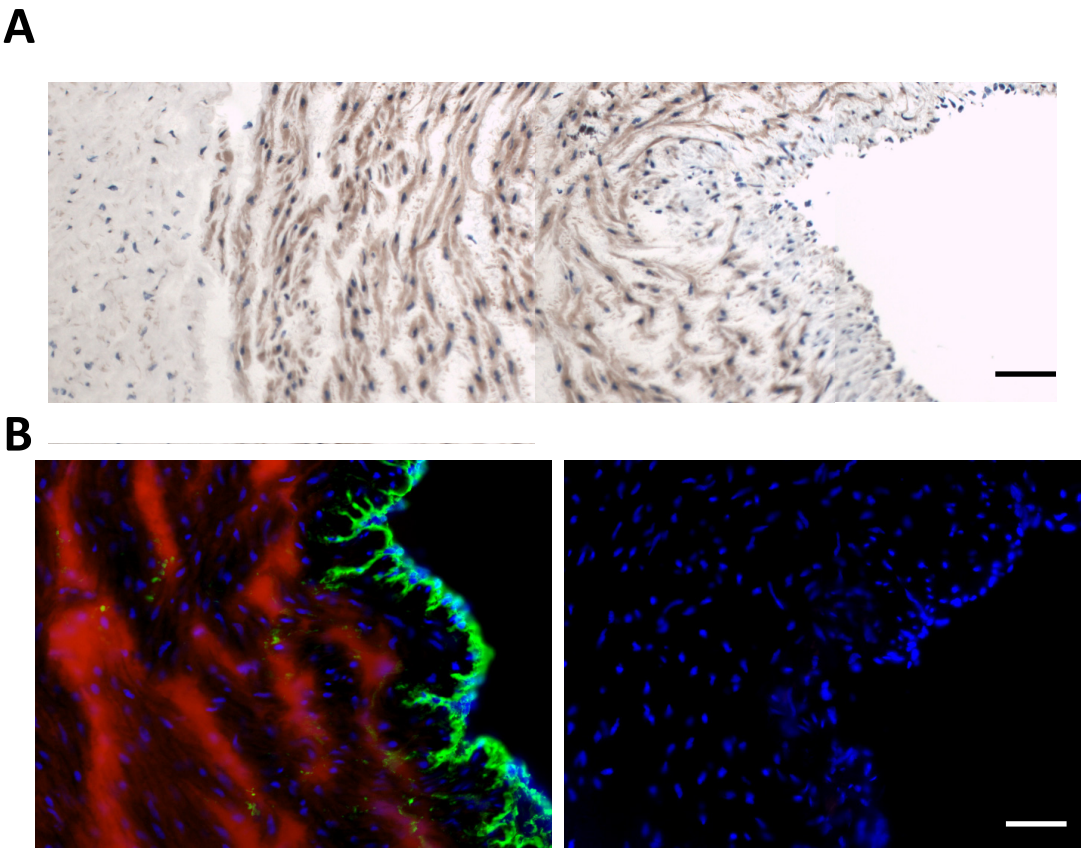

Figure 5.3 scFv A7 reactivity in umbilical cord vein endothelium

Biotinylated scFv A7 IHC staining in umbilical cord vein detected with ABC-HRP conjugate (A). Immunofluorescent double-staining with biotinylated scFv A7 (Texas Red – Avidin) and vWF-CD31 (Alexa 488 green) in umbilical cord vein with DAPI negative control (B). Scale bar = 50 µm.

In order to screen a cell population more closely related to the target tissue for scFv A7, the reactivity of this antibody was examined with primary synovial fibroblasts derived from RA synovial tissue (RASF) (240). Additionally, primary dermal fibroblasts derived from RA patients' skin (RADF) were used as control. Examination of scFv staining with these two primary fibroblast cell populations *in vitro* has shown that scFv A7 exhibits strong reactivity with the cell surface of both population tested (Figure 5.4) both of which obtained 100% positive cell staining. Further, both cell types showed positive cytoplasmic reactivity with scFv A7 (Figure 5.4). Confocal analysis of RASF stained with scFv A7 confirmed membrane and cytosol staining in non-permeabilised and permeabilised conditions respectively (Figure 5.5).

The synovial tissue in rheumatoid arthritis exists in the context of active inflammation. Cytokines are known to play an important role in the pathogenesis of rheumatoid arthritis with an imbalance towards proinflammatory cytokines (14, 30). In this context, cytokine stimulation may have a role in A7 target antigen expression. In order to evaluate the effect of cytokine stimulation in relation to A7 target antigen expression and scFv A7 binding, RASF cells were stimulated for 24h with human TNF-α. Staining was performed in non-permeabilised conditions as described in section 2.7.5. scFv A7 showed a dose-dependent increase in signal with both stimulated and unstimulated cells, significantly higher than the control scFv HEL (Figure 5.6 A). TNF stimulated RASF showed a significant increase in signal intensity of scFv A7 compared to unstimulated cells while maintaining a comparable curve profile, suggesting analogous binding kinetics and a possible role for cytokines in A7 target antigen up-regulation (Figure 5.6 B).

These results are in contrast with our earlier data where no detectable scFv A7 reactivity was observed with synovial fibroblast when sections of RA/OA synovial tissue were examined. Similarly, no detectable scFv A7 reactivity was observed with dermal fibroblasts when sections of human skin were examined (section 4.2). As mentioned above, *in vitro* culturing conditions might alter the protein expression profile of primary cells. In this light, reactivity of scFv A7 with primary synovial and

dermal fibroblasts in culture may represent promiscuous expression of proteins due to lack of signals from surrounding cells within the tissue matrix.

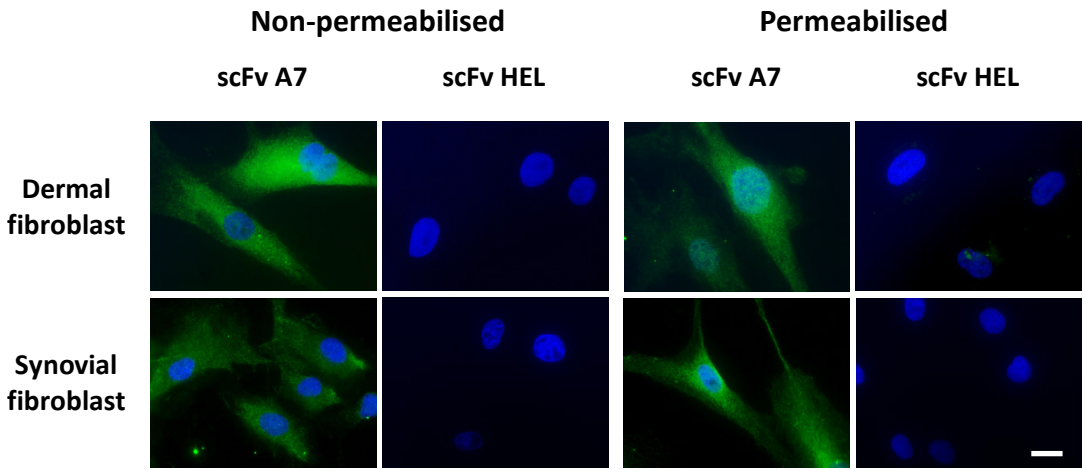

Figure 5.4 scFv A7 reactivity in cultured RA fibroblasts

Biotinylated scFv A7 IF staining in dermal and synovial fibroblast with scFv HEL staining as control, detected by α-myc antibody (Alexa 488 green). Cells were stained in non-permeabilised as well as in permeabilised condition after treatment with Triton X-100. Scale bar = 20 µm.

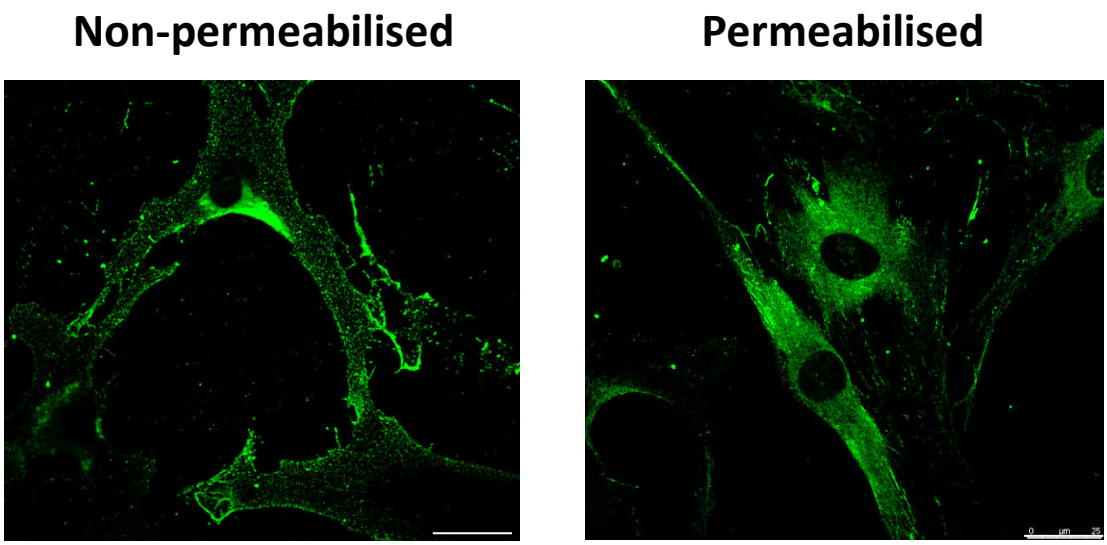

Figure 5.5 scFv A7 reactivity in RASF

Immunofluorescent staining in primary RASF with biotinylated scFv A7 detected by streptavidin-Alexa fluor 488 (green). Cells were stained in non-permeabilised as well as in permeabilised condition after treatment with Triton X-100. Pictures show confocal imaging Z-stack of positive cells. Scale Bar = 25 µm.

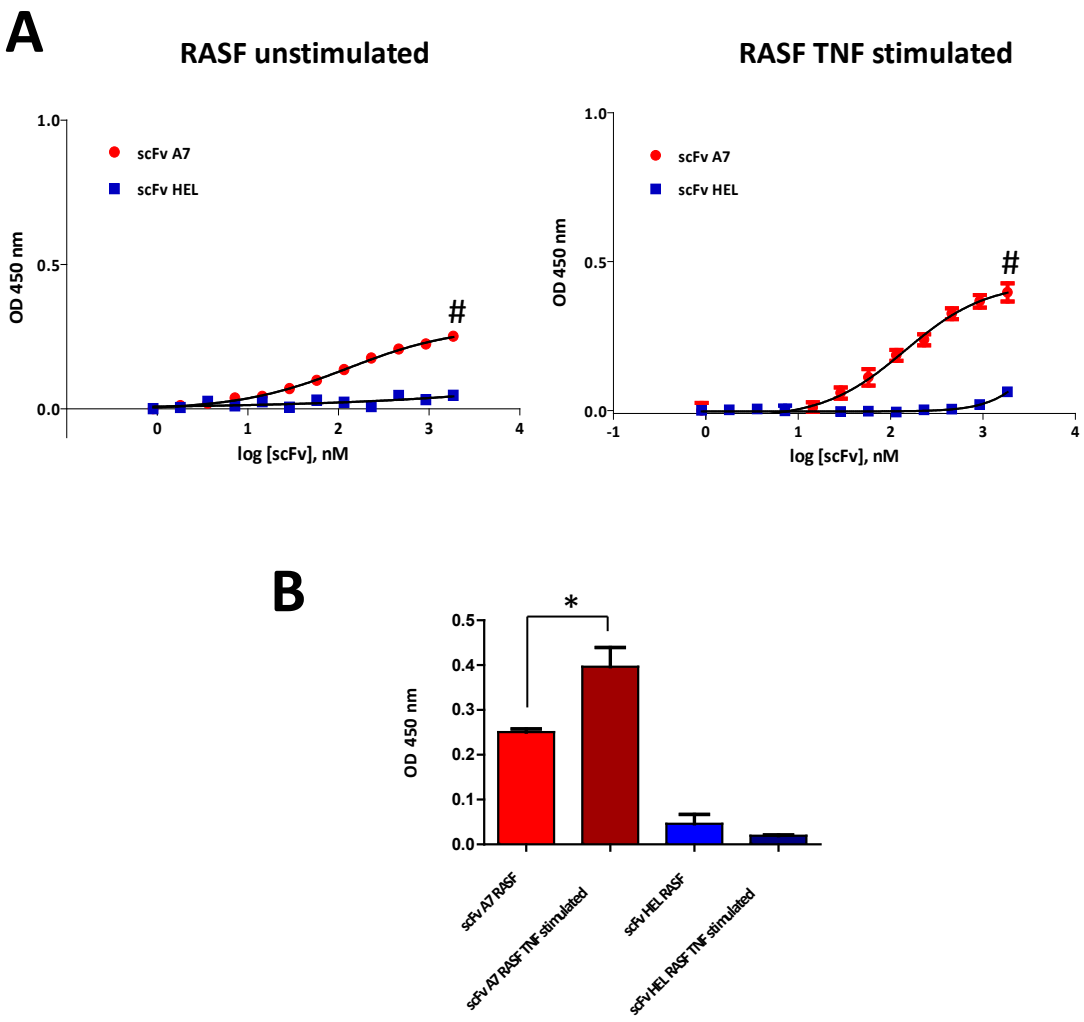

Figure 5.6 reactivity of scFv A7 in TNF stimulated RASF

Cellular ELISA on TNF stimulated and unstimulated RASF with scFv A7 and scFv HEL. Starting antibody concentration 1.85 µM with 1:2 serial dilution (A). Comparison of signal intensity between stimulated and unstimulated RASF with scFv A7 or HEL at 1.85 µM (B). Bound antibodies were detected with anti c-myc and anti-mouse IgG-HRP coupled antibody. Conversion of TMB substrate read in standard plate reader at 450 nm. (A) Unpaired t test # = p value <0.05. (B) Paired t test * = p value <0.05 (B).

5.2.2 Protein extraction from selected cell lines

The data previously described, demonstrate that scFv A7 shows reactivity with the cell surface of a number of cells grown in culture. These cells therefore, may represent a useful resource for identification of the target antigen for scFv A7 through a proteomics approach combining Western blot analysis, immunoprecipitation and protein sequencing. Towards this aim, the initial efforts sought to identify a detergent which best solublised the target molecule for scFv A7 in cells, for preparation of cell lysates for use in Western blot and immunoprecipitation studies.

Membrane bound and transmembrane proteins account for a high number of genes in the human genome, however, analysis of membrane proteins is aggravated by their low abundance in cells and low copy numbers of each individual protein (303). It is therefore crucial when aiming at isolating membrane proteins from live cells, to enrich for this class of proteins. A common feature of transmembrane proteins, is the presence of hydrophobic regions. Depending on the degree of hydrophobicity, a suitable detergent must be used in order to solubilise the antigen efficiently. To avoid cytosolic proteins contaminants and to enrich for a selected class of transmembrane protein, it is recommended to proceed with a multi-step purification process using detergents with specific properties (304). However, this procedure is time consuming and not applicable when aiming at the isolation of an unknown antigen.

The best strategy for protein enrichment was to select a number of detergents with different properties, in order to identify one able to better solubilise the unknown target antigen for scFv A7 in cells grown in culture. Since each detergent chosen would preferentially solubilise proteins with specific properties, this approach may also yield information regarding characteristic properties of the protein of interest. Specifically the following detergents were selected:

Triton X-100, a non-ionic detergent, most commonly used in protein extraction from cytoplasm, membrane and nucleus.

n-Octyl-β-D-thioglucopyranoside (OTG), a non–ionic, mild detergent used for solubilisation of membrane proteins.

Saponin, a non-ionic detergent able to remove cholesterol from the membrane. Treatment with saponin will facilitate subsequent solubilisation by Triton X-100 of the membrane proteins that would otherwise be inaccessible and insoluble in the same detergent.

Triton X-114, a non-ionic detergent used to solubilised highly hydrophobic proteins. Treatment with Triton X-114 will give two fractions: an aqueous phase rich in hydrophilic or mild hydrophobic proteins, and a detergent phase rich in highly hydrophobic proteins.

Radio Immunoprecipitation Assay (RIPA) buffer, a mild ionic detergent for efficient solubilisation of membrane-bound and soluble proteins avoiding protein degradation and interference with proteins' immunoreactivity.

The final approach used a hypotonic shock, where no detergent is used in preparation of cellular protein extract.

Although both endothelial cell line IE7 and prostate cancer cell line PC3 cell lines showed reactivity with scFv A7, this study focused initially on PC3 due to the rapid growth rate and easier culturing conditions. To this end, PC3 cell lysates prepared in the above listed detergents were resolved by SDS-PAGE, transferred onto nitrocellulose membrane and probed with anti E-cadherin and anti α-tubulin antibodies to examine the efficiency of extraction. As shown in Figure 5.6, E-cadherin, a trans-membrane protein of 124 kDa, was efficiently solubilised in all preparations with the only exception of the hypotonic shock and the supernatant from the saponin treatment. This is as expected since the hypotonic preparations should contain predominantly cytosolic proteins, while the saponin supernatant can contain some cytoplasmic proteins which are present in abundance and "leak" as the cell membrane is made more fluid due to removal of cholesterol. Indeed, this is seen with α-tubulin, an abundant intracellular protein with a molecular weight of

approximately 55 kDa (Figure 5.7). Similarly, presence of α-tubulin in the detergent phase of Triton X-114, which represents hydrophobic proteins, is most likely due to the abundance of this protein. As mentioned above, these one step protein extraction procedures are not sufficient to purify proteins but are useful for crude enrichment of specific classes of proteins.

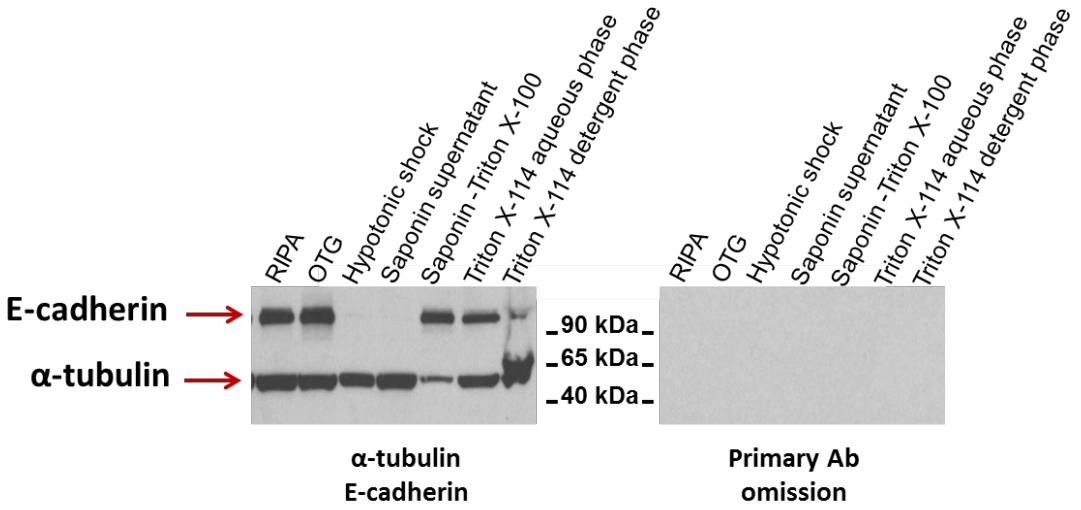

Figure 5.7 Western blot analysis of PC3 cell extracts

Western blotting of PC3 cell extracts probed with anti E-cadherin (124 kDa)/α-tubulin (55 kDa) as controls. Reactivity detected with HRP conjugated secondary antibody and ECL reagent.

5.2.2.1 Western blot analysis

Having established that the solubilisation protocols were functional and efficient in isolating transmembrane and cytosolic proteins, the above cell lysates were probed with scFv A7 in order to determine whether this antibody had applications in Western blot analysis. ScFv HEL was used as control. ScFv A7 and scFv HEL showed a similar staining pattern, highlighting protein bands at 35/37 kDa and 60 kDa (Figure 5.8). Since probing with secondary and tertiary antibodies (primary Ab omission) or tertiary antibody alone (secondary Ab omission) gave clean negative result, the reactivity detected with both A7 and HEL antibodies is probably a non-specific interaction due to the framework on the scFv format. Same result was obtained when lysates from IE7, HEK-293 and u937 cell lines were analysed by Western blot and probed for scFv A7 or control scFv HEL antibody (Figure 5.9).

ScFv antibodies are by definition single variable domains, despite maintaining comparable specificity and affinity to the parent IgG they are inherently limited by low avidity due to the monovalency of the antibody fragment. Since high avidity plays an important role in the stability of antibody-antigen complexes with a reduced dissociation rate resulting from multiple binding to antigen molecules (305), the use of the scFv-Fc construct described in section 3.3 could increase the chances of detecting the antigen in Western blot. Total cell lysate from PC3, HEK-293 and u937 cell lines using Laemmli lysis buffer (306) were resolved in SDS-PAGE and probed with A7 scFv-Fc and a control scFv-Fc antibody. No specific protein band could be detected in the A7 scFv-Fc blot when compared to the control antibody (Figure 5.10).

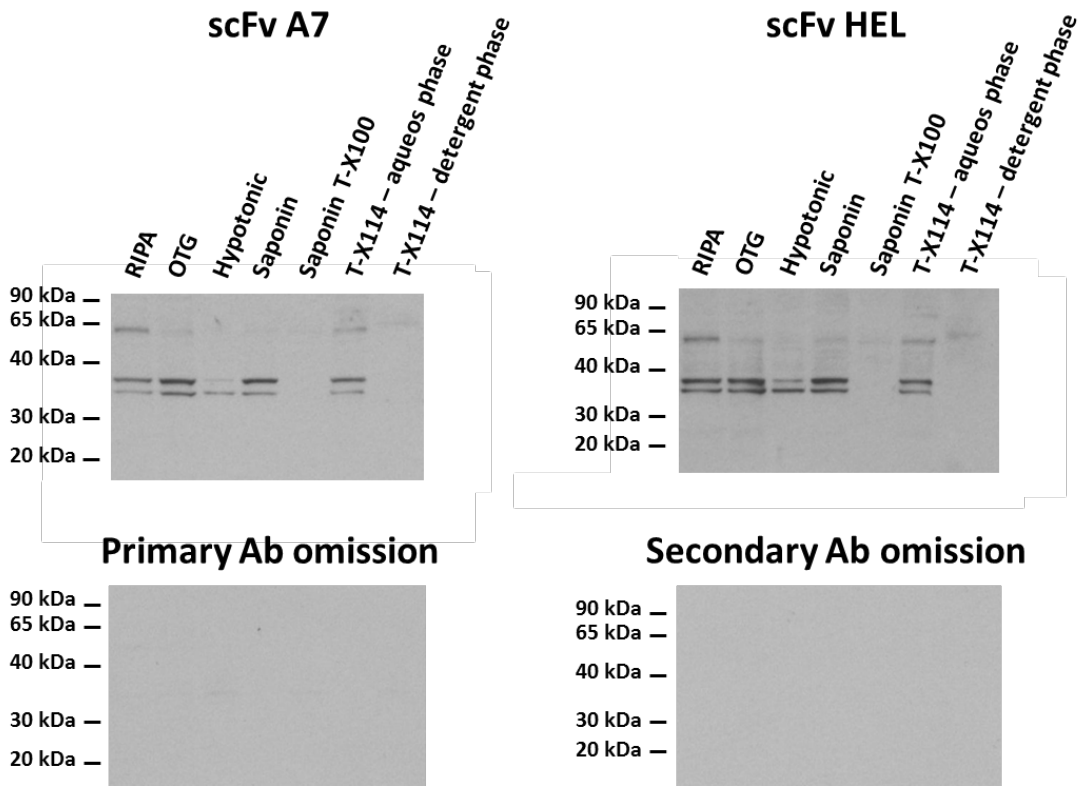

Figure 5.8 Western blot analysis of PC3 cell extracts with scFv A7

Western blotting of PC3 cell extracts probed with scFv A7 and scFv HEL as a control, at 5 µg/ml. Reactivity detected with anti c-myc and anti-mouse IgG-HRP conjugated antibody followed by incubation with ECL reagent.

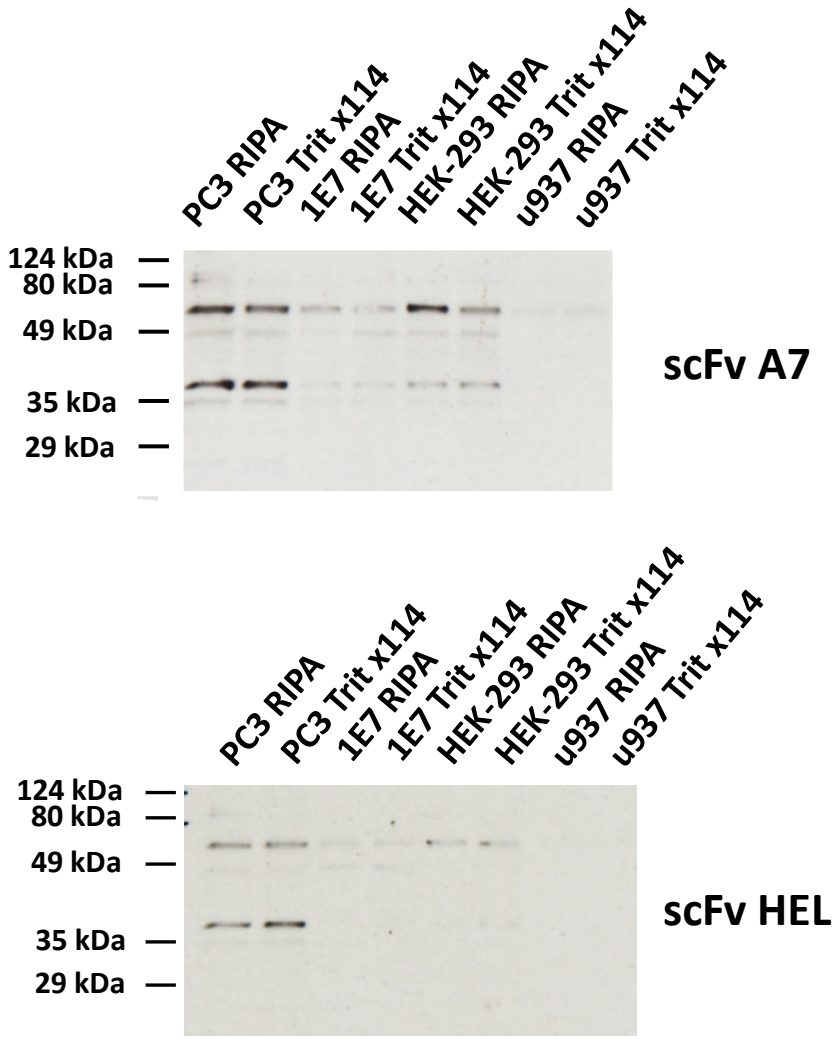

Figure 5.9 Western blot analysis of PC3, 1E7, HEK-293 and u937 cell extracts with scFv A7

Western blotting of PC3 cell extracts probed with scFv A7 or scFv HEL as control, at 5 µg/ml. Reactivity detected with anti c-myc and anti-mouse IgG-HRP conjugated antibody and ECL reagent.

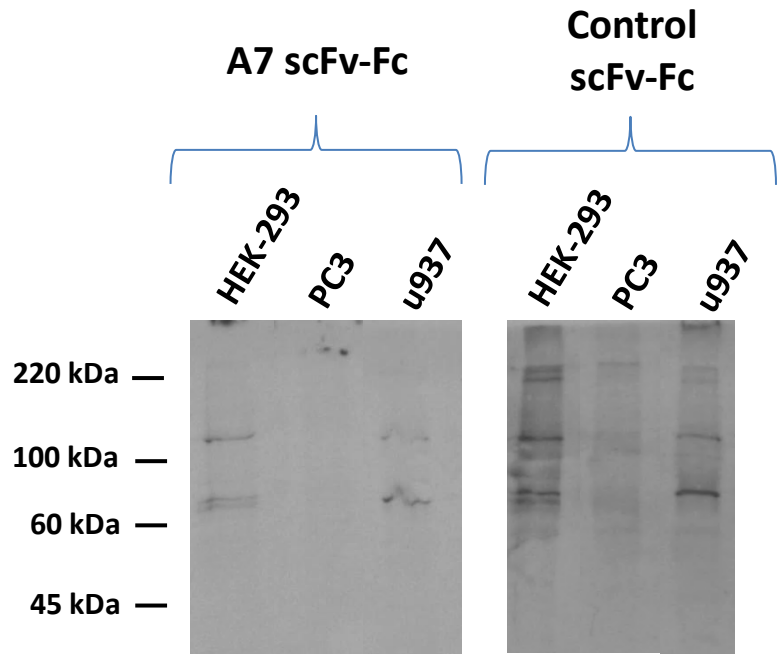

Figure 5.10 Western blot analysis of PC3, HEK-293 and u937 cell extracts with A7 scFv-Fc

Western blotting of PC3, HEK-293 and u937 cell extracts probed with A7 scFv-Fc or control scFv-Fc at 5 µg/ml. Reactivity detected with anti-human Fc-HRP conjugated antibody and ECL reagent.

5.2.2.2 Immunoprecipitation analysis

Western blot analysis using protein extracts from PC3 cell line did not provide a target candidate, showing only non-specific reactivity. Low antigen concentration in the cell lysate can often be the reason for lack of specific reactivity in Western blot. Protein concentration using filter systems is not suitable for antigens with unknown molecular weight. Immunoprecipitation, however, is a well-established method for isolating protein-protein complexes (291). The traditional method includes incubation of the test antibody with the antigen mixture, in this case the protein extract from the cell line, and subsequent binding to protein A beads. The resin containing protein A is able to selectively bind the Fc region of human IgG and the variable region of the V_HIII subgroup (248, 256). In this context, protein A will be able to pull down the antibody and the bound protein.

In the first attempt, cell lysates obtained from the PC3 cell line using RIPA buffer were incubated with the test scFv A7 or control scFv as described in section 2.9.1. Antibody-antigen complexes were then isolated from the total protein pool using agarose protein A/G. Resin-antibody-antigen complex was destabilised by using Laemmli lysis buffer and resolved by SDS-PAGE followed by Western blotting probing with scFv A7 or control scFv antibody. Data presented in Figure 5.11 show the presence of an intense band at 30 kDa corresponding to the scFv, a lower molecular weight band at 15 kDa corresponding to the scFv breakdown products and a high molecular weight band at approximately 65 kDa, visible also in the beads alone lane, which most likely corresponds to protein A/G leakage during elution. No specific band was detected with scFv A7 when compared to control scFv HEL.

Combined with the results described in section 5.2.2.1, the lack of reactivity with any specific protein band might be due to the fact that a conformational epitope is required for antibody-antigen binding. The SDS-PAGE and Western blot employed in the previous experiments involved boiling of the cell lysate in Laemmli lysis buffer containing DTT and SDS. These procedures cause reduction of disulphide bonds and denaturing of the proteins. Antibodies requiring conformational epitopes for antigen binding are therefore precluded from Western

blot application. Immunoprecipitation does not necessarily require identification of the precipitated proteins via Western blot. In this context, immunoprecipitation from cell lysate using A7 antibody should remove most of the non-specific proteins and then when resolved in SDS-PAGE should show enrichment of the target antigen that can be visualised using non-specific protein dyes. The IP procedure was repeated using scFv A7 and A7 scFv-Fc antibody formats, in parallel with the respective control antibodies, using lysates from PC3, HEK-293 cell line and primary RASF cells. SDS-PAGE resolved antibody-antigen complexes were stained with Sypro® ruby protein gel stain in order to detect total protein content and determine whether any protein enrichment was obtained in the A7 IP assays. In Figure 5.12, stained gels from PC3, HEK-293 and RASF are shown. Bands at approximately 60 kDa and 30 kDa could be detected in all gels and corresponded to the scFv-Fc and scFv molecules, respectively. Minor bands present in the gels were mirrored by the scFv-Fc and scFv alone lane and represented antibody breakdown products. No detectable protein enrichment was observed in any of the cell lines tested following IP.

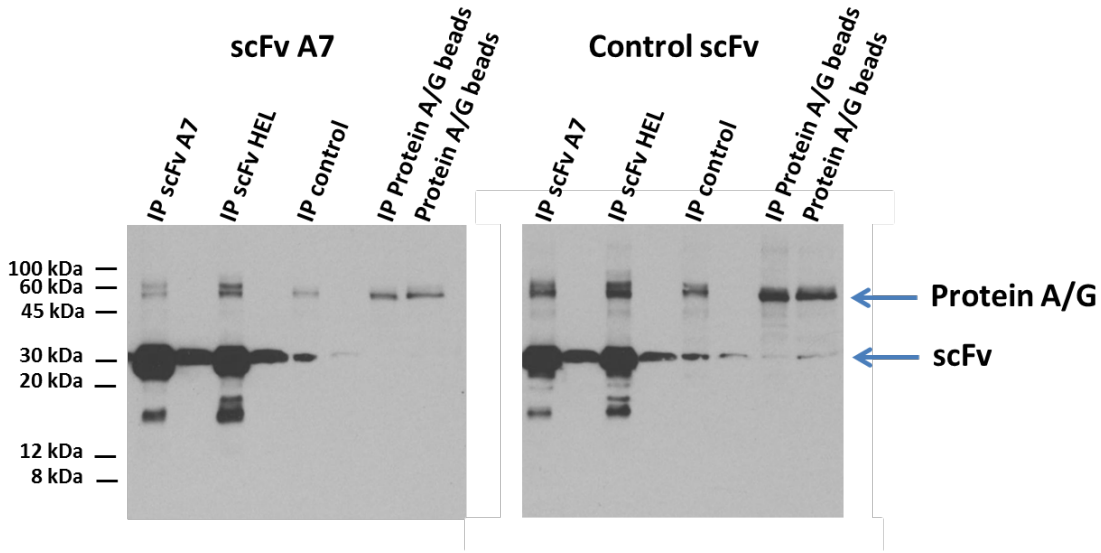

Figure 5.11 Immunoprecipitation analysis of PC3 cell extracts with scFv A7

Immunoprecipitation of PC3 RIPA cell lysates with scFv A7 and scFv HEL used as a control, at 10 µg. Recovered bound material analysed in Western blot and probed with scFv A7 or control scFv HEL. Reactivity detected with anti c-myc and anti-mouse IgG-HRP conjugated antibody and ECL reagent.

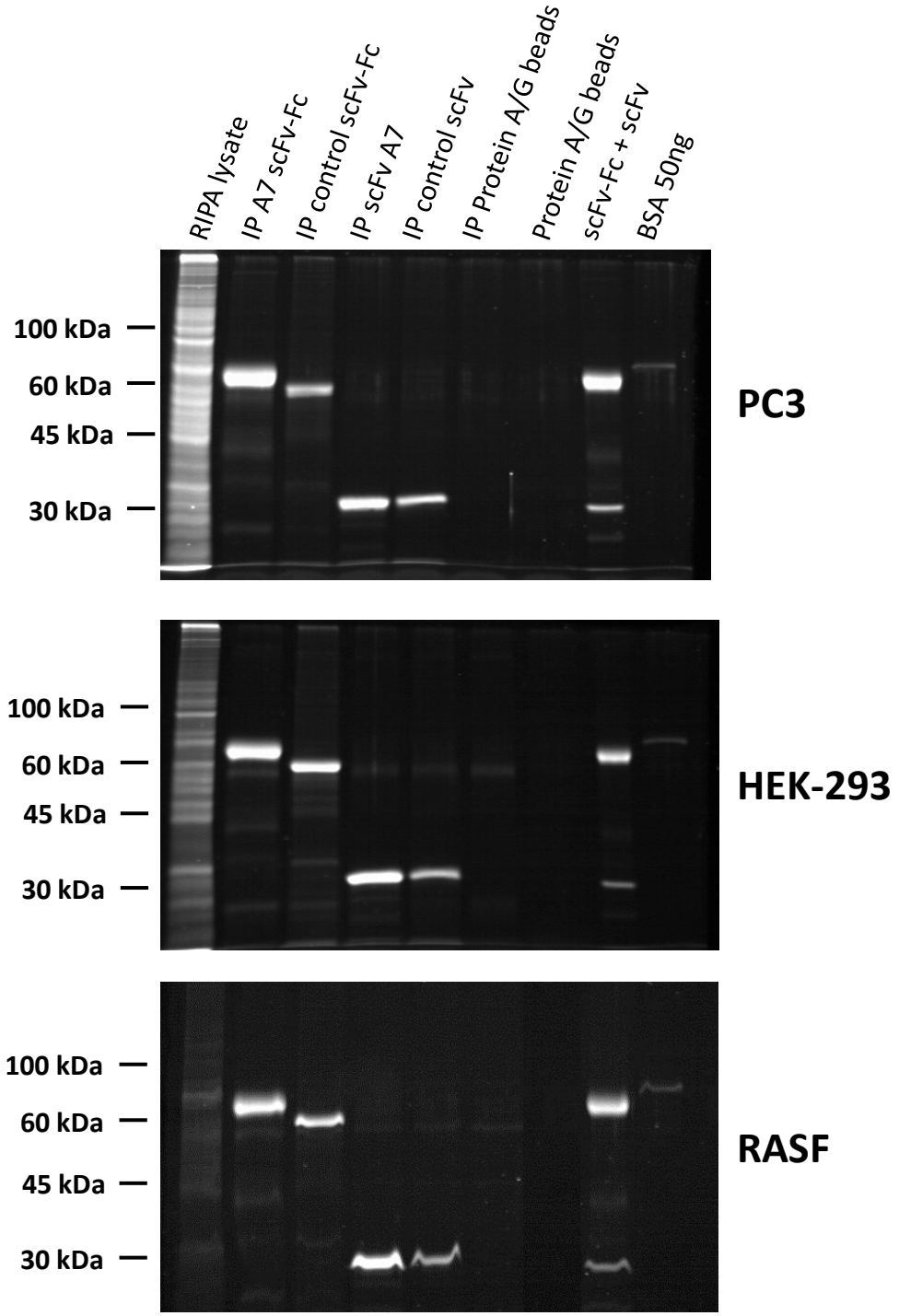

Figure 5.12 Immunoprecipitation analysis of PC3, HEK-293 and RASF cell extracts with scFv A7

Immunoprecipitation of PC3, HEK-293 and RASF RIPA cell lysates with A7 scFv-Fc, control scFv-Fc, scFv A7 and scFv HEL as control at 5 µg/ml. Recovered bound material resolved in SDS-PAGE and stained with Sypro® ruby protein gel stain.

Although the detergent approach used was able to efficiently solubilise the trans-membrane protein E-cadherin and the cytosolic protein α-tubulin (section 5.2.2), no direct proof of A7 target antigen solubilisation was obtained. In order to do so, a new lysis buffer optimised for cell lysate ELISA assay was used for PC3 protein extracts and screened for scFv A7 reactivity in ELISA. Data presented in Figure 5.13 show a dose dependent reactivity of scFv A7 with PC3 cell lysates. This result strongly indicates the presence of A7 target antigen in the protein extract.

In order to validate the IP procedure with the new lysis buffer, the trans-membrane protein ICAM-1 was chosen as a target for a proof of concept IP. The JU77 epithelial cell line expresses high levels of ICAM-1 upon 24 h TNF-α stimulation (Figure 5.14 A). The presence of ICAM-1 can be detected in stimulated JU77 cell lysates following Western blotting (Figure 5.14 B). To test the capacity to isolate ICAM-1 from TNF stimulated JU77 lysates, protein extracts were incubated with anti-ICAM 1 antibody and immune-precipitated using protein A/G beads. The elution profile shown in Figure 5.14 C, demonstrates the capacity to specifically isolate ICAM-1 using the immune-precipitation procedure.

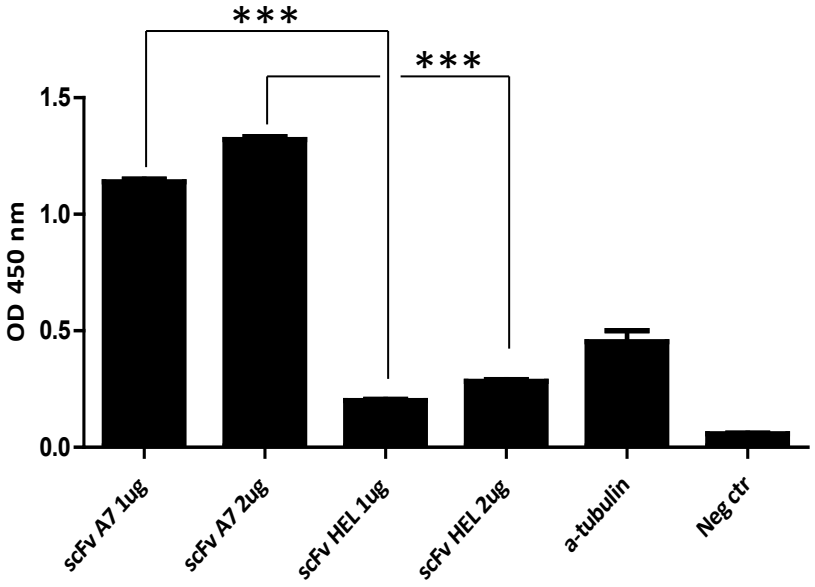

Figure 5.13 PC3 cell lysate ELISA with scFv A7

ELISA assay on PC3 cell lysate with scFv A7 or control scFv HEL. α-tubulin antibody included as positive control. Signal detected with streptavidin-HRP. Two tailed unpaired T-test ***= p value < 0.001.

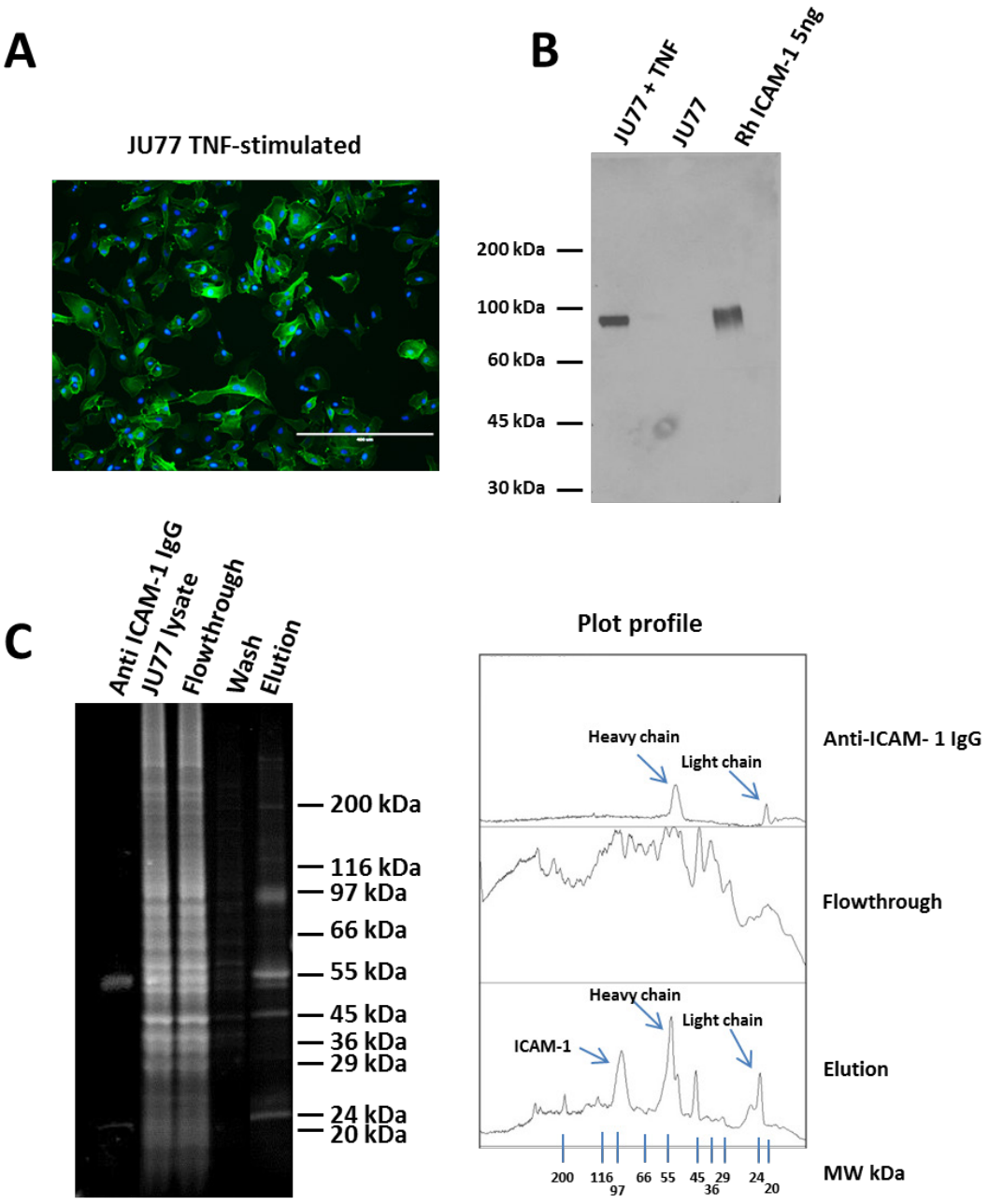

Figure 5.14 ICAM IP on JU77 protein extracts

JU77 stimulated with 10 ng/ml TNF-α for 24 h stained with anti-ICAM-1 antibody (green) and DAPI (blue) to depict nuclei (A). Scale bar 400 µm. Western blot on JU77 and TNF stimulated JU77 cell lysates probed with anti ICAM-1 antibody. Recombinant human ICAM-1 was used as a positive control (B). IP on TNF stimulated JU77 cell lysates using anti ICAM-1 antibody (C).

As previously described, protein A is able to bind the variable antibody region of the V_HIII subgroup (248). However, as shown in section 3.2.1, protein A is not as efficient as Talon in purifying scFv antibody fragments which may be due to low affinity for the variable region and suboptimal antigen retention compared to the interaction of Talon® for the 6His tag. In order to prevent early dissociation, scFv A7 and control scFv HEL were directly coupled to CNBr-activated agarose beads. In this process, CNBr reacts with the hydroxyl groups on agarose beads forming cyanate esters. These groups are able to react with primary amines under very mild conditions. The result is a covalent coupling of proteins/peptides to the agarose beads. Since this process is non-specific and will covalently bind any given protein, a pure antibody preparation has to be used in order to avoid unwanted contaminant protein coupling which can reduce the binding capacity of the resin and increase background noise. As demonstrated in section 3.2.2, the scFv purification process yielded a high quality pure antibody with limited breakdown contaminant products. Coupling efficiency of scFv A7/HEL with CNBr-activated agarose beads was measured via quantification of free scFv pre- and post-coupling (Figure 5.15). A coupling efficiency greater than 97% was obtained for both scFv antibodies.

The coupled agarose beads were used in an immunoprecipitation assay to identify interacting partners within the PC3 cell line. PC3 protein extract that showed positivity for scFv A7 in ELISA (Figure 5.13) was used as the antigen source. In order to include a positive control for the IP procedure and confirm functionality of the setup, recombinant hen egg lysozyme was added to the PC3 protein extract. IP was performed as described in section 2.9.2. Briefly, PC3 protein extract was incubated with the coupled resin to allow antibody-antigen interaction. The beads resin was then washed to eliminate non-specific and low affinity protein interactions and subsequently eluted in Laemmli lysis buffer to recover bound material. This final fraction should contain the antibody coupled to the resin and any protein that showed sufficient binding interaction. The recovered bound material was then resolved in SDS-PAGE and stained with Sypro® ruby protein gel stain to highlight protein content. In Figure 5.16 A is shown the resolved fractions

obtained from scFv A7 and scFv HEL IPs, including loaded material, flowthrough, washing steps and eluted bound material. Visual comparison between the resolved PC3 loaded material and the flowthrough fraction, containing the unbound protein from scFv A7 IP, does not show any significant protein depletion. The reduction in intensity of a band in the flowthrough compared to the total protein load would indicate a selective retention of the antigen in the coupled resin. Low protein content can be detected in the washing step fractions of both scFv A7 and scFv HEL and represents antigens with low affinity for the coupled resin. Finally, the elution fractions of both A7 and HEL show the presence of a marked band at 30 kDa corresponding to the molecular weight of the scFv molecule. However, high background is visible in both scFv A7 and scFv HEL recovered bound material. Analysis of the elution plot profile (Figure 5.16 B) shows the presence of several proteins with different intensity (peaks) but with no clear distinction between scFv A7 and the control scFv HEL samples. No detectable specific protein was isolated in the scFv A7 IP. Despite high protein contaminants in the elution fractions, the scFv HEL was able to selectively retain the recombinant hen egg lysozyme antigen which is represented by a peak at 14 kDa with considerably higher intensity compared to the scFv A7 elution fraction.

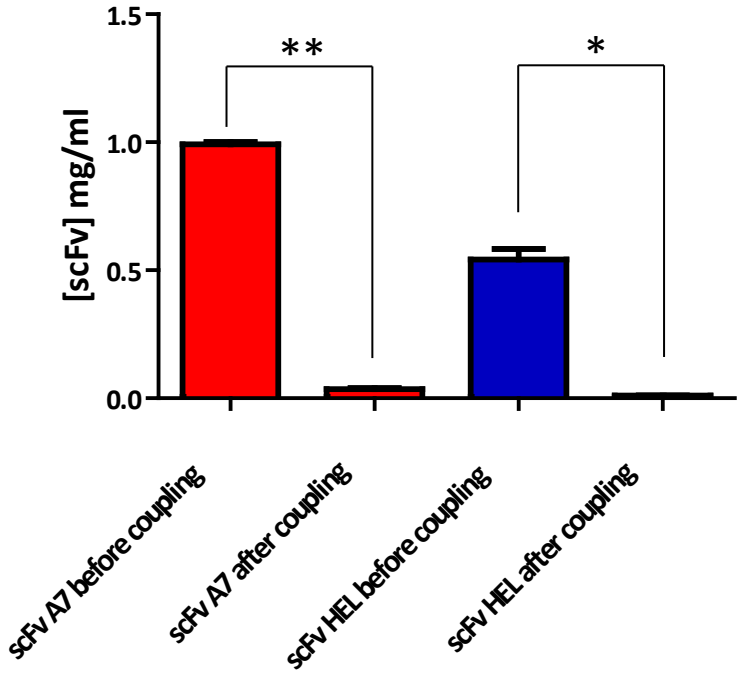

Figure 5.15 Agarose beads coupling efficiency

ScFv coupling efficiency on CNBr-activated agarose beads. Free scFv measured via spectrophotometric analysis at 280nm. Paired t test * = p value <0.05, ** = p value <0.01.

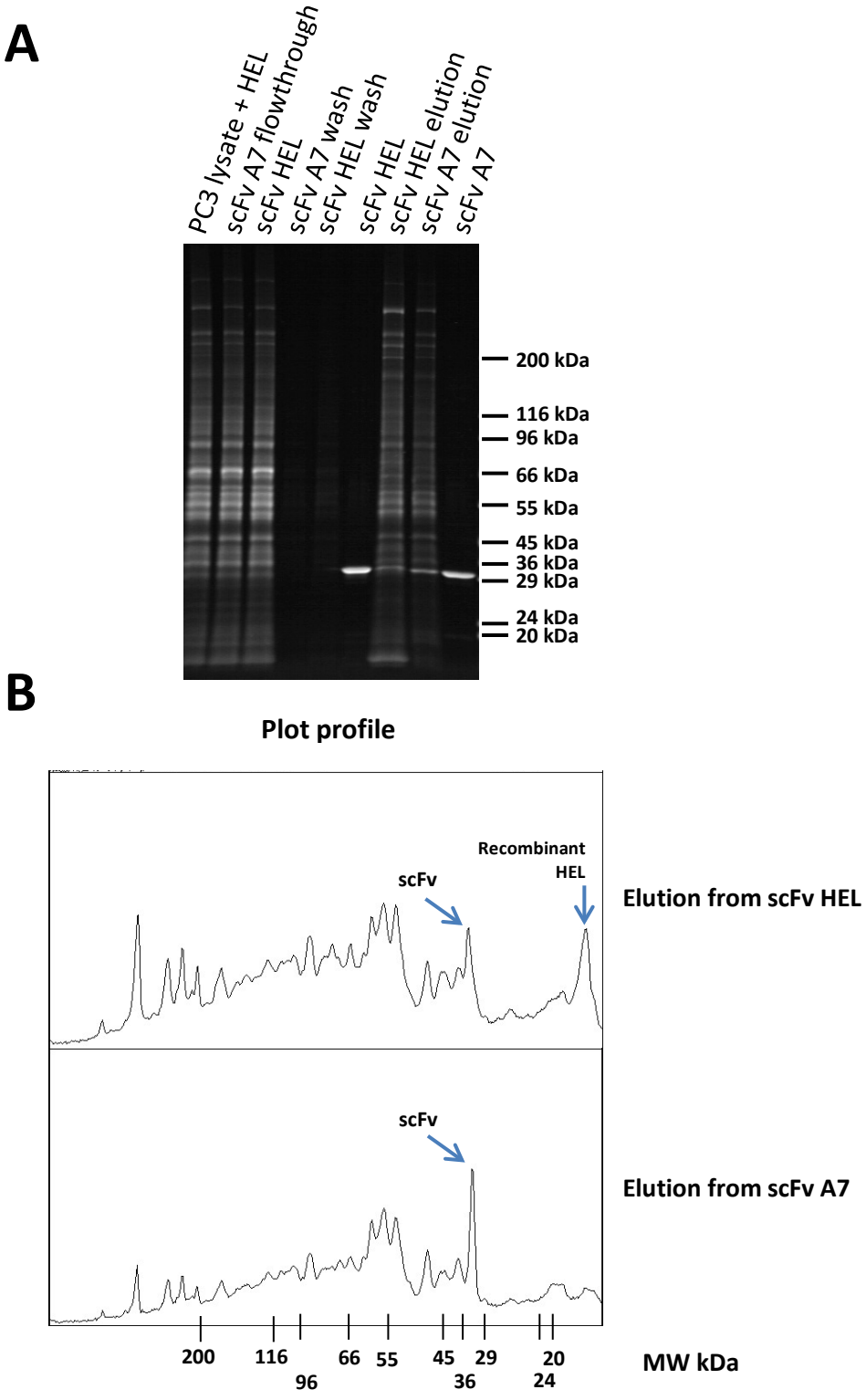

Figure 5.16 SDS-PAGE of scFv A7 IP with PC3 protein extract

SDS-PAGE resolved samples from PC3 protein extracts using scFv A7 and scFv HEL coupled agarose beads (A). Plot profile analysis of elution fraction of scFv A7 and scFv HEL using the image analysis tool ImageJ (B).

As already mentioned above, scFv antibodies may be limited in their binding capacity and antibody-antigen complex stability by low functional affinity and avidity (305). Since no clear antigen enrichment was obtained using scFv A7 and PC3 protein extracts, the scFv-Fc bivalent A7 antibody format was adopted in the subsequent experiments. In this IP setup, the scFv-Fc antibody obtained from concentrated CHO-S supernatant (section 3.3.1), was coupled to protein A beads. Unlike scFv antibody fragments, full human IgG molecules have shown high binding capacity to staphylococcal protein A (256), making protein A resin suitable for this purpose. In addition, to ensure a better washing step and limit the carry-over of unbound material, magnetic protein A coupled beads were used as binding resin. The use of a magnetic resin confers an advantage over classical protein A agarose beads, the beads can be separated from the liquid phase by applying a magnetic field to the suspension reducing the carry-over of unwanted sample/washing buffer, reducing loss of resin during washing steps and resulting in fewer interference bands and lower backgrounds (307). Subsequently, beads-protein A-antibody complex was added to the PC3 cell lysate or to the RASF cell lysate to allow antibody-antigen binding. After 3 washing steps, bound antigens were eluted in Laemmli lysis buffer following incubation at 90 °C.

As shown in Figure 5.17 A, most of the A7 scFv-Fc was successfully coupled to the beads with only limited uncoupled material left in the flowthrough (lane A7 scFv-Fc uncoupled FT). Similarly to what was observed in Figure 5.16, no clear protein depletion was identified between total PC3 lysate material and flowthrough following incubation with A7 scFv-Fc coupled resin. Analysis of the elution fraction obtained from PC3 lysate with A7 scFv-Fc or control scFv-Fc antibody, shows the presence of a predominant band at 60 kDa which corresponds to the reduced scFv-Fc molecule (Figure 5.17 A). Comparing plot profiles of A7 scFv-Fc loaded material, PC3 cell lysate and elution fraction from control and A7 scFv-Fc antibodies can help distinguish protein peaks deriving from the scFv-Fc loaded material and peaks deriving from the PC3 cell lysate (Figure 5.17 B). Several peaks are visible in the elution profile of A7 scFv-Fc, mostly shared by the control antibody elution profile and A7 scFv-Fc loaded sample plot. A peak at around 180 kDa was very intense in

the A7 elution sample compared to control (Figure 5.17 B dashed line). However, the same peak was present also in the A7 scFv-Fc loaded sample, indicating therefore a possible antibody aggregate. A second protein peak at around 50 kDa was more pronounced in the A7 scFv-Fc elution plot while being absent in the A7 scFv-Fc sample plot, suggesting a protein that is not a breakdown product of the antibody itself but rather a specific protein enrichment (Figure 5.17 B dotted line and blue arrow).

IP on RASF cell lysates showed a similar pattern when compared to PC3 IP (Figure 5.17 A). No clear protein depletion was visible between RASF lysate and flowthrough following incubation with A7 scFv-Fc coupled resin. Interestingly, the elution profile of IP performed with A7 scFv-Fc was remarkably similar with the one obtained in PC3 IP (Figure 5.17 B). An intense peak at 180 kDa was visible in the A7 elution profile (Figure 5.17 B dashed line) but was shared with both A7 scFv-Fc loaded sample and control antibody elution profiles and therefore representing most likely an antibody aggregate. The possible specific band observed at 50 kDa in PC3 IP was present also in the RASF IP. The peak was marked in the A7 elution sample while being undetectable in both control IP elution and A7 scFv-Fc loaded sample (Figure 5.17 B dotted line and blue arrow).

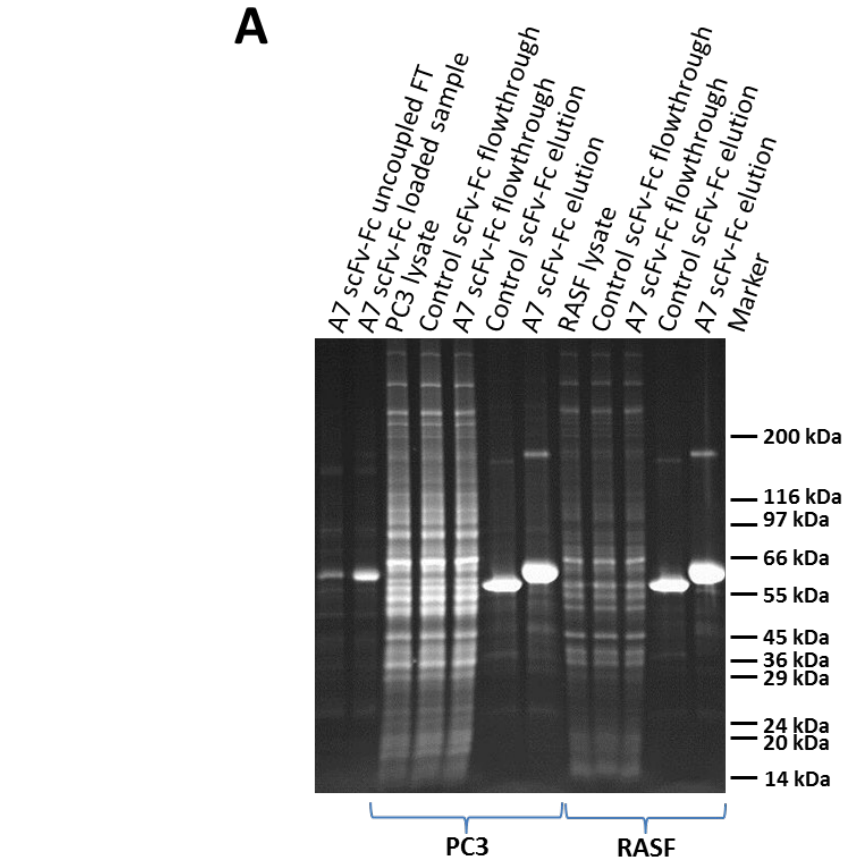
A
A7 scFv-Fc uncoupled FT
A7 scFv-Fc loaded sample
PC3 lysate
Control scFv-Fc flowthrough
A7 scFv-Fc flowthrough
Control scFv-Fc elution
A7 scFv-Fc elution
RASF lysate
Control scFv-Fc flowthrough
A7 scFv-Fc flowthrough
Control scFv-Fc elution
A7 scFv-Fc elution
Marker
200 kDa
116 kDa
97 kDa
66 kDa
55 kDa
45 kDa
36 kDa
29 kDa
24 kDa
20 kDa
14 kDa
PC3
RASF

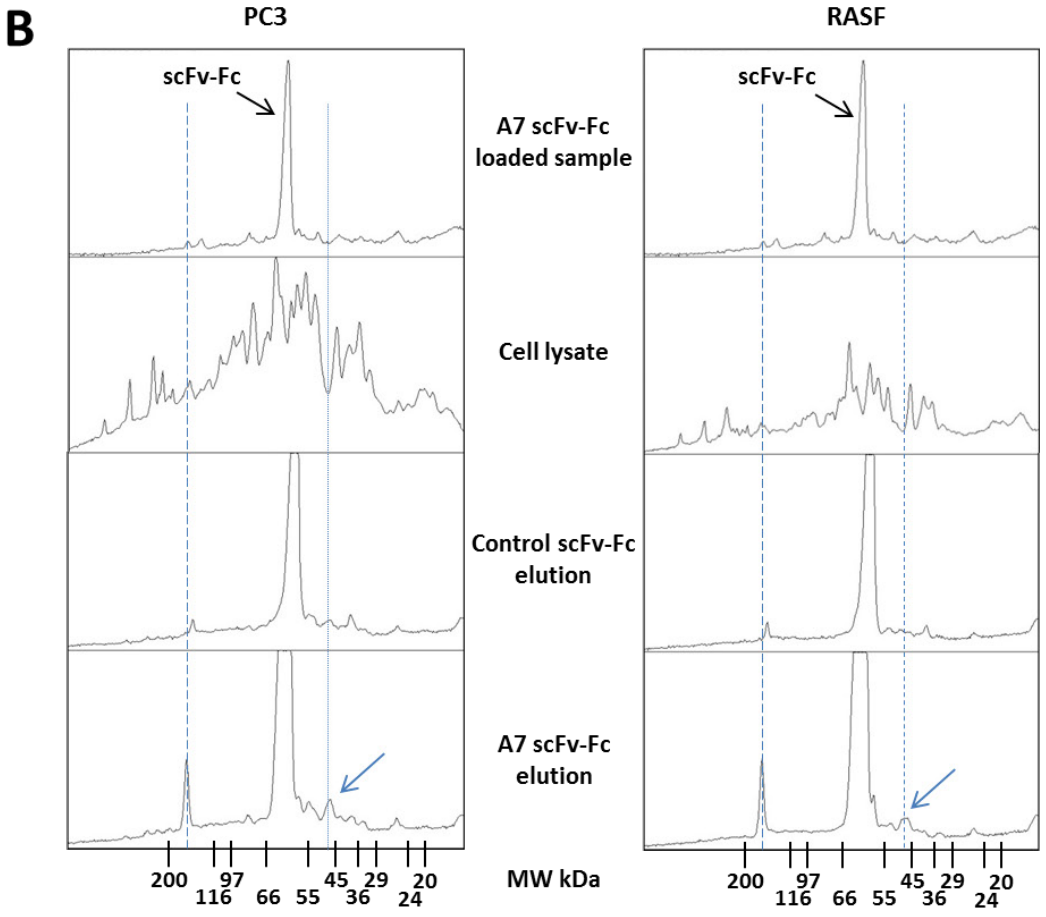
B
PC3
RASF
scFv-Fc
scFv-Fc
A7 scFv-Fc loaded sample
Cell lysate
Control scFv-Fc elution
A7 scFv-Fc elution
MW kDa
200
97
116
66
55
45
36
29
24
20

Figure 5.17 SDS-PAGE of A7 scFv-Fc IP with PC3 and RASF protein extracts

SDS-PAGE resolved samples from IP of PC3 and RASF protein extracts using A7 scFv-Fc coupled to protein A dynabeads (A). Plot profile analysis gel lanes using the image analysis tool ImageJ (B). Peak specific for scFv-Fc A7 elution marked with blue arrow and dotted line.

The IP experiments described so far were characterised by the elution of the IP antibody with the partner antigen. The Laemmli lysis buffer used to recover the bound antigens from the affinity purification resin contains SDS and DTT reagents, causing protein denaturation. While this is important for optimal band resolution in SDS-PAGE, together with the boiling step it also causes uncoupling of the antibody from the resin. Since the antibody is likely the most abundant protein in the IP mixture, its presence in the elution fraction might mask other proteins, preventing detection in standard SDS-PAGE analysis. In order to prevent antibody leakage during the elution step, a possible solution is cross-linking the protein to the resin.

For this purpose, A7 scFv-Fc antibody derived from concentrated supernatant of CHO-s cells was coupled to protein A beads and cross-linked using bis-sulfosuccinimdyl-suberate (BS3) as described in section 2.9.3. The BS3 is a water soluble molecule containing amino reactive sulfo-NHS esters on both ends that can be used to covalently orient antibody to immobilised protein A resin. Subsequently, the resin-antibody complex was added to the PC3 protein extract to allow antibody-antigen interaction. In order to limit possible antibody leakage, the elution step was conducted without Laemmli lysis buffer but using a pH 2.8 elution buffer instead. Before loading on SDS-PAGE for resolution, the elution fraction was equilibrated to pH 7.4 via buffer exchange in PBS using filter spin columns. The data presented in Figure 5.18 A, confirm the efficient coupling of scFv-Fc to the protein A beads, visible as a depleted 60 kDa band in the uncoupled flowthrough fraction in the stained SDS-PAGE. The scFv-Fc 60 kDa band was efficiently retained by the cross-linked protein A resin with no detectable leakage in the elution fractions of both A7 and control scFv-Fc. Virtually no proteins were eluted from the control IP, while two main bands could be detected in the A7 scFv-Fc IP elution. The presence of a smear in the A7 elution sample is reflected in the plot profile analysis in Figure 5.18 B by an elevated background noise. However, two main peaks are clearly visible at 95 kDa and 15 kDa, not being shared by the control elution sample and representing specific A7 scFv-Fc interactions (dotted line in Figure 5.18 B). A peak at 60 kDa, corresponding to the A7 scFv-Fc, was visible in the A7 scFv-Fc loaded sample but

not in the A7 or control IP elution, confirming the efficient retention of the antibody by the cross-linked protein A resin.

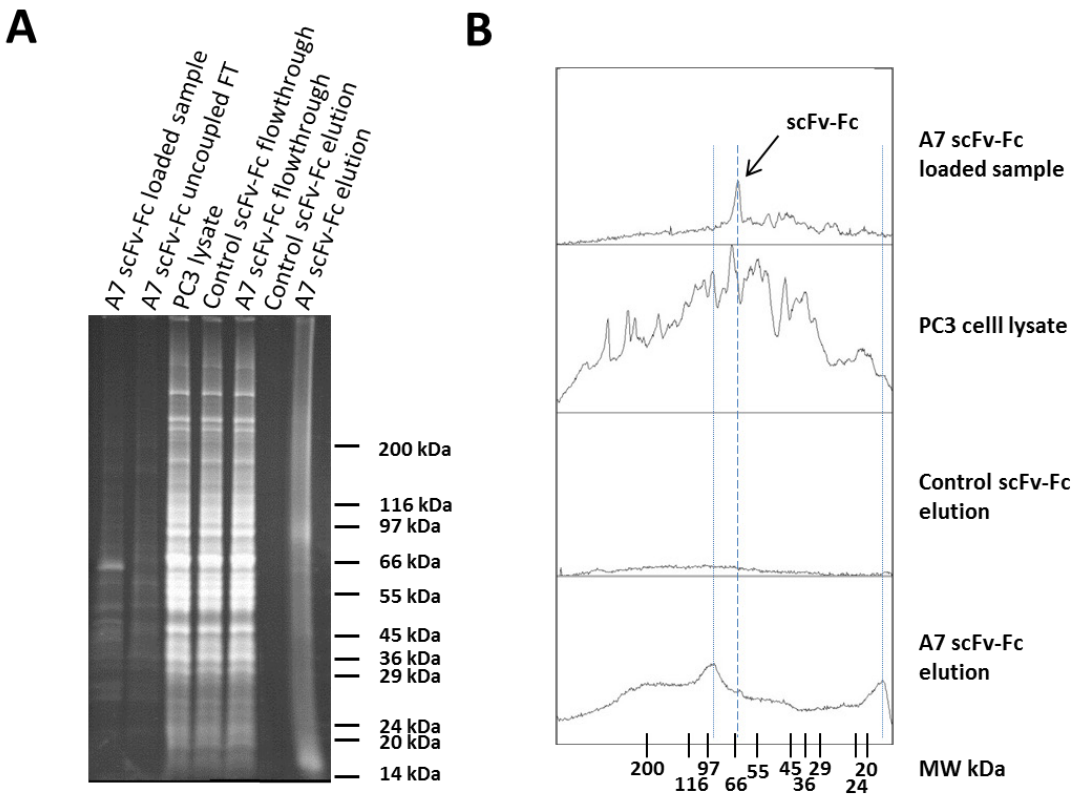

Figure 5.18 SDS-PAGE of cross-linked A7 scFv-Fc IP with PC3 protein extracts

SDS-PAGE resolved samples from IP of PC3 protein extracts using A7 scFv-Fc cross-linked to protein A dynabeads (A). Plot profile analysis gel lanes using the image analysis tool ImageJ (B). Peak specific for scFv-Fc A7 elution marked with dotted line. Peak corresponding to scFv-Fc antibody marked with dashed line.

5.3 Phage library screening

The second approach used for antibody target antigen identification was the screening of cDNA expression libraries. cDNA libraries have been successfully used to isolate protein-protein interactions over the years and phage display proved to be a versatile technology for large library screening (294, 308, 309). As already described in section 1.4.2 for scFv phage display isolation, phage libraries were expressed in permissive host *E.coli* strains allowing the formation of a full bacteriophage vehicle containing the foreign (test) antigen fused to the phage coat proteins. The test antigen is therefore exposed on the surface of the bacteriophage and free to interact with partner antigens during library biopanning. For the purpose of this project, a phage display cDNA expression library was used as a screening tool to identify interacting molecules to the A7 antibody.

Since phage libraries require amplification and expression in bacterial hosts, protein expression is characterised by the absence of post-translational modifications. This aspect represents a limitation for identification of protein-protein interactions when modifications such as glycosylation are important for protein activity and/or folding. In order to establish whether the glycosylation was required for scFv A7 binding to its target antigen, in collaboration with the University College of London the positive cell line IE7 (characterised in section 5.2.1) was treated with tunicamycin, PNGase F and benzyl-GalNAc. Tunicamycin is an antibiotic that blocks the reaction of UDP-GlcNAc in the first step of glycoprotein synthesis, inhibiting *N*-linked glycoprotein formation. PNGase F is an amidase able to cleave between GlcNAc and asparagine residues of complex oligosaccharides from *N*-linked glycoproteins. Benzyl-GalNAc inhibits glycosyltransferase incorporation of glucosamine into *O*-glycans, suppressing *O*-linked glycosylations. The data shown in Figure 5.19 suggest that the glycosylation is not required for scFv A7 binding. However, it doesn't exclude the presence of glycosylation in the target antigen.

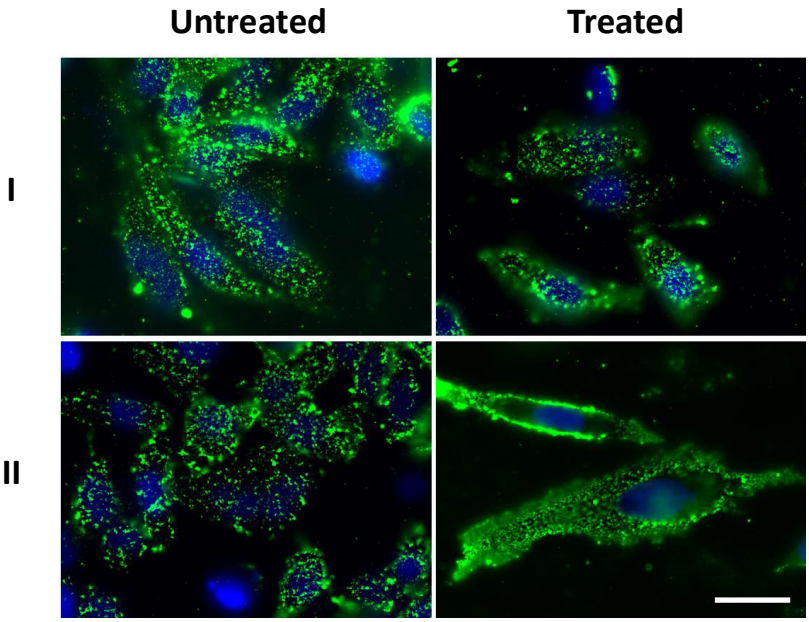

Figure 5.19 scFv A7 reactivity in IE7 cell line following inhibition of glycosylation

Immunofluorescent confocal microscopy was used to examine the reactivity of scFv A7 with the cell surface of 1E7 cells after treatment with tunicamycin together with the glycosidase PNGase F, for removal of N-linked carbohydrates (**I**), and benzyl-GalNAc for inhibition of O-linked glycosylation (**II**). Reactivity with the cell surface was examined using non-permeabilised cells. Bound scFv A7 was detected through anti c-myc antibody followed by Alexa fluor 488. DAPI was used to depict nuclei.

The cDNA library used for the proposed screening was developed and extensively characterised by Di Niro *et al.* (241). Briefly, the library was obtained from mRNA of human colon carcinoma, human lung fibroblasts and human pancreatic islets. The mRNA molecules were fragmented, reverse transcribed in cDNA, cloned into an appropriate vector and filtered for clones encoding for open reading frames (ORF). Massive sequencing of the entire cDNA library demonstrated the presence of over 18000 different human genes. In addition, the random fragmentation of the source mRNA provides the possibility to identify the minimum region required for protein-protein binding and determine the epitope recognised by the test antibody.

The phage display cDNA expression library screening was performed in collaboration with the University of Eastern Piedmont in Novara, Italy. Figure 5.20 shows a schematic for phage library biopanning on scFv A7. Briefly, in the first round of selection 4 μg/ml scFv A7 was coated on immunotubes, as described in section 2.14, and incubated with the phage library (10^{13} phage clones) in order to allow antibody-antigen interaction. Phage clones showing no specificity or low affinity for the scFv A7 were removed by serial washing steps using 0.1% tween 20 in PBS to increase stringency. Bound clones were then recovered via incubation with *E.coli* DH5α bacteria strain and plated for amplification. In Figure 5.21 an agarose gel analysis of PCR products from random clones derived from the first round of selection is shown. The PCR confirmed the selection of cDNA fragments from 200 to 700 bp which indicates a correct selection performance (Figure 5.21 A). Recovered infected bacteria were then infected with helper phage and phage clones harvested for a second round of selection. The second round of selection was performed using the same protocol adopted for the first round. One important characteristic that differentiates the first round from the second is the fact that this selection will start with a total phage population containing only phage clones showing high binding capacity for the test antibody. A total of 10^{12} phage were used for the second biopanning and in order to increase the stringency of the assay, the washing steps were doubled in number. The increased washing steps would allow the elimination of phage clones that showed moderate affinity for the scFv A7

during the first round of selection, contributing to enrich for the clones showing high binding capacity. The second round of selection gave a titre of 10^4 phage clones. Starting from a total of 10^{13} phage from the non-selected library, the output showed a 10^9 reduction in phage number which indicates positive selection and enrichment for specific phage clones. Random colonies from DH5α *E.coli* bacteria infected with the output from the second round of selection were screened in phage ELISA to confirm the specificity for scFv A7. In this assay, coated scFv A7 in a 96 well plate was challenged with phage obtained from the random colonies selected. Bound phage molecules were detected using an anti-M13 antibody (Figure 5.21 B). One clone (F2/B6) showed a good signal with scFv A7 and 6 showed only a moderate reactivity. When expressed as soluble protein extracted from the periplasmic compartment of infected bacteria, only the clone F2/B6 showed good expression and reactivity for scFv A7 (Figure 5.21 C). Sequencing analysis and BLAST alignment identified the clone F2/B6 as *Latent-transforming growth factor beta-binding protein 2* (LTBP2), a human extracellular matrix associated protein with multi-domain structure.

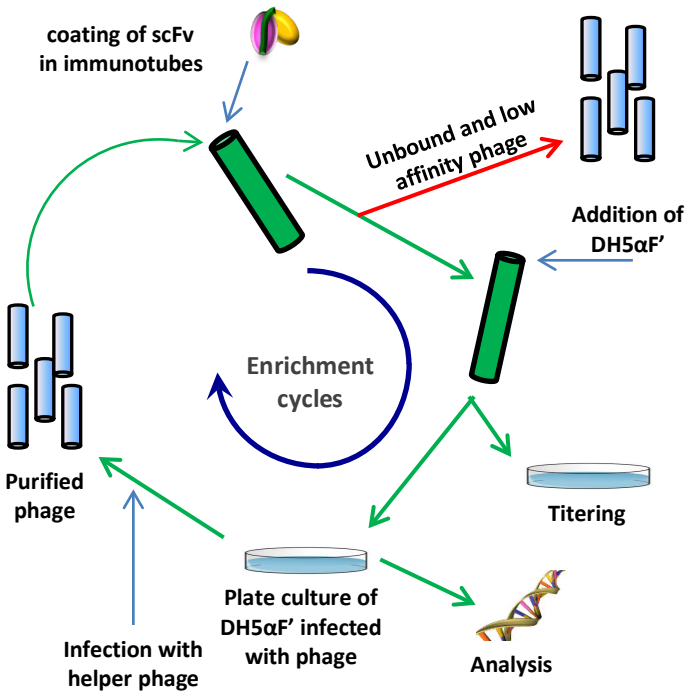

Figure 5.20 Phage display screening of cDNA expression library with scFv A7

Schematic of cDNA expression library biopanning on scFv A7 using phage display. Immobilised scFv antibodies in immunotubes were incubated with the phage library, unbound and low affinity phages removed by washing steps. Bound phage clones recovered via infection of DH5α *E.coli* strain and plated for amplification. The total output was then harvested and used for successive rounds of enrichment.

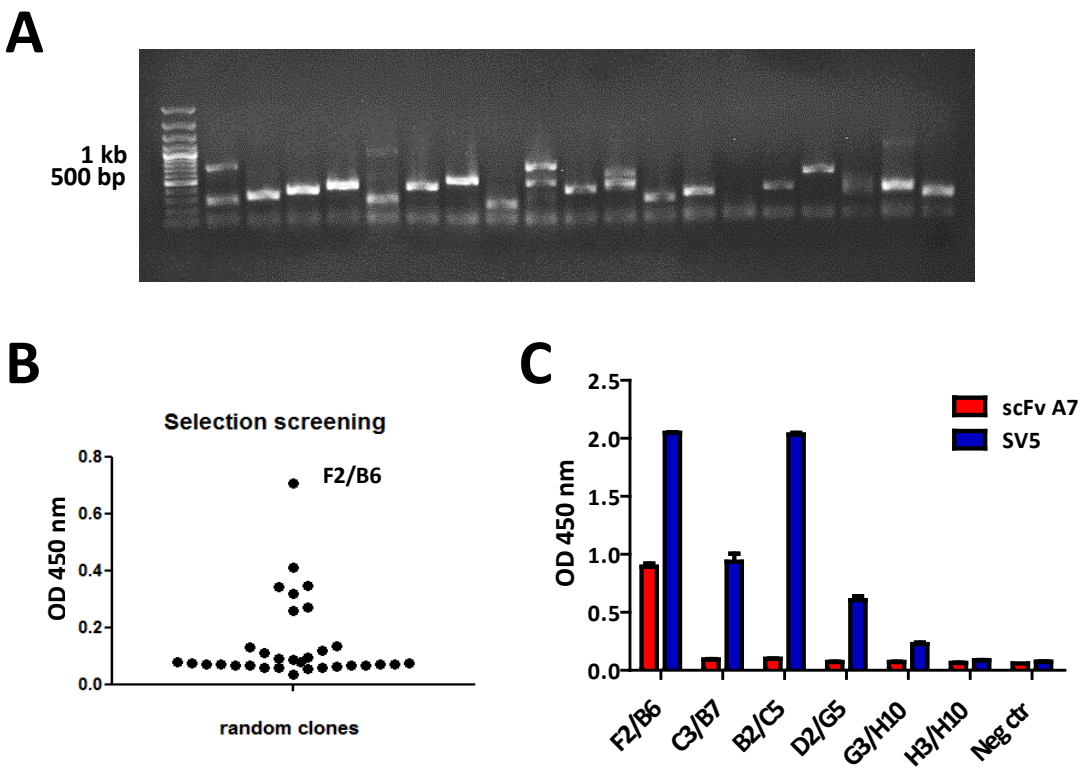

Figure 5.21 Analysis of phage clones from first phage display selection

PCR screening on random clones from the first round of selection on scFv A7. Fragment length from 200 to 700 bp, consistent with cDNA library characteristics (A). Analysis of selected phage clones from second round of selection on scFv A7. Phage ELISA on coated scFv A7 detected with anti-M13 HRP conjugated antibody (B). ELISA on periplasmic extract of selected clones on coated scFv A7 detected with anti SV5 tag and anti-mouse HRP conjugated antibody (C).

The phage display library screening was performed a second time using both scFv A7 and A7 scFv-Fc immobilised in immunotubes. The screening protocol was conducted in the same way as described above with the following modifications: 10 µg/ml of antibody was immobilised on a plastic surface and incubated with the phage library for a shorter time at room temperature (30 minutes standing and 1 hour on rotation). The output from the first round of selection was then amplified via infection of DH5α and used as input for a second round of selection against the same antibodies. As for the previous phage display selection, washing steps were increased in the second round. 50 random colonies were picked for both scFv A7 and A7 scFv-Fc selection and screened in phage ELISA as previously described (Figure 5.22 A). Clones that were shown to have a good signal on phage ELISA were screened by PCR to analyse insert length (Figure 5.22 B) and sequenced to determine identity via BLAST alignment on human nucleotide database (Table 5.1). Phage ELISA of clones that showed strong signal for A7 scFv-Fc (n=3) or scFv A7 (n=1) was repeated using two different concentrations and including the control scFv-Fc antibody as negative control (Figure 5.22 C). None of the selected clones gave a similar result for both scFv A7 and A7 scFv-Fc, while non-specific reactivity for the control scFv-Fc was detected for half of the samples.

phage	coating	N° cycle	clone	Sequence identity
output 1°cycle vs A7 scFv-Fc	A7 scFv-Fc	2	A5	Homo sapiens ras homologous gene family member B (RHOB)
			B4	Homo sapiens ring finger protein 1 (RING1)
			C2	serpin peptidase inhibitor, clade A (alpha-1 antiproteinase, antitrypsin)
			E4	Homo sapiens brain abundant, membrane attached signal protein 1 (BASP1)
			F2	Homo sapiens ras homologous gene family member B (RHOB)
			F5	TOP1
			G4	Homo sapiens nuclear receptor subfamily 1, group H, member 2 (NR1H2)
			G5	Homo sapiens serrate RNA effector molecule homolog (Arabidopsis) (SRRT)
output 1° cycle vs scFv A7	scFv A7	2	F7	Homo sapiens adenylate cyclase 5 (ADCY5)
			F9	Homo sapiens GABA(A) receptor-associated protein like 1 (GABARAPL1)
			H8	Homo sapiens GABA(A) receptor-associated protein like 1 (GABARAPL1)
			H12	Homo sapiens GABA(A) receptor-associated protein like 1 (GABARAPL1)

Table 5.1 Sequence identity of selected phage clones (round 2)

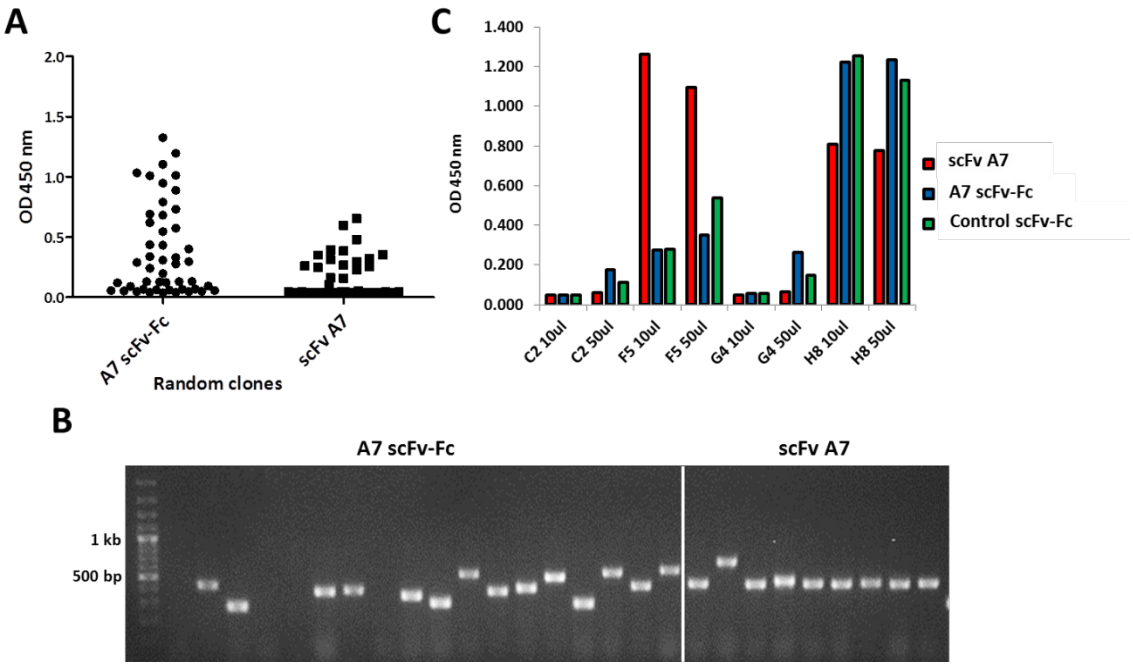

Figure 5.22 Analysis of second phage display screening

Analysis of selected phage clones from second round of selection on scFv A7 and A7 scFv-Fc. Phage ELISA on coated scFv A7 and A7 scFv-Fc detected with anti-M13 HRP conjugated antibody (A). PCR screening on clones from the second round of selection on scFv A7 and A7 scFv-Fc that showed good signal on phage ELISA (B). Phage ELISA on 4 high reactive phage clones at two different concentrations on coated scFv A7, A7 scFv-Fc or control scFv-Fc. Bound phage detected with anti-M13 HRP conjugated antibody (C).

Since no clear specific reactivity for either scFv A7 or A7 scFv-Fc was proved with the outcome of the previous phage selection, a third round of selection was performed inverting the input of the scFv A7 and A7 scFv-Fc screening. The output of the second round of selection for scFv A7 was incubated with coated A7 scFv-Fc and vice versa. This inverted selection should eliminate phage clones showing specificity for the framework of either antibody. In this selection round, the binding time was further reduced to retain only high affinity clones and washings increased to have more stringent conditions. 100 clones were randomly picked for each selection and screened against scFv A7 or A7 scFv-Fc in phage ELISA (Figure 5.23 A). Phage clones showing highest reactivity for scFv A7 or A7 scFv-Fc after the third round of selection were sequenced and the result is shown in Table 5.2. The *Homo sapiens myeloid leukemia factor 2* (MLF2) and *Homo sapiens GABA (A) receptor-associated protein like 1* (GABARAPL1) were the most represented among the selected phage clones. In order to determine the specificity of both enriched phage clones for A7, the phage ELISA was repeated on scFv A7 and A7 scFv-Fc, including the control scFv-Fc antibody (Figure 5.23 B). High reactivity could be detected with scFv A7. However, A7 scFv-Fc and control scFv-Fc antibodies gave similar results, suggesting a non-specific reactivity for the scFv format.

phages	coating	N° cycle	clone	Sequence identity
output 2°cycle vs A7 scFv-Fc	scFv A7	3	A3	Homo sapiens myeloid leukemia factor 2 (MLF2)
			A12	Homo sapiens GABA(A) receptor-associated protein like 1 (GABARAPL1)
			B9	Homo sapiens myeloid leukemia factor 2 (MLF2)
			B12	Homo sapiens myeloid leukemia factor 2 (MLF2)
			C12	Homo sapiens GABA(A) receptor-associated protein like 1 (GABARAPL1)
			D6	Homo sapiens myeloid leukemia factor 2 (MLF2)
			D8	Homo sapiens GABA(A) receptor-associated protein like 1 (GABARAPL1)
			E7	Homo sapiens GABA(A) receptor-associated protein like 1 (GABARAPL1)
			E8	Homo sapiens GABA(A) receptor-associated protein like 1 (GABARAPL1)
			E9	Homo sapiens GABA(A) receptor-associated protein like 1 (GABARAPL1)
output 2° cycle vs scFv A7	A7 scFv-Fc	3	B1	Homo sapiens integral membrane protein 2C (ITM2C)
			G9	Homo sapiens myeloid leukemia factor 2 (MLF2)
			H3	Homo sapiens myeloid leukemia factor 2 (MLF2)

Table 5.2 Sequence identity of selected phage clones (round 3)

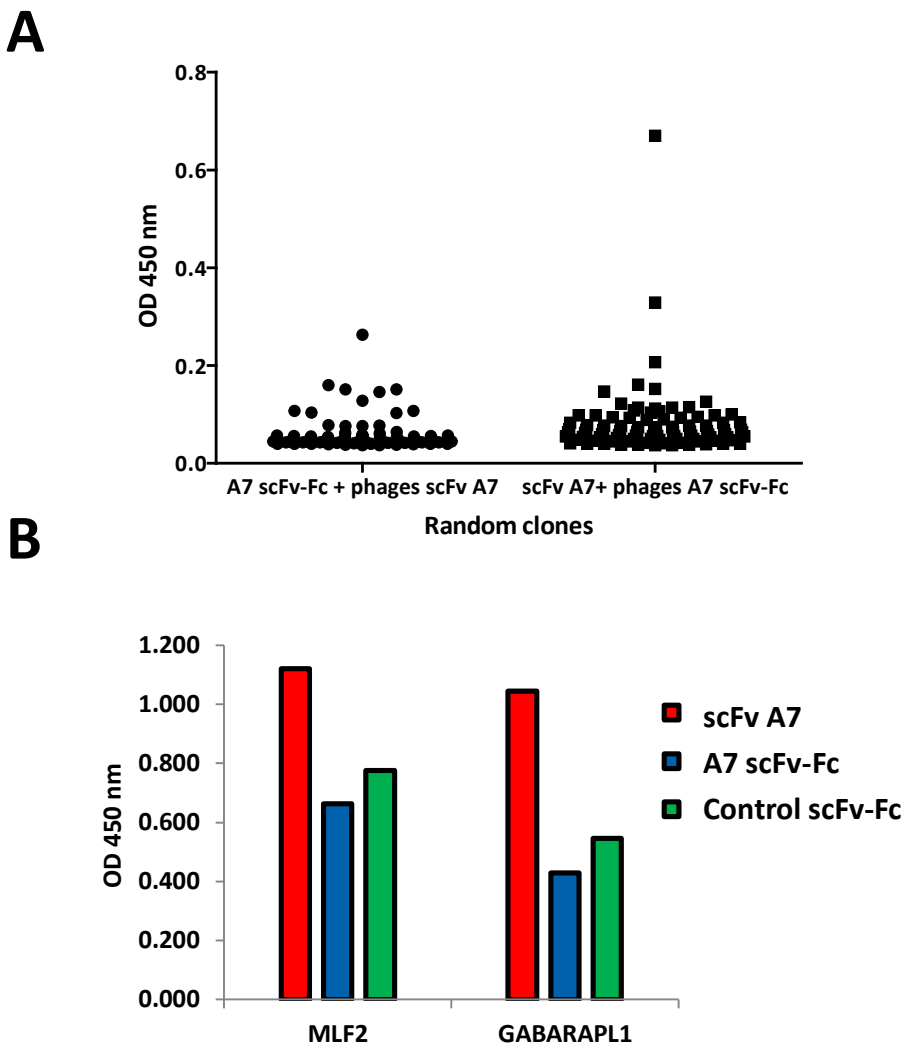

Figure 5.23 Phage ELISA on clones from inverted selection

Analysis of selected phage clones from the third round of selection on scFv A7 and A7 scFv-Fc via phage ELISA (A). Phage clones MLF2 and GABARAPL1 were tested in phage ELISA on coated scFv A7, A7 scFv-c or control scFv-Fc (B). Phage ELISA detected with anti-M13 HRP conjugated antibody.

5.3.1 Validation of LTBP2 as target antigen

The first phage display selection against scFv A7 identified LTBP2 as a putative interacting protein. Although the following round of selections against scFv A7 and A7 scFv-Fc failed to reproduce the same result, this protein represented a valid candidate as target antigen. LTBP2 is a protein belonging to the LTBP family, that has been previously described in synovium of OA and RA patients and associated with chondrocyte dedifferentiation (310-312). Furthermore, staining for LTBP2 on RA, OA and SLE synovium was reminiscent of the staining pattern obtained with scFv A7 (Figure 5.24 A) (310).

In order to produce a purified soluble LTBP2 protein, in collaboration with the University of Eastern Piedmont, the cDNA obtained from the phage clone F2/B6 (Figure 5.22) was subcloned in an expression vector containing the GST tag, forming a GST-LTBP2 fusion protein that can be easily purified using GSH resin. LTBP2 is a large protein of 1821 amino acids and 195 kDa. The design of the cDNA library does not allow the presence of the entire protein and therefore the selected phage clone contained only a fraction of the original protein. This fraction was characterised by a small 200 bp sequence coding for a 40 kDa peptide as visible in the purified protein fractions in Western blot or Coomassie stained gels (Figure 5.24 B). ELISA assay was used to validate the specificity of A7 for LTBP2. The LTBP2 fusion protein was coated on a 96 well plate along with the non-relevant protein DPP6 and the LTBP2 containing the SV5 tag obtained from supernatant and periplasmic extract of infected DH5α (Figure 5.24 C). ELISA was performed via incubation with scFv A7, scFv HEL, A7 scFv-Fc, control scFv-Fc and anti-GST or anti-SV5 as positive controls. Signal derived by anti-GST or anti-SV5 antibodies demonstrated efficient coating with the fusion proteins. No reactivity was detected with any test antibody on GST purified protein. Minor reactivity was detected with scFv A7 and A7 scFv-Fc on LTBP2-SV5 fusion protein. However, a similar signal was obtained using the corresponding control antibody.

As already mentioned above, the cDNA sequence obtained from the phage library contains only a fragment of the original LTBP2 gene. The absence of large

portions of the original protein and specific domains or secondary structures may impair proper protein folding and inhibit antibody-antigen interaction. During phage library screening the protein is expressed on the surface of the bacteriophage, fused to the g3p minor coat protein. Since in this format the antibody was able to target and retain the phage clone, a possible strategy was to clone the protein in fusion with a trans-membrane domain in order to express it on the cell surface of a mammalian cell line. This strategy has the dual advantage of providing a fast screening for protein expression and of exploiting the mammalian expression machinery. The peptide was then fused with the single trans-membrane domain of the platelet derived growth factor receptor (PDGFR) using the pDisplay vector (313). This vector contains the Ig κ-chain leader sequence at the N-terminus to direct the protein to the secretory pathway. In addition, the protein is fused to the hemagglutinin A (HA) epitope at the N-terminus and c-myc tag at the C-terminus to help identification of efficiently transfected cells. This construct was transfected in HEK-293T SV40 transformed cell line and screened in immunocytochemistry for scFv A7 reactivity. Transfected cells were stained for scFv A7 or control scFv HEL in a dual IF approach in combination with anti-HA antibody. HEK-293T cells were efficiently transfected with the LTBP2-PDGFR construct as shown from staining with anti-HA antibody. scFv A7 showed reactivity with the transfected cell line, however, the staining did not co-localise with the anti-HA signal and therefore was not related to the expression of the fusion protein. Furthermore, the reactivity of scFv A7 antibody could be detected also in the control non-transfected HEK-293T cells (Figure 5.25).

These results indicate that the LTBP2 protein is unlikely the target antigen for A7.

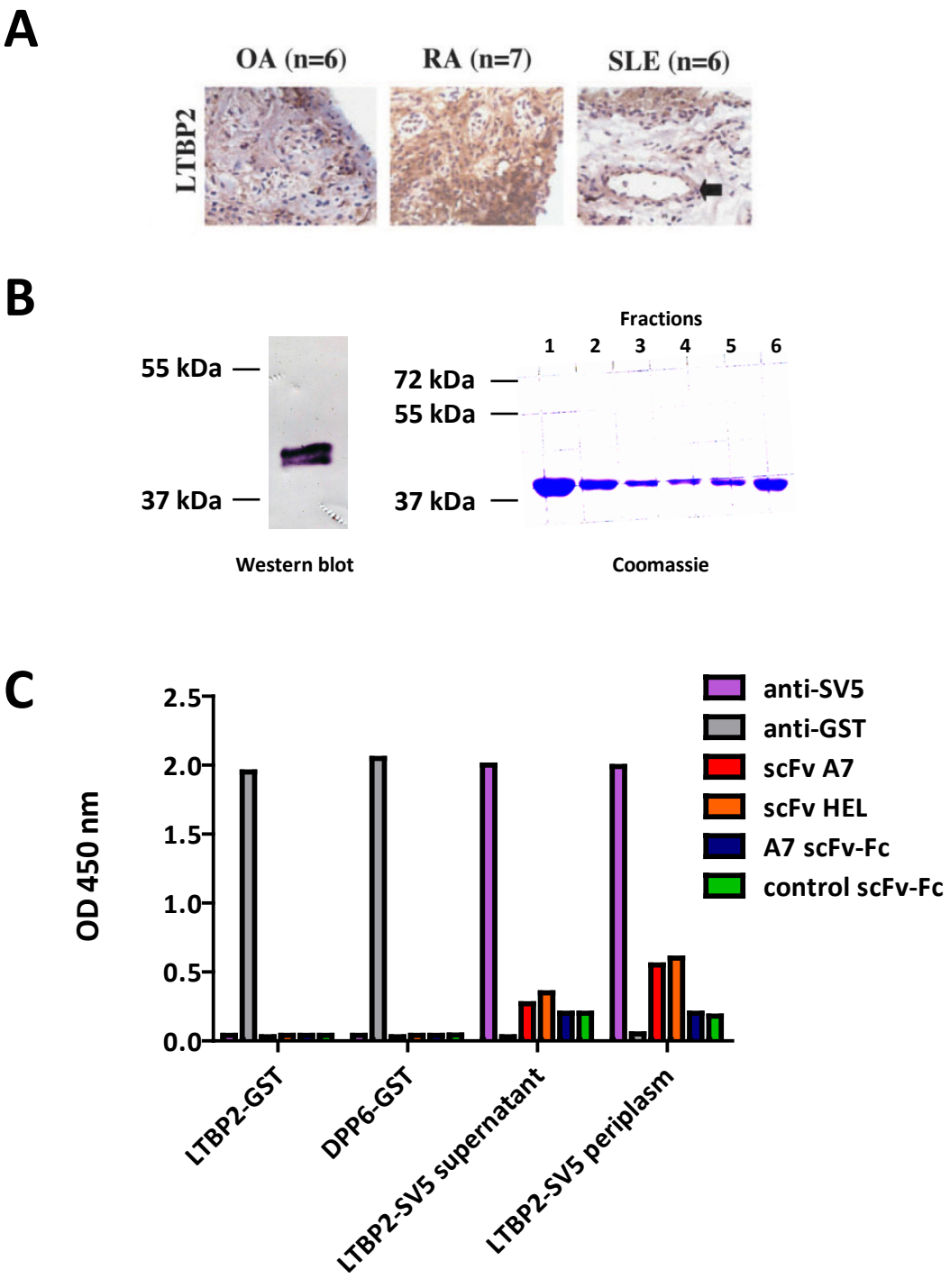

Figure 5.24 Analysis of A7 reactivity with LTBP2

Staining pattern on OA, RA and SLE synovium reported by Nzeusseu Toukap *et al*. 2007 (310) (A). SDS-PAGE of purified LTBP2-GST analysed in western blot using anti-GST HRP conjugated antibody (left) or stained with coomassie brilliant blue (right) (B). ELISA on coated purified LTBP2-GST, supernatant concentrated or periplasm extracted LTBP2-SV5 with scFv A7, scFv HEL, A7 scFv-Fc and control scFv-Fc (C).

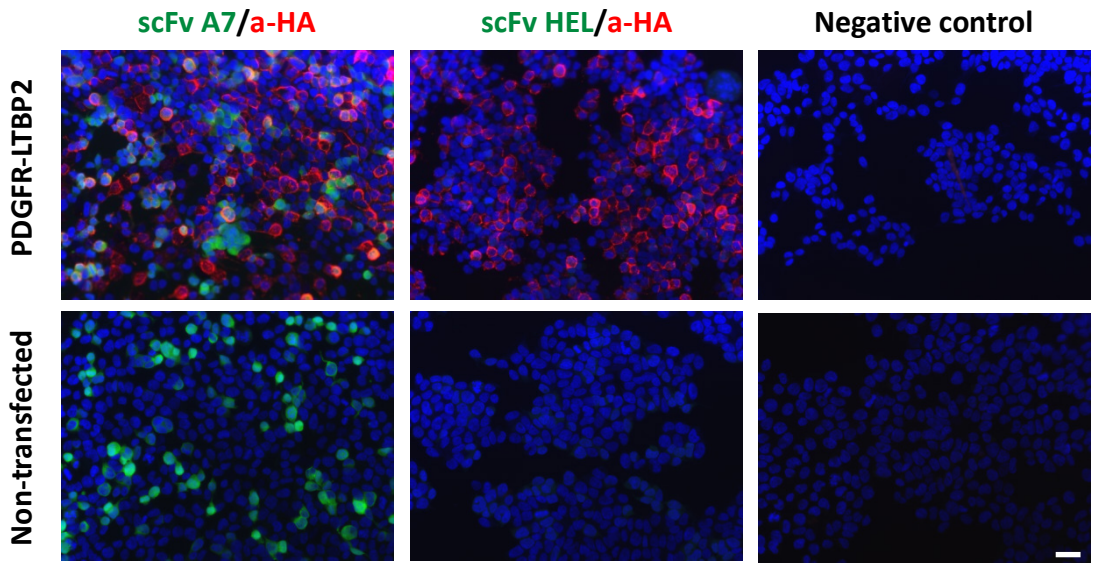

Figure 5.25 IF staining on LTBP2 transfected HEK-293T

HEK-293T transfected cells with PDGFR-LTBP2 construct. Dual IF staining with scFv A7 or scFv HEL (green) in combination with anti-HA tag (red) on transfected and non-transfected cells. Nuclei depicted with DAPI stain. Scale bar = 50 µm.

5.4 Literature survey and validation of C19 ORF 10

Analysis of the RASF proteome has provided insights on possible synovial specific markers or antigens that are characterised by over expression in stress conditions such as the inflammatory environment of arthritic synovium (314). Among those proteins, one in particular has raised interest: the product of C19 ORF 10. The mRNA of the C19 ORF 10 gene is widely expressed and does not appear to be lineage restricted. However, the role and biological activity of this protein still remains unclear. Further, analysis of tissue distribution of C19 ORF 10 in both OA and RA synovium has shown a perivascular localisation of the protein with occasional involvement of the lining layer (315). Due to the similarity of tissue distribution between the reported C19 ORF 10 and the staining pattern obtained with scFv A7, this protein represents an ideal target antigen candidate.

A vector for C19 ORF 10 was purchased from Origene. This vector coded for the C19 ORF 10 protein fused to the green fluorescent protein (GFP) at the C-terminus under the control of the CMV promoter. The GFP protein serves as a reporter protein to determine transfection efficiency and protein production. The vector was transfected in HEK-293T cell lines in parallel with a control GFP only plasmid. The cell line transfected with the control plasmid showed green fluorescence when stimulated with UV light, in over 80% of transfected cells. The cells transfected with C19 ORF 10-GFP plasmid showed a fluorescent signal only slightly increased compared to the non-transfected cells (Figure 5.26 A). When analysed using the SignalP 4.1 server protein analysis tool, the C19 ORF 10 is shown to have a putative signal peptide at the N-terminus consisting of 31 amino acids (MAAPSGGWNGVGASLWAALLLGAVALRPAEA) with a cleavage site between position 31 and 32 (316). The presence of a signal peptide suggests that the protein might be secreted by the transfected cell line in the culture media. Since GFP is a cytosolic protein, the secretory pathway causes improper folding of the protein and inhibition of fluorescent activity (317). For this reason, the presence of secreted C19 ORF 10 protein was evaluated in culture supernatant of transfected cells. Supernatant of both transfected and non-transfected HEK-293T cells were screened

in ELISA for scFv A7 or control scFv HEL reactivity (Figure 5.26 B). scFv A7 showed a stronger signal compared to scFv HEL and most importantly, the signal obtained in transfected supernatant was significantly higher than the supernatant from non-transfected cells. However, anti-GFP antibody tested did not confirm the presence of the target protein in the supernatant.

The experiment reported above gave the first indirect indication of a possible interaction between C19 ORF 10 and scFv A7. In order to further investigate the interaction between the two proteins, the protein was fused to the PDGFR trans-membrane domain using the pDisplay vector (313). As mentioned in section 5.3.1 for the LTBP2-PDGFR fusion protein, this construct carries the HA and the c-myc tags. Transfected HEK-293T cells were stained with scFv A7 or scFv HEL as control, in combination with anti-HA tag antibody (5.27). The presence of the signal peptide is further confirmed by the low intensity of staining with anti-HA tag. The HA tag was positioned at the N-terminus of the C19 ORF 10 protein and therefore gets cleaved when the signal peptide is removed. Efficient transfection and protein expression is confirmed by staining for the c-myc tag. scFv A7 showed reactivity for both transfected and non-transfected cells in a minor percentage of the cell population suggesting a signal not related to the expression of C19 ORF 10.

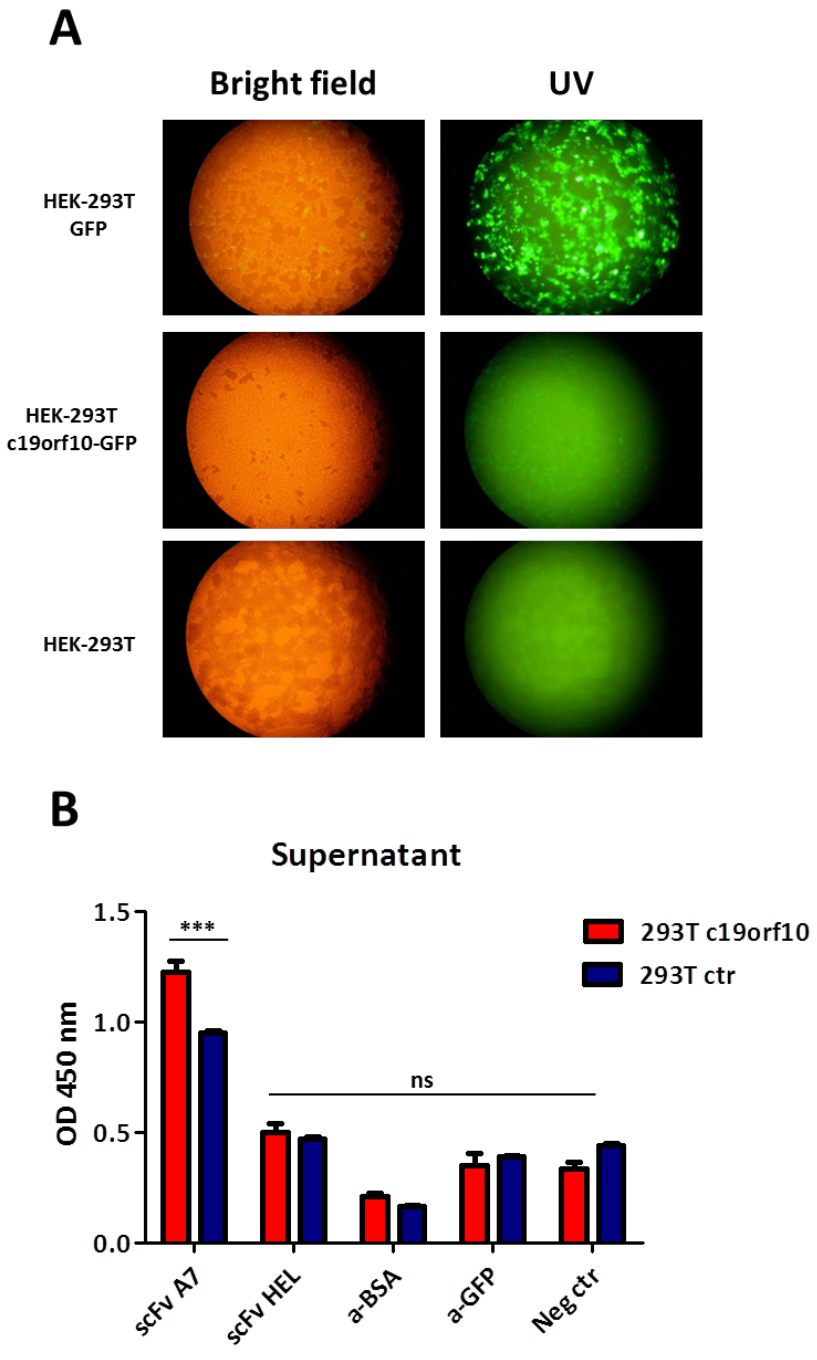

Figure 5.26 scFv A7 reactivity for C19 ORF 10

HEK-293T transfected cells with C19 ORF 10-GFP construct. Bright field and UV imaging of C19 ORF 10-GFP transfected cells, non-transfected and transfected with GFP control plasmid (A). ELISA assay on supernatant from transfected and non-transfected HEK-293T cells with scFv A7, control scFv HEL and including anti-BSA and anti-GFP as positive controls (B). 2 way ANOVA with Bonferroni post-test ***= p value <0.001.

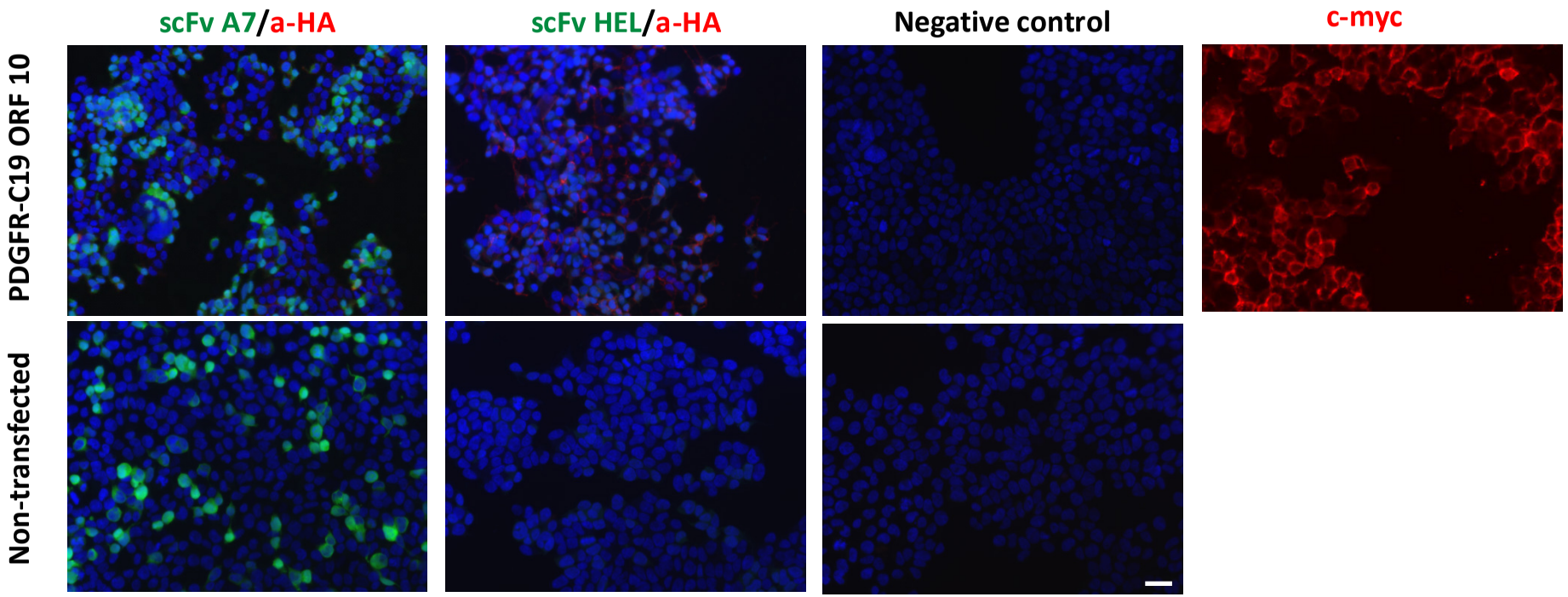

Figure 5.27 IF staining on C19 ORF 10 transfected HEK-293T

HEK-293T transfected cells with PDGFR-C19 ORF 10 construct. Dual IF staining with scFv A7 or scFv HEL (green) in combination with anti-HA tag (red) on transfected and non-transfected cells. Staining with anti-c-myc (red) to confirm efficient protein expression. Nuclei depicted with DAPI stain. Scale bar = 50 µm.

5.5 Discussion

The aim of this chapter was to identify the target antigen for the scFv A7. This is particularly important because of the tissue and disease specificity demonstrated for the scFv A7 in chapter 4 that suggest the targeting of an arthritic synovium specific marker with potential applications for imaging, drug targeting or as a diagnostic tool. The work reported in this chapter represents an on-going effort towards this goal.

The proteomic approach was used as a first strategy to isolate the target antigen. The classical method would involve the identification of a suitable source of the protein to be analysed for reactivity with the test antibody. However, this approach has the disadvantage of requiring large quantities of the target molecule. In this project the ideal antigen source would be the human arthritic synovium. Unfortunately, as mentioned earlier in this chapter, the limited availability of this tissue does not allow the employment of this source. Furthermore, the vascular localisation of the A7 target antigen suggests that the antigen is expressed only in a small area of the tissue, making a total synovium lysate an inefficient source of protein. Several cell lines were screened in order to identify a potential source of antigen. Interestingly, the scFv A7 showed reactivity with both intracellular and surface compartment of the positive cell lines PC3 and IE7 (Figure 5.1). Some protein can be kept in vesicles in the intracellular front of the membrane until a stimulus promotes secretion. However, the staining pattern of scFv A7 in permeabilised cells does not comply with a vesicle localisation. Several proteins have been reported to exhibit the phenomenon of dual localisation through a process of retrotranslocation or altered localisation signals (318). Of particular interest was also the reactivity of scFv A7 for the SV40 transformed endothelial cell line derived from the human umbilical cord vein, IE7. Since localisation experiments described in Figure 4.11 pointed towards perivascular reactivity, involving pericyte and smooth muscle layer but not the endothelial cells, examination of umbilical cord reactivity was necessary. Sections of human umbilical cord stained for scFv A7 in IHC and IF showed a strong reactivity with the stromal compartment of the

umbilical cord vein but not with the endothelial layer (Figure 5.3). As has been reported in the literature, an inflammatory environment may trigger the expression of oncofoetal antigens normally absent in adult tissues. Such is the case for the splicing variant of fibronectin containing the extra domain B (EDB) which has been shown to be re-expressed in arthritic synovium (319, 320). In this context, the A7 target antigen may be an oncofoetal protein up-regulated or re-expressed in disease conditions and therefore may be expressed in other foetal tissues such as the umbilical cord.

Primary synovial fibroblasts from RA patients were screened for A7 reactivity in order to analyse a cell population closely related to the target tissue. RASF showed strong reactivity with scFv A7 in both intracellular and membrane compartment (figure 5.4). Since synovial tissue in rheumatoid arthritis is subjected to extensive inflammation and normal synovium does not share the A7 target antigen (Figure 4.9), the expression of the target protein might be regulated by the inflammatory environment and specific cytokine stimuli. Although no sensible difference was detected in tissues with varying degree of cell infiltrates when screened for scFv A7 reactivity (Figure 4.3), no assumption could be made on the levels of cytokine present. *In vitro* TNF stimulation was able to increase the intensity of staining of scFv A7 on RASF, suggesting a role for cytokine tuning of A7 target antigen expression.

As a first approach, protein extracts obtained from cell lysis using detergents with different properties were resolved in SDS-PAGE and analysed in Western blots for scFv A7 reactivity. The rationale behind a multi detergent approach is to ensure protein enrichment and increase the chances of detection. Membrane bound proteins in particular are characterised by low abundance and often contain highly hydrophobic regions difficult to solubilise in conventional buffers (303). Both scFv A7 and the A7 scFv-Fc bivalent format did not provide a specific reactivity with any protein band. The detected bands in Western blots were shared by the respective control antibody and therefore represented non-specific interactions (Figures 5.8 to 5.10). The reason for this negative result may be attributed to the requirement of a conformational epitope for antibody-antigen interaction which is denatured in the

presence of DTT and SDS. A possible solution would be to run a gel in native conditions in which the protein is not subjected to denaturation prior to gel resolution. However, motility of proteins when exposed to electric field depends mainly on protein hydrodynamic size and superficial charge (321). The presence of SDS ensures a uniform negative charge and allows the resolution solely depending of protein size, moving from cathode to anode. Gel electrophoresis in native conditions of unknown proteins would probably convey a confusing picture with antigens potentially migrating in both directions and may therefore not be informative.

The IP strategy involves co-precipitation of antibody-antigen complex via use of an affinity resin. This is the method of choice for antigen isolation from complex protein solutions (291). The classical method involves isolation of the antibody-antigen complex from the protein solution, in this case the cell lysate, using protein A beads, resolution of the purified antigens in SDS-PAGE and analysis in Western blot. However, as reported for the Western blot approach described above, no specific protein isolation was detected (Figure 5.11). This result further indicates the requirement for a conformational epitope for antibody-antigen interaction to take place. In order to overcome this limitation, the proteins pulled down using IP were resolved in SDS-PAGE and stained with Sypro® ruby protein gel stain, able to non-selectively highlight the total protein content of the gel. Using a colorimetric or UV gel stain could allow the identification of an enriched protein band that can then be excised and analysed in mass spectroscopy to determine identity. No enriched band was detected in the IP experiment shown in Figure 5.12, suggesting low concentration of the target antigen in the cell lysate. Identification of a lysis buffer able to efficiently solubilise the target protein is therefore essential to increase the chances of isolation. One of the lysis buffers tested showed dose dependent reactivity with scFv A7, indicating efficient solubilisation of the target antigen and maintaining antibody binding capacity (Figure 5.13). This buffer was then used as standard lysis buffer for the subsequent experiments. Several strategies were studied to achieve efficient antigen isolation, using covalently coupled scFv antibodies to agarose beads (Figure 5.16), agarose-protein A coupled

scFv-Fc antibodies (Figure 5.17) or cross linked scFv-Fc antibodies to magnetic protein A beads (Figure 5.18). However, despite the fact that the system has shown to be able to selectively isolate ICAM-1 from JU77 cell lysates, no clear and unequivocal protein isolation could be claimed for A7 antibody in either format. Antibody efficiency in immunoprecipitation procedures can be affected by various factors: detergents in the lysis buffer may prevent antibody binding or retention, washing steps need to be optimised in order to reduce background but not remove specific antigen and finally antibody affinity plays a crucial role in antigen targeting. Antibodies isolated through phage display in scFv format are by design characterised by low avidity and scFv with a moderate affinity around 10^2 nM have been reported in the literature (322, 323). The range of this affinity is far from the high affinity values of affinity matured antibodies that are generally in the low pM range as is the case for Adalimumab (165, 324). If the k_{off} rate is the limiting factor in this approach, a possible solution would be by chemically cross-linking the antibody on the surface of positive cells to prevent dissociation and then immunoprecipitate the complex.

The second approach adopted for antigen identification was cDNA library screening. Since the removal of glycosylation from the positive cells did not impact on scFv A7 reactivity, it could be assumed that post-translational modifications are not required for antigen targeting (Figure 5.19). This is important because the phage display technique adopted in this screening requires bacterial expression of the phage clone (325). Although the cDNA library adopted was not derived from synovial tissue but from colon carcinoma, lung fibroblasts and pancreas, it had been characterised in the past and successfully employed for isolation of specific antigens (241). The library was shown to express nearly 18000 human genes. Most importantly, the library was expressing only true ORF sequences with different lengths (ranging from 200 to 700 bp) with multiple copies per antigen. This last characteristic allows the presence of different overlapping fragments for each antigen. In this context, isolation of multiple phage clones coding for the same protein but with different fragments can be used to identify the minimum binding region and potentially determine the target epitope. The first selection on scFv A7,

with two enrichment cycles, identified the LTBP2 antigen as the most reactive clone (Figure 5.21). This protein has been previously reported in the literature to be expressed in arthritic synovium, representing a potential target candidate (310). However, further characterisation of the putative target as a purified protein or in a cell surface expression system did not confirm the specificity (Figures 5.24 and 5.25). The second selection performed on both scFv A7 and A7 scFv-Fc did not produce the same outcome as the first screening. In order to reduce possible selection due to the framework, output from both selections were inverted and used for a third round of selection. Several low binding antigens were identified; with GABARAPL1 and MLF2 being the most represented clones (Table 5.2). GABARAPL1 antigen was reported to be expressed in brain, liver, kidney, heart, placenta and skeletal muscle (326), while the MLF2 was found to be ubiquitously expressed at mRNA level (327). Since no correlation with arthritic synovium appeared evident, further validation of these antigens was not performed. It has to be mentioned that the main limitation of phage display library screening resides on the time consuming step of random picking for assessment of individual clones. The screening procedure in the assays reported in this chapter was characterised by limited clone analysis, generally limited to 96 well plate format, and may not be representative of the total phage output. Massive sequencing of the total outcome pool can be performed using the deep-sequencing system 454 pyrosequencing (328). This strategy would allow a more comprehensive analysis of the phage outcome and identify the most represented clone population, potentially identifying previously missed clones (241).

Additionally, a potential target candidate was identified via literature screening. The C19 ORF 10 is a secreted protein that has been associated with arthritic synovium (314, 315). Tulin and colleagues suggested a role in cellular proliferation and identified the C19 ORF 10 as a murine bone marrow stroma-derived growth factor (SF20/IL-25) (329). However, proliferation data could not be reproduced and the paper was withdrawn (330). Further, the C19 ORF 10 was reported to be over expressed in hepatocellular carcinoma (HCC), activating the Akt/MAPK pathway and contributing to proliferation (331), and in preadipocyte

cells (332). The staining pattern reported by Weiler and colleagues in rheumatoid and osteoarthritic synovium was strikingly similar to the staining obtained with A7, involving the perivascular compartment and showing occasional involvement of the synovial lining layer (315). Transfection of HEK-293T cells with a vector coding for the C19 ORF 10 protein fused to the reporter GFP antigen showed a significantly higher signal in the supernatant from transfected cells compared to non-transfected counterpart (Figure 5.27). This result indicates the specific targeting of a soluble antigen in the culture medium. However, anti-GFP antibody failed to confirm the presence of the recombinant protein in the supernatant. Due to the variety of GFP proteins available on the market, the negative reactivity of the anti-GFP antibody could be blamed on the non-specificity of the antibody clone used in the assay. To further characterize the reactivity with scFv A7, the protein has been fused with the PDGFR transmembrane domain to be exposed on the cell surface of transfected HEK-293T cells (Figure 5.28). The presence of a putative signal peptide at the N-terminus of the protein was detected with the SignalP 4.1 server tool (316) and confirmed by the cleavage of the HA tag domain on the fusion protein. Efficient transfection was confirmed by the presence of c-myc reactivity. However, no specific reactivity was detected with scFv A7. To finally validate the antigen and determine whether or not it represents the long sought target antigen, analyses using the soluble recombinant protein need to be performed in ELISA and IP.

The strategies employed for target antigen identification described in this chapter did not provide a suitable identity. The proposed approaches that will be evaluated in the future will be described in chapter 7.

Chapter 6

Development of a novel tissue specific therapeutic

6.1 Introduction

In the therapy for arthritis, biologic agents have acquired increasing interest over the years. In particular, anti-cytokine therapy, specifically anti-TNF agents, have proved to be the most promising therapeutics currently available for rheumatoid arthritis (139). Good clinical response can be achieved for the majority of patients after treatment with any of the 5 available TNF inhibitors, showing pain control, reduction of inflammation and prevention of joint damage (333, 334). However, an inadequate number of patients can actually achieve treatment free remission and loss of efficacy over time is not rare (139). Despite being generally well tolerated, systemic toxicity can still be devastating for individuals with side effects mainly involving increased risk of infectious complications (335). In addition, costs related to biologic therapy in the treatment of arthritis are high and constitute a considerable burden for national health systems (20-22).

In this project we aimed at the development of a novel tissue specific therapeutic for rheumatoid arthritis. Lately, bispecific antibodies have gained momentum especially in cancer treatment, with one FDA approved antibody and many other showing promising results in clinical trials, demonstrating good pharmacological capacities and improved potency compared to a standard antibody approach (205). The scFv A7 antibody described in chapters 3 and 4 displayed all the characteristics of a synovium specific antibody that most importantly was able to discriminate between arthritic and non-arthritic tissue. In this chapter the development of a new therapeutic agent combining the tissue specific properties of the A7 antibody with the gold standard for anti-TNF therapy Adalimumab in a bispecific antibody format will be described. Bispecific antibody design and characterisation of *in vitro* reactivity will be described in the following sections.

6.2 Adalimumab conversion in IgG-like scFv-Fc format

In order to obtain an IgG-like molecule equivalent to the one presented in section 3.3, characterised by a scFv fused to the Fc domain of human IgG1, the anti-TNF antibody Adalimumab was converted into a scFv format using the V_H and V_L sequences published in the original patent and available in the public domain (165). Cloning strategy and rational for the development of a scFv-Fc fusion protein are described in section 2.2.1 and 3.3. Briefly, V_H and V_L nucleotide sequences obtained from the Adalimumab patent application were optimised for CHO expression and linked via the same Serine-Glycine peptide linker used for scFv A7, in a V_H-L-V_L orientation. This construct was cloned in the pHygro vector in frame with the hinge, C_H2 and C_H3 domains of human IgG1, ensuring efficient homodimerisation and correct glycosylation pattern of the IgG-like antibody (153, 252-254). This scFv-Fc format displays the same characteristics and properties of the parent Adalimumab IgG, maintaining bivalency for TNF binding capacity and normal Fc effector functions. Figure 6.1 presents a schematic of Adalimumab scFv-Fc antibody construct and pHygro vector structure.

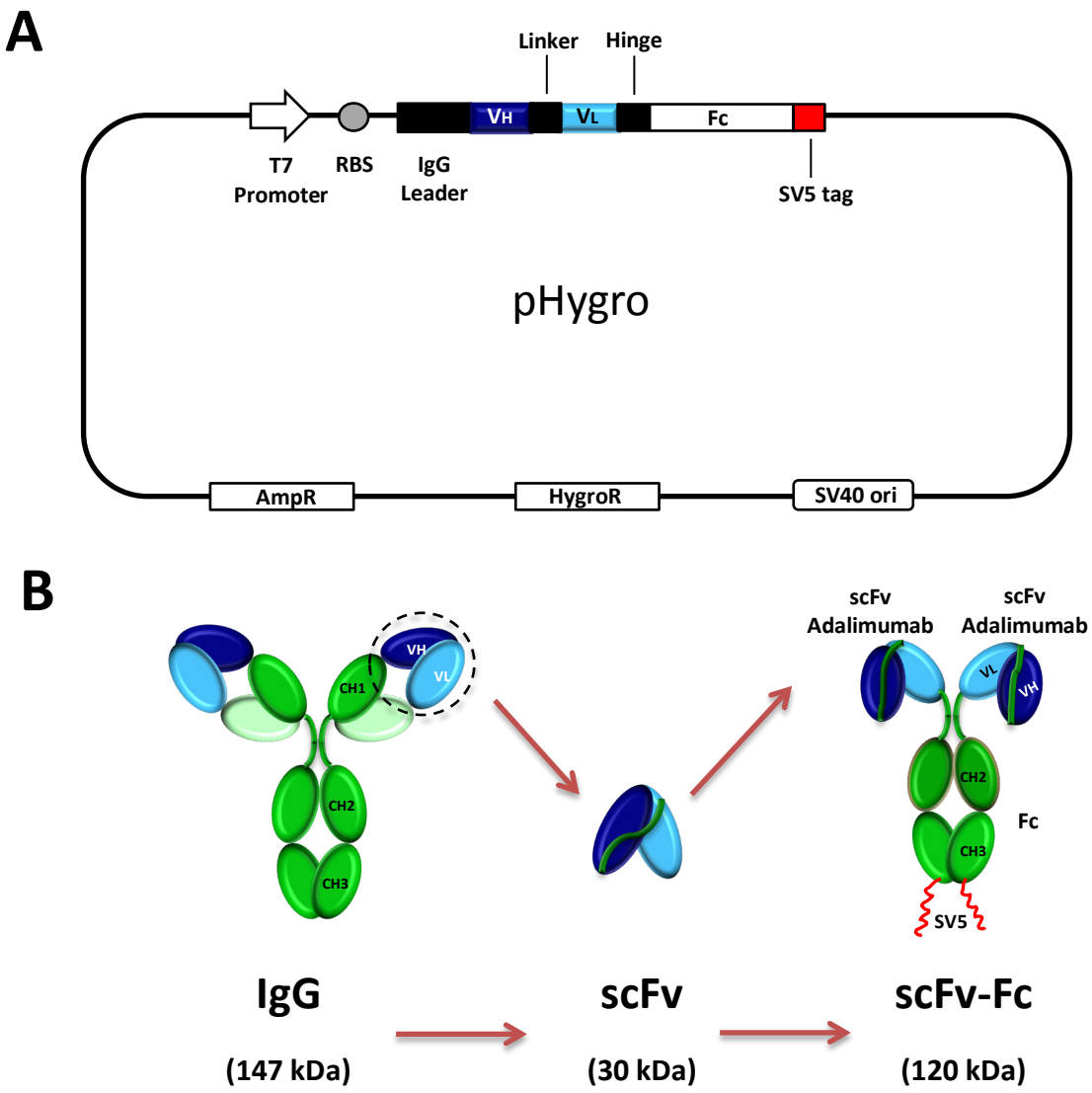

Figure 6.1 pHygro vector and Adalimumab scFv-Fc protein structure

Schematic of pHygro vector encoding the scFv-Fc gene with the IgG leader sequence containing a mini intron (A). Schematic of the conversion of Adalimumab from full IgG to scFv to scFv-Fc format showing the scFv domain linked to the CH2-CH3 Fc IgG1 domain and carrying the SV5 tag (B).

6.2.1 Adalimumab scFv-Fc expression and quality control

The CHO expression system proved to efficiently produce the A7 scFv-Fc construct with high yields and high purity (section 3.3.1 and 3.3.2). The optimised expression protocol used for A7 scFv-Fc was applied to Adalimumab scFv-Fc production. CHO-s cells able to grow in suspension in serum free medium were transfected with the pHygro vector carrying the Adalimumab scFv-Fc construct, in a culture medium containing the selective agent hygromycin B to select for efficiently transfected cells, as described in section 2.2.2.1. The surviving cell population was diluted to a single cell suspension and protein production capacity was evaluated in culture supernatant via ELISA assay (Figure 6.2 A). The clone 17 proved to efficiently produce the antibody with higher yields compared to the clone 12 selected for scFv A7 (shown in Figure 3.12 A). However, the selected clone gradually lost production capacity over time and frozen vials kept in liquid nitrogen for 1 year showed a high growth rate but a low antibody expression (Figure 6.2 B) and as a result was less efficient when compared to the A7 scFv-Fc CHO clone 12 (Figure 3.12 B). The presence of Adalimumab scFv-Fc was further confirmed by Coomassie stained SDS-PAGE and Western blot analysis (Figure 6.3).

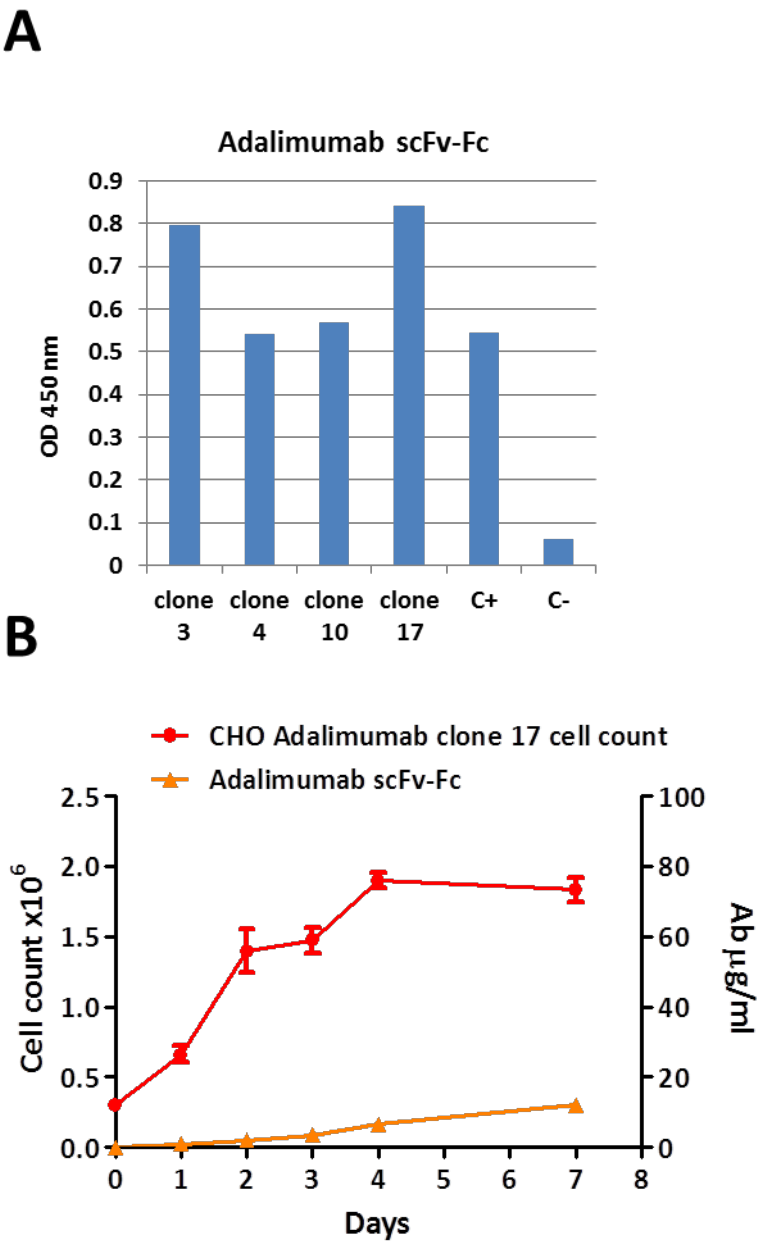

Figure 6.2 Selection of Adalimumab scFv-Fc CHO-s expressing clone

ELISA assay on culture supernatant of transfected CHO-s clones carrying the A7 scFv-Fc construct. ELISA performed on anti-Human Fc coated plates and presence of scFv-Fc antibody detected using anti-SV5 and anti-mouse HRP conjugated antibody. Positive clone (C+) and negative clone (C-) included as control (A). Correlation between cell number and scFv-Fc protein content in CHO-s clone 17 supernatant after 1 year from transfection. Cell count and protein content detected at various time points (B).

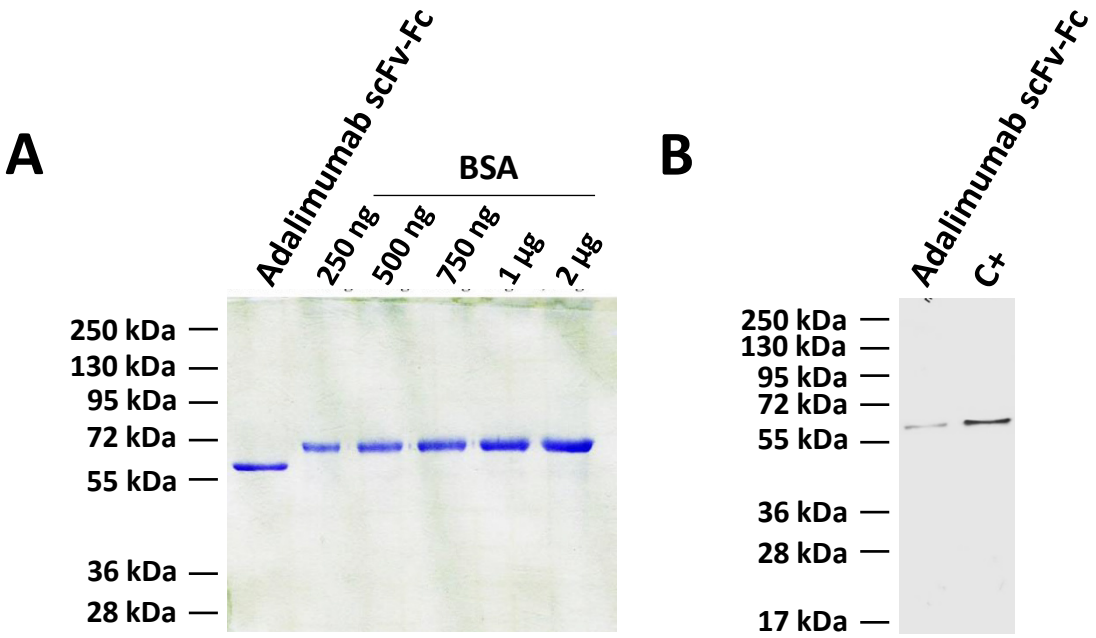

Figure 6.3 Adalimumab scFv-Fc production from CHO-s

SDS-PAGE resolved Adalimumab scFv-Fc from protein A stained with Coomassie brilliant blue (A) or probed with anti-SV5 and anti-mouse AP antibody following Western blotting (B). Positive clone (C+) included as control.

Protein A Sepharose beads were used as purification system due to the ability for IgG targeting (256) and the efficiency demonstrated in A7 scFv-Fc purification (section 3.3.1). Culture supernatant from CHO-s clone 17 transfected with Adalimumab scFv-Fc encoding vector was incubated with protein A resin, as described in section 2.2.3.1, and purification performed using gravity flow chromatography. Analysis of the eluted fractions using UV detection at 280 nm showed that the majority of the bound antibody was eluted within the first fractions collected (Figure 6.4 A). Presence of Adalimumab scFv-Fc was confirmed in Coomassie stained SDS-PAGE (Figure 6.4 B) and Western blot probing with anti-SV5 tag antibody (Figure 6.4 C). The SDS-PAGE confirmed the presence of a predominant band at 60 kDa, consistent with the expected molecular weight of the reduced scFv-Fc fusion product. A minor proportion of breakdown products at around 30 kDa was visible in the Western blot and represents the Fc portion bearing the SV5 tag. This purification protocol was able to purify up to 5 mg/L, however, frozen vials kept in liquid nitrogen for 1 year showed a decrease in antibody production down to 1.6 mg/L.

To further characterise and quantify the purity of Adalimumab scFv-Fc production from CHO-s cells, a SDS-PAGE resolved protein batch was stained using the high sensitive Sypro® ruby protein gel stain reagent. The plot profile of Adalimumab scFv-Fc purified from CHO-s cells analysed using the image analysis tool ImageJ, showed the presence of a predominant band at 60 kDa accounting for 71% of signal above background (Figure 6.5 A and B).

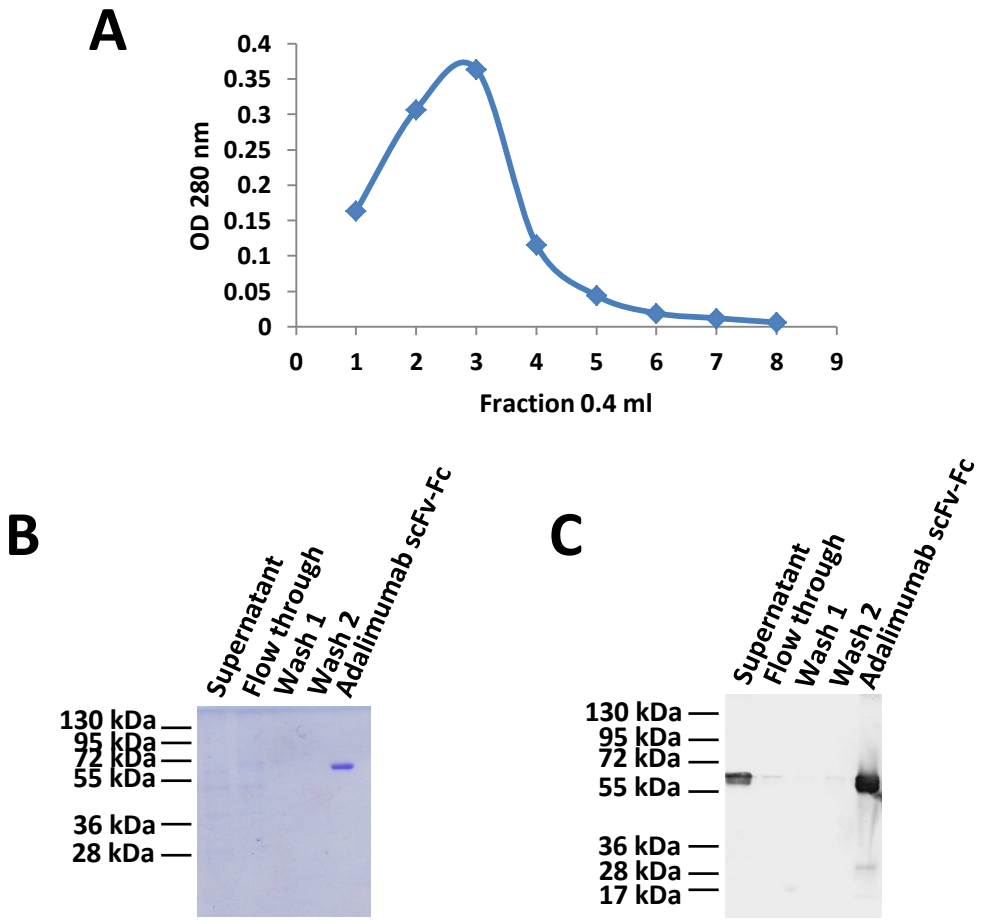

Figure 6.4 Adalimumab scFv-Fc production and purification via CHO-s

Optical density analysis of Adalimumab scFv-Fc eluted fractions from CHO-s supernatant using protein A purification system (A). SDS-PAGE resolved protein A purified Adalimumab scFv-Fc fractions from CHO-s stained with Coomassie brilliant blue (B) or probed with anti-SV5 and anti-mouse HRP antibody following Western blotting (C).

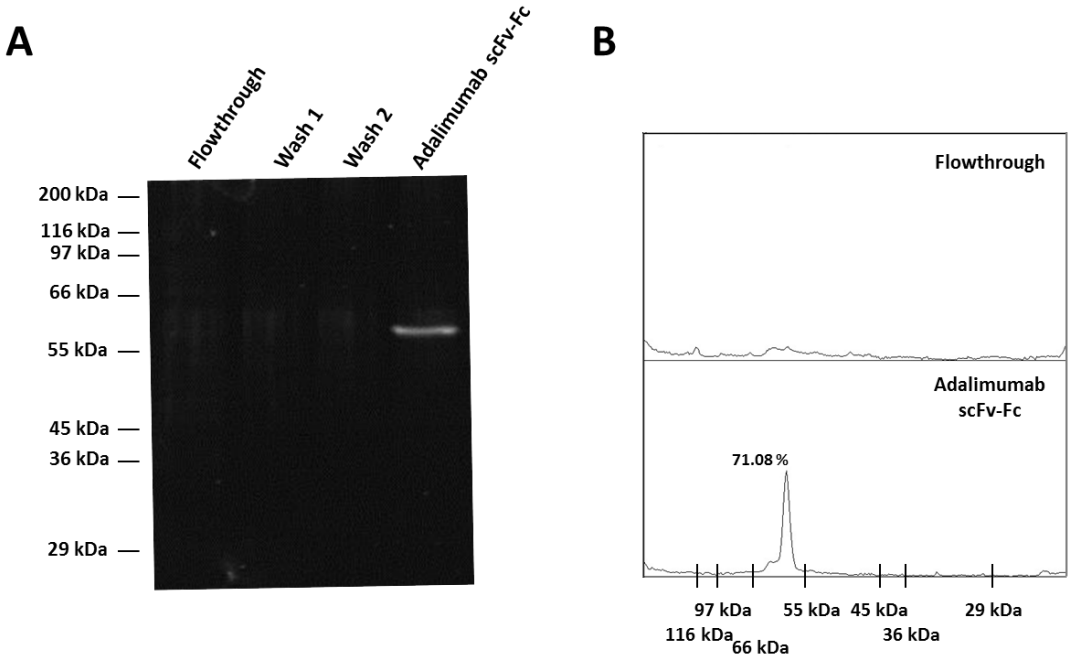

Figure 6.5 Quality assessment of CHO-s produced Adalimumab scFv-Fc

SDS-PAGE resolved Adalimumab scFv-Fc produced in CHO-s (A) stained with Sypro® ruby protein gel stain. Analysis of plot profile from the purified Adalimumab scFv-Fc lane (B) reveals a high purity in the CHO-s produced protein (71%).

6.2.2 Characterisation of Adalimumab scFv-Fc specificity

As reported in the previous section, the new Adalimumab scFv-Fc format proved to be efficiently produced using CHO-s expression system (Figure 6.4 and 6.5). A key element in the design of this approach is that the Adalimumab antibody currently used in the clinic was isolated using phage display, therefore in scFv format, and subsequently converted into a fully human IgG antibody (324). In addition, when expressed in scFv format, Adalimumab maintains similar binding kinetics, affinity and potency in neutralising TNF as the parent antibody (336, 337). Based on this, the scFv-Fc fusion construct created in our lab should display optimal TNF binding and neutralising properties. However, every new construct may cause unforeseen structural changes and binding to target antigen may be blocked or impaired by protein mis-folding or steric hindrance. In order to assess the capacity to bind human TNF-α, an ELISA assay was employed in which varying concentrations of Adalimumab IgG or Adalimumab scFv-Fc were added to the coated TNF (detail in section 2.11). The results presented in Figure 6.6 show an almost identical dose-response curve with similar EC50 when comparing the two antibody formats, while no binding could be detected with the control antibody A7 scFv-Fc.

Further, the capacity of the Adalimumab scFv-Fc antibody to neutralise the biological effects of human TNF-α was assessed in a TNF induced cytotoxicity assay as described in section 2.10. Briefly, a murine fibroblastic cell line was incubated for 24 hours in complete medium with the presence of the protein synthesis inhibitor actinomycin D, 0.45 ng/ml human TNF-α and varying concentrations of the test antibodies. Cell viability was assessed by measuring the production of a violet dye visible at 560 nm after incubation with MTT substrate. Results presented in Figure 6.7 show a similar dose-response curve between Adalimumab and Adalimumab scFv-Fc antibodies while no rescue could be detected with A7 scFv-Fc (Figure 6.7 A). Comparison of half maximal inhibitory concentration (IC50), the concentration at which the antibody exerts 50% inhibition of TNF induced cytotoxicity, Adalimumab scFv-Fc shows a significant 2 fold increase compared to the parent antibody, rising from 0.17 nM to 0.34 nM (Figure 6.7 B). The IC50 value obtained with the IgG

Adalimumab is in line with reported values in literature (216, 337). On the basis of this last result, the Adalimumab scFv-Fc format shows good inhibitory capacity with only a minor increase in the IC50.

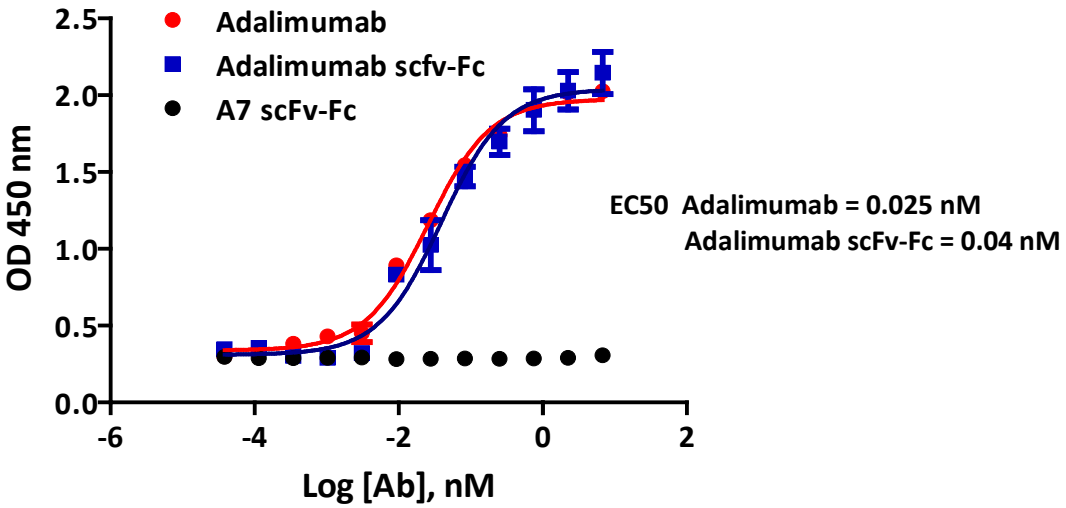

Figure 6.6 TNF binding assay

ELISA assay on 100 ng/ml coated human TNF-α. 6.8 nM starting antibody concentration with 1:3 serial dilution. Bound antibodies detected using anti-human Fc HRP conjugated antibody. Intensity of converted TMB substrate detected at 450 nm. Values presented as Mean ± SEM.

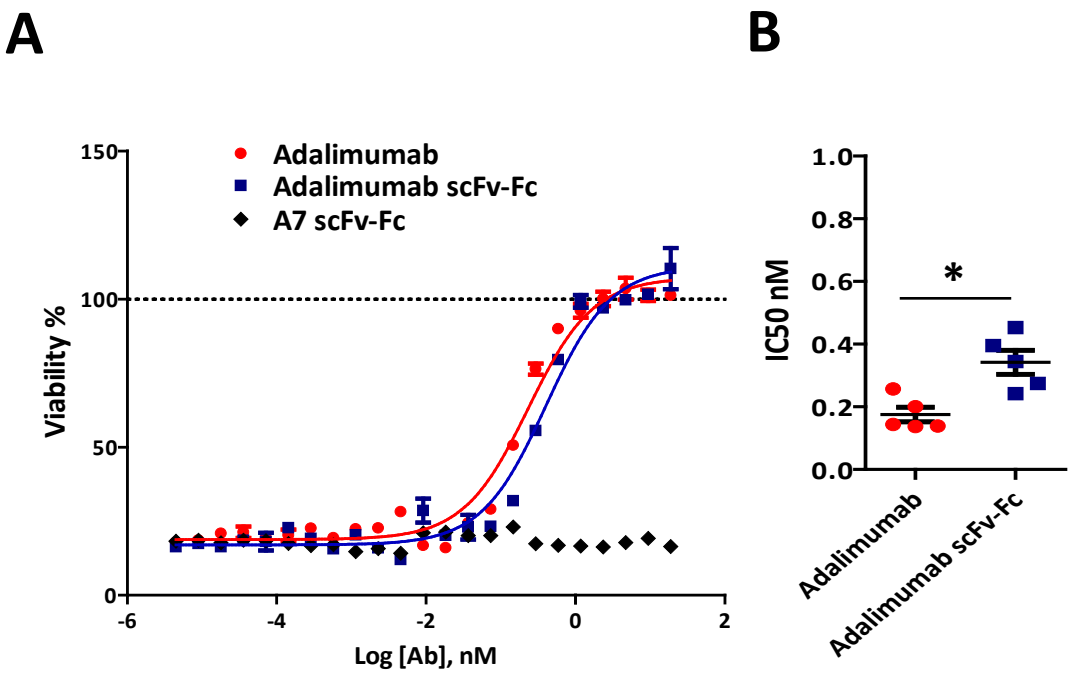

Figure 6.7 TNF induced cytotoxicity assay on L-929

$3x10^4$ L-929 cells seeded in a 96 well plate in complete DMEM medium. Cells were incubated with 1 µg/ml actinomycin D and 0.45 ng/ml TNF-α in the presence of varying concentrations of test antibodies for 24 hours. Antibody starting concentration 18.8 nM with 1:3 serial dilutions. Viability measured upon conversion of 5 µg/ml MTT substrate in a violet dye and measure at 560 nm in standard plate reader. Values are representative of 5 independent experiments expressed as Mean ± SEM (A). IC50 values of 5 independent cytotoxicity assay (B). Mean IC50 for Adalimumab = 0.17 nM. Mean IC50 for Adalimumab scFv-Fc = 0.34 nM. Mann-Whitney test * = p value <0.05.

6.3 Bispecific antibody development

Bispecific antibodies are a class of antibody molecules able to specifically target two different antigens at the same time. Several engineering strategies are available for bispecific antibody development, including small scFv based diabodies, symmetric and asymmetric IgG-like antibodies and IgG fusion molecules (205, 338). For the purpose of this project, a scFv-Fc fusion bispecific antibody format was employed. The strategy adopted to ensure efficient heterodimerisation is an adaptation of the well characterised knobs-into-Holes technology developed by Ridgway and colleagues in 1996 (211). In this section the cloning strategy adopted for A7/Adalimumab bispecific antibody production and characterisation of the expression efficiency, purity and *in vitro* functionality will be described.

6.3.1 Cloning strategy

The knobs-into-Holes technology is based on the replacement of a small amino acid with a larger one in the C_H3 domain of human IgG of the first heavy chain, specifically the residue 366 will be converted from threonine to tyrosine (T366Y) creating a knob. On the paired heavy chain, a large amino acid is converted into a smaller one, in this case the residue 407 will be converted from a tyrosine to a threonine (Y407T) creating a hole (211). With this strategy, the chain containing the T366Y mutation will preferentially dimerise in a heterodimer fashion with the chain containing the Y407T mutation. Homodimerisation of either chain is impaired due to steric hindrance and protein instability. The cloning procedure employed for the development of the pHygro bispecific vector is described in detail in section 2.3. Briefly, the T366Y and Y407T mutations were inserted in the C_H3 sequence via site directed mutagesis. The two mutated heavy chains were cloned in separate vectors in order to allow the insertion of the desired scFv sequence independently. The first vector, containing the Y407T mutation carries also the Simian-virus 5 (SV5) tag and a portion of the 2A peptide sequence. The second vector containing the T366Y mutation carries the second part of the 2A peptide sequence at 5' end and the 6-His tag at 3'. After cloning of the suitable scFv sequences in the two heavy chain mutated vectors, the two vectors were fused into one, reconstituting the entire 2A

peptide sequence and generating a single open reading frame sequence encoding both chains. The final vector construct (pDuo-opt) will encode both chains separated by a short peptide sequence. The most important features of the vector will be discussed in this section. Figure 6.8 shows a schematic representation of the cloning strategy adopted.

The vector encoding the bispecific construct carries a Kozak consensus sequence at the 5' end of the sequence, important for the initiation of the translation process (339). The coding sequence starts with a human Ig leader sequence of 20 amino acids including a mini-intron sequence that while not transcribed is able to increase transcription efficiency. The leader sequence allows the translocation of the first antibody chain to the endoplasmic reticulum and subsequent release in the culture medium (340). The first scFv sequence in V_H-V_L orientation is linked to the Fc sequence carrying the C_H3 Y407T mutation via the human IgG hinge region. At the end of the Fc region, a short 14 amino acid sequence (GKPIPNPLLGLDST) derived from the SV5 is added as a tag in order to allow a selective targeting of the first antibody chain. The first peptide chain is linked to the second scFv-Fc chain via the presence of a 2A peptide. First a furin protease cleavage site of 4 amino acids (RAKR) is present at the end of the SV5 region. The following 24 amino acids (APVKQTLNFDLLKLAGDVESNPGP) constitute the 2A peptide sequence derived from the Foot-and-Mouth Disease Virus. The characteristic of this peptide is the ability to separate the previous and the subsequent peptide chains. The mechanism of action of this short sequence does not involve mRNA processing or proteolytic activity but rather a ribosomal skip during translation process in a stop codon-independent manner. In this mechanism, the nascent peptide chain will undergo hydrolysis at the -N-P-G sequence at the C-terminus of the 2A sequence, releasing the first chain and allowing the ribosome to continue the synthesis of the second peptide chain without being released from the mRNA (341). The furin cleavable site located after the SV5 tag will allow the removal of the remaining amino acid residues. Since the 2A peptide determines the processing of the peptide chain at the moment of translation, a second Ig leader sequence is required to produce and release the second encoded scFv-Fc chain.

This second leader is equivalent to the one present at the 5' end of the first scFv-Fc chain and contains the same mini-intron sequence. Following, the second scFv sequence is linked to the Fc domain carrying the C_H3 T366Y mutation via the human IgG hinge region. At the end of the Fc, a 6 times repeated histidine is added as a tag to allow specific targeting of the second scFv-Fc chain. In Figure 6.9 is shown a schematic representation of the pDuo-opt vector and bispecific antibody construct with the first scFv Adalimumab fused to the Fc region containing the Y407T mutation and SV5 tag, while the second scFv A7 is fused to the Fc domain containing the T366Y knob mutation and 6-His tag.

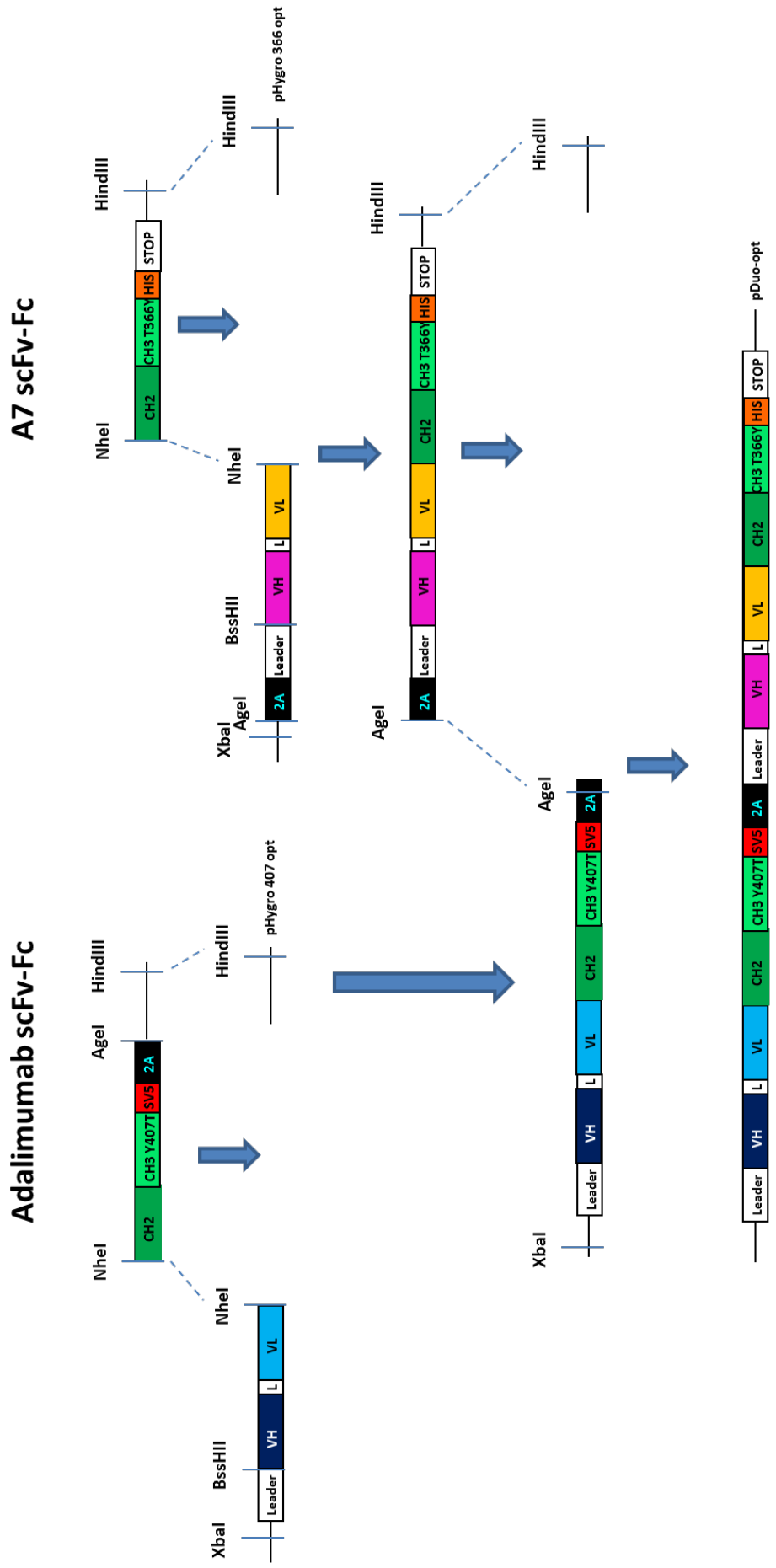
A7 scFv-Fc
Adalimumab scFv-Fc
HindIII
NheI
BssHII
XbaI
AgeI
pHygro 366 opt
pHygro 407 opt
pDuo-opt
Leader
VH
L
VL
CH2
CH3 T366Y
HIS
STOP
CH3 Y407T
SV5
2A

Figure 6.8 Schematic of cloning strategy for pDuo-opt

Vector pHygro 407 generated via cloning of the first leader-scFv-Fc region using XbaI-NheI restriction sites to the Y407T mutated Fc region carrying the SV5 tag and the first part of the 2A peptide using NheI-HindIII restriction sites in the original pHygro vector. Vector pHygro 366 generated via cloning of the second leader-scFv-Fc region using XbaI-NheI restriction sites to the T366Y mutated Fc region carrying the 6-His tag and the second part of the 2A peptide using NheI-HindIII restriction sites in the original pHygro vector. pDuo-opt vector formed by cloning the second leader-scFv-Fc-6 His sequence to the pHygro 407 via AgeI-HindIII restriction sites.

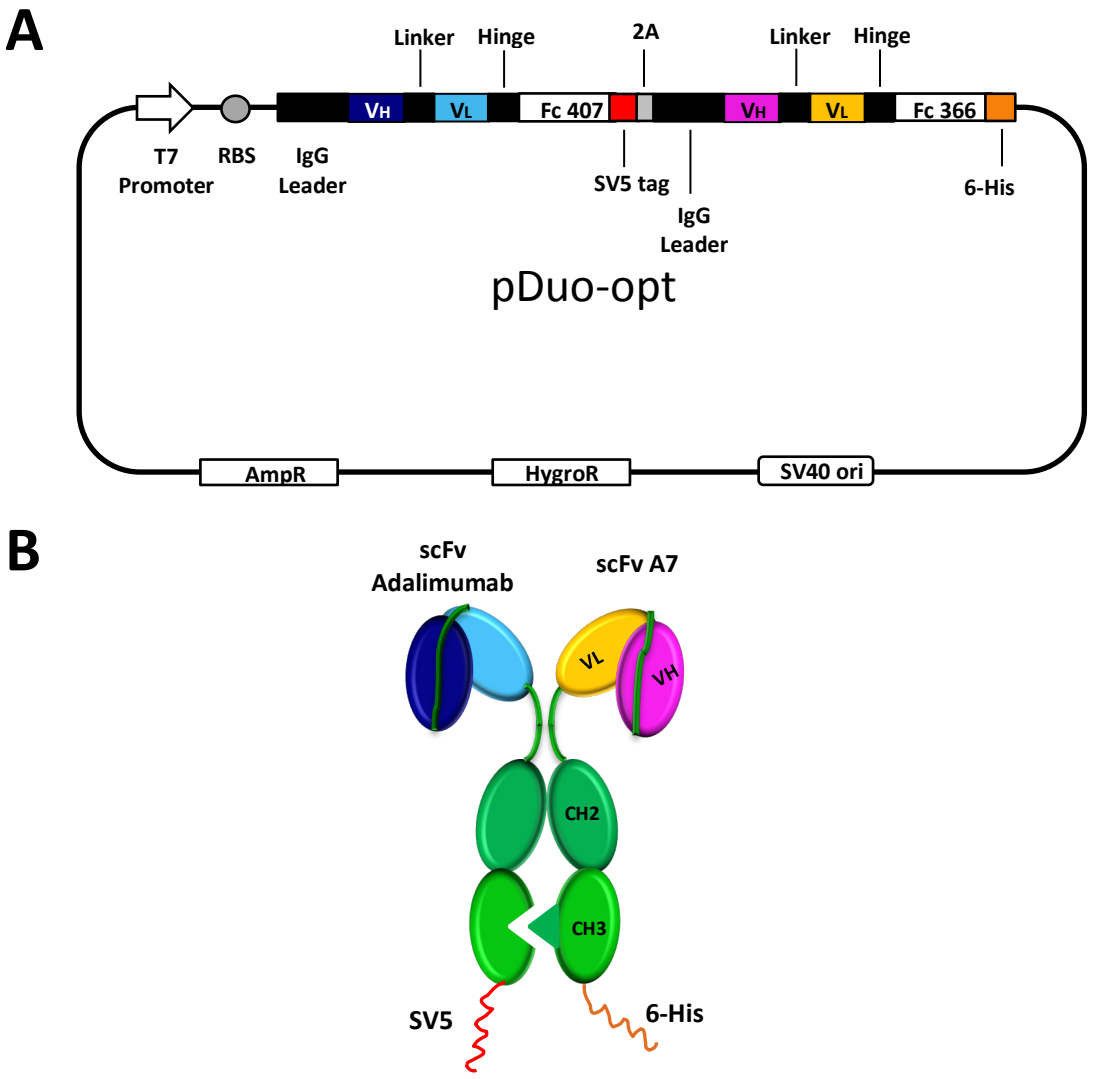

Figure 6.9 pDuo-opt vector and bispecific A7-Adalimumab protein structure

Schematic of pDuo-opt vector encoding the bispecific scFv-Fc gene with the IgG leader sequence containing a mini intron (A). Schematic of the bispecific A7/Adalimumab antibody carrying the knobs-into-Holes mutation in the CH3 domain and carrying the SV5 and 6-His tags (B).

6.3.2 Antibody expression and quality control

The CHO-s expression system adopted for A7 scFv-Fc and Adalimumab scFv-Fc protein production was employed for the A7/Adalimumab bispecific antibody expression and for the control bispecific antibody E2/Adalimumab (section 3.3 and 6.2.1). The E2 scFv antibody fragment used in the control antibody is specific for the intracellular domain of the dipeptidyl aminopeptidase-like protein 6 (DPP6) a protein implicated in ion channel modulation in human neuronal and heart tissue (342, 343). As described in section 6.3.1 for the bispecific antibody A7/Adalimumab, the scFv E2 antibody fragment was cloned in the pDuo-opt vector in the position previously occupied by scFv A7, generating the E2/Adalimumab bispecific antibody.

6.3.2.1 Bispecific antibody production

Stably transfected CHO-s cells with the two bispecific antibodies were grown in serum free medium containing the selective agent hygromycin B to bias for efficiently transfected cells. Since the bispecific antibody bears both the SV5 and the 6-His tags, the Talon® metal affinity purification system can be employed to purify the antibody from the culture supernatant. Due to the higher protein yield obtained with Talon® purification over protein A approach in scFv isolation, described in section 3.2.1, and to the reduced activity observed in A7 scFv-Fc antibodies purified using protein A compared to culture medium concentration, as described in section 3.3.3, the Talon® purification was chosen as the primary purification system.

Analysis of the eluted fractions of A7/Adalimumab under UV 280 nm showed high readings, demonstrating the presence of protein in the collected fractions (Figure 6.10 A). Fractions showing similar protein content, calculated through OD absorbance, were pooled and dialysed O/N in PBS to remove excess free imidazole and equilibrated in standard buffer. Yields of up to 12 mg/L were obtained for A7/Adalimumab bispecific antibody. SDS-PAGE analysis of reduced protein, showed the presence of two distinct bands around 60 kDa (Figure 6.10 B). The difference in apparent molecular weight between A7 scFv-Fc and Adalimumab scFv-Fc was already observed in the bivalent monospecifc antibody, described in

sections 3.3 and 6.2.1, and is probably due to a different glycosylation pattern. No detectable contaminant proteins were present in the purified antibody pool. Western blot analysis of anti 6-His or anti-SV5 probed membranes show the presence of the A7 scFv-Fc and Adalimumab scFv-Fc band respectively (Figure 6.10 C).

Analysis of eluted fractions of E2/Adalimumab under UV 280 nm, showed a good protein production although lower than the one obtained with A7/Adalimumab, with a yield of up to 8.5 mg/L (Figure 6.11 A). SDS-PAGE analysis of reduce protein previously dialysed in PBS, showed the presence of two bands around 60 kDa representing the two scFv-Fc chains (Figure 6.11 B). A difference in the apparent molecular weight between the two chains can be appreciated also in this bispecific construct. This time however, the E2 scFv-Fc chain appears smaller than the Adalimumab portion. Western blot analysis confirms the specificity of the bands detected in Coomassie stained SDS-PAGE, showing reactivity in anti-6-His and anti-SV5 probed membranes (Figure 6.11 C).

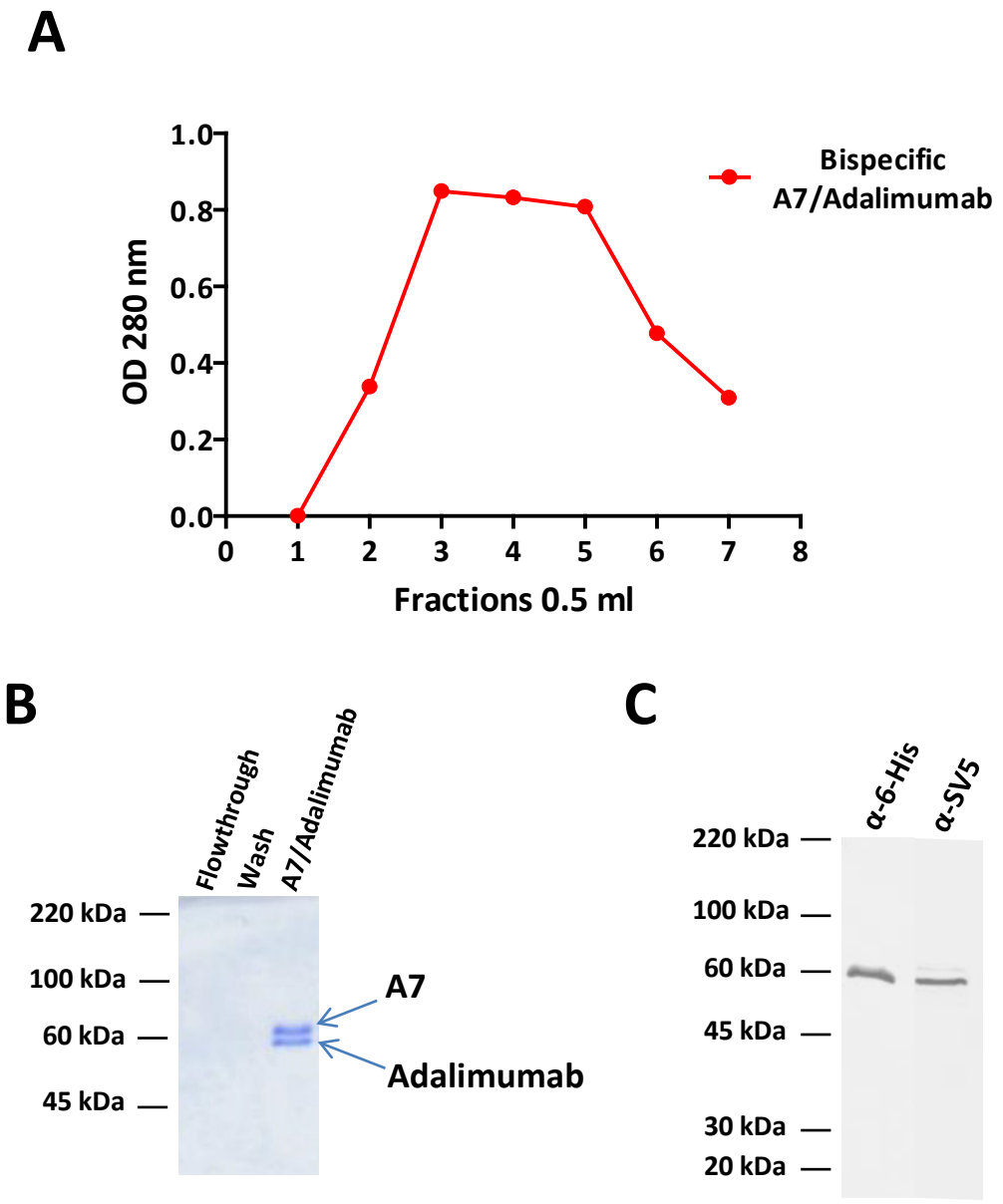

Figure 6.10 A7/Adalimumab bispecific antibody production and purification via CHO-s

Optical density analysis of A7/adalimumab bispecific antibody eluted fractions from 150ml CHO-s supernatant using Talon® purification system (A). SDS-PAGE resolved purified A7/Adalimumab fractions from CHO-s stained with Coomassie brilliant blue (B) or probed with anti-6-His (A7 chain) or anti-SV5 (Adalimumab chain) and anti-mouse HRP antibody following Western blotting (C).

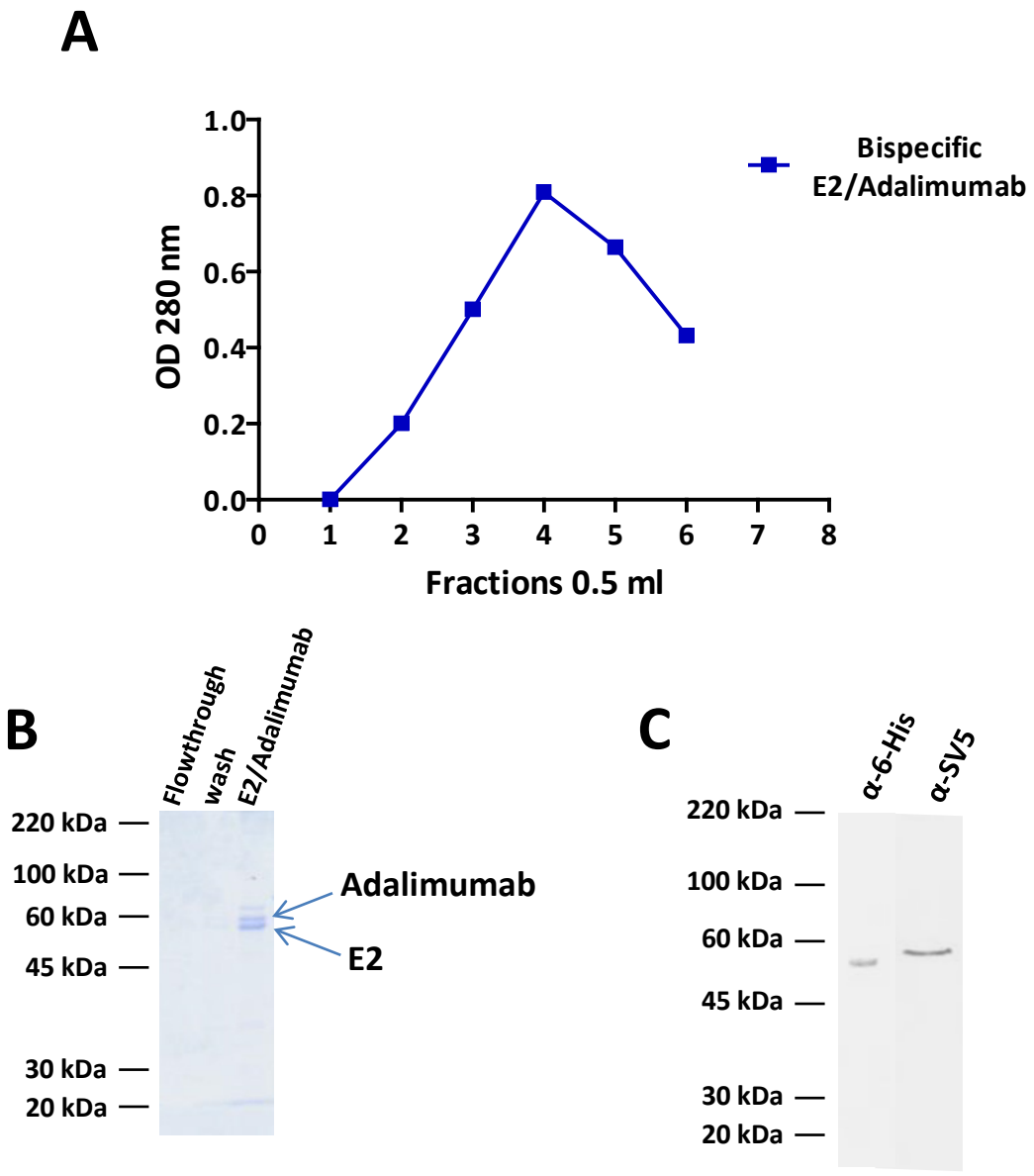

Figure 6.11 E2/Adalimumab bispecific antibody production and purification via CHO-s

Optical density analysis of E2/adalimumab bispecific antibody eluted fractions from 150 ml CHO-s supernatant using Talon® purification system (A). SDS-PAGE resolved purified E2/Adalimumab fractions from CHO-s stained with Coomassie brilliant blue (B) or probed with anti-6-His (E2 chain) or anti-SV5 (Adalimumab chain) and anti-mouse HRP antibody following Western blotting (C).

6.3.2.2 Heterodimerisation efficiency

A key element in the production of an efficient and optimal bispecific antibody is the degree of heterodimerisation. The knobs-into-holes technology employed for bispecific antibody production in this project, has reported up to 92% of efficient heterodimerisation (211). However, the reproducibility of this dimerisation efficiency varies depending on the protein synthesis strategy and antibody structure. The antibody format used in this project significantly differs from the IgG format adopted in the original knobs-into-holes publication. It is therefore pivotal to determine the degree of heterodimerisation obtained and rule out the possibility of any effect being due to the presence of homodimers of either chain.

The production of bispecific antibodies, independently of the technology used, can potentially produce antibodies in heterodimer format, homodimer for the first chain and homodimer for the second chain. The data presented in Figure 6.10 B, SDS-PAGE resolved reduced A7/Adalimumab antibody, shows a similar concentration of the two chains. This is due to the efficient 1:1 ratio obtained using the 2A peptide self-processing sequence. This analysis, however, is not informative with regard to the degree of dimerisation. In order to investigate this, bispecific antibodies were resolved in SDS-PAGE under non-reducing conditions and stained with the highly sensitive colloidal Coomassie brilliant blue stain (EZBlue). The Adalimumab IgG antibody shows a molecular weight of about 150 kDa, consistent with the IgG format. Adalimumab scFv-Fc shows an approximate molecular weight of 120 kDa. The bispecific antibodies show a molecular weight smaller than the IgG but higher than the Adalimumab scFv-Fc, however, due to the limitations in the resolution power of the acrylamide gel electrophoresis, it is difficult to discriminate subtle differences in size (Figure 6.12).

In order to overcome this limitation and have a clear distinction between the three possible dimer molecules, the bispecific antibody encoding vector was engineered to remove the second scFv sequence as described in detail in section 2.3.1. In doing so, the first chain maintained the correct Adalimumab scFv-hinge-Fc

sequence, while the second chain displayed only the hinge-Fc region (Adalimumab/Fc truncated). In this way the three possible dimers displayed a molecular weight size of 120 kDa, 60 kDa and 90 kDa, representing the homodimer for Adalimumab, the homodimer for the truncated chain and the heterodimer, respectively. Figure 6.13 shows a schematic of the vector and the antibodies structure.

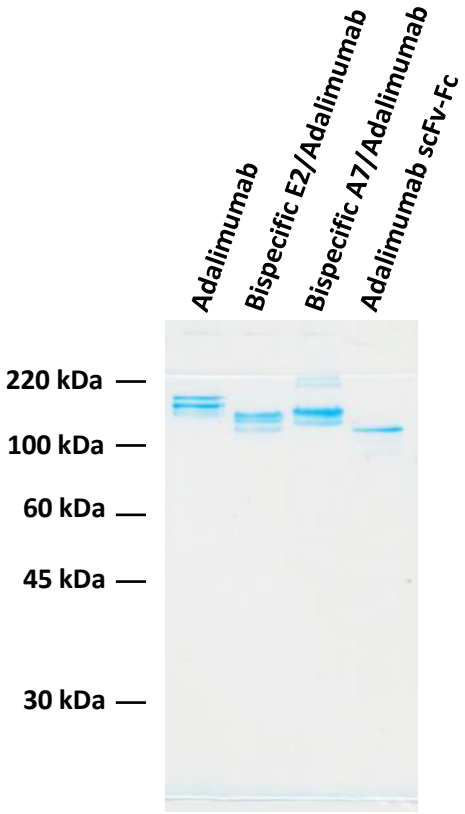

Figure 6.12 SDS-PAGE analysis of bispecific antibodies

SDS-PAGE analysis in non-reducing conditions of bispecific antibodies compared to original Adalimumab and Adalimumab scFv-Fc. Gel stained with colloidal Coomassie brilliant blue (EZBlue).

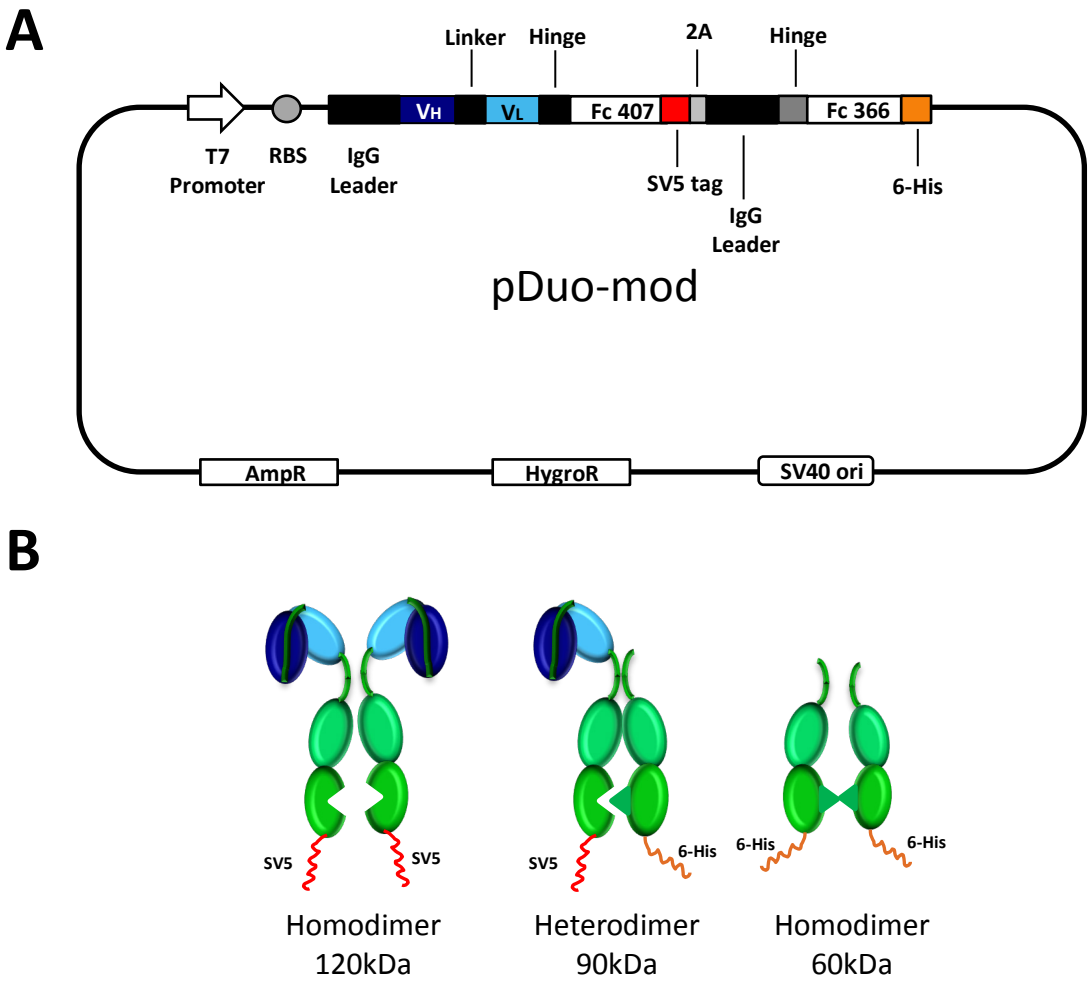

Figure 6.13 pDuo-mod vector and bispecific antibody protein structures

Schematic of pDuo-mod vector encoding the bispecific scFv-Fc antibody with deletion of the second scFv (A). Schematic of the possible bispecific antibody dimer structures (B).

HEK-293T cell line was transiently transfected with the pDuo-mod vector and incubated in serum free medium. Culture supernatant was purified using a double purification step. First the medium was dialysed overnight in PBS and then incubated with protein A Sepharose beads as described in section 2.2.3.1. Protein A Sepharose beads are able to purify antibodies by targeting the Fc region. By doing so, the protein A will purify the antibody from the supernatant mixture without discriminating between the three different possible dimers. The second purification step employed is the Talon® metal affinity resin, the standard approach used for the bispecific antibody isolation. This resin by being able to selectively target the 6-His tag, will discriminate in favour of the 90 kDa heterodimer and the 60 kDa homodimer. Both resins were able to purify the antibody as shown in Figure 6.14.

The asymmetric antibody construct created carried only one scFv domain and it was chosen to maintain the Adalimumab scFv order to be able to determine correct antibody function in a convenient ELISA assay. The ability to bind TNF was then assessed in comparison to the Adalimumab scFv-Fc antibody previously described (section 6.2). Both antibodies purified with protein A or Talon® were able to selectively target the TNF-α with only a slight increase in the EC50 values when compared to Adalimumab scFv-Fc to be ascribed to the monovalency of the asymmetric antibody construct (Figure 6.15).

Western blot analysis of non-reduced antibody derived from protein A or Talon® purification and probed for anti-6His tag showed as expected no change in the protein content between the two, figuring the 90 kDa and 60 kDa molecules. When probed for anti-SV5 however, the lane corresponding to protein A purification showed the bands at 120 kDa and 90 kDa while the lane from Talon® purification showed predominantly one band at 90 kDa (Figure 6.16 A). This data signifies that Talon® purification can significantly reduce the concentration of one of the two contaminating homodimers.

In order to quantify the relative proportion of the three dimer forms potentially present in the purified antibody pool and define the degree of purity of the functional heterodimeric antibody, SDS-PAGE resolved antibody from protein A

or Talon® purification were resolved in non-reducing conditions and stained with colloidal Coomassie brilliant blue (Figure 6.16 B). Analysis of the plot profile obtained from the protein A lane, showed the presence of the three molecular weight products with a relative proportion of 8.5%, 79.2% and 12.2% for the 120 kDa homodimer, 90 kDa heterodimer and 60 kDa homodimer respectively. Analysis of the Talon® lane, showed a reduction of the 120 kDa homodimer down to 3.2%, and increase of the 90 kDa heterodimer format to 85.1% of the total protein pool and maintaining unaltered the 60 kDa homodimer with 11.7% (Figure 6.16 C). This result demonstrates that an efficient heterodimerisation rate of 85% can be achieved using our construct following Talon® purification.

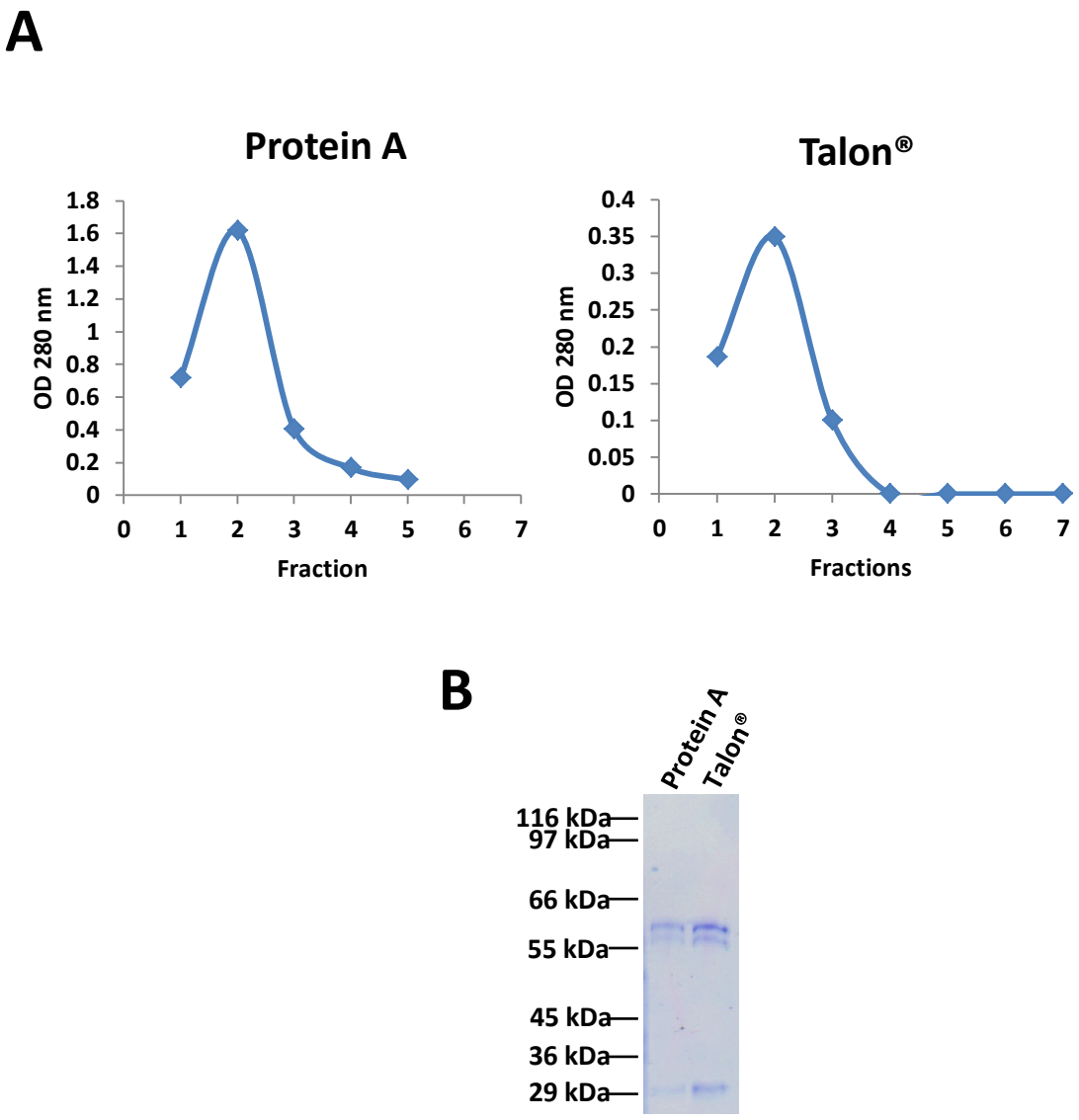

Figure 6.14 Adalimumab/Fc truncated bispecific antibody production

Optical density analysis of Adalimumab/Fc truncated antibody eluted fractions from 80 ml HEK-293T supernatant using protein A purification system and 1 mg antibody purified using Talon® metal affinity chromatography (A). SDS-PAGE resolved reduced purified Adalimumab/Fc truncated antibody from protein A and Talon® stained with Coomassie brilliant blue (B).

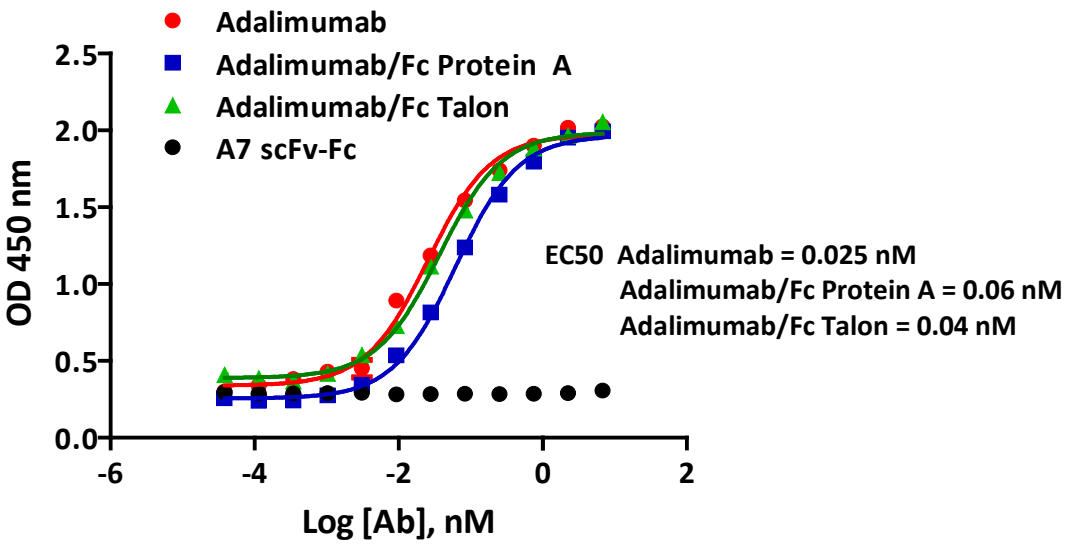

Figure 6.15 Reactivity of Adalimumab/Fc truncated antibody for TNF

ELISA on coated 100 ng/ml TNF-α. Antibody starting concentration 6.8 nM with 1:3 serial dilutions. Bound antibodies detected using anti-human Fc HRP conjugated antibody. Intensity of converted TMB substrate measured at 450 nm in a standard plate reader. Values expressed as Mean ± SEM.

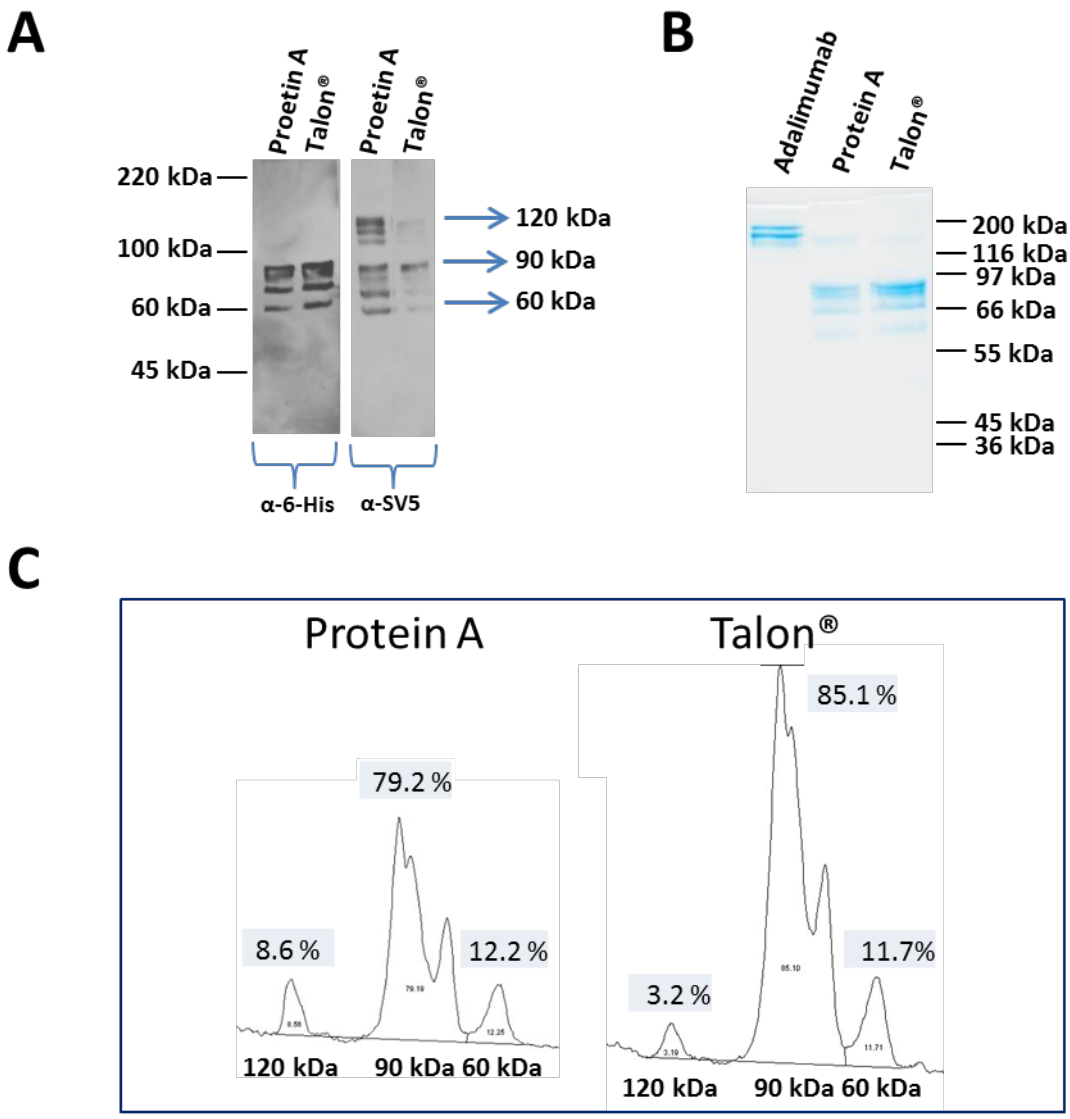

Figure 6.16 Quality analysis of Adalimumab/Fc truncated antibody

Western blot of non-reduced Adalimumab/Fc truncated antibody probed with anti 6-His or anti-SV5 antibody and detected with anti-mouse HRP conjugated antibody (A). SDS-PAGE resolved Adalimumab/Fc truncated antibody in non-reduced condition stained with colloidal Coomassie brilliant blue (B). Analysis of plot profile of protein A and Talon® purified antibody resolved in SDS-PAGE (C).

6.3.3 Characterisation of bispecific antibody specificity

A bispecific antibody is by definition an antibody able to target two different antigen epitopes at the same time. The bispecific antibodies developed for this project are designed to target human TNF-α and either the A7 target antigen or DPP6. In order to define whether the scFv domains in the new antibody format were able to retain their original antigen specificity, each antibody was tested for their specific reactivity *in vitro*.

6.3.3.1 A7 specificity

The specificity for synovium conferred by the scFv A7 domain was assessed in IHC and immunofluorescence on human arthritic synovium as described in sections 2.6.3 and 2.6.4. When compared to A7 scFv-Fc, the bispecific A7/Adalimumab antibody showed the classical perivascular staining characterised for scFv A7. Additionally, staining in sparse cell population across the tissue section could be detected in both A7/Adalimumab and E2/Adalimumab bispecific antibodies. This staining pattern was mirrored by Adalimumab scFv-Fc antibody and probably represents TNF-α targeting in TNF producing cells (Figure 6.17).

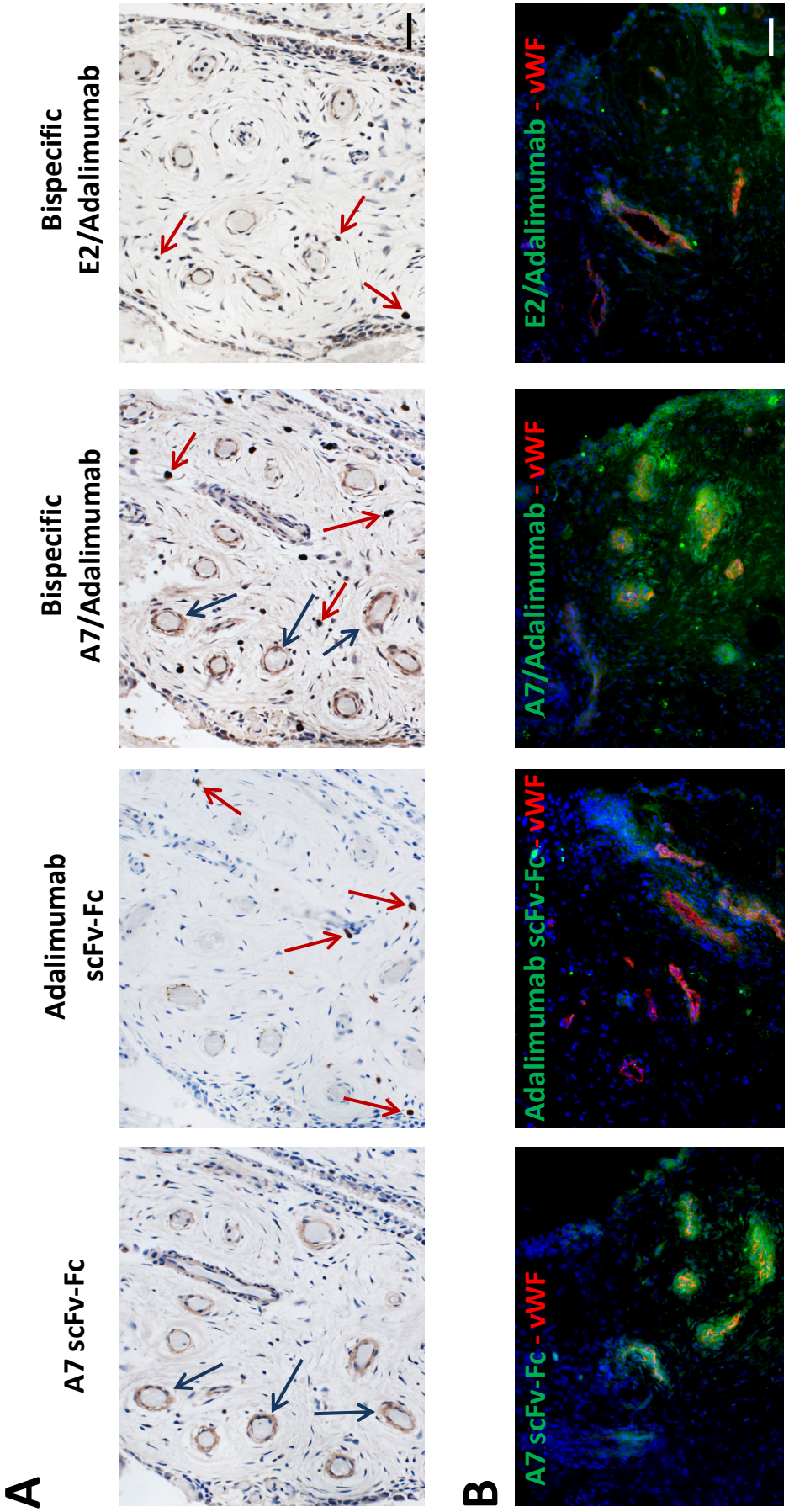
A
A7 scFv-Fc
Adalimumab scFv-Fc
Bispecific A7/Adalimumab
Bispecific E2/Adalimumab
B
A7 scFv-Fc - vWF
Adalimumab scFv-Fc - vWF
A7/Adalimumab - vWF
E2/Adalimumab - vWF

Figure 6.17 Reactivity in human arthritic synovium

IHC on OA synovium stained with biotinylated A7 scFv-Fc, Adalimumab scFv-Fc, bispecific A7/Adalimumab and bispecific E2/Adalimumab at 20 μg/ml (n=3). Binding of antibody to the tissue section detected with ABC-HRP conjugated. Blue arrows showing A7 staining. Red arrows showing Adalimumab staining (A). Immunofluorescent staining on OA synovium with biotinylated A7 scFv-Fc, Adalimumab scFv-Fc, bispecific A7/Adalimumab and bispecific E2/Adalimumab at 20 μg/ml in combination with anti-vWF. Biotinylated antibody detected with streptavidin-Alexa fluor 488 (green). Anti-vWF detected with anti-mouse Alexa 555 (red) (B).

6.3.3.2 E2 specificity

Staining with E2/Adalimumab bispecific antibody on synovium showed a light reactivity in the vascular compartment and extracellular matrix. The presence of DPP6 protein has not yet been reported in the human synovium, while being documented in neuronal and heart tissues (342, 343). In order to further evaluate the reactivity in human arthritic synovium, a bivalent mono-specific version of scFv E2 using the same scFv-Fc format adopted for A7 and Adalimumab was developed. Staining in OA and RA synovium shows a distinct staining pattern compared to A7 or Adalimumab, targeting the endothelial layer of the vessels and sparse cells within lymphoid infiltrates (Figure 6.18).

E2/Adalimumab bispecific antibody reactivity for DPP6 was evaluated in an ELISA assay showing specific dose dependent reactivity for its target (Figure 6.19).

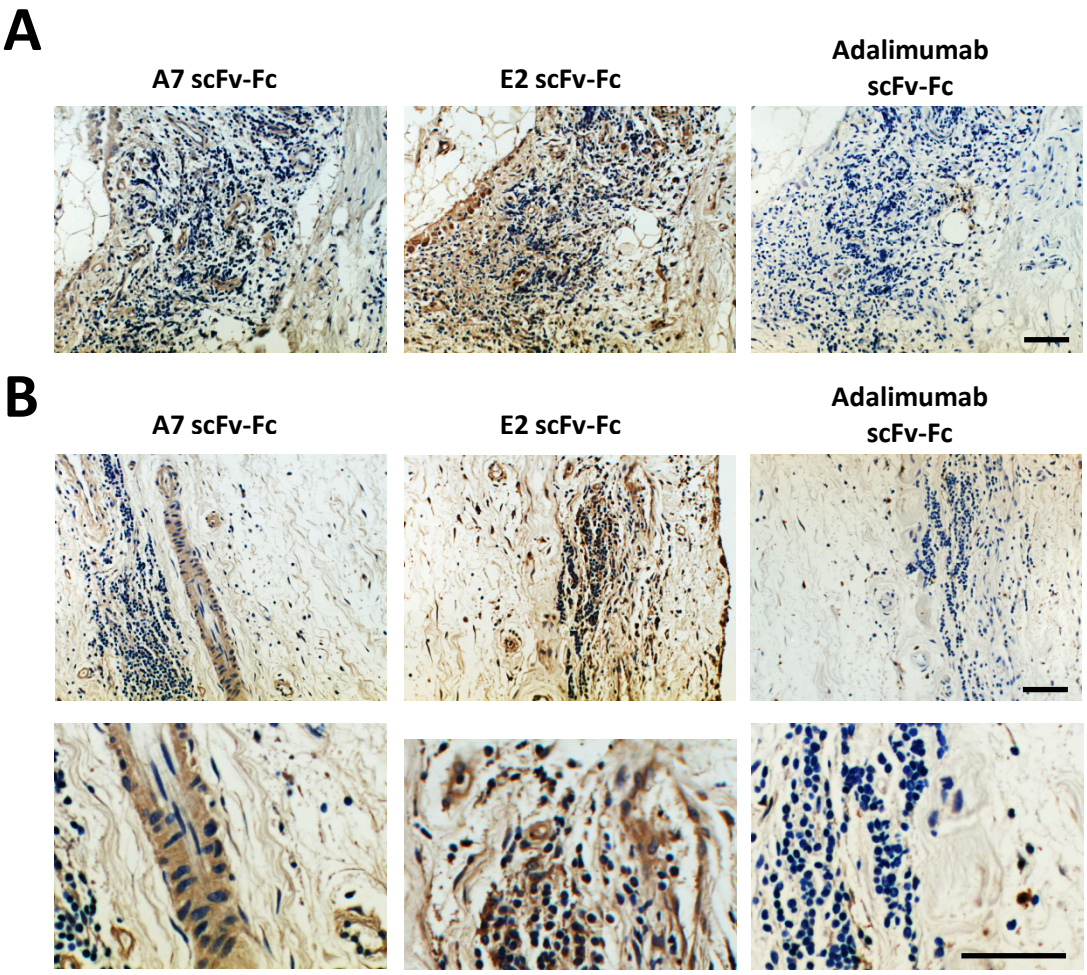

Figure 6.18 E2 scFv-Fc reactivity in human arthritic synovium

IHC on RA synovium (A) and OA synovium (B) stained with biotinylated A7 scFv-Fc, E2 scFv-Fc and Adalimumab scFv-Fc at 50 µg/ml. Binding of antibody to the tissue section detected with ABC-HRP conjugate.

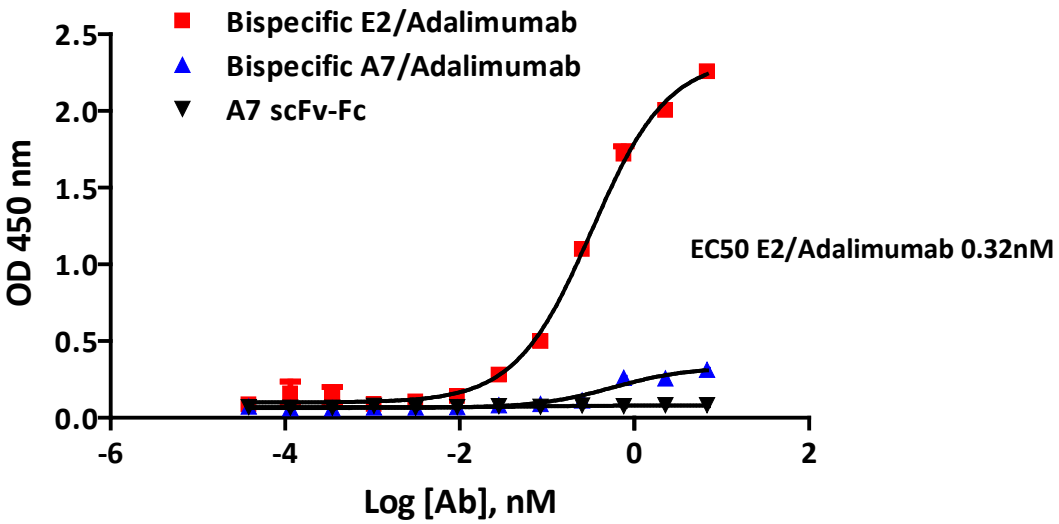

Figure 6.19 Analysis of DPP6 reactivity

ELISA on coated 1 µg/ml DPP6. Antibody starting concentration 6.8 nM with 1:3 serial dilutions. Bound antibodies detected using anti-human Fc HRP conjugated antibody. Intensity of converted TMB substrate measured at 450 nm in standard plate reader. Values expressed as Mean ± SEM.

6.3.3.3 Adalimumab specificity

Adalimumab reactivity for human TNF-α was assessed using an ELISA assay in which varying concentrations of the test antibodies were added to TNF coated plates. Dose dependent reactivity was detected for the antibodies carrying the scFv Adalimumab domain, while no reactivity could be detected with the control antibody A7 scFv-Fc (Figure 6.20). Both the A7/Adalimumab and the E2/Adalimumab antibodies showed an EC50 of 0.06 nM, in a similar range to the Adalimumab scFv-Fc and the parent Adalimumab antibody (0.04 nM and 0.025 nM respectively). In addition, when the E2/Adalimumab bispecific antibody was added to the TNF coated plates in the presence of the E2 specific target antigen DPP6, no change in EC50 value could be detected, indicating that the Adalimumab scFv arm remains active when the second scFv is engaged.

In order to further characterise the TNF binding kinetics of the newly produced antibodies and determine association (k_{on}) and dissociation (k_{off}) rates, surface plasmon resonance data are required (344). This method allows the measurement of the rates at which soluble TNF binds and dissociates from single antigen-binding regions of the antibody. The CM5 sensor chip, with a matrix of carboxymethylated dextran covalently attached to the gold surface, was used to covalently couple the anti-human Fc antibody, exploiting the primary amine groups (described in detail in section 2.13). An anti-human Fc antibody was used as a capture molecule for the test antibodies (ligand), with the advantage of allowing efficient and reproducible chip regeneration for serial experimental cycles. Test antibody was then added to the sensor chip to be captured by the anti-Fc antibody. Finally, the human TNF-α substrate (analyte) at five different concentrations (20, 8, 3.2, 1.28 and 0.512 nM) was injected over the sensor surface in separate cycles for accurate kinetic measurements. The data obtained with the Biacore T200 were analysed using the BIAevaluation software adopting the 1:1 Langmuir binding model (Figure 6.21). The kinetic parameters obtained showed consistency with previously published data, with a K_D of 23.3 pM and 31.6 pM for Adalimumab scFv-Fc and A7/Adalimumab bispecific antibody respectively (Table 6.1) (345). When sensograms from Adalimumab scFv-Fc and A7/Adalimumab antibodies challenged

with 20 nM TNF-α are compared, a clear decrease in RU is visible in the bispecific antibody plot (Figure 6.22). This discrepancy can be partially explained by the reduced TNF binding capacity of the bispecific antibody in which only one arm is dedicated to the task. This characteristic translates to fewer bound TNF molecules and, as a consequence, a reduced signal. The similar K_D values obtained with both antibodies suggest unaltered TNF binding kinetics, therefore confirming the functionality of the bispecific antibody construct.

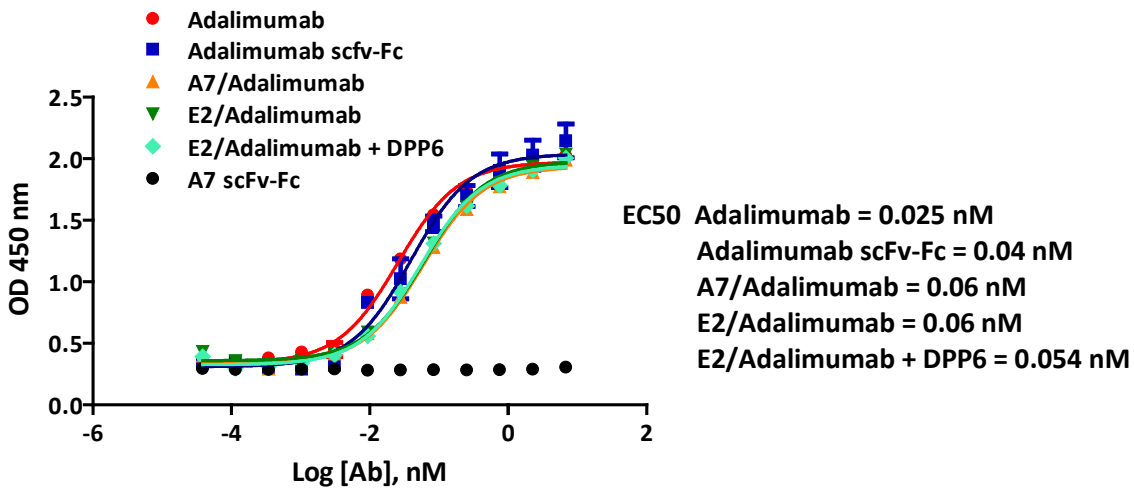

Figure 6.20 Analysis of TNF-α reactivity

ELISA coated on 100 ng/ml TNF-α. Antibody starting concentration 6.8 nM with 1:3 serial dilutions. Bound antibodies detected using anti-human Fc HRP conjugated antibody. Intensity of converted TMB substrate measured at 450 nm in a standard plate reader. Values expressed as Mean ± SEM.

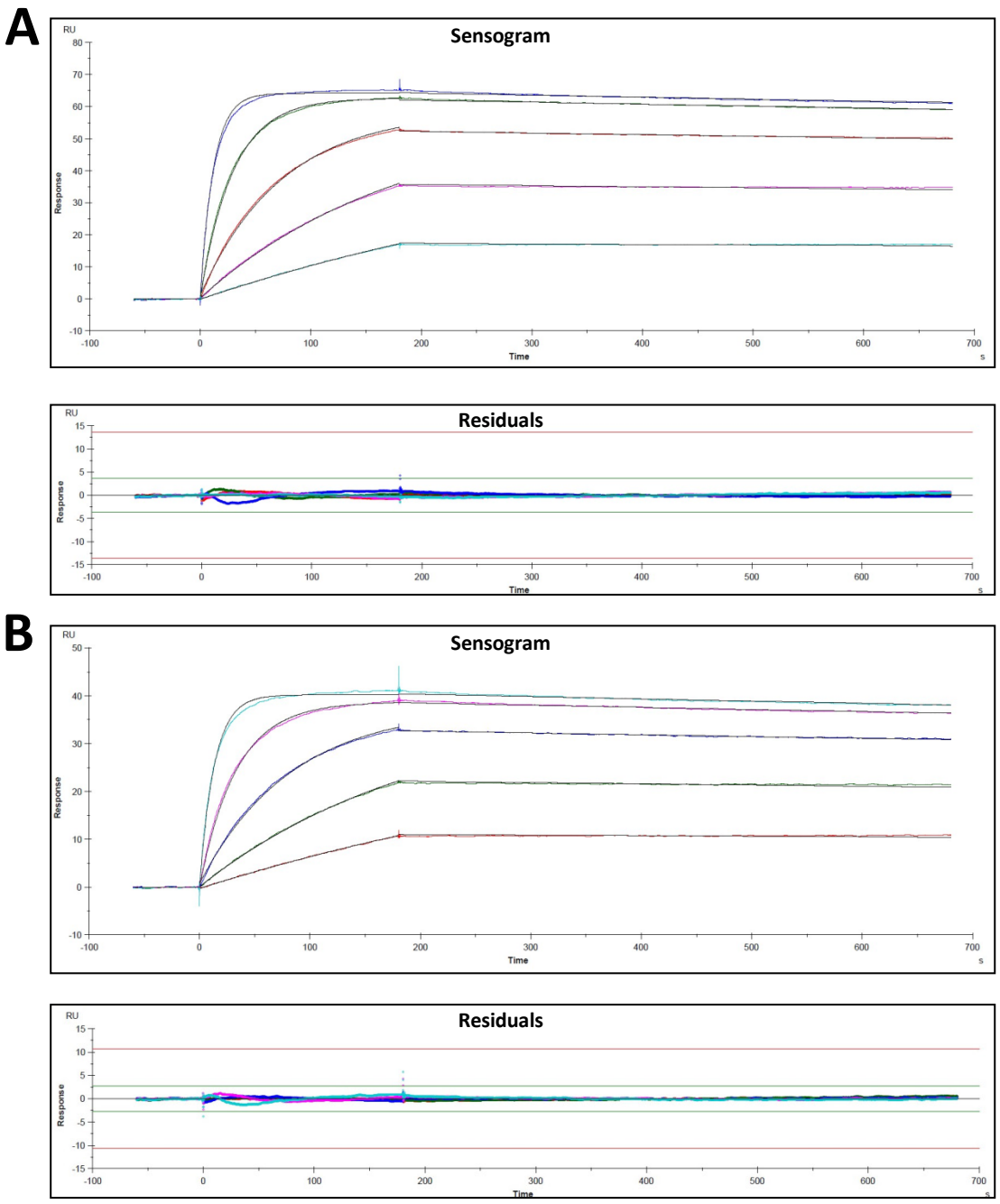

Figure 6.21 Biacore analysis of TNF-α reactivity

Biacore data analysed using Bia-evaluation software tool. Sensogram fitted with Langmuir binding model for (A) Adalimumab scFv-Fc antibody (TNF 20 nM dark blue, 8 nM green, 3.2 nM orange, 1.28 nM pink and 0.512 nM light blue) and (B) A7/Adalimumab bispecific antibody (TNF 20 nM light blue, 8 nM pink, 3.2 nM dark blue, 1.28 nM green and 0.512 nM orange). Residuals included to indicate degree of discrepancy between experimental data points and the 1:1 Langmuir model fit.

	Curve	k_{on} (1/Ms) [SE]	k_{off} (1/s) [SE]	K_D (M)	Rmax (RU) [SE]	Chi^2 (RU^2)
Adalimumab scFv-Fc		4.193E+6 [3.1E+3]	9.768E-5 [3.1E-7]	2.330E-11		0.127
	TNF 20 nM				64.42 [0.01]	
	TNF 8 nM				62.42 [0.01]	
	TNF 3.2 nM				57.84 [0.01]	
	TNF 1.28 nM				58.17 [0.02]	
	TNF 0.512 nM				54.56 [0.03]	
Bispecific A7/Adalimumab		3.739E+6 [3.5E+3]	1.181E-4 [3.9E-7]	3.157E-11		0.075
	TNF 20 nM				40.42 [0.01]	
	TNF 8 nM				38.85 [0.01	
	TNF 3.2 nM				37.19 [0.01]	
	TNF 1.28 nM				38.68 [0.02]	
	TNF 0.512 nM				38.21 [0.03]	
Adalimumab (345)		1.69E+6	4.71E-5	3.04E-11		

Table 6.1 Kinetics of Adalimumab scFv-Fc and A7/Adalimumab binding with TNF-α

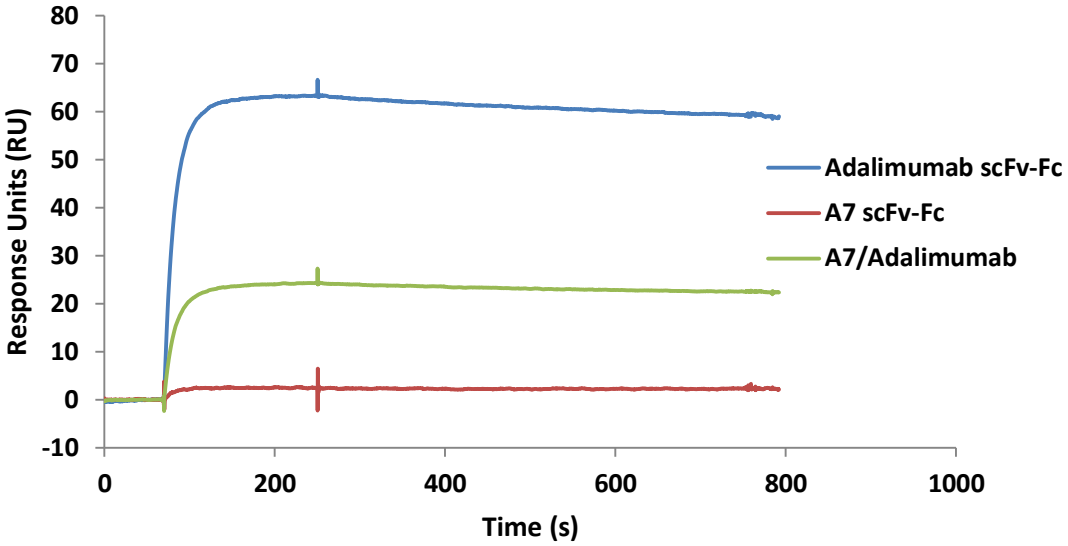

Figure 6.22 Biacore sensogram analysis on anti-TNF constructs

Sensograms from Biacore analysis of Adalimuab scFv-Fc, A7/Adalimumab and A7 scFv-Fc challenged with 20 nM TNF-α compared to reveal change in magnitude of response. A7 scFv-Fc shows no interaction with TNF while the A7/Adalimumab bispecific antibody shows 30-40% of RU detected with Adalimumab scFv-Fc, suggesting a monovalent capacity of TNF binding in the bispecific construct.

6.3.4 Pharmacodynamics of bispecific antibody *in vitro*

As already mentioned in section 6.2.2, the ability to target TNF *in vitro* is important but not sufficient to determine inhibition of the biological activity of TNF in a cell based environment. This ability is pivotal in the mechanism of action of Adalimumab (346). In order to evaluate the capacity to inhibit TNF induced cytotoxicity, a murine fibroblastic cell line was incubated for 24 hours in complete medium with the presence of the protein synthesis inhibitor actinomycin D, 0.45 ng/ml human TNF-α and varying concentrations of the test antibodies. Cell viability was assessed by measuring the production of a violet dye visible at 560 nm after incubation with MTT substrate as described in section 2.10. Data presented in Figure 6.23 confirm the ability of the bispecific antibodies produced to inhibit the TNF induced cytotoxicity in a dose dependent manner. The bispecific antibodies showed an increase in the IC50 values compared to the original Adalimumab antibody.

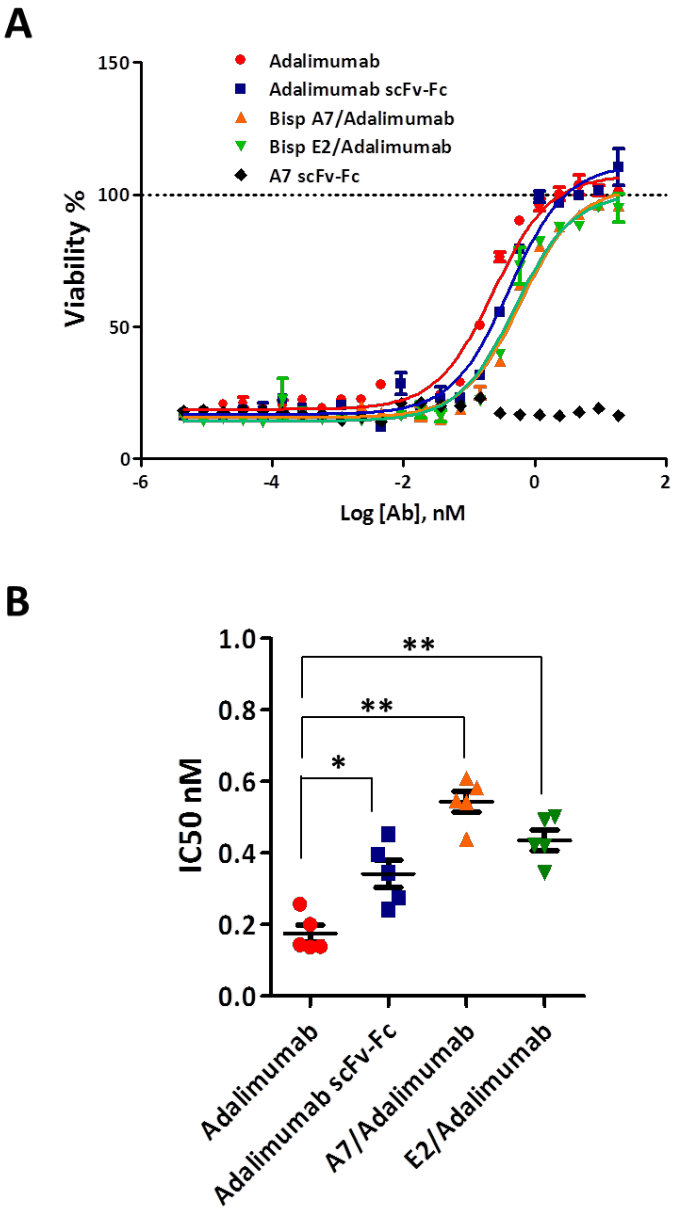

Figure 6.23 TNF induced cytotoxicity assay on L-929

$3x10^4$ L-929 cells seeded in a 96 well plate in complete DMEM medium. Cells were incubated with 1 µg/ml actinomycin D and 0.45 ng/ml TNF-α in the presence of varying concentrations of test antibodies for 24 hours. Antibody starting concentration 18.8nM with 1:3 serial dilutions. Viability measured upon conversion of 5 µg/ml MTT substrate in a violet dye and measure at 560 nm in standard plate reader. Values expressed as Mean +- SEM (A). IC50 values of 5 independent cytotoxicity assay (B). Mean IC50 for Adalimumab = 0.17 nM, Adalimumab scFv-Fc = 0.34 nM, A7/Adalimumab = 0.5 nM and E2/Adalimumab 0.4 nM. Mann-Whitney test * = p value <0.05, **= p value <0.01.

6.4 Discussion

In this chapter the development of a synovium specific molecule with potential application as a therapeutic agent in the field of arthritis was presented. Following the results described in chapter 3, the scFv A7 antibody fragment proved to be able to specifically target the human arthritic synovium with little if any reactivity with other human tissues both in healthy and disease condition. This remarkable capacity has led us to further develop the molecule into a therapeutic agent. Ligand-based vascular targeting of disease is a new attractive strategy for treatment of conditions characterised by extensive neo-angiogenesis and vascular remodelling. This approach is likely to improve the therapeutic index of available therapeutic agents and increase safety. By targeting disease specific antigens in the vascular compartment, a selective drug localisation can be achieved *in vivo*, sparing healthy organs and decreasing systemic toxicity. Recently, antibodies specific for alternatively spliced extra-domain of fibronectin, up-regulated in tumour and inflammatory conditions, have been successfully conjugated with effector moieties, showing improved functionalities (261, 320, 347). As a proof of concept, the gold standard for anti-TNF therapy Adalimumab (Humira) (139) was chosen as the molecule for A7 functionalization in this project. In order to do so, it was chosen to use a bispecific antibody approach adopting the well characterised knobs-into-Holes technology (211).

First, the original Adalimumab IgG antibody had to be converted into a format suitable for efficient production and rapid engineering. The same scFv-Fc antibody format (described in section 3.3) has been adopted for Adalimumab. This strategy is made possible by the fact that originally Adalimumab derives from a scFv molecule isolated through phage display (324). Adalimumab has already been shown in the literature to be able to maintain binding specificity and pharmacokinetics in scFv format (336, 337), a characteristic that is crucial to assume similar therapeutic efficacy. The new antibody format adopted is structurally identical to the one presented in section 3.3 for A7, characterised by a scFv domain fused to the human IgG hinge and C_H2 – C_H3 domains, restoring Fc

effector functions, dimerization capacity and increased serum half-life to the scFv molecule (153, 252, 262). The results presented in section 6.2.1, demonstrate that the new Adalimumab scFv-Fc antibody can be readily produced by stably transfected CHO-s cell line with high efficiency and high purity following protein A purification (Figure 6.4 and 6.5). However, a reduction in protein production was detected following long term storing of transfected clones (Figure 6.2). Decreased protein production over time is an issue that can affect small scale laboratory based antibody production as well as large industrial facilities. Protein expression rates depend on numerous factors, such as transcriptional regulatory elements and DNA sequence, and can be altered by change in surrounding chromatin structure or specific DNA methylation (348). These changes can occur rapidly and are difficult to foresee. Often the only way to recover protein expression is by repeating the transfection step. A possible way to overcome this limitation and maintain a more stable and prolonged protein expression would be by using of vectors containing specific ubiquitous chromatin-opening elements (UCOEs), that are characterised by methylation-free CpG islands preventing heterochromatin formation and transgene silencing (348). Despite yield fluctuations, the Adalimumab scFv-Fc was fully functional and able to specifically target TNF *in vitro* as observed in ELISA essay (Figure 6.6). EC50 value comparison with the original Adalimumab antibody showed an almost identical binding capacity. Additionally, Adalimumab scFv-Fc was able to efficiently block TNF biological activity in a TNF induced cytotoxicity assay. This assay is the standard approach for *in vitro* determination of anti-TNF activity in a biological environment (165, 349). Results presented in Figure 6.7 showed an efficient inhibition of TNF induced cytotoxicity with Adalimumab scFv-Fc with a small, although significant, increase in IC50 value compared to the commercial Adalimumab antibody. This increase is likely due to the presence of impurities in the produced scFv-Fc protein deriving from in-house production and protein handling. Production of the antibody under good manufacturing practice (GMP) conditions and in dedicated facilities would probably ameliorate the quality and reactivity of the product.

Many strategies are currently available to produce bispecific antibodies (as described in section 1.3.3), ranging from chemically cross-linked antibodies to tandem scFv and scFv-IgG fusion proteins (205). The approach used in this project was the knobs-into-Holes, one of the first described methods for efficient heterodimerisation of bispecific antibodies (211). The rational for choosing this method lies on the fact that it requires little engineering of the Fc region by introducing single amino acid substitutions. These mutations consist of the substitution of a small amino acid side chain with a larger one on the first peptide chain to create a knob and substitution of a large amino acid with a smaller one on the second chain creating a hole. Among the different possible mutations reported in the literature, the T366Y and Y407T were chosen. Recently, mutations on the 407 residue with charged amino acids or glutamine have been proven to influence the degree and nature of glycosylation, leading to dimer destabilisation and impaired activity (350). However, substitution with a polar non-charged amino acid has shown to conserve functionality of the heterodimer by retaining the Fc effector functions, eliciting ADCC and complement-mediated cytotoxicity (CMC) (211). The knobs-into-Holes method was adapted to the scFv-Fc fusion construct already described in section 3.3 for A7 bivalent molecule. Having adopted a scFv-Fc fusion approach allowed a more efficient antibody expression. In this context, other bispecific antibody strategies, such as the Quadromas approach in which two monoclonal antibody producing hybridomas are fused (351) or the TriomAbs approach in which rat IgG2b and mouse IgG2a are used to create bispecific constructs (210), have the inherent limitation of heavy-light chain mis-pair. The scFv-Fc fusion construct developed overcomes this limitation by directly linking the heavy and light variable regions and preventing mismatch. The bispecific A7/Adalimumab and control E2/Adalimumab antibodies were efficiently expressed and secreted by CHO-s cells as described in Figure 6.10 and 6.11. SDS-PAGE analysis confirmed correct expression of the two chains in comparable levels; however, heterodimerisation efficiency could not be assessed using this format. Correct heterodimerisation is the limiting step in bispecific antibody efficacy. The knobs-into-Holes technology has been reported to provide up to 92% of correct dimerization by inherent instability of the homodimers due to steric hindrance.

However, efficient heterodimerisation is often dependent on molecules expression performance. In order to improve our chances of obtaining a 1:1 ratio between the two chains, the vector construct described in Figure 6.9 contains the 2A peptide sequence. As previously mentioned this sequence allows a ribosomal skip during protein translation, causing the release of the first peptide chain before continuing with the second part (341). This self-processing peptide does not require ribosome release and re-attachment using internal ribosome entry sequences (IRES) and should therefore provide a better efficiency in chain expression. However, contrasting reports are described in the literature, showing both higher 2A peptide performance and higher IRES efficiency (352, 353). Probably these contrasting reports are influenced by host environment and primary protein sequence. To determine the degree of heterodimerisation that can be obtained with the developed construct described in this chapter, an asymmetric version of the bispecific antibody was engineered by removing one of the two scFv but maintaining both hinge and Fc region (Figure 6.13). This engineered version of the bispecific antibody allowed for a clear MW distinction between the three possible dimer formats. Analysis of the HEK-293T expressed protein purified with protein A or Talon®, the standard approach used for bispecific antibody purification in this project, revealed up to 85% of heterodimer formation with the latter (Figure 6.16). In addition, the Talon® purification could discriminate for the heterodimer and the dimer containing the 6-His tag (85% and 12% in comparison to 3% for the SV5 tagged homodimer). Since the A7/Adalimumab antibody has the SV5 tag on the Adalimumab arm and the 6-His tag on the A7 side, the Talon® purification will preferentially purify the heterodimer and the homodimer for A7, reducing the quantity of homodimer for Adalimumab. This is important for the *in vivo* characterisation of the bispecific antibody functionality in which the presence of a full Adalimumab antibody contaminant in the bispecific antibody mixture should be minimised. Further, characterisation of *in vitro* functionality of the two scFv domains constituting the bispecific antibodies showed an unaltered binding capacity for their target antigen. This was demonstrated via synovial staining for A7 scFv portion (Figure 6.17), DPP6 ELISA assay for E2 scFv (Figure 6.19) and TNF ELISA for Adalimumab scFv domain (Figure 6.20). Of particular interest is the notion that

bispecific E2/Adalimumab antibody can target TNF in the presence of DPP6 without altering the EC50 value. This indicates that the bispecific scFv-Fc format does not suffer from competitive binding between the two arms due to steric hindrance. Biacore analysis of Adalimumab scFv-Fc and A7/Adalimumab bispecific antibody binding kinetics with TNF-α showed consistent K_D values with previously reported measurement for the commercial Adalimumab in the literature (345). These data further confirm the functionality of the scFv format of Adalimumab, providing additional proof to the validity of the developed bispecific antibody format. Lastly, both bispecific antibodies were able to efficiently rescue the L-929 murine cell line from TNF induced cytotoxicity with only a slightly elevated IC50 compared to the original Adalimumab antibody (Figure 6.23). This variation is likely to be due to the monovalency of the bispecific construct for TNF binding. By developing a bispecific but monovalent antibody for each functional domain, the construct in our hands probably displays a reduced avidity and an altered binding potential, translating into a reduced inhibitory efficiency. In this context, it has been demonstrated that Adalimumab is able to form complex multimeric structures with soluble TNF with the most stable binding configuration consisting of three separate TNF homotrimers and three Adalimumab antibodies (176). Furthermore, the data obtained from the Biacore analysis of anti-TNF kinetics (Figure 6.21) fit in the Langmuir 1:1 binding model when TNF is considered as a homotrimer, suggesting that each anti-TNF arm is able to interact with one TNF trimer (345).

In conclusion, the conversion of Adalimumab into scFv-Fc format didn't significantly alter the biological activity of the antibody. Coupling with the A7 scFv-Fc molecule allowed the formation of a bispecific antibody construct with high efficiency and high quality. The *in vitro* characterisation demonstrated the functional properties of the newly generated bispecific antibody, providing excellent ground bases for further preclinical studies as a biotherapeutic in the treatment of rheumatoid arthritis.

Chapter 7

Discussion and future plans

7.1 General discussion

Rheumatoid arthritis is a common autoimmune disease affecting diarthrodial joints and causing chronic inflammation and profound disability (14, 15). Over the past decades, the introduction of recombinant antibodies targeting inflammatory cytokines, has rapidly transformed the established treatments for RA. However, a high-magnitude response and treatment-free remission remain an elusive goal. One explanation for the failure to achieve remission routinely could be due to the fact that they all target inflammatory cytokines or cells involved in immune inflammation rather than the actual cause of the disease. Therefore new therapeutics with higher effectiveness and improved safety profiles are still needed in the treatment of arthritic diseases. An interesting approach would be the development of targeting tools able to selectively deliver drugs to the site of interest, improving the levels of pharmaceuticals where needed, prolonging the local activity and limiting the systemic influence of the current anti-cytokine therapeutics.

Towards this goal, identification of synovial specific antigens is of paramount importance and may have significant commercial impact. The ability of migrating leukocytes to preferentially accumulate in specific tissues has further sustained the notion of organ specific antigens expressed by the vascular endothelium. Indeed, *in vivo* phage display screenings have successfully isolated peptides able to specifically target vessels of different tissues, confirming the heterogeneity of the tissue microvasculature and the possibility to exploit such markers for targeted delivery approaches (130, 131, 133). With the same intent, our group has pioneered a chimeric mouse model using SCID mice grafted with human arthritic synovium, demonstrating the viability of the grafted tissue and the preservation of the natural human homeostatic and disease responses in the murine context (231, 232). This model was adopted to identify short peptides with specificity for the human arthritic synovium microvasculature, with potential as drug delivery vectors *in vivo* (132, 136). More recently, we adopted this model for the isolation of scFv antibody fragments showing preferential homing specificity for

the arthritic synovial tissue (230). Antibodies are evolutionally designed for antigen binding and retention, providing a unique opportunity for the identification of synovial specific markers to be used as diagnostic tools or for targeted drug delivery. Hence, the main goal of this project was to provide a direct translational application for the isolated scFv A7 antibody fragment, moving from the bench to the clinic by developing a targeted therapeutic agent with synovial specificity for the treatment of rheumatoid arthritis.

Specifically, there were four objectives in this project and these were described in chapters three, four, five and six:

1. Optimisation of scFv A7 antibody fragment production and quality assessment of the soluble antibody were the ground base conditions for further characterisation of the target antibody. In addition, a scFv-Fc IgG-like molecule was produced to take advantage of the increased avidity and Fc effector functions.

2. Characterisation of scFv A7 reactivity was evaluated using immunohistochemistry, with an emphasis on tissue, disease and species reactivity, to provide supporting evidences for the human arthritic synovial specificity of the selected antibody. This investigation was pivotal to the development of the A7 antibody into a therapeutic tool.

3. Subsequently, chapter five was centred on the efforts towards identification of the target antigen, providing an overview of the methods employed for A7 target antigen isolation and characterisation. This step would be important to provide information on the arthritic synovium specific marker targeted by A7.

4. Finally, the well-established anti-TNF antibody Adalimumab was combined with scFv-Fc A7 to form a bispecific antibody with synovium specificity and TNF inhibiting properties. Both production optimisation and quality control were assessed, alongside characterisation of tissue reactivity, providing excellent ground bases for *in vivo* evaluation of antibody potency.

7.1.1 Optimisation of scFv A7 and A7 scFv-Fc production and quality control

The phage display technology has allowed the isolation of a selective agent with specificity for the microvasculature of human arthritic synovium. One of the most important characteristics of this technology when applied to antibody isolation, is the ability to express a small antibody fragment (such as scFv or Fab) on the surface of the phagemid particle via fusion with the pIII or pVIII coat protein (226, 227). Complex multi-domain molecules such as full IgG antibodies require glycosylation and disulphide bond formation for efficient folding and function. This post-translational modification is not provided by bacterial hosts, making the antibody fragments the optimal solution to allow fast antibody screening and production in bacteria.

Two approaches are available for bacterial protein production, either directing the protein to the reducing cytoplasmic compartment of the cell or to the oxidising environment of the periplasmic compartment between the cytoplasmic membrane and the outer membrane. Cytoplasmic expression has both advantages and disadvantages: when directed by a strong promoter high yields can be achieved, however, the absence of disulphide bond formation (due to the reducing environment) and the presence of high protein content often causes the formation of insoluble inclusion bodies, characterised by mis-folded protein precipitates. These protein aggregates can be easily separated from the cellular components due to their size and density but need to be converted into their natural conformation via laborious, time-consuming and complex *in vitro* renaturation. This step has variable success rates, depending on the protein sequence, and by the additional need to separate the correctly folded proteins (354, 355). Alternatively, the protein can be directed towards the periplasmic compartment mimicking the IgG secretion pathway in eukaryotic cells. In this instance, a leader signal is required to direct the nascent molecule towards the periplasm (234, 247). In this compartment, the presence of an oxidising environment and chaperone proteins ensures a more efficient protein folding, yielding functional proteins (244-246). An additional limiting step during production is inherent to the protein itself. Efficiency in the transfer to the periplasm can influence the yields of functional proteins and lengths

and composition of the linker can determine expression and formation of insoluble aggregates (355).

For the purpose of isolating a human antibody able to target human arthritic synovium, the use of naïve and immune libraries was excluded since autoreactive clones would not be included in the pool. The Tomlinson library however, is a synthetic library based on the common V_HIII framework with diversified CDR2 and CDR3, high clone diversity ($1.47x10^8$) and good antibody production (233). However, the synthetic nature of the CDR2 and CDR3 sequences introduce an unknown variable in the antigen that can result in clone dependent expression efficiency. Presence of an amber codon is the most common yield limiting factor in scFv expression since it is not detected by the permissive *E.coli* host used for phage expression but is then recognised by the non-suppressive *E.coli* strains used for soluble scFv production, resulting in the abrupt termination of protein synthesis (356).

The scFv A7 antibody however, proved to be efficiently produced by the *E.coli* strain HB2151 following IPTG stimulation and using pelB driven periplasmic transfer. The soluble protein showed the expected 30 kDa molecular weight and presence of both c-myc and 6-His tags, indicating full protein length. Two purification methods were compared: staphylococcal protein A and the cobalt based metal affinity chromatography Talon®. The design of the Tomlinson library allows the use of protein A for a fast and easy purification, exploiting the V_HIII framework in the absence of the more conventional Fc binding region. Targeting the 6-His tag proved to be more efficient, with a 1.8 fold increase in protein yield and up to 3 mg from 100 ml shake flask cultures, in line with the 0.1-100 mg/L yield for antibody fragments reported in the literature (355). Importantly, the purified scFv antibody showed limited contaminant proteins and breakdown products as detected by SDS-PAGE analysis, HPLC and FPLC. Furthermore, synovial reactivity of the scFv A7 purified antibody separated via size exclusion chromatography in FPLC showed no difference between the total scFv pool and the pure monomeric form. These results indicate not only that the scFv A7 was readily produced by *E.coli* using standard laboratory equipment, but also that the method adopted was able to

efficiently purify the scFv antibody from the bacterial culture with a single purification step.

ScFv antibody fragments have revolutionised the field of recombinant antibody development, providing small molecules with binding capacity that can easily be expressed by eukaryotic as well as prokaryotic hosts and have been successfully adapted to phage display technology for fast screening (205, 222, 227). ScFvs are by design small monovalent molecules with low avidity and fast blood clearance. However, these characteristics may offer several advantages over conventional full-length IgG antibodies. Generally scFvs have a molecular weight of 30 kDa, below the kidney filtration limit which translates in fast renal clearance and short serum half-life. In specific circumstances however, this property is more than welcome: functionalization with effector moieties such as radionuclides for imaging or radiotherapy requires fast clearance rates to minimise the risk of healthy tissue exposure (357, 358). In addition, the small size allows a better and faster tissue penetration (359). For other applications though, longer half-life and increased antigen retention via high avidity may be preferable. Due to their plasticity, scFv have been extensively used as building blocks for the full IgG development, resulting in 13 antibodies currently in clinical trials (205).

In order to increase avidity and restore Fc effector functions, we designed a scFv-Fc fusion protein linking the scFv domain to the C_H2-C_H3 regions, acquiring the structural and functional characteristics of a native IgG molecule. This new format was not compatible with the bacterial expression machinery due to the requirement of Fc glycosylation for homodimer stability and effector functions (153, 252, 254). Although bacteria are still considered the most efficient and cost effective way of producing recombinant proteins, 32 among the 58 biopharmaceutical molecules approved in the clinic are currently produced in mammalian expression systems (263), 70% of which are produced using CHO cells (360). The main reason for the success of this cell line lies in the ability of these cells to adapt to serum free culture conditions, efficient post-translational modifications compatible and bioactive in humans, and compliance to FDA criteria and regulations (264). Since the well-established anti-TNF Adalimumab was produced

using CHO, we adopted this expression system as the standard approach for scFv-Fc expression. The IgG-like construct was readily produced by CHO cells and secreted in the medium directed by the IgG leader sequence. A yield of up to 20 mg/L could be achieved using high density cultures of CHO-s cells in suspension using serum-free medium. This yield however, is far from optimal when yields of more than 10 g/L have been reported for industry productions. A possible way to increase the production efficiency could be the use of shaker incubators allowing a continuous re-suspension of cells during culturing, increasing cell growth and protein production. This system could be easily applied to laboratory based productions. An additional strategy could be the use of hollow fiber bioreactors that can house 10-100 times higher cell density than conventional T-flasks. In this system, small tube-like filters create a semi-permeable membrane filtering nutrients and waste material allowing high cell density, continuous cell culturing and long term protein production (361). However, although this system is available for small and large scale productions, it requires specialised equipment. Another way of addressing yield efficiency would be engineering of the expression vector. Simple integration of UCOE sequences, characterised by methylation-free CpG islands upstream of the promoter sequence, preventing heterochromatin formation and transgene silencing, have shown to significantly increase scFv-Fc antibody production in CHO-s cells, providing long term stable expression of the exogenous antigen (348).

Finally, synovium specific reactivity was confirmed via IHC on arthritic synovial tissue sections with comparable efficiency to the parent scFv A7. However, the gained avidity did not seem to substantially increase the binding capacity of scFv-Fc antibody. Analysis of the scFv A7 sequence revealed the presence of two glycosylation sites within the CDR2 and CDR3, specifically N-S-T and N-A-S respectively. Presence of N-glycosylation sites within the antigen recognition regions can seriously impair binding capacity and potentially influence pharmacokinetic properties and should therefore be avoided (362). Furthermore, bacterial scFv expression does not include glycosylation, introducing an additional variable for the scFv-Fc construct. Removal of the glycosylation consensus sequence can be easily achieved via site-directed mutagenesis; however, modifications in

such critical regions can alter the specificity of the antibody and therefore require scrupulous screening to confirm retention of original targeting capacity.

7.1.2 Characterisation of scFv A7 reactivity

The reactivity of the soluble scFv A7 antibody was previously proven *in vivo* in the SCID mouse transplantation model, showing preferential homing specificity for the human arthritic synovium compared to the normal human skin and mouse tissues (230). ScFv A7 was also shown to specifically target the microvasculature of both RA and OA human synovium *in vitro* with no detectable reactivity with normal human skin. As already mentioned in section 4.6, the targeting of both RA and OA vasculature is not uncommon. A previously isolated peptide using *in vivo* phage display in the same SCID mouse model showed synovial homing specificity irrespectively of RA or OA origin (279). This can indicate the targeting of a synovium specific antigen or an antigen undergoing expression or up-regulation in arthritic disease and therefore shared by the two conditions. Further investigations using synovium biopsies from patients with inexplicable knee pain that did not develop arthritic conditions in a 5 year follow-up survey (271), showed no reactivity with vasculature or other cell components within the tissue. This is of particular importance since it points toward the identification of an arthritic synovium specific antigen and therefore may lead to a possible diagnostic tool.

It would be of interest to further characterise the prevalence and expression of the target antigen in different therapeutic stages of the disease, analysing tissues from patients not previously treated with DMARD or biologic agents to detect changes in expression patterns. Additionally, screening patients with early or advanced arthritis would provide insights into whether the target antigen or scFv A7 may be used as a marker for early diagnosis of the pathology.

Towards this aim we have performed a screen on tissue sections form OA and RA synovium characterised by varying degrees of immune cell infiltrates. Tissue samples can show low amount of infiltrating cells, diffuse infiltration with no clear distribution and aggregates of varying size that can present features of ectopic lymphoid structures (50). However, no significant difference in reactivity could be detected with A7. It is worth mentioning that the infiltration levels detected in the tissue sections are not representative of the entire synovium of a single patient and

different regions may present different phenotypes (50). In this light, the stimulus required for A7 target antigen expression may be independent of tissue cellularity or may distribute across the tissue and therefore migrate in adjacent regions. It could be speculated that the A7 target antigen expression is promoted by the inflammatory environment itself and therefore be non-disease specific. In order to shed light on this possible scenario, the reactivity of scFv A7 was evaluated in inflammatory bowel disease, a class of disease characterised by extensive angiogenesis and chronic inflammation (268). An additional reason for testing IBD lies in the fact that mucosal leukocytes are capable of binding to synovial vessels, causing arthritic complications in mucosal disorders or aggravating pre-existing arthritis, indicating a common migratory pathway (363, 364). All of the samples tested were negative for scFv A7 reactivity in the vascular compartment; however, 3 Crohn's disease and 2 colorectal cancer tissues showed confined reactivity to the muscular layer. Further, reactivity was tested in psoriatic skin and melanoma samples with associated colon and axillary lymph node metastasis showed a negative outcome. The arthritic synovium specificity of scFv A7 was further proved by screening a comprehensive panel of normal human tissue from various organs, where no targeting was detected with the vasculature or other tissue components. These results demonstrate that the expression of the epitope for scFv A7 is likely to be tissue specific and restricted to the microvasculature of the arthritic synovium.

The use of animal model of arthritis for testing antibody distribution, pharmacokinetics and possible biological effect would be an invaluable resource in the development of scFv A7 into a therapeutic agent for the treatment of rheumatoid arthritis. Collagen induced arthritis is a well-known and extensively studied model of the pathology, showing classical RA immunological and pathological features (272). However, despite the presence of an extensive angiogenesis, associated with T- and B-cell infiltrates and synovial hypertrophy, no reactivity could be detected with scFv A7. As already mentioned in section 4.6, this result could indicate the targeting of a human specific antigen with little homology to the murine counterpart. Screening of other models of arthritis in mouse or other species, with different triggering systems may identify a suitable alternative.

Collagen-antibody induced arthritis (CAIA) for example, exploits the same principle as CIA but it is characterised by more pronounced macrophage and polymorphonuclear cell infiltrates with no associated T- and B-cell response (365). Other models include Saccharomyces cell wall immunisation acting via TLR2 stimulation, BSA-induced arthritis and TNF transgenic mouse models (365). While the identification of a suitable animal model of arthritis might provide a simple way of monitoring disease progression and A7 potency *in vivo*, the SCID xenograft model adopted in this project can be applied for the same purpose. Specifically, since the grafted arthritic synovium has been proven to maintain the phenotypic appearance of the *in vivo* rheumatoid tissue and maintained homeostatic and disease specific tissue response (231, 232), monitoring intragraft cellularity and cytokine expression would provide insights towards evaluation of the therapeutic properties of the tested molecule.

Despite the impact that rheumatoid arthritis exerts both in personal and social life, in terms of life impairment with disability, associated morbidity and mortality, considerable health care cost and high investments from the pharmaceutical companies, to date, there is a paucity of specific synovial markers. The use of synovial specific markers for selective delivery of drugs to the synovium, may improve the levels of pharmaceuticals *in situ*, prolong the local activity and limit systemic side effects. Identification of synovial specific antigens may hence be an interesting avenue for the development of novel targeted therapeutics for treatment of arthritic disease. However, to date, only a few synovial markers have been reported. In this context, synoviolin/Hrd1, an E3 ubiquitin ligase has been shown to be involved in the pathogenesis of arthritis (366) through its antiapoptotic effects (367, 368). Although ubiquitously expressed in all human tissues, synoviolin protein expression is up-regulated in the endoplasmic reticulum of synoviocytes of patients with RA (366). Cadherin-11 has been shown to be important for the synovial tissue architecture, providing adherent junctions between fibroblast-like synoviocytes and hence support to the proliferating synovium. Specifically, prominent protein expression was detected in the lining of RA, OA and normal synovium and in rare cells in the sublining region (369). Although the complete

distribution of Cadherin-11 in adult human tissue is currently unknown, evidence suggest that the protein is ubiquitously expressed, rendering this protein not specific to the synovium (369-372). Finally, gene expression profiling studies have identified the *TLE1* gene as an excellent discriminator of synovial sarcoma from other sarcomas (373). TLE proteins (human homologues of Groucho) are transcriptional co-repressors that inhibit Wnt signaling and other cell fate determination signals. Specifically, TLE has been implicated as a diagnostic marker for synovial sarcoma. However, although up-regulated in synovial sarcomas, TLE protein expression is found ubiquitously in human tissues (374-376). Further, expression of TLE in arthritic synovium has not yet been reported. In this light, currently, there is a dearth of markers specific to normal and arthritic synovium (Table 7.1).

Here the development and characterisation of a scFv antibody was reported, which shows specificity for the stromal compartment of the microvasculature of arthritic synovium with undetectable levels of the target antigen in a broad spectrum of normal and disease human tissues. This suggests that the A7 antibody represents a more selective and specific marker for arthritic synovium than those mentioned above. ScFv A7 hence represents a strong candidate for targeted therapy of arthritic disease.

Marker	Presence in arthritic synovium	Presence in normal synovium	Presence in cancer tissues	Tissue specificity	Cellular localisation	Activity
Synoviolin	Yes	Not available	Not available	Ubiquitous	Cytosol	Protection from apoptosis
Cadherin-11	Yes	Yes	Not available	Ubiquitous	Membrane	Homophilic cell-to-cell adhesion
TLE1	Not available	Not available	Yes	Ubiquitous	Nucleus	Transcriptional co-repressor
scFv A7 target	Yes	No	Not available	Arthritic synovium	Cytosol Membrane	Not available

Table 7.1 Expression profile of synovial markers

The *in vivo* phage display approach used in this project was intended to selectively isolate a scFv antibody with high specificity for a microvascular determinant within the arthritic synovium. To this intent, the phage library injected intravenously in mice, would diffuse in the murine blood stream and reach the human vessels in the synovial grafts through the anastomoses between mouse and human vasculature. To ascertain which cellular compartment within the synovial microvasculature scFv A7 was binding to, a range of endothelial and stromal markers were used in immunohistological analysis. A panel of currently available vascular markers is shown in Table 7.2. CD31 is a platelet endothelial cell adhesion molecule normally found on endothelial cells, platelets and macrophages (282) and is primarily used to demonstrate the presence of endothelial cells; CD34 is a member of the transmembrane sialomucin proteins, expressed mainly in hematopoietic stem cells, endothelial progenitor cells and endothelial cells (377) and is employed as a marker for immature vessels; vWF is constitutively produced by the endothelium and megakaryocytes (280) and is used as a marker for endothelial cells in mature vessels. IHC stainings in a range of human tissues demonstrated a lack of correlation between scFv A7 antigen expression and the endothelial markers tested. Furthermore, a direct dual staining in RA synovium with scFv A7 and anti-vWF showed that the scFv A7 staining is not present in the endothelium.

Regarding the vascular stromal compartment, endosialin (CD248) has recently been identified as a marker of mural (pericyte/smooth muscle) cells and fibroblasts associated with tumour vasculature (276, 277), however the expression detected in RA and OA synovium was not shared by the perivascular cells and showed a different profile compared to scFv A7. Additionally, smoothelin, a cytoskeletal protein, has been reported as a specific marker of differentiated (contractile) smooth muscle cells. In particular, smoothelin-A is found in viscera smooth muscle cells while the smoothelin B is found in the vascular smooth muscle cells in adult organs (378). In this context, it is unlikely that smoothelin is the target molecule for scFv A7 since the expression profile of these two antigens is different. Specifically, scFv A7 antibody does not show reactivity with the intestinal or

esophageal smooth muscle cells within the muscularis mucosa, where smoothelin A shows clear and strong reactivity (379, 380). Further, within the vasculature, smoothelin B is expressed in the tunica media of large and contractile vessels (378) and not the pericytes whilst scFv A7 exhibits reactivity with the pericytes as well as the smooth muscle cells of the microvasculature found in arthritic synovium. To date, expression of smoothelin in the arthritic joint has not yet been reported.

NG2, α-smooth muscle actin and desmin are the most commonly used markers of perivascular cells. NG2 is expressed by pericytes but not shared by the smooth muscle cells, allowing a clear discrimination between the two populations (283). α-smooth muscle actin and desmin, are both important for muscle cell architecture and therefore are a shared feature of smooth muscle cells and pericytes (284, 285). Staining in arthritic human synovium tissues showed a similar staining profile between scFv A7 and the perivascular marker described above. A dual immunofluorescent staining in RA synovium with NG2 showed significant co-localisation, therefore suggesting that the expression of the scFv A7 target antigen is confined to the perivascular compartment. This aspect is not in contrast with the principle of vascular *in vivo* bio-panning, since the presence of chronic inflammation, hypoxia and angiogenesis can facilitate extravasation of the phage clones during recirculation and allows the targeting of perivascular antigens. Further, since the *in vivo* selection guarantees the accessibility of the antigen in physiological conditions, it confirms the validity and potential of the selected scFv clone. In this regard, a scFv antibody fragment targeting the extra-domain A of fibronectin has been recently developed for RA synovium targeting (347). This antibody has been conjugated with the anti-inflammatory IL-10, showing promising results in animal models of arthritis and is now in phase Ib clinical trial, confirming the therapeutic potential of extravascular targeted therapy (347, 381).

Comparison between scFv A7 and other markers of vasculature lies outside of the primary aim of this project and was not pursued further.

Marker	Vascular localisation	Tissue specificity	Cellular localisation
CD31	Endothelium	Ubiquitous	Membrane
CD34	Endothelium	Ubiquitous	Membrane
vWF	Endothelium	Ubiquitous	Cytosol/soluble
NG2	Pericytes	Ubiquitous	Membrane
Desmin	Pericytes Smooth muscle cells	Ubiquitous	Cytosol
α-smooth muscle actin	Pericytes Smooth muscle cells	Ubiquitous	Cytosol
Smoothelin	Smooth muscle cells	Ubiquitous	Cytosol
Endosialin	Pericytes Fibroblasts	Ubiquitous	Membrane
scFv A7 target antigen	Pericytes Smooth muscle cells	Arthritic synovium	Cytosol/Membrane

Table 7.2 Expression profile of best established vascular marker

7.1.3 Identification of scFv A7 target antigen

From the data presented in chapter 4 and discussed in the above section, it is evident that scFv A7 and the target antigen may have potential as a therapeutic and/or diagnostic tool. In a scenario such as rheumatoid arthritis in which a specific and selective marker is not yet available, the identification of a tissue and disease specific antigen may have a profound impact. Unlike general antibody development strategies in which animal hosts are immunised with a known antigen to promote specific immunoglobulin production, this project started with the isolation of a scFv antibody from an *in vivo* screening. Although this strategy allowed the isolation of an antibody fragment with specificity for the natural environment of the target organ, the target antigen remains unknown. It is therefore one of the primary goals of this project to identify this antigen.

Scarce availability of RA and OA synovium has been a limiting factor in the use of the diseased tissue as the primary source of the antigen. However, the data described in chapter 5 show a defined perivascular staining in the synovium, representative of only a minor percentage of the total tissue. In this light, isolation of the antigen from tissue protein extracts might be limited by the target protein concentration. Cell lines were subsequently screened for antigen expression, in order to identify a suitable line to use as source of expressed protein to be applied to the conventional proteomic approaches. PC3 and IE7 cell lines showed reactivity with scFv A7 on the cell surface (although only on a minor percentage of the total population) and in the intracellular compartment. It is important to bear in mind that protein expression pattern can be altered following *in vitro* culturing conditions as a result of extrapolation from the three dimensional context of the native tissue (301, 302). Screening of umbilical cord tissue sections indeed proved the absence of endothelial staining with scFv A7 as was detected in HUVEC derived IE7 cell line. Interestingly, vascular staining was detected in in the perivascular compartment of the umbilical cord vein which may suggest that the target antigen for A7 displays the properties of an oncofoetal protein reactivated in disease conditions. Primary RA synovial fibrablasts were also found to be positive for scFv A7, providing an antigen source closely related to the pathology.

The classical proteomic approach using multiple detergents to enrich for specific class of proteins, followed by SDS-PAGE resolution and Western blotting, failed to provide a clear antigen candidate due to the presence of background bands detectable also with the control antibody. Furthermore, an attempt to enrich for the target antigen using IP pull-down, followed by SDS-PAGE resolution and Western blotting, did not shown a detectable reactive band. The requirement of a conformational epitope for efficient antibody-antigen binding may be the reason for the failure of the Western blot approach. Sypro® ruby protein gel stain in SDS-PAGE resolved proteins following IP, could overcome the necessity of the antibody dependent detection in Western blot by marking all protein content and detect enrichment of a specific antigen. However, no protein enrichment was detected, suggesting low concentration of the target antigen in the cell lysate.

The identification of a lysis buffer that showed scFv A7 reactivity when tested in ELISA, provided the necessary confidence for pursuing the IP strategy using the additional advantage given by the developed IgG-like format of A7. In this approach, protein A or chemically coupled beads were used to capture the A7 antibody followed by incubation with the cell lysate and analysed in Sypro® ruby stained SDS-PAGE. Despite the increased avidity of the IgG-like format compared to the scFv molecule, no clear enrichment was detected. Some bands were showing increased intensity compared to the control IP and may therefore deserve further investigation. The IP procedure mirrors what happens *in vivo* between antibody and target antigen, forming immune-complexes with stability dependent on affinity and avidity effects between the two molecules. Surprisingly, only a minor percentage of commercial antibodies are able to efficiently immuno-precipitate when not developed for this purpose. In addition, the scFv A7 antibody isolated via phage display was not affinity maturated and it did not appear to have a high affinity interaction. This may be the reason why despite the increased avidity an antigen pull-down was not achieved. Since the antibody showed a strong staining of the cell surface in RASF, a possible solution could be to cross-link the antibody to the antigen directly on the cell surface using the BS3 cross-linking reagent prior to cell lysis and analyse the shift in size of the A7 antibody. Cross-linking the antibody to

the target will prevent fast dissociation and retain the antigen during IP procedure. A possible drawback is the concomitant cross-linking of adjacent proteins, potentially resulting in a confounding picture when analysed by SDS-PAGE. A more refined strategy could be the use of sulfo-SBED Biotin (sulfo-N-hydroxysuccinimidyl-2-(6-[biotinamido]-2-(p-azido benzamido)-hexanoamido) ethyl-1,3'-dithioproprionate) (382, 383). Sulfo-SBED biotin conjugated antibodies can be incubated with the cell target or protein lysates to stimulate binding. When exposed to UV light, the biotin is transferred to the bound protein within a 20 Å distance, reducing non-specific and broad cross-linking. The antibody-sulfo-SBED-biotin-antigen complex can then be disassembled in reducing conditions, leaving the biotin attached to the target antigen. The protein can then be easily detected in western blot using HRP coupled streptavidin.

cDNA library screening was also adopted for isolation of A7 target antigen using phage display technology. The library employed was not derived from synovium but rather from colon carcinoma, lung fibroblasts and pancreatic cells, and was shown to express nearly 18000 human genes (241). The use of phage display for target antigen screening was deemed possible by the retention of A7 staining in IE7 cells treated for glycosylation inhibition. The outcome of the first phage screening indicated LTBP2 as a putative target antigen for scFv A7. Subsequent validation of the antigen in ELISA as a soluble protein or using a HEK-293 trans-membrane expression failed to confirm the specificity. A second selection on scFv A7 and A7 scFv-Fc antibody provided alternative candidates, with GABARAPL1 and MLF2 as the most represented clones. However, phage ELISA assay showed contradicting results and since no correlation with arthritic synovium appeared evident the validation was not continued. Under-representation of the total phage output could be a reason for the failure of this technique. Massive sequencing using deep sequencing systems could potentially identify previously missed clones (241). As an alternative, the yeast-two-hybrid system could be used for the same purpose. Although the general principle remains the same, the use of a eukaryotic system would allow the screening of more complex proteins. The main concern however, is the efficient folding of the scFv antibody in the cytosolic

compartment, which may impair the binding capacity of the molecule. In the literature the successful use of this system for the identification of scFv antibody targets has been reported, providing a proof of concept for the intended application (297, 298). The limiting step for these techniques comes down to the cDNA library used. For this reason, the development of an arthritic synovium library could be very beneficial and many companies now offer custom library development as a service.

Further, use of synthetic protein microarrays could be useful for target identification and have been successfully employed for antibody profiling in autoimmune diseases (299, 300). However, since protein arrays are able to house fewer proteins than the ones expressed by cDNA libraries, the protein content needs to be carefully selected and tailored to the necessity of each particular screening. Commercially available protein arrays usually contain a broad spectrum of human proteins and can be customised according to personal requests. Synovial proteome microarrays have been described in the literature (299), containing known common autoantigens, including citrullinated forms, and abundant synovial antigens. The use of such arrays may provide a more disease oriented assay and increase the chances of identifying the interacting protein.

As described in section 7.1.2, the current vascular and synovial markers do not fit with the scFv A7 staining distribution across the synovium and other tissues. A literature survey however, unveiled a yet unknown protein with strikingly similar tissue distribution to the A7 antibody (315). This protein is known as the product of the C19 ORF 10 gene and has been shown to be overexpressed in RA and OA synovium. This protein represented the optimal candidate for the A7 target antigen. Validation of the antigen using expression of soluble protein in HEK-293T or as a trans-membrane protein has been controversial. Additional experiments need to be performed in order to clearly define whether this protein represents the long sought target. Specifically, expression of the protein in soluble recombinant format will allow the testing in ELISA to determine antibody binding affinity and could be used in competitive assays in IHC on RA synovium to show inhibition of A7 targeting capacity.

The failing of the proteomic approaches and library screening performed so far can be attributed to low affinity of the antibody, high false-positive results due to non-specific interactions or to false-negative results due to low concentration of the target antigen in the lysates and testing material. However, the possibility remains that scFv A7 does not bind a protein but rather a lipid based molecule and therefore not detectable with conventional proteomic approach. Analysis of the lipidome in rheumatoid arthritis is not yet available but the capacity of lipids to act as autoantigens has been reported in autoimmune diseases (384). Further investigation with total lipid extract from cell lines, followed by thin layer chromatography and antibody probing could provide insights into whether the A7 antibody binds lipids.

In conclusion, the identification of the A7 target antigen did not provide a clear answer with the conventional proteomic approaches. Nonetheless, the isolation of the antigen remains a pivotal point in the development of A7 as a therapeutic tool and will be further pursued.

7.1.4 Development of a novel tissue specific therapeutic

Development of tissue and/or disease selective drugs represents a unique opportunity to increase pharmaceutical potency and reduce systemic side effects. The possible strategies involve the identification of a molecule able to selectively inhibit the biological function of the target antigen or the isolation of a molecule with no direct effect but with the capacity to be used for targeted delivery approaches. Conceptually these two strategies are fundamentally different, with the first aiming at the development of an active compound with intrinsic therapeutic capacities, while the latter is aimed at the development of a molecule able to selectively localise in the target organ. In the latter strategy therefore, the effector function is delegated to a second molecule. This aspect confers a high versatility to the targeting agent. Imaging is one of the possible applications of a targeting agent, via conjugation with radionuclides, fluorophores or magnetic nanoparticles. For this purpose, the scFv format appears more suited for the task, due to the small size and short *in vivo* half-life which guarantees fast clearance and deep tissue penetration, translating into low systemic exposure (357, 359, 385). For therapeutic applications, targeting antibodies can be conjugated with a vast variety of effector moieties, including radionuclides, cytokines, loaded liposomes, active or pro-drugs, photosensitizers or active proteins such as full IgG or derivatives (386). Of note is the recent development of scFv antibodies directed towards splicing variants of fibronectin, specifically extradomain (ED) A and B, that have been successfully conjugated with effector molecules, retaining the targeting capacities. The L19 clone directed against the EDB was conjugated to IL-2 and TNF displaying potent anti-tumour activity in animal models and are currently in clinical development phase I and II (386-388). Furthermore, conjugation with photosensitizer agents demonstrated selective vascular occlusion as a result of treatment with red light in rodents with subcutaneous tumours (389). The F8 clone directed against the EDA was conjugated with IL-10, showing significant reduction of arthritis in CIA mouse models (347). More recently our group and collaborators demonstrated the successful delivery of IL-4 *in vivo* using a synovium targeting peptide in the xenograft SCID mouse model, and the selective accumulation of an

anti-C5 antibody fused to the same synovium targeting peptide in affected joints of rodent models of arthritis, further confirming the validity of targeted therapy in an arthritic context (136, 390).

The A7 antibody described in this thesis was isolated *in vivo* with the purpose of identifying a scFv antibody with specificity for the microvasculature of human arthritic synovium. Indeed, the scFv A7 and A7 scFv-Fc antibodies proved to specifically target the vasculature in the arthritic synovium without detectable reactivity with normal human tissues or other disease conditions. In this light, the A7 displays all the requirements for a targeted delivery tool applied to rheumatoid and osteoarthritis. This is especially true since one of the key characteristic of a targeting agent is the accessibility of the target antigen when challenged *in vivo*. This feature is intrinsic in the *in vivo* isolation strategy adopted for the phage display screening and further confirmed in *in vivo* recirculation assays performed with the soluble scFv A7 (230). As a proof of concept and evaluate the capacity of A7 to act as a targeting molecule and develop a novel therapeutic agent in the treatment of rheumatoid arthritis, the A7 antibody was combined to the gold standard for anti-TNF therapeutics Adalimumab using a bispecific antibody strategy.

Antibodies are still considered the molecules of choice for targeting applications due to the natural binding properties and established manufacturing processes. In addition, development of antibody screening strategies such as scFv phage display, allows fast isolation of clones of interest that can be readily engineered to introduce specific functions and properties. In this context, the bispecific antibody format combines the binding specificities of two independent antibodies, maintaining the structural and functional characteristics of a natural IgG molecule. As already described in section 1.3.3, bispecific antibodies are acquiring increasing interest from pharmaceutical companies with one FDA approved antibody and many other currently in clinical trials (205). Since a standard asymmetric IgG bispecific antibody combines two independent antibodies, two main issues need to be addressed to ensure optimal antibody production: correct light chain association and correct heavy chain heterodimerisation. Regarding the first aspect, the correct pairing of heavy and light chains for both components is

pivotal to the formation of functional molecules. Use of species restricted heavy-light chain pairing can provide better outcomes but it is not applicable to fully human antibodies (210). Another strategy involves the combination of antibodies with common light chains, overcoming the problem of erroneous pairing but with the shortcoming of not being applicable to pre-existing antibodies and requiring development of ad hoc molecules (391). Alternatively, Roche laboratories developed a platform called CrossMab characterised by CH1-CL domain inversion on one arm, providing a better pairing outcome with reduced non-functional side products (392). For the purpose of this study, the format adopted was the scFv-Fc IgG-like antibody which confers advantages over the conventional IgG structure by overcoming the issues addressed above. Specifically, by using scFv domains, the light and heavy variable regions are linked in order to prevent chain mis-pair and provide only functional antibodies with the desired specificity. In addition, the expression of heavy and light chains in a single peptide circumvents the need to ensure a 1:1 ratio between the expressed heavy and light chain. To address the second issue, the developed bispecific antibody carried the Y407T and T366Y mutations in the CH3 domains, resulting in preferential heavy chain heterodimerisation due to steric instability of the homodimeric counterparts (211). Although this technology was developed in the late 1990's and is not therefore the most innovative strategy, it has the advantage of requiring minimal alteration of the Fc region, maintaining unaltered the Fc effector functions (211). In our hands this method allowed an efficient heterodimerisation of 85% following a simple purification step.

Towards the development of a novel bispecific therapeutic for the treatment of rheumatoid arthritis and as a proof of concept for targeted delivery using A7, the anti-TNF antibody Adalimumab was chosen as the effector moiety to be coupled to A7. Adalimumab is a potent biologic agent in the treatment of rheumatoid arthritis characterised by considerable clinical success (described in section 1.3.2). However, high treatment cost, safety concerns and a high number of non-responder patients, indicate the need of improved therapeutic agents. In this light, the bispecific antibody developed in this work may provide a better safety

profile by reducing systemic exposure, increase pharmacological potency via accumulation of the active molecule at the site of interest and as a consequence reduced administration doses and related costs. A second important aspect considered while choosing Adalimumab resides on the fact that Adalimumab was originally isolated from phage display in scFv format (324). Reports in the literature show that Adalimumab maintains binding and kinetic properties as a scFv when compared to the commercial IgG format (336, 337), providing supporting evidence for the bispecific antibody design described here. The scFv-Fc format of Adalimumab showed TNF binding capacity with similar EC50 values and kinetic properties compared to the original antibody. In addition, the scFv-Fc antibody was biologically active rescuing L-929 cells from TNF induced cytotoxicity with an IC50 value closely comparable to the parent antibody. The bispecific antibody A7/Adalimumab was readily produced by CHO-s cell line and showed both TNF and human arthritic synovium binding specificity. As already mentioned in section 6.4, the bispecific but monovalent nature of the A7/Adalimumab antibody is likely to be the reason for the slightly elevated IC50 compared to the commercial Adalimumab detected in the TNF cytotoxicity assay. It may be argued therefore that the reduced inhibitory efficiency of the bispecific antibody will work against it *in vivo*, possibly resulting in a reduced therapeutic efficacy. However, the synovial homing properties of A7 may provide a gain of function to the molecule and allow the selective accumulation in the site of interest, as has been reported for other synovium homing constructs (136, 390), conferring increased pharmacological activity by reducing the systemic and non-specific distribution.

Bispecific antibodies reveal huge potential for therapeutic applications with an estimated market of 4.4 billion USD to be reached in the next 10 years (393). In this light, the bispecific antibody developed in this project may provide proof of concept for antibody based delivery in arthritic synovium with the final aim of improving available therapeutics by addressing the safety concerns characterising anti-cytokine biologics. The A7/Adalimumab bispecific antibody construct showed unaltered TNF blocking capacity and synovial specificity that may allow reduction in the dosage and/or administration frequency, with the ultimate goal to reduce the

systemic exposure, achieve a better therapeutic index and decreasing health care costs.

7.2 Future directions

Identification and isolation of the target antigen remains a primary goal of the project. Standard proteomic approaches described in this work failed to produce reliable results, despite the presence of A7 reactivity on cell lines detected using immunofluorescent staining. Future work towards this goal can follow two main paths, involving engineering of the A7 antibody and more refined proteomic strategies.

It is possible the affinity of scFv A7 for its target antigen may be the reason for the difficulties encountered in antigen identification. Conversion into an IgG-like format would have provided an increase in functional affinity (i.e. avidity) via formation of a bivalent molecule. However, the increased avidity did not result in a stronger binding to synovial tissues and subsequently did not translate into a more efficient IP. Although structurally similar, scFv-Fc and IgG differ mainly for the absence of the C_L-C_H1 region in the former molecule. This region is necessary for heavy and light chain stability via formation of a disulphide bond (153, 252) but can be efficiently substituted by a short peptide linking the V_L and V_H regions, without altering the Fc effector functions (234). This substitution results in approximately 30 kDa size reduction and shortened arm span. This last aspect may be relevant in the context of antigen binding when high clearance is required to accommodate the antigen. In this context, a native IgG format might provide the necessary flexibility to allow simultaneous binding of both arms and increase binding capacity. scFv conversion in IgG format is a well-established procedure commonly adopted for scFv antibodies to be developed into therapeutic agents (394). Specifically, commercially available vectors can be employed to fuse the V_L and V_H regions to the C_L and C_H1-C_H2-C_H3 domains respectively. This strategy however, will substantially alter the Fv structure and, as performed for the scFv-Fc construct, careful screenings on reactive synovial tissue will be required to confirm preservation of specificity.

As already mentioned in section 7.1.1, the scFv A7 carries two putative N-glycosylation sequences located in the CDR2 and CDR3 regions. Glycosylation in the

variable region is fairly common among natural IgGs, preferentially in the CDR2 region, and can introduce unforeseen variables in the antibody properties, influencing binding capacity and pharmacokinetics (362). Since the scFv antibody was produce in bacterial hosts, the N-glycosylation was initially not incorporated in the molecule but became evident in the scFv-Fc construct expressed in CHO cells, characterised by a higher apparent molecular weight when compared to similar constructs. The expected improved performances of the scFv-Fc format may therefore be partially neutralised by the presence of glycosylation in the site of antigen interaction. In order to assess the influence of the two glycosylation in the binding capacity, the A7 scFv-Fc could be treated enzymatically with PNGase F and compared with the untreated antibody. However, enzymatic treatment is subjected to site accessibility and may result in uneven cleavage. A second potential strategy may be site directed mutagenesis in order to substitute the asparagine residue and disrupt the consensus sequence. The IgG variable domains, especially the CDR regions, are extremely delicate and small changes in the amino acidic sequence can substantially alter binding capacity and antigen specificity. This key aspect is exploited by B cells themselves during affinity maturation in a process defined as somatic hypermutation (395). In this specific case however, the binding to the target antigen needs to be preserved in order to maintain synovial targeting. A possible way of tackling this problem would be to apply conservative mutations to the consensus sequence, removing key amino acids and replacing them with amino acids showing either similar chemical properties or similar steric burden (396). Specifically, the asparagine, present in the NXS/T sequence, is a polar uncharged amino acid in physiological conditions, containing an amine group in the side chain. This amino acid could be substituted with glutamine without altering its chemical properties (396). Glutamine is also a polar uncharged amino acid with an amine group but carries an extra methylene group compared to asparagine. In a less conservative approach, the asparagine could be substituted with the closely related aspartic acid, with the advantage of maintaining a similar side chain size. However, this substitution would introduce a negative charge in the CDR region with potential deleterious effects.

Once identified the target molecule, the antibody could be further optimised via affinity maturation to obtain a reagent with both high affinity and high specificity. In order to do so, the antibody could undergo random mutagenesis using error-prone PCR (397) or look-through mutagenesis in which primers are designed in order to constitute a small library with random substitutions with selected amino acids in the CDR regions (337). The newly created libraries can then be screened using display techniques, such as phage display, ribosome display or yeast surface display, to detect clones with improved binding kinetics (362).

Indeed the observed low affinity may be related to the inefficient IP of scFvA7 and A7 scFv-Fc when tested with protein extracts from reactive cell lines. As introduced in section 7.1.3, chemically cross-linking the antibody to the antigen on the cell surface may preserve the immune-complex and facilitate the isolation of the target antigen from the total protein pool. However, in order to limit the cross-linking to the nearest protein, the sulfo-SBED biotin reagent with a 20 Å range of interaction would guarantee a minimum degree of non-specific cross-linking and provide more robust results (382, 383). The possibility of detaching the antibody using reducing conditions would allow the identification of the interacting protein free from the immune-complex. Alternatively, the cross-linking could be performed on synovial tissue sections, preferably non-fixed frozen sections, in order to adopt the best possible source of target antigen. In this instance, the conjugated antibody could be incubated with the tissue section, similarly to the way in which IHC staining is performed, and cross-linked using UV light. Following efficient cross-linking, the tissue would be scraped from the glass slide and solubilised, obtaining total protein extract and simultaneously releasing the antibody from the target. The presence of biotinylated target antigen could then be detected by Western blot with streptavidin-HRP reagent. Finally, identity of the putative interacting antigen would be identified using mass spectrometry following resolution of protein content in 2D gel electrophoresis and excision of relevant protein spot (398).

Screening of protein expression libraries would provide an alternative route for target antigen identification. Screening of a phage expression library however was not successful and failed to reveal reliable target candidates (described in

section 5.3). The main limitation in such an approach relies on the library used. Indeed, in the absence of a rheumatoid synovial library, the use of a human placental library would increase the chances of identifying the A7 target since it represents the most generic library available and the application has been proven in several studies (399, 400). Screening of protein microarrays could offer a valid alternative, with the advantage of the availability of human synovial arrays. Specifically, a human rheumatoid synovial protein array has been developed at Stanford University in Professor Robinson's laboratory and could be used to identify reacting proteins with A7 antibody (299). This strategy could provide a more disease oriented approach although limited by relatively low protein diversity and a restriction to known antigens.

Finally, in order to evaluate the biological activity of the bispecific A7/Adalimumab antibody in an *in vivo* context, the xenograft SCID mouse model of arthritis could be employed in order to mimic the human arthritic synovial environment (231, 232). Since the scFv A7 antibody failed to demonstrate reactivity in the CIA mouse model, the human synovial milieu in this approach would provide the best chances of demonstrate biological functionality of the A7 antibody. Specifically, the bispecific A7/Adalimumab antibody would be injected via the tail vein in SCID mice bearing human synovial xenograft. Subsequently, the synovial xenografts will be harvested, evaluating the effect on cellularity within the tissue, processed for IHC to detect the presence of antibody and for QT-PCR to analyse gene expression of pro-inflammatory cytokines such as TNFα, IL-1β and IL-6 (73), an approach which has already proved successful in testing the effects of Infliximab (data not published). In parallel, the bispecific E2/Adalimumab and A7 scFv-Fc antibodies could be used as negative control molecules and the original Adalimumab antibody would serve as a positive control, collectively allowing a direct comparison of the *in vivo* biological efficacy of the newly developed bispecific antibody and the gold standard TNF blocker therapeutic.

7.3 Final conclusion

Rheumatoid arthritis is a relatively common disease worldwide with substantial impact on the life of affected people (18). With a 1% incidence rate it also represents a significant market share with growing interest and investment from pharmaceutical companies (137). However, despite the advent of biological agents in the management of rheumatoid arthritis, true treatment-free remission is still difficult to achieve and 20-40% of the patients do not respond to the available therapeutics (138, 139). Furthermore, the biologic agents currently approved are targeting inflammatory cytokines or immune cells, in an attempt to dampen the inflammatory response and limit the damages that occur during chronic inflammation. At the same time however, targeting the downstream effects rather than the leading cause of the disease exposes the patients to higher risk of developing infections, due to the systemic activity of such therapeutic agents. In this light there is therefore the need to develop new compounds with higher potency, broader efficacy and improved safety profiles.

In this thesis the characterisation of a scFv antibody isolated following *in vivo* phage display selection is described. The scFv A7 showed specificity for the human arthritic synovium with no detectable reactivity with normal synovium or other human tissues, suggesting that the target molecule for A7 may have applications as a biomarker and/or immunotherapeutic target in arthritis. The selective arthritic synovium binding capacity confers to the A7 antibody unique properties that can be exploited for the development of diagnostic or therapeutic agents. Towards this end, a novel bispecific antibody combining the anti-TNF properties of Adalimumab and the synovium targeting capacity of A7 was developed, providing proof of concept for antibody based pharmaco-delivery of existing therapeutics in an arthritic context, potentially allowing reduction in the dosage and/or administration frequency, with the ultimate goal of reducing the systemic exposure, achieve better therapeutic index and decreasing related health care costs.

With growing interest from pharmaceutical companies over bispecific antibody constructs (393), mostly deriving from the success obtained in the field of cancer therapy (205), the work presented in this thesis represents an innovative therapeutic development with potential impact in the therapy of rheumatoid arthritis.

References

1. Barland P, Novikoff A, Hamerman D. Electron microscopy of the human synovial membrane. The Journal of cell biology. 1962;14:207-20.
2. Hamerman D, Barland P. Structure and function of the synovial membrane. Bulletin on the rheumatic diseases. 1966;16(5):396-9.
3. Athanasou N. Synovial macrophages. Annals of the Rheumatic Diseases. 1995;54(5):392-4.
4. Demaziere A, Athanasou N. Adhesion receptors of intimal and subintimal cells of the normal synovial membrane. The Journal of pathology. 1992;168(2):209-15.
5. Revell P, al-Saffar N, Fish S, Osei D. Extracellular matrix of the synovial intimal cell layer. Annals of the Rheumatic Diseases. 1995;54(5):404-7.
6. Danen E, Sonneveld P, Brakebusch C, Fassler R, Sonnenberg A. The fibronectin-binding integrins alpha5beta1 and alphavbeta3 differentially modulate RhoA-GTP loading, organization of cell matrix adhesions, and fibronectin fibrillogenesis. The Journal of cell biology. 2002;159(6):1071-86.
7. Mor A, Abramson S, Pillinger M. The fibroblast-like synovial cell in rheumatoid arthritis: a key player in inflammation and joint destruction. Clinical immunology (Orlando, Fla). 2005;115(2):118-28.
8. Buckwalter JA, Mankin HJ, Grodzinsky AJ. Articular cartilage and osteoarthritis. Instr Course Lect. 2005;54:465-80.
9. Vuorio E, de Crombrugghe B. The family of collagen genes. Annual review of biochemistry. 1990;59:837-72.
10. Morales T, Hascall V. Factors involved in the regulation of proteoglycan metabolism in articular cartilage. Arthritis and rheumatism. 1989;32(10):1197-201.
11. Lotz M, Blanco F, von Kempis J, Dudler J, Maier R, Villiger P, et al. Cytokine regulation of chondrocyte functions. The Journal of rheumatology Supplement. 1995;43:104-8.
12. Callahan LF. Awareness of the prevalence and impact of arthritis: the role of health professionals. Arthritis Care Res. 1995 Jun;8(2):63-5.
13. Young A, Koduri G, Batley M, Kulinskaya E, Gough A, Norton S, et al. Mortality in rheumatoid arthritis. Increased in the early course of disease, in ischaemic heart disease and in pulmonary fibrosis. Rheumatology (Oxford). 2007 Feb;46(2):350-7.
14. McInnes I, Schett G. The pathogenesis of rheumatoid arthritis. The New England journal of medicine. 2011;365(2171818d-3eef-0320-e5b8-4896f32b6664):2205-24.
15. Firestein G. Evolving concepts of rheumatoid arthritis. Nature. 2003;423(65ab7ba6-b66b-1522-cd74-4896f3773728):356-417.
16. Gabriel SE, Crowson CS. Risk factors for cardiovascular disease in rheumatoid arthritis. Curr Opin Rheumatol. 2012 Mar;24(2):171-6.
17. Gullick NJ, Scott DL. Co-morbidities in established rheumatoid arthritis. Best Pract Res Clin Rheumatol. 2011 Aug;25(4):469-83.
18. Symmons D, Turner G, Webb R, Asten P, Barrett E, Lunt M, et al. The prevalence of rheumatoid arthritis in the United Kingdom: new estimates for a new century. Rheumatology (Oxford). 2002 Jul;41(7):793-800.
19. Scott D, Wolfe F, Huizinga T. Rheumatoid arthritis. Lancet. 2010;376(9746):1094-108.
20. Rat AC, Boissier MC. Rheumatoid arthritis: direct and indirect costs. Joint Bone Spine. 2004 Nov;71(6):518-24.
21. Kavanaugh A. Economic consequences of established rheumatoid arthritis and its treatment. Best Pract Res Clin Rheumatol. 2007 Oct;21(5):929-42.

22. Cooper NJ. Economic burden of rheumatoid arthritis: a systematic review. Rheumatology (Oxford). 2000 Jan;39(1):28-33.
23. Aletaha D, Neogi T, Silman A, Funovits J, Felson D, Bingham C, et al. 2010 Rheumatoid arthritis classification criteria: an American College of Rheumatology/European League Against Rheumatism collaborative initiative. Arthritis and rheumatism. 2010;62(1cec97b1-9f23-afc7-2694-4896f1dab0de):2569-650.
24. Berglin E, Dahlqvist S. Comparison of the 1987 ACR and 2010 ACR/EULAR classification criteria for rheumatoid arthritis in clinical practice: a prospective cohort study. Scand J Rheumatol. 2013 Apr 23.
25. MacGregor AJ, Snieder H, Rigby AS, Koskenvuo M, Kaprio J, Aho K, et al. Characterizing the quantitative genetic contribution to rheumatoid arthritis using data from twins. Arthritis Rheum. 2000 Jan;43(1):30-7.
26. Silman AJ, MacGregor AJ, Thomson W, Holligan S, Carthy D, Farhan A, et al. Twin concordance rates for rheumatoid arthritis: results from a nationwide study. Br J Rheumatol. 1993 Oct;32(10):903-7.
27. Newton J, Harney S, Wordsworth B, Brown M. A review of the MHC genetics of rheumatoid arthritis. Genes and immunity. 2004;5(3):151-7.
28. Bowes J, Barton A. Recent advances in the genetics of RA susceptibility. Rheumatology (Oxford, England). 2008;47(4):399-402.
29. Gregersen P, Silver J, Winchester R. The shared epitope hypothesis. An approach to understanding the molecular genetics of susceptibility to rheumatoid arthritis. Arthritis and rheumatism. 1987;30(11):1205-13.
30. Boissier M-C, Semerano L, Challal S, Saidenberg-Kermanac'h N, Falgarone G. Rheumatoid arthritis: from autoimmunity to synovitis and joint destruction. Journal of autoimmunity. 2012;39(3):222-8.
31. Ling S, Pi X, Holoshitz J. The rheumatoid arthritis shared epitope triggers innate immune signaling via cell surface calreticulin. Journal of immunology (Baltimore, Md : 1950). 2007;179(9):6359-67.
32. De Almeida D, Ling S, Pi X, Hartmann-Scruggs A, Pumpens P, Holoshitz J. Immune dysregulation by the rheumatoid arthritis shared epitope. Journal of immunology (Baltimore, Md : 1950). 2010;185(3):1927-34.
33. Hill RJ, Zozulya S, Lu YL, Ward K, Gishizky M, Jallal B. The lymphoid protein tyrosine phosphatase Lyp interacts with the adaptor molecule Grb2 and functions as a negative regulator of T-cell activation. Exp Hematol. 2002 Mar;30(3):237-44.
34. Rieck M, Arechiga A, Onengut-Gumuscu S, Greenbaum C, Concannon P, Buckner JH. Genetic variation in PTPN22 corresponds to altered function of T and B lymphocytes. J Immunol. 2007 Oct 1;179(7):4704-10.
35. Hameed K, Gibson T. A comparison of the prevalence of rheumatoid arthritis and other rheumatic diseases amongst Pakistanis living in England and Pakistan. Br J Rheumatol. 1997 Jul;36(7):781-5.
36. Costenbader KH, Feskanich D, Mandl LA, Karlson EW. Smoking intensity, duration, and cessation, and the risk of rheumatoid arthritis in women. Am J Med. 2006 Jun;119(6):503 e1-9.
37. Makrygiannakis D, Hermansson M, Ulfgren AK, Nicholas AP, Zendman AJ, Eklund A, et al. Smoking increases peptidylarginine deiminase 2 enzyme expression in human lungs and increases citrullination in BAL cells. Ann Rheum Dis. 2008 Oct;67(10):1488-92.
38. Kallberg H, Jacobsen S, Bengtsson C, Pedersen M, Padyukov L, Garred P, et al. Alcohol consumption is associated with decreased risk of rheumatoid arthritis:

results from two Scandinavian case-control studies. Ann Rheum Dis. 2009 Feb;68(2):222-7.
39. Maxwell JR, Gowers IR, Moore DJ, Wilson AG. Alcohol consumption is inversely associated with risk and severity of rheumatoid arthritis. Rheumatology (Oxford). 2010 Nov;49(11):2140-6.
40. Fujinami RS, Oldstone MB, Wroblewska Z, Frankel ME, Koprowski H. Molecular mimicry in virus infection: crossreaction of measles virus phosphoprotein or of herpes simplex virus protein with human intermediate filaments. Proc Natl Acad Sci U S A. 1983 Apr;80(8):2346-50.
41. Ercolini A, Miller S. Molecular mimics can induce novel self peptide-reactive CD4+ T cell clonotypes in autoimmune disease. Journal of immunology (Baltimore, Md : 1950). 2007;179(10):6604-12.
42. Graham JP, Arcipowski KM, Bishop GA. Differential B-lymphocyte regulation by CD40 and its viral mimic, latent membrane protein 1. Immunol Rev. 2010 Sep;237(1):226-48.
43. Mancao C, Hammerschmidt W. Epstein-Barr virus latent membrane protein 2A is a B-cell receptor mimic and essential for B-cell survival. Blood. 2007 Nov 15;110(10):3715-21.
44. Gravallese EM, Goldring SR. Cellular mechanisms and the role of cytokines in bone erosions in rheumatoid arthritis. Arthritis Rheum. 2000 Oct;43(10):2143-51.
45. Rantapää-Dahlqvist S, de Jong B, Berglin E, Hallmans G, Wadell G, Stenlund H, et al. Antibodies against cyclic citrullinated peptide and IgA rheumatoid factor predict the development of rheumatoid arthritis. Arthritis and rheumatism. 2003;48(10):2741-9.
46. Jansen LM, van Schaardenburg D, van der Horst-Bruinsma I, van der Stadt RJ, de Koning MH, Dijkmans BA. The predictive value of anti-cyclic citrullinated peptide antibodies in early arthritis. J Rheumatol. 2003 Aug;30(8):1691-5.
47. Takemura S, Braun A, Crowson C, Kurtin PJ, Cofield RH, O'Fallon WM, et al. Lymphoid neogenesis in rheumatoid synovitis. J Immunol. 2001 Jul 15;167(2):1072-80.
48. Manzo A, Bombardieri M, Humby F, Pitzalis C. Secondary and ectopic lymphoid tissue responses in rheumatoid arthritis: from inflammation to autoimmunity and tissue damage/remodeling. Immunological reviews. 2010;233(e54c30a6-c084-5293-b73c-4896f1d911fb):267-352.
49. Strand V, Kimberly R, Isaacs JD. Biologic therapies in rheumatology: lessons learned, future directions. Nat Rev Drug Discov. 2007 Jan;6(1):75-92.
50. Pitzalis C, Kelly S, Humby F. New learnings on the pathophysiology of RA from synovial biopsies. Current opinion in rheumatology. 2013;25(3):334-44.
51. Melnyk VO, Shipley GD, Sternfeld MD, Sherman L, Rosenbaum JT. Synoviocytes synthesize, bind, and respond to basic fibroblast growth factor. Arthritis Rheum. 1990 Apr;33(4):493-500.
52. Allen JB, Manthey CL, Hand AR, Ohura K, Ellingsworth L, Wahl SM. Rapid onset synovial inflammation and hyperplasia induced by transforming growth factor beta. J Exp Med. 1990 Jan 1;171(1):231-47.
53. Firestein GS, Echeverri F, Yeo M, Zvaifler NJ, Green DR. Somatic mutations in the p53 tumor suppressor gene in rheumatoid arthritis synovium. Proc Natl Acad Sci U S A. 1997 Sep 30;94(20):10895-900.
54. Perlman H, Georganas C, Pagliari LJ, Koch AE, Haines K, 3rd, Pope RM. Bcl-2 expression in synovial fibroblasts is essential for maintaining mitochondrial homeostasis and cell viability. J Immunol. 2000 May 15;164(10):5227-35.

55. Perlman H, Pagliari LJ, Volin MV. Regulation of apoptosis and cell cycle activity in rheumatoid arthritis. Curr Mol Med. 2001 Nov;1(5):597-608.
56. Bartok B, Firestein G. Fibroblast-like synoviocytes: key effector cells in rheumatoid arthritis. Immunological reviews. 2010;233(31ee0c85-ab37-c46b-090d-4896f4611005):233-88.
57. Lin J, Zhou Z, Huo R, Xiao L, Ouyang G, Wang L, et al. Cyr61 induces IL-6 production by fibroblast-like synoviocytes promoting Th17 differentiation in rheumatoid arthritis. J Immunol. 2012 Jun 1;188(11):5776-84.
58. Bombardieri M, Kam NW, Brentano F, Choi K, Filer A, Kyburz D, et al. A BAFF/APRIL-dependent TLR3-stimulated pathway enhances the capacity of rheumatoid synovial fibroblasts to induce AID expression and Ig class-switching in B cells. Ann Rheum Dis. 2011 Jul 27.
59. Cope A, Ettinger R, McDevitt H. The role of TNF alpha and related cytokines in the development and function of the autoreactive T-cell repertoire. Res Immunol. 1997 Jun;148(5):307-12.
60. Cope AP, Londei M, Chu NR, Cohen SB, Elliott MJ, Brennan FM, et al. Chronic exposure to tumor necrosis factor (TNF) in vitro impairs the activation of T cells through the T cell receptor/CD3 complex; reversal in vivo by anti-TNF antibodies in patients with rheumatoid arthritis. J Clin Invest. 1994 Aug;94(2):749-60.
61. Isomaki P, Panesar M, Annenkov A, Clark JM, Foxwell BM, Chernajovsky Y, et al. Prolonged exposure of T cells to TNF down-regulates TCR zeta and expression of the TCR/CD3 complex at the cell surface. J Immunol. 2001 May 1;166(9):5495-507.
62. Zhang Z, Gorman CL, Vermi AC, Monaco C, Foey A, Owen S, et al. TCRzetadim lymphocytes define populations of circulating effector cells that migrate to inflamed tissues. Blood. 2007 May 15;109(10):4328-35.
63. Manoury-Schwartz B, Chiocchia G, Bessis N, Abehsira-Amar O, Batteux F, Muller S, et al. High susceptibility to collagen-induced arthritis in mice lacking IFN-gamma receptors. J Immunol. 1997 Jun 1;158(11):5501-6.
64. Nakae S, Nambu A, Sudo K, Iwakura Y. Suppression of immune induction of collagen-induced arthritis in IL-17-deficient mice. J Immunol. 2003 Dec 1;171(11):6173-7.
65. Lubberts E, Koenders MI, Oppers-Walgreen B, van den Bersselaar L, Coenen-de Roo CJ, Joosten LA, et al. Treatment with a neutralizing anti-murine interleukin-17 antibody after the onset of collagen-induced arthritis reduces joint inflammation, cartilage destruction, and bone erosion. Arthritis Rheum. 2004 Feb;50(2):650-9.
66. Baecher-Allan C, Brown JA, Freeman GJ, Hafler DA. CD4+CD25high regulatory cells in human peripheral blood. J Immunol. 2001 Aug 1;167(3):1245-53.
67. Taams LS, van Amelsfort JM, Tiemessen MM, Jacobs KM, de Jong EC, Akbar AN, et al. Modulation of monocyte/macrophage function by human CD4+CD25+ regulatory T cells. Hum Immunol. 2005 Mar;66(3):222-30.
68. Zhao DM, Thornton AM, DiPaolo RJ, Shevach EM. Activated CD4+CD25+ T cells selectively kill B lymphocytes. Blood. 2006 May 15;107(10):3925-32.
69. Misra N, Bayry J, Lacroix-Desmazes S, Kazatchkine MD, Kaveri SV. Cutting edge: human CD4+CD25+ T cells restrain the maturation and antigen-presenting function of dendritic cells. J Immunol. 2004 Apr 15;172(8):4676-80.
70. van Amelsfort JM, Jacobs KM, Bijlsma JW, Lafeber FP, Taams LS. CD4(+)CD25(+) regulatory T cells in rheumatoid arthritis: differences in the presence, phenotype, and function between peripheral blood and synovial fluid. Arthritis Rheum. 2004 Sep;50(9):2775-85.

71. Flores-Borja F, Jury EC, Mauri C, Ehrenstein MR. Defects in CTLA-4 are associated with abnormal regulatory T cell function in rheumatoid arthritis. Proc Natl Acad Sci U S A. 2008 Dec 9;105(49):19396-401.
72. Pasare C, Medzhitov R. Toll pathway-dependent blockade of CD4+CD25+ T cell-mediated suppression by dendritic cells. Science. 2003 Feb 14;299(5609):1033-6.
73. Humby F, Bombardieri M, Manzo A, Kelly S, Blades M, Kirkham B, et al. Ectopic lymphoid structures support ongoing production of class-switched autoantibodies in rheumatoid synovium. PLoS medicine. 2009;6(5be2e776-5191-2579-843d-4896f45d2f6e).
74. Cornish AL, Campbell IK, McKenzie BS, Chatfield S, Wicks IP. G-CSF and GM-CSF as therapeutic targets in rheumatoid arthritis. Nat Rev Rheumatol. 2009 Oct;5(10):554-9.
75. Haringman JJ, Gerlag DM, Zwinderman AH, Smeets TJ, Kraan MC, Baeten D, et al. Synovial tissue macrophages: a sensitive biomarker for response to treatment in patients with rheumatoid arthritis. Ann Rheum Dis. 2005 Jun;64(6):834-8.
76. Cascao R, Rosario HS, Souto-Carneiro MM, Fonseca JE. Neutrophils in rheumatoid arthritis: More than simple final effectors. Autoimmun Rev. 2010 Jun;9(8):531-5.
77. Arden N, Nevitt MC. Osteoarthritis: epidemiology. Best Pract Res Clin Rheumatol. 2006 Feb;20(1):3-25.
78. Grotle M, Hagen KB, Natvig B, Dahl FA, Kvien TK. Obesity and osteoarthritis in knee, hip and/or hand: an epidemiological study in the general population with 10 years follow-up. BMC Musculoskelet Disord. 2008;9:132.
79. Arden N, Leyland K. Osteoarthritis year 2013 in review: Clinical. Osteoarthritis and cartilage / OARS, Osteoarthritis Research Society. 2013.
80. Haynes MK, Hume EL, Smith JB. Phenotypic characterization of inflammatory cells from osteoarthritic synovium and synovial fluids. Clin Immunol. 2002 Dec;105(3):315-25.
81. Benito M, Veale D, FitzGerald O, van den Berg W, Bresnihan B. Synovial tissue inflammation in early and late osteoarthritis. Annals of the Rheumatic Diseases. 2005;64(9):1263-7.
82. Tetlow LC, Adlam DJ, Woolley DE. Matrix metalloproteinase and proinflammatory cytokine production by chondrocytes of human osteoarthritic cartilage: associations with degenerative changes. Arthritis Rheum. 2001 Mar;44(3):585-94.
83. Fan Z, Bau B, Yang H, Soeder S, Aigner T. Freshly isolated osteoarthritic chondrocytes are catabolically more active than normal chondrocytes, but less responsive to catabolic stimulation with interleukin-1beta. Arthritis Rheum. 2005 Jan;52(1):136-43.
84. Nietfeld JJ, Wilbrink B, Helle M, van Roy JL, den Otter W, Swaak AJ, et al. Interleukin-1-induced interleukin-6 is required for the inhibition of proteoglycan synthesis by interleukin-1 in human articular cartilage. Arthritis Rheum. 1990 Nov;33(11):1695-701.
85. Chadjichristos C, Ghayor C, Kypriotou M, Martin G, Renard E, Ala-Kokko L, et al. Sp1 and Sp3 transcription factors mediate interleukin-1 beta down-regulation of human type II collagen gene expression in articular chondrocytes. J Biol Chem. 2003 Oct 10;278(41):39762-72.
86. Haseeb A, Haqqi T. Immunopathogenesis of osteoarthritis. Clinical immunology (Orlando, Fla). 2013;146(3):185-96.
87. Ishii H, Tanaka H, Katoh K, Nakamura H, Nagashima M, Yoshino S. Characterization of infiltrating T cells and Th1/Th2-type cytokines in the synovium of patients with osteoarthritis. Osteoarthritis and cartilage / OARS, Osteoarthritis Research Society. 2002;10(4):277-81.

88. Sakkas L, Platsoucas C. The role of T cells in the pathogenesis of osteoarthritis. Arthritis and rheumatism. 2007;56(2):409-24.
89. Xiang Y, Sekine T, Nakamura H, Imajoh-Ohmi S, Fukuda H, Nishioka K, et al. Proteomic surveillance of autoimmunity in osteoarthritis: identification of triosephosphate isomerase as an autoantigen in patients with osteoarthritis. Arthritis Rheum. 2004 May;50(5):1511-21.
90. Hu CJ, Wang LY, Chodosh LA, Keith B, Simon MC. Differential roles of hypoxia-inducible factor 1alpha (HIF-1alpha) and HIF-2alpha in hypoxic gene regulation. Mol Cell Biol. 2003 Dec;23(24):9361-74.
91. Folkman J, Klagsbrun M. Angiogenic factors. Science (New York, NY). 1987;235(4787):442-7.
92. Gerhardt H, Golding M, Fruttiger M, Ruhrberg C, Lundkvist A, Abramsson A, et al. VEGF guides angiogenic sprouting utilizing endothelial tip cell filopodia. J Cell Biol. 2003 Jun 23;161(6):1163-77.
93. Bergers G, Song S. The role of pericytes in blood-vessel formation and maintenance. Neuro-oncology. 2005;7(04d1fa1e-e152-bf76-32c4-4896f1ee0112):452-516.
94. Hellstrom M, Kalen M, Lindahl P, Abramsson A, Betsholtz C. Role of PDGF-B and PDGFR-beta in recruitment of vascular smooth muscle cells and pericytes during embryonic blood vessel formation in the mouse. Development. 1999 Jun;126(14):3047-55.
95. Sims D. Diversity within pericytes. Clinical and experimental pharmacology & physiology. 2000;27(a8401d48-ef3a-180d-60af-4896f475608d):842-8.
96. Rucker HK, Wynder HJ, Thomas WE. Cellular mechanisms of CNS pericytes. Brain Res Bull. 2000 Mar 15;51(5):363-9.
97. Hayashi K, Nakao S, Nakaoke R, Nakagawa S, Kitagawa N, Niwa M. Effects of hypoxia on endothelial/pericytic co-culture model of the blood-brain barrier. Regul Pept. 2004 Dec 15;123(1-3):77-83.
98. Betsholtz C. Insight into the physiological functions of PDGF through genetic studies in mice. Cytokine Growth Factor Rev. 2004 Aug;15(4):215-28.
99. Sivakumar B, Akhavani MA, Winlove CP, Taylor PC, Paleolog EM, Kang N. Synovial hypoxia as a cause of tendon rupture in rheumatoid arthritis. J Hand Surg Am. 2008 Jan;33(1):49-58.
100. Giatromanolaki A, Sivridis E, Maltezos E, Athanassou N, Papazoglou D, Gatter KC, et al. Upregulated hypoxia inducible factor-1alpha and -2alpha pathway in rheumatoid arthritis and osteoarthritis. Arthritis Res Ther. 2003;5(4):R193-201.
101. Koch AE, Harlow LA, Haines GK, Amento EP, Unemori EN, Wong WL, et al. Vascular endothelial growth factor. A cytokine modulating endothelial function in rheumatoid arthritis. J Immunol. 1994 Apr 15;152(8):4149-56.
102. Hitchon C, Wong K, Ma G, Reed J, Lyttle D, El-Gabalawy H. Hypoxia-induced production of stromal cell-derived factor 1 (CXCL12) and vascular endothelial growth factor by synovial fibroblasts. Arthritis Rheum. 2002 Oct;46(10):2587-97.
103. Ahn JK, Koh EM, Cha HS, Lee YS, Kim J, Bae EK, et al. Role of hypoxia-inducible factor-1alpha in hypoxia-induced expressions of IL-8, MMP-1 and MMP-3 in rheumatoid fibroblast-like synoviocytes. Rheumatology (Oxford). 2008 Jun;47(6):834-9.
104. Westra J, Brouwer E, Bos R, Posthumus MD, Doornbos-van der Meer B, Kallenberg CG, et al. Regulation of cytokine-induced HIF-1alpha expression in rheumatoid synovial fibroblasts. Ann N Y Acad Sci. 2007 Jun;1108:340-8.

105. Konisti S, Kiriakidis S, Paleolog E. Hypoxia--a key regulator of angiogenesis and inflammation in rheumatoid arthritis. Nature reviews Rheumatology. 2012;8(3):153-62.
106. Proudfoot AE, Handel TM, Johnson Z, Lau EK, LiWang P, Clark-Lewis I, et al. Glycosaminoglycan binding and oligomerization are essential for the in vivo activity of certain chemokines. Proc Natl Acad Sci U S A. 2003 Feb 18;100(4):1885-90.
107. Butcher EC, Picker LJ. Lymphocyte homing and homeostasis. Science. 1996 Apr 5;272(5258):60-6.
108. del Pozo MA, Cabanas C, Montoya MC, Ager A, Sanchez-Mateos P, Sanchez-Madrid F. ICAMs redistributed by chemokines to cellular uropods as a mechanism for recruitment of T lymphocytes. J Cell Biol. 1997 Apr 21;137(2):493-508.
109. Allport JR, Ding H, Collins T, Gerritsen ME, Luscinskas FW. Endothelial-dependent mechanisms regulate leukocyte transmigration: a process involving the proteasome and disruption of the vascular endothelial-cadherin complex at endothelial cell-to-cell junctions. J Exp Med. 1997 Aug 18;186(4):517-27.
110. Engelhardt B, Wolburg H. Mini-review: Transendothelial migration of leukocytes: through the front door or around the side of the house? Eur J Immunol. 2004 Nov;34(11):2955-63.
111. Tak PP, Thurkow EW, Daha MR, Kluin PM, Smeets TJ, Meinders AE, et al. Expression of adhesion molecules in early rheumatoid synovial tissue. Clin Immunol Immunopathol. 1995 Dec;77(3):236-42.
112. Koch AE, Burrows JC, Haines GK, Carlos TM, Harlan JM, Leibovich SJ. Immunolocalization of endothelial and leukocyte adhesion molecules in human rheumatoid and osteoarthritic synovial tissues. Lab Invest. 1991 Mar;64(3):313-20.
113. Szekanecz Z, Besenyei T, Paragh G, Koch A. Angiogenesis in rheumatoid arthritis. Autoimmunity. 2009;42(7):563-73.
114. Storgard C, Stupack D, Jonczyk A, Goodman S, Fox R, Cheresh D. Decreased angiogenesis and arthritic disease in rabbits treated with an alphavbeta3 antagonist. The Journal of clinical investigation. 1999;103(29f3463e-cac1-8cb9-06ff-4896f42617d9):47-101.
115. Nanki T, Hayashida K, El-Gabalawy HS, Suson S, Shi K, Girschick HJ, et al. Stromal cell-derived factor-1-CXC chemokine receptor 4 interactions play a central role in CD4+ T cell accumulation in rheumatoid arthritis synovium. J Immunol. 2000 Dec 1;165(11):6590-8.
116. Pablos JL, Santiago B, Galindo M, Torres C, Brehmer MT, Blanco FJ, et al. Synoviocyte-derived CXCL12 is displayed on endothelium and induces angiogenesis in rheumatoid arthritis. J Immunol. 2003 Feb 15;170(4):2147-52.
117. Shi K, Hayashida K, Kaneko M, Hashimoto J, Tomita T, Lipsky PE, et al. Lymphoid chemokine B cell-attracting chemokine-1 (CXCL13) is expressed in germinal center of ectopic lymphoid follicles within the synovium of chronic arthritis patients. J Immunol. 2001 Jan 1;166(1):650-5.
118. Szekanecz Z, Koch AE. Vascular involvement in rheumatic diseases: 'vascular rheumatology'. Arthritis Res Ther. 2008;10(5):224.
119. Bono MR, Elgueta R, Sauma D, Pino K, Osorio F, Michea P, et al. The essential role of chemokines in the selective regulation of lymphocyte homing. Cytokine Growth Factor Rev. 2007 Feb-Apr;18(1-2):33-43.
120. Garrood T, Lee L, Pitzalis C. Molecular mechanisms of cell recruitment to inflammatory sites: general and tissue-specific pathways. Rheumatology (Oxford). 2006 Mar;45(3):250-60.
121. Rosen SD. Ligands for L-selectin: homing, inflammation, and beyond. Annu Rev Immunol. 2004;22:129-56.

122. Arbones ML, Ord DC, Ley K, Ratech H, Maynard-Curry C, Otten G, et al. Lymphocyte homing and leukocyte rolling and migration are impaired in L-selectin-deficient mice. Immunity. 1994 Jul;1(4):247-60.
123. Campbell JJ, Murphy KE, Kunkel EJ, Brightling CE, Soler D, Shen Z, et al. CCR7 expression and memory T cell diversity in humans. J Immunol. 2001 Jan 15;166(2):877-84.
124. Berlin C, Berg EL, Briskin MJ, Andrew DP, Kilshaw PJ, Holzmann B, et al. Alpha 4 beta 7 integrin mediates lymphocyte binding to the mucosal vascular addressin MAdCAM-1. Cell. 1993 Jul 16;74(1):185-95.
125. Hamann A, Andrew DP, Jablonski-Westrich D, Holzmann B, Butcher EC. Role of alpha 4-integrins in lymphocyte homing to mucosal tissues in vivo. J Immunol. 1994 Apr 1;152(7):3282-93.
126. Miles A, Liaskou E, Eksteen B, Lalor PF, Adams DH. CCL25 and CCL28 promote alpha4 beta7-integrin-dependent adhesion of lymphocytes to MAdCAM-1 under shear flow. Am J Physiol Gastrointest Liver Physiol. 2008 May;294(5):G1257-67.
127. Campbell JJ, Haraldsen G, Pan J, Rottman J, Qin S, Ponath P, et al. The chemokine receptor CCR4 in vascular recognition by cutaneous but not intestinal memory T cells. Nature. 1999 Aug 19;400(6746):776-80.
128. Berg EL, Yoshino T, Rott LS, Robinson MK, Warnock RA, Kishimoto TK, et al. The cutaneous lymphocyte antigen is a skin lymphocyte homing receptor for the vascular lectin endothelial cell-leukocyte adhesion molecule 1. J Exp Med. 1991 Dec 1;174(6):1461-6.
129. Picker LJ, Michie SA, Rott LS, Butcher EC. A unique phenotype of skin-associated lymphocytes in humans. Preferential expression of the HECA-452 epitope by benign and malignant T cells at cutaneous sites. Am J Pathol. 1990 May;136(5):1053-68.
130. Rajotte D, Arap W, Hagedorn M, Koivunen E, Pasqualini R, Ruoslahti E. Molecular heterogeneity of the vascular endothelium revealed by in vivo phage display. J Clin Invest. 1998 Jul 15;102(2):430-7.
131. Arap W, Kolonin M, Trepel M, Lahdenranta J, Cardó-Vila M, Giordano R, et al. Steps toward mapping the human vasculature by phage display. Nature medicine. 2002;8(2):121-7.
132. Lee L, Buckley C, Blades M, Panayi G, George A, Pitzalis C. Identification of synovium-specific homing peptides by in vivo phage display selection. Arthritis and rheumatism. 2002;46(156ac775-2c8c-a8a2-b795-4896f4a38406):2109-29.
133. Arap W, Haedicke W, Bernasconi M, Kain R, Rajotte D, Krajewski S, et al. Targeting the prostate for destruction through a vascular address. Proceedings of the National Academy of Sciences of the United States of America. 2002;99(98fbbfc0-752f-2d1e-e137-4896f3439a6e):1527-58.
134. Arap W, Pasqualini R, Ruoslahti E. Cancer treatment by targeted drug delivery to tumor vasculature in a mouse model. Science. 1998 Jan 16;279(5349):377-80.
135. Ruoslahti E. Targeting tumor vasculature with homing peptides from phage display. Semin Cancer Biol. 2000 Dec;10(6):435-42.
136. Wythe S, Dicara D, Taher T, Finucane C, Jones R, Bombardieri M, et al. Targeted delivery of cytokine therapy to rheumatoid tissue by a synovial targeting peptide. Annals of the rheumatic diseases. 2012(7f361865-2b46-2910-b0b0-4396cfbd1943).
137. GBI. Monoclonal Antibodies Market in Rheumatoid Arthritis to 2018 - Market Characterized by Large and Diversified Pipeline and Low Threat of Biosimilar Sales Erosion: GBI Research2013 Contract No.: GBIHC273MR.
138. van der Woude D, Young A, Jayakumar K, Mertens BJ, Toes RE, van der Heijde D, et al. Prevalence of and predictive factors for sustained disease-modifying

antirheumatic drug-free remission in rheumatoid arthritis: results from two large early arthritis cohorts. Arthritis Rheum. 2009 Aug;60(8):2262-71.
139. Taylor PC, Feldmann M. Anti-TNF biologic agents: still the therapy of choice for rheumatoid arthritis. Nat Rev Rheumatol. 2009 Oct;5(10):578-82.
140. Kremer JM. Rational use of new and existing disease-modifying agents in rheumatoid arthritis. Ann Intern Med. 2001 Apr 17;134(8):695-706.
141. Fransen J, van Riel PL. The Disease Activity Score and the EULAR response criteria. Clin Exp Rheumatol. 2005 Sep-Oct;23(5 Suppl 39):S93-9.
142. Ranganath V, Khanna D, Paulus H. ACR remission criteria and response criteria. Clinical and experimental rheumatology. 2006;24(6 Suppl 43).
143. van Vollenhoven RF. Treatment of rheumatoid arthritis: state of the art 2009. Nat Rev Rheumatol. 2009 Oct;5(10):531-41.
144. Lee D, Weinblatt M. Rheumatoid arthritis. Lancet. 2001;358(9285):903-11.
145. Cherwinski HM, Cohn RG, Cheung P, Webster DJ, Xu YZ, Caulfield JP, et al. The immunosuppressant leflunomide inhibits lymphocyte proliferation by inhibiting pyrimidine biosynthesis. J Pharmacol Exp Ther. 1995 Nov;275(2):1043-9.
146. Osiri M, Shea B, Robinson V, Suarez-Almazor M, Strand V, Tugwell P, et al. Leflunomide for treating rheumatoid arthritis. Cochrane Database Syst Rev. 2003(1):CD002047.
147. Donahue K, Gartlehner G, Jonas… D. Systematic review: comparative effectiveness and harms of disease-modifying medications for rheumatoid arthritis. Annals of Internal …. 2008(1a2d0ba9-cc14-2f67-33f5-4896f425c79e).
148. Smolen JS, Kalden JR, Scott DL, Rozman B, Kvien TK, Larsen A, et al. Efficacy and safety of leflunomide compared with placebo and sulphasalazine in active rheumatoid arthritis: a double-blind, randomised, multicentre trial. European Leflunomide Study Group. Lancet. 1999 Jan 23;353(9149):259-66.
149. O'Dell JR, Leff R, Paulsen G, Haire C, Mallek J, Eckhoff PJ, et al. Treatment of rheumatoid arthritis with methotrexate and hydroxychloroquine, methotrexate and sulfasalazine, or a combination of the three medications: results of a two-year, randomized, double-blind, placebo-controlled trial. Arthritis Rheum. 2002 May;46(5):1164-70.
150. O'Dell JR, Haire CE, Erikson N, Drymalski W, Palmer W, Eckhoff PJ, et al. Treatment of rheumatoid arthritis with methotrexate alone, sulfasalazine and hydroxychloroquine, or a combination of all three medications. N Engl J Med. 1996 May 16;334(20):1287-91.
151. Köhler G, Milstein C. Continuous cultures of fused cells secreting antibody of predefined specificity. 1975. Journal of immunology (Baltimore, Md : 1950). 1975;174(5):2453-5.
152. Hansel TT, Kropshofer H, Singer T, Mitchell JA, George AJ. The safety and side effects of monoclonal antibodies. Nat Rev Drug Discov. 2010 Apr;9(4):325-38.
153. Liu H, May K. Disulfide bond structures of IgG molecules: structural variations, chemical modifications and possible impacts to stability and biological function. MAbs. 2012 Jan-Feb;4(1):17-23.
154. Dayer JM, Beutler B, Cerami A. Cachectin/tumor necrosis factor stimulates collagenase and prostaglandin E2 production by human synovial cells and dermal fibroblasts. J Exp Med. 1985 Dec 1;162(6):2163-8.
155. Bertolini DR, Nedwin GE, Bringman TS, Smith DD, Mundy GR. Stimulation of bone resorption and inhibition of bone formation in vitro by human tumour necrosis factors. Nature. 1986 Feb 6-12;319(6053):516-8.
156. Butler DM, Maini RN, Feldmann M, Brennan FM. Modulation of proinflammatory cytokine release in rheumatoid synovial membrane cell cultures. Comparison of

monoclonal anti TNF-alpha antibody with the interleukin-1 receptor antagonist. Eur Cytokine Netw. 1995 Jul-Dec;6(4):225-30.
157. Keffer J, Probert L, Cazlaris H, Georgopoulos S, Kaslaris E, Kioussis D, et al. Transgenic mice expressing human tumour necrosis factor: a predictive genetic model of arthritis. EMBO J. 1991 Dec;10(13):4025-31.
158. Williams RO, Feldmann M, Maini RN. Anti-tumor necrosis factor ameliorates joint disease in murine collagen-induced arthritis. Proc Natl Acad Sci U S A. 1992 Oct 15;89(20):9784-8.
159. Rigby W. Drug insight: different mechanisms of action of tumor necrosis factor antagonists-passive-aggressive behavior? Nature clinical practice Rheumatology. 2007;3(bd5bd7db-176b-770d-e27b-4896f1f10de0):227-60.
160. Grell M, Douni E, Wajant H, Lohden M, Clauss M, Maxeiner B, et al. The transmembrane form of tumor necrosis factor is the prime activating ligand of the 80 kDa tumor necrosis factor receptor. Cell. 1995 Dec 1;83(5):793-802.
161. Kontoyiannis D, Pasparakis M, Pizarro TT, Cominelli F, Kollias G. Impaired on/off regulation of TNF biosynthesis in mice lacking TNF AU-rich elements: implications for joint and gut-associated immunopathologies. Immunity. 1999 Mar;10(3):387-98.
162. O'Donnell M, Ting A. Chronicles of a death foretold: dual sequential cell death checkpoints in TNF signaling. Cell cycle (Georgetown, Tex). 2010;9(6):1065-71.
163. Peppel K, Crawford D, Beutler B. A tumor necrosis factor (TNF) receptor-IgG heavy chain chimeric protein as a bivalent antagonist of TNF activity. The Journal of experimental medicine. 1991;174(6):1483-9.
164. Knight D, Trinh H, Le J, Siegel S, Shealy D, McDonough M, et al. Construction and initial characterization of a mouse-human chimeric anti-TNF antibody. Molecular immunology. 1993;30(16):1443-53.
165. Salfeld; Jochen G. (North Grafton M, Allen; Deborah J. (London, GB), Hoogenboom; Hendricus R. J. M. (Hasselt, BE), Kaymakcalan; Zehra (Westboro, MA), Labkovsky; Boris (Framingham, MA), Mankovich; John A. (Andover, MA), McGuinness; Brian T. (Hauxton, GB), Roberts; Andrew J. (Cambridge, GB), Sakorafas; Paul (Shrewsbury, MA), Schoenhaut; David (Clifton, NJ), Vaughan; Tristan J. (Impington, GB), White; Michael (Framingham, MA), Wilton; Alison J. (Cambridge, GB), inventor BASF Aktiengesellschaft (DE), assignee. Human antibodies that bind human TNF.alpha. United States patent 6090382. 1996.
166. Sohini M, David G. Golimumab. MAbs. 2009;1.
167. Niti G, Sue S. Certolizumab Pegol. MAbs. 2010;2.
168. Geborek P, Crnkic M, Petersson IF, Saxne T. Etanercept, infliximab, and leflunomide in established rheumatoid arthritis: clinical experience using a structured follow up programme in southern Sweden. Ann Rheum Dis. 2002 Sep;61(9):793-8.
169. Weaver AL, Lautzenheiser RL, Schiff MH, Gibofsky A, Perruquet JL, Luetkemeyer J, et al. Real-world effectiveness of select biologic and DMARD monotherapy and combination therapy in the treatment of rheumatoid arthritis: results from the RADIUS observational registry. Curr Med Res Opin. 2006 Jan;22(1):185-98.
170. Gartlehner G, Hansen RA, Jonas BL, Thieda P, Lohr KN. The comparative efficacy and safety of biologics for the treatment of rheumatoid arthritis: a systematic review and metaanalysis. J Rheumatol. 2006 Dec;33(12):2398-408.
171. Sandborn WJ, Hanauer SB, Katz S, Safdi M, Wolf DG, Baerg RD, et al. Etanercept for active Crohn's disease: a randomized, double-blind, placebo-controlled trial. Gastroenterology. 2001 Nov;121(5):1088-94.

172. ten Hove T, van Montfrans C, Peppelenbosch MP, van Deventer SJ. Infliximab treatment induces apoptosis of lamina propria T lymphocytes in Crohn's disease. Gut. 2002 Feb;50(2):206-11.
173. Papadakis KA, Shaye OA, Vasiliauskas EA, Ippoliti A, Dubinsky MC, Birt J, et al. Safety and efficacy of adalimumab (D2E7) in Crohn's disease patients with an attenuated response to infliximab. Am J Gastroenterol. 2005 Jan;100(1):75-9.
174. Van den Brande JM, Braat H, van den Brink GR, Versteeg HH, Bauer CA, Hoedemaeker I, et al. Infliximab but not etanercept induces apoptosis in lamina propria T-lymphocytes from patients with Crohn's disease. Gastroenterology. 2003 Jun;124(7):1774-85.
175. Scallon B, Cai A, Solowski N, Rosenberg A, Song XY, Shealy D, et al. Binding and functional comparisons of two types of tumor necrosis factor antagonists. J Pharmacol Exp Ther. 2002 May;301(2):418-26.
176. Santora L, Kaymakcalan Z, Sakorafas P, Krull I, Grant K. Characterization of noncovalent complexes of recombinant human monoclonal antibody and antigen using cation exchange, size exclusion chromatography, and BIAcore. Analytical biochemistry. 2001;299(f25cbe3e-b1c9-3391-f869-4896f376cdb9):119-48.
177. Watts AD, Hunt NH, Wanigasekara Y, Bloomfield G, Wallach D, Roufogalis BD, et al. A casein kinase I motif present in the cytoplasmic domain of members of the tumour necrosis factor ligand family is implicated in 'reverse signalling'. EMBO J. 1999 Apr 15;18(8):2119-26.
178. Mitoma H, Horiuchi T, Hatta N, Tsukamoto H, Harashima S, Kikuchi Y, et al. Infliximab induces potent anti-inflammatory responses by outside-to-inside signals through transmembrane TNF-alpha. Gastroenterology. 2005 Feb;128(2):376-92.
179. Keane J, Gershon S, Wise RP, Mirabile-Levens E, Kasznica J, Schwieterman WD, et al. Tuberculosis associated with infliximab, a tumor necrosis factor alpha-neutralizing agent. N Engl J Med. 2001 Oct 11;345(15):1098-104.
180. Keane J. TNF-blocking agents and tuberculosis: new drugs illuminate an old topic. Rheumatology (Oxford). 2005 Jun;44(6):714-20.
181. van Schouwenburg PA, Rispens T, Wolbink GJ. Immunogenicity of anti-TNF biologic therapies for rheumatoid arthritis. Nat Rev Rheumatol. 2013 Mar;9(3):164-72.
182. Abramson SB, Amin A. Blocking the effects of IL-1 in rheumatoid arthritis protects bone and cartilage. Rheumatology (Oxford). 2002 Sep;41(9):972-80.
183. Goldring SR. Pathogenesis of bone erosions in rheumatoid arthritis. Curr Opin Rheumatol. 2002 Jul;14(4):406-10.
184. Jiang Y, Genant HK, Watt I, Cobby M, Bresnihan B, Aitchison R, et al. A multicenter, double-blind, dose-ranging, randomized, placebo-controlled study of recombinant human interleukin-1 receptor antagonist in patients with rheumatoid arthritis: radiologic progression and correlation of Genant and Larsen scores. Arthritis Rheum. 2000 May;43(5):1001-9.
185. Mertens M, Singh JA. Anakinra for rheumatoid arthritis: a systematic review. J Rheumatol. 2009 Jun;36(6):1118-25.
186. Hashizume M, Mihara M. The roles of interleukin-6 in the pathogenesis of rheumatoid arthritis. Arthritis. 2011;2011:765624.
187. Schiff MH, Kremer JM, Jahreis A, Vernon E, Isaacs JD, van Vollenhoven RF. Integrated safety in tocilizumab clinical trials. Arthritis Res Ther. 2011;13(5):R141.
188. Edwards JC, Cambridge G. Sustained improvement in rheumatoid arthritis following a protocol designed to deplete B lymphocytes. Rheumatology (Oxford). 2001 Feb;40(2):205-11.
189. Clynes RA, Towers TL, Presta LG, Ravetch JV. Inhibitory Fc receptors modulate in vivo cytotoxicity against tumor targets. Nat Med. 2000 Apr;6(4):443-6.

190. Edwards JC, Szczepanski L, Szechinski J, Filipowicz-Sosnowska A, Emery P, Close DR, et al. Efficacy of B-cell-targeted therapy with rituximab in patients with rheumatoid arthritis. N Engl J Med. 2004 Jun 17;350(25):2572-81.
191. Edwards JC, Leandro MJ, Cambridge G. B lymphocyte depletion in rheumatoid arthritis: targeting of CD20. Curr Dir Autoimmun. 2005;8:175-92.
192. Roll P, Palanichamy A, Kneitz C, Dorner T, Tony HP. Regeneration of B cell subsets after transient B cell depletion using anti-CD20 antibodies in rheumatoid arthritis. Arthritis Rheum. 2006 Aug;54(8):2377-86.
193. Ho LY, Mok CC, To CH, Anselm M, Cheung MY, Yu KL. Rituximab for refractory rheumatoid arthritis: a 24-week open-label prospective study. Open Rheumatol J. 2007;1:1-4.
194. Mease PJ, Revicki DA, Szechinski J, Greenwald M, Kivitz A, Barile-Fabris L, et al. Improved health-related quality of life for patients with active rheumatoid arthritis receiving rituximab: Results of the Dose-Ranging Assessment: International Clinical Evaluation of Rituximab in Rheumatoid Arthritis (DANCER) Trial. J Rheumatol. 2008 Jan;35(1):20-30.
195. Kavanaugh A, Rosengren S, Lee SJ, Hammaker D, Firestein GS, Kalunian K, et al. Assessment of rituximab's immunomodulatory synovial effects (ARISE trial). 1: clinical and synovial biomarker results. Ann Rheum Dis. 2008 Mar;67(3):402-8.
196. Thurlings RM, Vos K, Wijbrandts CA, Zwinderman AH, Gerlag DM, Tak PP. Synovial tissue response to rituximab: mechanism of action and identification of biomarkers of response. Ann Rheum Dis. 2008 Jul;67(7):917-25.
197. Verweij CL, Vosslamber S. New insight in the mechanism of action of rituximab: the interferon signature towards personalized medicine. Discov Med. 2011 Sep;12(64):229-36.
198. McInnes I, O'Dell J. State-of-the-art: rheumatoid arthritis. Annals of the Rheumatic Diseases. 2010;69(11):1898-906.
199. Rosman Z, Shoenfeld Y, Zandman-Goddard G. Biologic therapy for autoimmune diseases: an update. BMC Med. 2013;11:88.
200. Moreland L, Bate G, Kirkpatrick P. Abatacept. Nature reviews Drug discovery. 2006;5(3):185-6.
201. Kremer JM, Dougados M, Emery P, Durez P, Sibilia J, Shergy W, et al. Treatment of rheumatoid arthritis with the selective costimulation modulator abatacept: twelve-month results of a phase iib, double-blind, randomized, placebo-controlled trial. Arthritis Rheum. 2005 Aug;52(8):2263-71.
202. Kremer JM, Russell AS, Emery P, Abud-Mendoza C, Szechinski J, Westhovens R, et al. Long-term safety, efficacy and inhibition of radiographic progression with abatacept treatment in patients with rheumatoid arthritis and an inadequate response to methotrexate: 3-year results from the AIM trial. Ann Rheum Dis. 2011 Oct;70(10):1826-30.
203. Weinblatt M, Combe B, Covucci A, Aranda R, Becker JC, Keystone E. Safety of the selective costimulation modulator abatacept in rheumatoid arthritis patients receiving background biologic and nonbiologic disease-modifying antirheumatic drugs: A one-year randomized, placebo-controlled study. Arthritis Rheum. 2006 Sep;54(9):2807-16.
204. Genovese MC, Cohen S, Moreland L, Lium D, Robbins S, Newmark R, et al. Combination therapy with etanercept and anakinra in the treatment of patients with rheumatoid arthritis who have been treated unsuccessfully with methotrexate. Arthritis Rheum. 2004 May;50(5):1412-9.
205. Chames P, Baty D. Bispecific antibodies for cancer therapy: the light at the end of the tunnel? MAbs. 2009 Nov;1(6):539-47.

206. Kufer P, Lutterbuse R, Baeuerle PA. A revival of bispecific antibodies. Trends Biotechnol. 2004 May;22(5):238-44.
207. Karpovsky B, Titus JA, Stephany DA, Segal DM. Production of target-specific effector cells using hetero-cross-linked aggregates containing anti-target cell and anti-Fc gamma receptor antibodies. J Exp Med. 1984 Dec 1;160(6):1686-701.
208. Staerz UD, Kanagawa O, Bevan MJ. Hybrid antibodies can target sites for attack by T cells. Nature. 1985 Apr 18-24;314(6012):628-31.
209. Nolan O, O'Kennedy R. Bifunctional antibodies: concept, production and applications. Biochim Biophys Acta. 1990 Aug 1;1040(1):1-11.
210. Lindhofer H, Mocikat R, Steipe B, Thierfelder S. Preferential species-restricted heavy/light chain pairing in rat/mouse quadromas. Implications for a single-step purification of bispecific antibodies. Journal of immunology (Baltimore, Md : 1950). 1995;155(1):219-25.
211. Ridgway J, Presta L, Carter P. 'Knobs-into-holes' engineering of antibody CH3 domains for heavy chain heterodimerization. Protein engineering. 1996;9(7):617-21.
212. Davis J, Aperlo C, Li Y, Kurosawa E, Lan Y, Lo K-M, et al. SEEDbodies: fusion proteins based on strand-exchange engineered domain (SEED) CH3 heterodimers in an Fc analogue platform for asymmetric binders or immunofusions and bispecific antibodies. Protein engineering, design & selection : PEDS. 2010;23(4):195-202.
213. Wu C, Ying H, Grinnell C, Bryant S, Miller R, Clabbers A, et al. Simultaneous targeting of multiple disease mediators by a dual-variable-domain immunoglobulin. Nat Biotechnol. 2007 Nov;25(11):1290-7.
214. Kainer M, Antes B, Wiederkum S, Wozniak-Knopp G, Bauer A, Ruker F, et al. Correlation between CD16a binding and immuno effector functionality of an antigen specific immunoglobulin Fc fragment (Fcab). Arch Biochem Biophys. 2012 Oct 15;526(2):154-8.
215. Qi J, Kan F, Ye X, Guo M, Zhang Y, Ren G, et al. A bispecific antibody against IL-1beta and IL-17A is beneficial for experimental rheumatoid arthritis. Int Immunopharmacol. 2012 Dec;14(4):770-8.
216. Kanakaraj P, Puffer B, Yao X-T, Kankanala S, Boyd E, Shah R, et al. Simultaneous targeting of TNF and Ang2 with a novel bispecific antibody enhances efficacy in an in vivo model of arthritis. MAbs. 2012;4(5):600-13.
217. Veri MC, Burke S, Huang L, Li H, Gorlatov S, Tuaillon N, et al. Therapeutic control of B cell activation via recruitment of Fcgamma receptor IIb (CD32B) inhibitory function with a novel bispecific antibody scaffold. Arthritis Rheum. 2010 Jul;62(7):1933-43.
218. Nelson A, Dhimolea E, Reichert J. Development trends for human monoclonal antibody therapeutics. Nature reviews Drug discovery. 2010;9(10):767-74.
219. Mirick GR, Bradt BM, Denardo SJ, Denardo GL. A review of human anti-globulin antibody (HAGA, HAMA, HACA, HAHA) responses to monoclonal antibodies. Not four letter words. Q J Nucl Med Mol Imaging. 2004 Dec;48(4):251-7.
220. Lonberg N. Human antibodies from transgenic animals. Nat Biotechnol. 2005 Sep;23(9):1117-25.
221. Smith GP. Filamentous fusion phage: novel expression vectors that display cloned antigens on the virion surface. Science. 1985 Jun 14;228(4705):1315-7.
222. Marks JD, Hoogenboom HR, Bonnert TP, McCafferty J, Griffiths AD, Winter G. By-passing immunization. Human antibodies from V-gene libraries displayed on phage. J Mol Biol. 1991 Dec 5;222(3):581-97.
223. Kehoe JW, Kay BK. Filamentous phage display in the new millennium. Chem Rev. 2005 Nov;105(11):4056-72.

224. Riechmann L, Holliger P. The C-terminal domain of TolA is the coreceptor for filamentous phage infection of E. coli. Cell. 1997 Jul 25;90(2):351-60.
225. Nakamura M, Tsumoto K, Kumagai I, Ishimura K. A morphologic study of filamentous phage infection of Escherichia coli using biotinylated phages. FEBS Lett. 2003 Feb 11;536(1-3):167-72.
226. Clackson T, Hoogenboom HR, Griffiths AD, Winter G. Making antibody fragments using phage display libraries. Nature. 1991 Aug 15;352(6336):624-8.
227. Hoogenboom HR, Griffiths AD, Johnson KS, Chiswell DJ, Hudson P, Winter G. Multi-subunit proteins on the surface of filamentous phage: methodologies for displaying antibody (Fab) heavy and light chains. Nucleic Acids Res. 1991 Aug 11;19(15):4133-7.
228. Kristensen P, Winter G. Proteolytic selection for protein folding using filamentous bacteriophages. Fold Des. 1998;3(5):321-8.
229. Harrison JL, Williams SC, Winter G, Nissim A. Screening of phage antibody libraries. Methods Enzymol. 1996;267:83-109.
230. Kamperidis P, Kamalati T, Ferrari M, Jones M, Garrood T, Smith M, et al. Development of a novel recombinant biotherapeutic with applications in targeted therapy of human arthritis. Arthritis and rheumatism. 2011;63(f16cf6b6-cad3-1020-9c1d-51f07b5627da):3758-825.
231. Blades M, Ingegnoli F, Wheller S, Manzo A, Wahid S, Panayi G, et al. Stromal cell-derived factor 1 (CXCL12) induces monocyte migration into human synovium transplanted onto SCID Mice. Arthritis and rheumatism. 2002;46(3):824-36.
232. Wahid S, Blades M, De Lord D, Brown I, Blake G, Yanni G, et al. Tumour necrosis factor-alpha (TNF-alpha) enhances lymphocyte migration into rheumatoid synovial tissue transplanted into severe combined immunodeficient (SCID) mice. Clinical and experimental immunology. 2000;122(b52100b2-0d70-93fc-0fe0-4896f4a4007f):133-75.
233. de Wildt R, Mundy C, Gorick B, Tomlinson I. Antibody arrays for high-throughput screening of antibody-antigen interactions. Nature biotechnology. 2000;18(9):989-94.
234. Di Niro R, Ziller F, Florian F, Crovella S, Stebel M, Bestagno M, et al. Construction of miniantibodies for the in vivo study of human autoimmune diseases in animal models. BMC biotechnology. 2007;7(1ba058d9-1893-8499-3161-4896f32bfcb7):46.
235. Abramoff MD, Magelhaes PJ, Ram SJ. Image processing with ImageJ. Biophotonics International. 2004;11:36-42.
236. Towbin H, Staehelin T, Gordon J. Electrophoretic transfer of proteins from polyacrylamide gels to nitrocellulose sheets: procedure and some applications. Proc Natl Acad Sci U S A. 1979 Sep;76(9):4350-4.
237. Ruifrok AC, Johnston DA. Quantification of histochemical staining by color deconvolution. Anal Quant Cytol Histol. 2001 Aug;23(4):291-9.
238. Barlow AL, Macleod A, Noppen S, Sanderson J, Guerin CJ. Colocalization analysis in fluorescence micrographs: verification of a more accurate calculation of pearson's correlation coefficient. Microsc Microanal. 2010 Dec;16(6):710-24.
239. Nakamura K, Watakabe A, Hioki H, Fujiyama F, Tanaka Y, Yamamori T, et al. Transiently increased colocalization of vesicular glutamate transporters 1 and 2 at single axon terminals during postnatal development of mouse neocortex: a quantitative analysis with correlation coefficient. Eur J Neurosci. 2007 Dec;26(11):3054-67.
240. Hirth A, Skapenko A, Kinne RW, Emmrich F, Schulze-Koops H, Sack U. Cytokine mRNA and protein expression in primary-culture and repeated-passage synovial fibroblasts from patients with rheumatoid arthritis. Arthritis Res. 2002;4(2):117-25.

241. Di Niro R, Sulic A-M, Mignone F, D'Angelo S, Bordoni R, Iacono M, et al. Rapid interactome profiling by massive sequencing. Nucleic acids research. 2010;38(27659e36-0731-9afb-a6fa-4896f32bfdf8).
242. Worn A, Pluckthun A. Stability engineering of antibody single-chain Fv fragments. J Mol Biol. 2001 Feb 2;305(5):989-1010.
243. Skerra A, Plückthun A. Assembly of a functional immunoglobulin Fv fragment in Escherichia coli. Science (New York, NY). 1988;240(4855):1038-41.
244. Kadokura H, Katzen F, Beckwith J. Protein disulfide bond formation in prokaryotes. Annu Rev Biochem. 2003;72:111-35.
245. Galat A. Peptidylprolyl cis/trans isomerases (immunophilins): biological diversity--targets--functions. Curr Top Med Chem. 2003;3(12):1315-47.
246. Skorko-Glonek J, Sobiecka-Szkatula A, Narkiewicz J, Lipinska B. The proteolytic activity of the HtrA (DegP) protein from Escherichia coli at low temperatures. Microbiology. 2008 Dec;154(Pt 12):3649-58.
247. Schlegel S, Rujas E, Ytterberg AJ, Zubarev RA, Luirink J, de Gier JW. Optimizing heterologous protein production in the periplasm of E. coli by regulating gene expression levels. Microb Cell Fact. 2013;12:24.
248. Ibrahim S, Seppala I, Makela O. V-region-mediated binding of human Ig by protein A. J Immunol. 1993 Oct 1;151(7):3597-603.
249. Hochuli E, Dobeli H, Schacher A. New metal chelate adsorbent selective for proteins and peptides containing neighbouring histidine residues. J Chromatogr. 1987 Dec 18;411:177-84.
250. Porath J, Carlsson J, Olsson I, Belfrage G. Metal chelate affinity chromatography, a new approach to protein fractionation. Nature. 1975 Dec 18;258(5536):598-9.
251. Kortt AA, Dolezal O, Power BE, Hudson PJ. Dimeric and trimeric antibodies: high avidity scFvs for cancer targeting. Biomol Eng. 2001 Oct 15;18(3):95-108.
252. Harris L, Larson S, Hasel K, McPherson A. Refined structure of an intact IgG2a monoclonal antibody. Biochemistry. 1997;36(7):1581-97.
253. Hu S, Shively L, Raubitschek A, Sherman M, Williams L, Wong J, et al. Minibody: A novel engineered anti-carcinoembryonic antigen antibody fragment (single-chain Fv-CH3) which exhibits rapid, high-level targeting of xenografts. Cancer research. 1996;56(33de8719-5802-e518-298b-4896f1ec6df7):3055-116.
254. Huhn C, Selman M, Ruhaak L, Deelder A, Wuhrer M. IgG glycosylation analysis. Proteomics. 2009;9(4):882-913.
255. Verma R, Boleti E, George A. Antibody engineering: comparison of bacterial, yeast, insect and mammalian expression systems. Journal of immunological methods. 1998;216(1-2):165-81.
256. Goding J. Use of staphylococcal protein A as an immunological reagent. Journal of immunological methods. 1978;20:241-53.
257. Arakawa T, Philo J, Tsumoto K, Yumioka R, Ejima D. Elution of antibodies from a Protein-A column by aqueous arginine solutions. Protein expression and purification. 2004;36(2):244-8.
258. Mayer SW, Tompkins ER. Ion exchange as a separations method; a theoretical analysis of the column separations process. J Am Chem Soc. 1947 Nov;69(11):2866-74.
259. Arap W, Kolonin MG, Trepel M, Lahdenranta J, Cardo-Vila M, Giordano RJ, et al. Steps toward mapping the human vasculature by phage display. Nat Med. 2002 Feb;8(2):121-7.
260. Villa A, Trachsel E, Kaspar M, Schliemann C, Sommavilla R, Rybak J-N, et al. A high-affinity human monoclonal antibody specific to the alternatively spliced EDA domain of fibronectin efficiently targets tumor neo-vasculature in vivo.

International journal of cancer Journal international du cancer. 2008;122(2f94b386-0057-2620-96fa-4896f2fc5c77):2405-18.
261. Rybak J-N, Trachsel E, Scheuermann J, Neri D. Ligand-based vascular targeting of disease. ChemMedChem. 2007;2(b845b548-88e9-1837-4d5d-4896f301bdbe):22-62.
262. Powers DB, Amersdorfer P, Poul M, Nielsen UB, Shalaby MR, Adams GP, et al. Expression of single-chain Fv-Fc fusions in Pichia pastoris. J Immunol Methods. 2001 May 1;251(1-2):123-35.
263. Walsh G. Biopharmaceutical benchmarks 2010. Nat Biotechnol. 2010 Sep;28(9):917-24.
264. Kim J, Kim Y-G, Lee G. CHO cells in biotechnology for production of recombinant proteins: current state and further potential. Applied microbiology and biotechnology. 2012;93(edc86c63-ccfd-d14a-6214-4896f1e1b345):917-47.
265. Ley K, Kansas GS. Selectins in T-cell recruitment to non-lymphoid tissues and sites of inflammation. Nat Rev Immunol. 2004 May;4(5):325-35.
266. Aloisi F, Pujol-Borrell R. Lymphoid neogenesis in chronic inflammatory diseases. Nature reviews Immunology. 2006;6(3):205-17.
267. Corsiero E, Bombardieri M, Manzo A, Bugatti S, Uguccioni M, Pitzalis C. Role of lymphoid chemokines in the development of functional ectopic lymphoid structures in rheumatic autoimmune diseases. Immunology letters. 2012;145(1-2):62-7.
268. Geboes K. Pathology of inflammatory bowel diseases (IBD): variability with time and treatment. Colorectal Dis. 2001 Jan;3(1):2-12.
269. Pousa I, Maté J, Gisbert J. Angiogenesis in inflammatory bowel disease. European journal of clinical investigation. 2008;38(2):73-81.
270. Gladman DD. Psoriatic arthritis. Dermatol Ther. 2009 Jan-Feb;22(1):40-55.
271. Smith M, Barg E, Weedon H, Papengelis V, Smeets T, Tak P, et al. Microarchitecture and protective mechanisms in synovial tissue from clinically and arthroscopically normal knee joints. Annals of the Rheumatic Diseases. 2003;62(4):303-7.
272. Kannan K, Ortmann R, Kimpel D. Animal models of rheumatoid arthritis and their relevance to human disease. Pathophysiology : the official journal of the International Society for Pathophysiology / ISP. 2005;12(8f8a3ff1-4f2c-8ba6-7e6b-4896f1ecdbf7):167-248.
273. von Tell D, Armulik A, Betsholtz C. Pericytes and vascular stability. Experimental cell research. 2006;312(cea378f5-51d1-6b81-44fa-4896f1eddffc):623-32.
274. Armulik A, Genové G, Betsholtz C. Pericytes: developmental, physiological, and pathological perspectives, problems, and promises. Developmental cell. 2011;21(9c30a559-0df9-a8c0-846c-52553beaaec5):193-408.
275. Adler J, Parmryd I. Quantifying colocalization by correlation: the Pearson correlation coefficient is superior to the Mander's overlap coefficient. Cytometry A. 2010 Aug;77(8):733-42.
276. MacFadyen JR, Haworth O, Roberston D, Hardie D, Webster MT, Morris HR, et al. Endosialin (TEM1, CD248) is a marker of stromal fibroblasts and is not selectively expressed on tumour endothelium. FEBS Lett. 2005 May 9;579(12):2569-75.
277. Simonavicius N, Robertson D, Bax DA, Jones C, Huijbers IJ, Isacke CM. Endosialin (CD248) is a marker of tumor-associated pericytes in high-grade glioma. Mod Pathol. 2008 Mar;21(3):308-15.
278. Lax S, Hou TZ, Jenkinson E, Salmon M, MacFadyen JR, Isacke CM, et al. CD248/Endosialin is dynamically expressed on a subset of stromal cells during lymphoid tissue development, splenic remodeling and repair. FEBS Lett. 2007 Jul 24;581(18):3550-6.

279. Lee L, Buckley C, Blades MC, Panayi G, George AJ, Pitzalis C. Identification of synovium-specific homing peptides by in vivo phage display selection. Arthritis Rheum. 2002 Aug;46(8):2109-20.
280. Sadler JE. Biochemistry and genetics of von Willebrand factor. Annu Rev Biochem. 1998;67:395-424.
281. Newman PJ, Berndt MC, Gorski J, White GC, 2nd, Lyman S, Paddock C, et al. PECAM-1 (CD31) cloning and relation to adhesion molecules of the immunoglobulin gene superfamily. Science. 1990 Mar 9;247(4947):1219-22.
282. Albelda SM, Muller WA, Buck CA, Newman PJ. Molecular and cellular properties of PECAM-1 (endoCAM/CD31): a novel vascular cell-cell adhesion molecule. J Cell Biol. 1991 Sep;114(5):1059-68.
283. Ozerdem U, Grako KA, Dahlin-Huppe K, Monosov E, Stallcup WB. NG2 proteoglycan is expressed exclusively by mural cells during vascular morphogenesis. Dev Dyn. 2001 Oct;222(2):218-27.
284. Skalli O, Pelte MF, Peclet MC, Gabbiani G, Gugliotta P, Bussolati G, et al. Alpha-smooth muscle actin, a differentiation marker of smooth muscle cells, is present in microfilamentous bundles of pericytes. J Histochem Cytochem. 1989 Mar;37(3):315-21.
285. Diaz-Flores L, Gutierrez R, Varela H, Rancel N, Valladares F. Microvascular pericytes: a review of their morphological and functional characteristics. Histol Histopathol. 1991 Apr;6(2):269-86.
286. Hall AP. Review of the pericyte during angiogenesis and its role in cancer and diabetic retinopathy. Toxicol Pathol. 2006;34(6):763-75.
287. Wahid S, Blades MC, De Lord D, Brown I, Blake G, Yanni G, et al. Tumour necrosis factor-alpha (TNF-alpha) enhances lymphocyte migration into rheumatoid synovial tissue transplanted into severe combined immunodeficient (SCID) mice. Clin Exp Immunol. 2000 Oct;122(1):133-42.
288. Nginamau E, Maehle B, Jonsson R. An experimental protocol for the fractionation and 2DE separation of HeLa and A-253 cell lysates suitable for the identification of the individual antigenic proteome in Sjögren's syndrome. Autoimmunity. 2011;44(8):652-63.
289. Klose J, Zeindl E. An attempt to resolve all the various proteins in a single human cell type by two-dimensional electrophoresis: I. Extraction of all cell proteins. Clinical chemistry. 1984;30(12 Pt 1):2014-20.
290. Zabel C, Klose J. Protein extraction for 2DE. Methods in molecular biology (Clifton, NJ). 2009;519:171-96.
291. Kaboord B, Perr M. Isolation of proteins and protein complexes by immunoprecipitation. Methods in molecular biology (Clifton, NJ). 2008;424:349-64.
292. Yarmush M, Jayaraman A. Advances in proteomic technologies. Annual review of biomedical engineering. 2002;4(316448c9-2262-da24-ca43-4896f1eed608):349-422.
293. Egelhofer V, Bussow K, Luebbert C, Lehrach H, Nordhoff E. Improvements in protein identification by MALDI-TOF-MS peptide mapping. Anal Chem. 2000 Jul 1;72(13):2741-50.
294. D'Angelo S, Mignone F, Deantonio C, Di Niro R, Bordoni R, Marzari R, et al. Profiling celiac disease antibody repertoire. Clinical immunology (Orlando, Fla). 2013;148(1):99-109.
295. Pluckthun A. Ribosome display: a perspective. Methods Mol Biol. 2012;805:3-28.
296. He M, Liu H, Turner M, Taussig M. Detection of protein-protein interactions by ribosome display and protein in situ immobilisation. New biotechnology. 2009;26(6):277-81.

297. Vielemeyer O, Nizak C, Jimenez A, Echard A, Goud B, Camonis J, et al. Characterization of single chain antibody targets through yeast two hybrid. BMC biotechnology. 2010;10(e85797fc-ab9d-f04e-131c-4896f1f2228f):59.
298. Jakobsen C, Rasmussen N, Laenkholm A-V, Ditzel H. Phage display derived human monoclonal antibodies isolated by binding to the surface of live primary breast cancer cells recognize GRP78. Cancer research. 2007;67(6f2d7938-3366-ce06-9674-4896f1dfe463):9507-24.
299. Hueber W, Kidd B, Tomooka B, Lee B, Bruce B, Fries J, et al. Antigen microarray profiling of autoantibodies in rheumatoid arthritis. Arthritis and rheumatism. 2005;52(9):2645-55.
300. Di Niro R, D'Angelo S, Secco P, Marzari R, Santoro C, Sblattero D. Profiling the autoantibody repertoire by screening phage-displayed human cDNA libraries. Methods in molecular biology (Clifton, NJ). 2009;570:353-69.
301. George A, Lee L, Pitzalis C. Isolating ligands specific for human vasculature using in vivo phage selection. Trends in biotechnology. 2003;21(0b94b39b-c6f1-3ce4-b449-4896f343a64c):199-402.
302. Smalley MJ, Titley J, Paterson H, Perusinghe N, Clarke C, O'Hare MJ. Differentiation of separated mouse mammary luminal epithelial and myoepithelial cells cultured on EHS matrix analyzed by indirect immunofluorescence of cytoskeletal antigens. J Histochem Cytochem. 1999 Dec;47(12):1513-24.
303. Santoni V, Molloy M, Rabilloud T. Membrane proteins and proteomics: un amour impossible? Electrophoresis. 2000 Apr;21(6):1054-70.
304. Lehner I, Niehof M, Borlak J. An optimized method for the isolation and identification of membrane proteins. Electrophoresis. 2003 Jun;24(11):1795-808.
305. Kortt A, Dolezal O, Power… B. Dimeric and trimeric antibodies: high avidity scFvs for cancer targeting. Biomolecular engineering. 2001(73eedf1b-d4fa-fb67-5369-4896f22c91cf).
306. Laemmli UK. Cleavage of structural proteins during the assembly of the head of bacteriophage T4. Nature. 1970 Aug 15;227(5259):680-5.
307. Worlock AJ, Sidgwick A, Horsburgh T, Bell PR. The use of paramagnetic beads for the detection of major histocompatibility complex class I and class II antigens. Biotechniques. 1991 Mar;10(3):310-5.
308. Caberoy NB, Maiguel D, Kim Y, Li W. Identification of tubby and tubby-like protein 1 as eat-me signals by phage display. Exp Cell Res. 2010 Jan 15;316(2):245-57.
309. Voss M, Lettau M, Janssen O. Identification of SH3 domain interaction partners of human FasL (CD178) by phage display screening. BMC Immunol. 2009;10:53.
310. Nzeusseu Toukap A, Galant C, Theate I, Maudoux A, Lories R, Houssiau F, et al. Identification of distinct gene expression profiles in the synovium of patients with systemic lupus erythematosus. Arthritis and rheumatism. 2007;56(5):1579-88.
311. Appleton C, Pitelka V, Henry J, Beier F. Global analyses of gene expression in early experimental osteoarthritis. Arthritis and rheumatism. 2007;56(6):1854-68.
312. Goessler U, Bugert P, Bieback K, Deml M, Sadick H, Hormann K, et al. In-vitro analysis of the expression of TGFbeta -superfamily-members during chondrogenic differentiation of mesenchymal stem cells and chondrocytes during dedifferentiation in cell culture. Cellular & molecular biology letters. 2005;10(2):345-62.
313. Chesnut JD, Baytan AR, Russell M, Chang MP, Bernard A, Maxwell IH, et al. Selective isolation of transiently transfected cells from a mammalian cell population with vectors expressing a membrane anchored single-chain antibody. J Immunol Methods. 1996 Jun 14;193(1):17-27.

314. Dasuri K, Antonovici M, Chen K, Wong K, Standing K, Ens W, et al. The synovial proteome: analysis of fibroblast-like synoviocytes. Arthritis research & therapy. 2004;6(2ef0deef-0718-e466-ee32-95d48a2742d1):8.
315. Weiler T, Du Q, Krokhin O, Ens W, Standing K, El-Gabalawy H, et al. The identification and characterization of a novel protein, c19orf10, in the synovium. Arthritis research & therapy. 2007;9(1ef30e78-c367-ebbf-c8a3-4896f1dd375a).
316. Petersen TN, Brunak S, von Heijne G, Nielsen H. SignalP 4.0: discriminating signal peptides from transmembrane regions. Nat Methods. 2011;8(10):785-6.
317. Tanudji M, Hevi S, Chuck SL. Improperly folded green fluorescent protein is secreted via a non-classical pathway. J Cell Sci. 2002 Oct 1;115(Pt 19):3849-57.
318. Arnoys E, Wang J. Dual localization: proteins in extracellular and intracellular compartments. Acta histochemica. 2007;109(2):89-110.
319. Berndt A, Borsi L, Luo X, Zardi L, Katenkamp D, Kosmehl H. Evidence of ED-B+ fibronectin synthesis in human tissues by non-radioactive RNA in situ hybridization. Investigations on carcinoma (oral squamous cell and breast carcinoma), chronic inflammation (rheumatoid synovitis) and fibromatosis (Morbus Dupuytren). Histochemistry and cell biology. 1998;109(3):249-55.
320. Trachsel E, Bootz F, Silacci M, Kaspar M, Kosmehl H, Neri D. Antibody-mediated delivery of IL-10 inhibits the progression of established collagen-induced arthritis. Arthritis Res Ther. 2007;9(1):R9.
321. Fesmire J. A brief review of other notable electrophoretic methods. Methods in molecular biology (Clifton, NJ). 2012;869:445-50.
322. Cattepoel S, Hanenberg M, Kulic L, Nitsch RM. Chronic intranasal treatment with an anti-Abeta(30-42) scFv antibody ameliorates amyloid pathology in a transgenic mouse model of Alzheimer's disease. PLoS One. 2011;6(4):e18296.
323. Li Y, Siegel DL, Scholler N, Kaplan DE. Validation of glypican-3-specific scFv isolated from paired display/secretory yeast display library. BMC Biotechnol. 2012;12:23.
324. Salfeld J, Kaymakcalan Z, Tracey D, Roberts A, Kamen R. Generation of fully human anti-TNF antibody D2E7. Arthritis Rheum. 1998;41(suppl 9).
325. Pande J, Szewczyk M, Grover A. Phage display: concept, innovations, applications and future. Biotechnology advances. 2010;28(6):849-58.
326. Xin Y, Yu L, Chen Z, Zheng L, Fu Q, Jiang J, et al. Cloning, expression patterns, and chromosome localization of three human and two mouse homologues of GABA(A) receptor-associated protein. Genomics. 2001 Jun 15;74(3):408-13.
327. Kuefer MU, Look AT, Williams DC, Valentine V, Naeve CW, Behm FG, et al. cDNA cloning, tissue distribution, and chromosomal localization of myelodysplasia/myeloid leukemia factor 2 (MLF2). Genomics. 1996 Jul 15;35(2):392-6.
328. Margulies M, Egholm M, Altman W, Attiya S, Bader J, Bemben L, et al. Genome sequencing in microfabricated high-density picolitre reactors. Nature. 2005;437(7057):376-80.
329. Tulin E, Onoda N, Nakata Y, Maeda M, Hasegawa M, Nomura H, et al. SF20/IL-25, a novel bone marrow stroma-derived growth factor that binds to mouse thymic shared antigen-1 and supports lymphoid cell proliferation. Journal of immunology (Baltimore, Md : 1950). 2001;167(11):6338-47.
330. Tulin E, Onoda N, Nakata Y, Maeda M, Hasegawa M, Nomura H, et al. SF20/IL-25, a novel bone marrow stroma-derived growth factor that binds to mouse thymic shared antigen-1 and supports lymphoid cell proliferation. Journal of immunology (Baltimore, Md : 1950). 2003;170(3):1593.
331. Sunagozaka H, Honda M, Yamashita T, Nishino R, Takatori H, Arai K, et al. Identification of a secretory protein c19orf10 activated in hepatocellular

carcinoma. International journal of cancer Journal international du cancer. 2011;129(5cf5b41f-392c-cb46-5941-4896f1dbcba3):1576-661.
332. Wang P, Mariman E, Keijer J, Bouwman F, Noben JP, Robben J, et al. Profiling of the secreted proteins during 3T3-L1 adipocyte differentiation leads to the identification of novel adipokines. Cellular and molecular life sciences : CMLS. 2004;61(ef5f82db-8832-0a58-60a7-4896f1e7fd3b):2405-22.
333. Chen YF, Jobanputra P, Barton P, Jowett S, Bryan S, Clark W, et al. A systematic review of the effectiveness of adalimumab, etanercept and infliximab for the treatment of rheumatoid arthritis in adults and an economic evaluation of their cost-effectiveness. Health technology assessment (Winchester, England). 2006;10(42).
334. Taylor P, Peters A, Paleolog E, Chapman P, Elliott M, McCloskey R, et al. Reduction of chemokine levels and leukocyte traffic to joints by tumor necrosis factor alpha blockade in patients with rheumatoid arthritis. Arthritis and rheumatism. 2000;43(1):38-47.
335. Askling J, Dixon W. The safety of anti-tumour necrosis factor therapy in rheumatoid arthritis. Curr Opin Rheumatol. 2008 Mar;20(2):138-44.
336. Yang K, Basu A, Wang M, Chintala R, Hsieh MC, Liu S, et al. Tailoring structure-function and pharmacokinetic properties of single-chain Fv proteins by site-specific PEGylation. Protein Engineering Design and Selection. 2003;16(077d1375-378c-9dd8-f089-4896f3788b33).
337. Rajpal A, Beyaz N, Haber L, Cappuccilli G, Yee H, Bhatt R, et al. A general method for greatly improving the affinity of antibodies by using combinatorial libraries. Proceedings of the National Academy of Sciences of the United States of America. 2005;102(4afd8c82-05f0-3a84-4cbf-4896f3758a70):8466-537.
338. Dhimolea E, Reichert J. World Bispecific Antibody Summit, September 27-28, 2011, Boston, MA. MAbs. 2012;4(1):4-13.
339. Kozak M. An analysis of 5'-noncoding sequences from 699 vertebrate messenger RNAs. Nucleic Acids Res. 1987 Oct 26;15(20):8125-48.
340. Rakestraw JA, Sazinsky SL, Piatesi A, Antipov E, Wittrup KD. Directed evolution of a secretory leader for the improved expression of heterologous proteins and full-length antibodies in Saccharomyces cerevisiae. Biotechnol Bioeng. 2009 Aug 15;103(6):1192-201.
341. Donnelly M, Luke G, Mehrotra A, Li X, Hughes L, Gani D, et al. Analysis of the aphthovirus 2A/2B polyprotein 'cleavage' mechanism indicates not a proteolytic reaction, but a novel translational effect: a putative ribosomal 'skip'. The Journal of general virology. 2001;82(Pt 5):1013-25.
342. Yokotani N, Doi K, Wenthold RJ, Wada K. Non-conservation of a catalytic residue in a dipeptidyl aminopeptidase IV-related protein encoded by a gene on human chromosome 7. Hum Mol Genet. 1993 Jul;2(7):1037-9.
343. Radicke S, Cotella D, Graf EM, Ravens U, Wettwer E. Expression and function of dipeptidyl-aminopeptidase-like protein 6 as a putative beta-subunit of human cardiac transient outward current encoded by Kv4.3. J Physiol. 2005 Jun 15;565(Pt 3):751-6.
344. Thillaivinayagalingam P, Gommeaux J, McLoughlin M, Collins D, Newcombe A. Biopharmaceutical production: Applications of surface plasmon resonance biosensors. Journal of chromatography B, Analytical technologies in the biomedical and life sciences. 2010;878(2):149-53.
345. Kaymakcalan Z, Sakorafas P, Bose S, Scesney S, Xiong L, Hanzatian D, et al. Comparisons of affinities, avidities, and complement activation of adalimumab,

infliximab, and etanercept in binding to soluble and membrane tumor necrosis factor. Clinical immunology (Orlando, Fla). 2009;131(2):308-16.
346. Tracey D, Klareskog L, Sasso E, Salfeld J, Tak P. Tumor necrosis factor antagonist mechanisms of action: a comprehensive review. Pharmacology & therapeutics. 2008;117(ae995bdc-1834-b17d-e268-4896f1e3dcee):244-323.
347. Schwager K, Kaspar M, Bootz F, Marcolongo R, Paresce E, Neri D, et al. Preclinical characterization of DEKAVIL (F8-IL10), a novel clinical-stage immunocytokine which inhibits the progression of collagen-induced arthritis. Arthritis Res Ther. 2009;11(5):R142.
348. Boscolo S, Mion F, Licciulli M, Macor P, De Maso L, Brce M, et al. Simple scale-up of recombinant antibody production using an UCOE containing vector. New biotechnology. 2012;29(4a43d3a0-1b2d-5ad7-944e-4896f32cdcd5):477-561.
349. Kanakaraj P, Puffer B, Yao X-T, Kankanala S, Boyd E, Shah R, et al. Simultaneous targeting of TNF and Ang2 with a novel bispecific antibody enhances efficacy in an in vivo model of arthritis. MAbs. 2012;4(5):600-13.
350. Rose R, van Berkel P, van den Bremer E, Labrijn A, Vink T, Schuurman J, et al. Mutation of Y407 in the CH3 domain dramatically alters glycosylation and structure of human IgG. MAbs. 2013;5(2):219-28.
351. Milstein C, Cuello AC. Hybrid hybridomas and their use in immunohistochemistry. Nature. 1983 Oct 6-12;305(5934):537-40.
352. Ho S, Bardor M, Li B, Lee J, Song Z, Tong Y, et al. Comparison of internal ribosome entry site (IRES) and Furin-2A (F2A) for monoclonal antibody expression level and quality in CHO cells. PloS one. 2013;8(5).
353. Anderson R, Voziyanova E, Voziyanov Y. Flp and Cre expressed from Flp-2A-Cre and Flp-IRES-Cre transcription units mediate the highest level of dual recombinase-mediated cassette exchange. Nucleic acids research. 2012;40(8).
354. Lee MH, Park TI, Park YB, Kwak JW. Bacterial expression and in vitro refolding of a single-chain fv antibody specific for human plasma apolipoprotein B-100. Protein Expr Purif. 2002 Jun;25(1):166-73.
355. Arbabi-Ghahroudi M, Tanha J, MacKenzie R. Prokaryotic expression of antibodies. Cancer Metastasis Rev. 2005 Dec;24(4):501-19.
356. Barderas R, Shochat S, Martinez-Torrecuadrada J, Altschuh D, Meloen R, Ignacio Casal J. A fast mutagenesis procedure to recover soluble and functional scFvs containing amber stop codons from synthetic and semisynthetic antibody libraries. J Immunol Methods. 2006 May 30;312(1-2):182-9.
357. Kobayashi N, Odaka K, Uehara T, Imanaka-Yoshida K, Kato Y, Oyama H, et al. Toward in vivo imaging of heart disease using a radiolabeled single-chain Fv fragment targeting tenascin-C. Anal Chem. 2011 Dec 1;83(23):9123-30.
358. Cheng KT. Radioiodinated-anti-TAG-72 covalently linked CC49 divalent single-chain Fv antibody. 2004.
359. Monnier PP, Vigouroux RJ, Tassew NG. In Vivo Applications of Single Chain Fv (Variable Domain)(scFv) Fragments. Antibodies. 2013;2(2):193-208.
360. Jayapal KP, Wlaschin KF, Hu W, Yap MGS. Recombinant protein therapeutics from CHO cells-20 years and counting. Chemical Engineering Progress. 2007;103(10):40.
361. Gramer M, Poeschl D. Comparison of cell growth in T-flasks, in micro hollow fiber bioreactors, and in an industrial scale hollow fiber bioreactor system. Cytotechnology. 2000;34(1-2):111-9.
362. Igawa T, Tsunoda H, Kuramochi T, Sampei Z, Ishii S, Hattori K. Engineering the variable region of therapeutic IgG antibodies. MAbs. 2011 May-Jun;3(3):243-52.

363. Salmi M, Jalkanen S. Human leukocyte subpopulations from inflamed gut bind to joint vasculature using distinct sets of adhesion molecules. J Immunol. 2001 Apr 1;166(7):4650-7.
364. Salmi M, Andrew DP, Butcher EC, Jalkanen S. Dual binding capacity of mucosal immunoblasts to mucosal and synovial endothelium in humans: dissection of the molecular mechanisms. J Exp Med. 1995 Jan 1;181(1):137-49.
365. Asquith DL, Miller AM, McInnes IB, Liew FY. Animal models of rheumatoid arthritis. Eur J Immunol. 2009 Aug;39(8):2040-4.
366. Amano T, Yamasaki S, Yagishita N, Tsuchimochi K, Shin H, Kawahara K, et al. Synoviolin/Hrd1, an E3 ubiquitin ligase, as a novel pathogenic factor for arthropathy. Genes Dev. 2003 Oct 1;17(19):2436-49.
367. Imai Y, Soda M, Takahashi R. Parkin suppresses unfolded protein stress-induced cell death through its E3 ubiquitin-protein ligase activity. J Biol Chem. 2000 Nov 17;275(46):35661-4.
368. Kaneko M, Ishiguro M, Niinuma Y, Uesugi M, Nomura Y. Human HRD1 protects against ER stress-induced apoptosis through ER-associated degradation. FEBS Lett. 2002 Dec 4;532(1-2):147-52.
369. Valencia X, Higgins JM, Kiener HP, Lee DM, Podrebarac TA, Dascher CC, et al. Cadherin-11 provides specific cellular adhesion between fibroblast-like synoviocytes. J Exp Med. 2004 Dec 20;200(12):1673-9.
370. Kawaguchi J, Takeshita S, Kashima T, Imai T, Machinami R, Kudo A. Expression and function of the splice variant of the human cadherin-11 gene in subordination to intact cadherin-11. J Bone Miner Res. 1999 May;14(5):764-75.
371. Shibata T, Ochiai A, Gotoh M, Machinami R, Hirohashi S. Simultaneous expression of cadherin-11 in signet-ring cell carcinoma and stromal cells of diffuse-type gastric cancer. Cancer Lett. 1996 Feb 6;99(2):147-53.
372. Kokkinos MI, Murthi P, Wafai R, Thompson EW, Newgreen DF. Cadherins in the human placenta--epithelial-mesenchymal transition (EMT) and placental development. Placenta. 2010 Sep;31(9):747-55.
373. Terry J, Saito T, Subramanian S, Ruttan C, Antonescu CR, Goldblum JR, et al. TLE1 as a diagnostic immunohistochemical marker for synovial sarcoma emerging from gene expression profiling studies. Am J Surg Pathol. 2007 Feb;31(2):240-6.
374. Stifani S, Blaumueller CM, Redhead NJ, Hill RE, Artavanis-Tsakonas S. Human homologs of a Drosophila Enhancer of split gene product define a novel family of nuclear proteins. Nat Genet. 1992 Dec;2(4):343.
375. Ota T, Suzuki Y, Nishikawa T, Otsuki T, Sugiyama T, Irie R, et al. Complete sequencing and characterization of 21,243 full-length human cDNAs. Nat Genet. 2004 Jan;36(1):40-5.
376. Wang JC, Waltner-Law M, Yamada K, Osawa H, Stifani S, Granner DK. Transducin-like enhancer of split proteins, the human homologs of Drosophila groucho, interact with hepatic nuclear factor 3beta. J Biol Chem. 2000 Jun 16;275(24):18418-23.
377. Nielsen JS, McNagny KM. Novel functions of the CD34 family. J Cell Sci. 2008 Nov 15;121(Pt 22):3683-92.
378. van Eys GJ, Niessen PM, Rensen SS. Smoothelin in vascular smooth muscle cells. Trends Cardiovasc Med. 2007 Jan;17(1):26-30.
379. Niessen P, Rensen S, van Deursen J, De Man J, De Laet A, Vanderwinden JM, et al. Smoothelin-a is essential for functional intestinal smooth muscle contractility in mice. Gastroenterology. 2005 Nov;129(5):1592-601.

380. Montani M, Thiesler T, Kristiansen G. Smoothelin is a specific and robust marker for distinction of muscularis propria and muscularis mucosae in the gastrointestinal tract. Histopathology. 2010 Aug;57(2):244-9.
381. Schwager K. Trial update; A phase Ib clinical trial with Dekavil (F8-IL10), an anti-inflammatory immunocytokine for the treatment of rheumatoid arthritis, used in combination with methotrexate. In: EULAR, editor. Annual European Congress of Rheumatology EULAR; Berlin, Germany2012.
382. Yan H, Gu C-G, Xu F-L, Wu X-H, Yin H-H, Hu C-X, et al. Identification of synthetic peptides that inhibit lipopolysaccharide (LPS) binding to myeloid differentiation protein-2 (MD-2). Journal of immunotherapy (Hagerstown, Md : 1997). 2013;36(3):197-207.
383. Chang C, Takayanagi A, Yoshida T, Shimizu N. Screening of scFv-displaying phages recognizing distinct extracellular domains of EGF receptor by target-guided proximity labeling method. Journal of immunological methods. 2011;372(58c87c10-09da-e8b0-1a43-06a0f8ae7ae9):127-63.
384. Jovanovic V, Abdul Aziz N, Lim YT, Ng Ai Poh A, Jin Hui Chan S, Ho Xin Pei E, et al. Lipid anti-lipid antibody responses correlate with disease activity in systemic lupus erythematosus. PLoS One. 2013;8(2):e55639.
385. Shimizu Y, Temma T, Hara I, Makino A, Yamahara R, Ozeki E-I, et al. Micelle-based activatable probe for in vivo near-infrared optical imaging of cancer biomolecules. Nanomedicine : nanotechnology, biology, and medicine. 2013.
386. Rybak JN, Trachsel E, Scheuermann J, Neri D. Ligand-based vascular targeting of disease. ChemMedChem. 2007 Jan;2(1):22-40.
387. Carnemolla B, Borsi L, Balza E, Castellani P, Meazza R, Berndt A, et al. Enhancement of the antitumor properties of interleukin-2 by its targeted delivery to the tumor blood vessel extracellular matrix. Blood. 2002 Mar 1;99(5):1659-65.
388. Borsi L, Balza E, Carnemolla B, Sassi F, Castellani P, Berndt A, et al. Selective targeted delivery of TNFalpha to tumor blood vessels. Blood. 2003 Dec 15;102(13):4384-92.
389. Fabbrini M, Trachsel E, Soldani P, Bindi S, Alessi P, Bracci L, et al. Selective occlusion of tumor blood vessels by targeted delivery of an antibody-photosensitizer conjugate. International journal of cancer Journal international du cancer. 2006;118(0410a0d2-f32e-789e-86ef-4896f41c7ab5):1805-18.
390. Macor P, Durigutto P, De Maso L, Garrovo C, Biffi S, Cortini A, et al. Treatment of experimental arthritis by targeting synovial endothelium with a neutralizing recombinant antibody to C5. Arthritis and rheumatism. 2012;64(8):2559-67.
391. Jackman J, Chen Y, Huang A, Moffat B, Scheer JM, Leong SR, et al. Development of a two-part strategy to identify a therapeutic human bispecific antibody that inhibits IgE receptor signaling. J Biol Chem. 2010 Jul 2;285(27):20850-9.
392. Schaefer W, Regula JT, Bahner M, Schanzer J, Croasdale R, Durr H, et al. Immunoglobulin domain crossover as a generic approach for the production of bispecific IgG antibodies. Proc Natl Acad Sci U S A. 2011 Jul 5;108(27):11187-92.
393. Ltd. RAP. Bispecific Antibody Therapeutics Market, 2013 - 20232013 September 2013.
394. Boel E, Verlaan S, Poppelier M, Westerdaal N, Van Strijp J, Logtenberg T. Functional human monoclonal antibodies of all isotypes constructed from phage display library-derived single-chain Fv antibody fragments. Journal of immunological methods. 2000;239(1-2):153-66.
395. Maul R, Gearhart P. AID and somatic hypermutation. Advances in immunology. 2010;105:159-91.

396. Man Sung Co DAS, Cary L. Queen, inventor INCREASING ANTIBODY AFFINITY BY ALTERING GLYCOSYLATION IN THE IMMUNOGLOBULIN VARIABLE REGION. USA patent 5,714,350. 1998.
397. Martineau P. Error-prone polymerase chain reaction for modification of scFvs. Methods in molecular biology (Clifton, NJ). 2002;178:287-94.
398. Meleady P. 2D gel electrophoresis and mass spectrometry identification and analysis of proteins. Methods in molecular biology (Clifton, NJ). 2011;784:123-37.
399. Parrini MC, Sadou-Dubourgnoux A, Aoki K, Kunida K, Biondini M, Hatzoglou A, et al. SH3BP1, an exocyst-associated RhoGAP, inactivates Rac1 at the front to drive cell motility. Mol Cell. 2011 Jun 10;42(5):650-61.
400. Bodemann BO, Orvedahl A, Cheng T, Ram RR, Ou YH, Formstecher E, et al. RalB and the exocyst mediate the cellular starvation response by direct activation of autophagosome assembly. Cell. 2011 Jan 21;144(2):253-67.

Supplementary material

ARTHRITIS & RHEUMATISM
Vol. 63, No. 12, December 2011, pp 3758–3767
DOI 10.1002/art.30650

Development of a Novel Recombinant Biotherapeutic With Applications in Targeted Therapy of Human Arthritis

Panagiotis Kamperidis,[1] Tahereh Kamalati,[1] Mathieu Ferrari,[1] Margaret Jones,[1] Toby Garrood,[1] Malcolm D. Smith,[2] Soraya Diez-Posada,[3] Chris Hughes,[1] Ciara Finucane,[1] Stephen Mather,[1] Ahuva Nissim,[1] Andrew J. T. George,[4] and Costantino Pitzalis[1]

Objective. **To isolate recombinant antibodies with specificity for human arthritic synovium and to develop targeting reagents with joint-specific delivery capacity for therapeutic and/or diagnostic applications.**

Methods. **In vivo single-chain Fv (scFv) antibody phage display screening using a human synovial xenograft model was used to isolate antibodies specific to the microvasculature of human arthritic synovium. Single-chain Fv antibody tissue-specific reactivity was assessed by immunostaining of synovial tissues from normal controls and from patients with rheumatoid arthritis and osteoarthritis, normal human tissue arrays, and tissues from other patients with inflammatory diseases displaying neovasculogenesis. In vivo scFv antibody tissue-specific targeting capacity was examined in the human synovial xenograft model using both ^{125}I-labeled and biotinylated antibody.**

Results. **We isolated a novel recombinant human antibody, scFv A7, with specificity for the microvasculature of human arthritic synovium. We showed that in vivo, this antibody could efficiently target human synovial microvasculature in SCID mice transplanted with human arthritic synovial xenografts. Our results demonstrated that scFv A7 antibody had no reactivity with the microvasculature or with other cellular components found in a comprehensive range of normal human tissues including normal human synovium. Further, we showed that the reactivity of the scFv A7 antibody was not a common feature of neovasculogenesis associated with chronic inflammatory conditions.**

Conclusion. **Here we report for the first time the identification of an scFv antibody, A7, that specifically recognizes an epitope expressed in the microvasculature of human arthritic synovium and that has the potential to be developed as a joint-specific pharmaceutical.**

Rheumatoid arthritis (RA) is a chronic inflammatory disease that principally affects synovial joints, causing disability with significant associated morbidity and mortality (1,2). In RA, the synovium becomes hyperplastic and locally invasive at the interface between the cartilage and bone, resulting in the destruction of articular cartilage and subchondral bone, leading to joint damage and disability. Notably, in RA, the synovium becomes heavily infiltrated by T and B cells, plasma cells, and monocytes through the development of new blood vessels (angiogenesis) (3,4). It is now clear that synovial angiogenesis contributes significantly to disease pathogenesis and progression (5,6) and may precede other pathologic features of RA, since synovial hypercellularity is sustained by an increase in the number and density of synovial blood vessels (6–8). Further, not only angiogenesis but also vasculogenesis may contribute to the increased vascularity observed in the RA synovium (9), making the newly formed blood vessels a particularly attractive therapeutic target for the manage-

Supported by the Nuffield Foundation (an Oliver Bird Rheumatism Programme PhD studentship to Dr. Kamperidis; Dr. Pitzalis Programme Principal Investigator) and Arthritis Research UK (grant 17606).

[1]Panagiotis Kamperidis, PhD, Tahereh Kamalati, PhD, Mathieu Ferrari, MSc, Margaret Jones, MIAT, Toby Garrood, MD, MRCP, PhD, Chris Hughes, PhD, Ciara Finucane, PhD, Stephen Mather, PhD, Ahuva Nissim, PhD, Costantino Pitzalis, MD, PhD, FRCP: Barts and the London School of Medicine and Dentistry, Queen Mary University of London, London, UK; [2]Malcolm D. Smith, MBBS, FRACP: Repatriation General Hospital, Daw Park, Adelaide, South Australia, Australia; [3]Soraya Diez-Posada, PhD: University College London, London, UK; [4]Andrew J. T. George, PhD, FRCPath, FRSA, FHEA: Imperial College London, Hammersmith Campus, London, UK.

Drs. Kamperidis and Kamalati contributed equally to this work.

Address correspondence to Costantino Pitzalis, MD, PhD, FRCP, William Harvey Research Institute, Barts and the London School of Medicine and Dentistry, Charterhouse Square, London EC1M 6BQ, UK. E-mail: c.pitzalis@qmul.ac.uk.

Submitted for publication April 1, 2011; accepted in revised form August 23, 2011.

ment of inflammatory arthritis (10). In support of this, blockade of inflammatory neovascularization has been shown to lead to the suppression of synovial inflammation and proliferation and to an attenuation of synovitis in RA (11).

The treatment of this condition has been transformed in the last decade by the use of recombinant antibodies targeting proinflammatory cytokines such as tumor necrosis factor α (TNFα) (12). However, despite the obvious impact of such therapies, 20–40% of patients do not respond (13), sustained and high-magnitude clinical response is achieved only in a minority of cases (14), and prolonged treatment-free remission has not been obtained. Additionally, these therapies exhibit several adverse side effects that make persistent administration undesirable (14–16). Therefore, the development of new agents that offer greater efficacy and improved safety profiles remains an important goal for the treatment of RA. In this context, tissue-specific drug delivery systems for targeting and improving the retention of bioactive agents are particularly important, as they could be used to achieve higher levels of pharmaceuticals at the site of therapeutic interference and thus prolong local activity within the joint, thereby reducing systemic exposure and toxicity. Recombinant, single-chain antibodies lend themselves well to the development of such targeted pharmacodelivery strategies.

To date, joint-specific targeting for the treatment of arthritic disease remains an unmet clinical goal. In order to address this, we have developed a synovial xenograft model in SCID mice where functional vascular anastomoses allow the delivery of agents targeting human synovial tissue to be assessed in vivo (17). Previously, we successfully used this model for in vivo peptide phage display and imaging of synovial tissue (18,19). Here, we have extended the use of this model system to carry out in vivo single-chain Fv (scFv) antibody phage display screening, in order to identify scFv antibody clones with specificity for the human synovial vasculature of the xenografts. We report for the first time the isolation and characterization of an scFv antibody (A7) that exhibits specificity for the microvasculature of human arthritic synovial tissue, and we discuss its potential application as an innovative recombinant pharmaceutical agent for the treatment of arthritic diseases.

MATERIALS AND METHODS

Human tissue transplantation into SCID mice. Beige SCID CB17 mice ages 4–10 weeks were used in this study. Human tissues (synovium and skin) were transplanted subcutaneously in a dorsal position distal to the shoulder joints (2 transplants per animal) as previously described (20). Mice were inspected daily, and animal work was performed under a Project License (PPL 70-6109). Human synovial tissue was obtained from RA patients or osteoarthritis (OA) patients undergoing joint replacement. Human skin tissue was obtained from patients undergoing cosmetic surgery. Informed consent was obtained from all patients. Additionally, ethical approval to use human synovial and skin tissue for research purposes was obtained from the Ethics Committee (Local Research Ethics Committee no. 05/Q0703/198).

In vivo selection of synovium-specific scFv phage. The human scFv libraries I + J (Tomlinson I + J) (21) were kindly provided by Dr. Greg Winter (Medical Research Council Centre for Protein Engineering, Cambridge, UK). Synovium-specific phage was isolated following 4 rounds of enrichment in SCID mice carrying human arthritic synovial tissue and skin tissue xenografts (18, 19). Selection and enrichment were monitored by phage titration, and the integrity of scFv coding regions from phage from the final round of selection was assessed by polymerase chain reaction using LMB3 and pHEN seq primers (see below). Clones that showed expression of full-length scFv fragments were used to infect the nonsuppressor strain *Escherichia coli* HB2151 for the production of soluble scFv protein. One hundred colonies were selected and analyzed for scFv expression by enzyme-linked immunosorbent assay for protein A and protein L binding (22).

DNA sequence analysis of scFv coding regions. The DNA sequences encoding the scFv inserts of phage clones from the final round of selection were determined using the vector primers LMB3 (CAGGAAACAGCTATGAC) and pHEN seq (CTATGCGGCCCCATTCA) (21,23). Sequencing was performed using the Big Dye Terminator v3.1 Cycle Sequencing kit (Applied Biosystems) on an ABI PRISM 3130 Genetic analyzer.

Production of soluble scFv antibodies. Single-chain Fv fragments encoded by phage from the final round of selection were expressed in *E coli* HB2151 as soluble, secreted proteins and purified from bacterial culture supernatants by affinity chromatography using protein A–Sepharose Fast Flow Resin (GE Healthcare), as described previously (24). Purified antibodies were analyzed by sodium dodecyl sulfate–polyacrylamide gel electrophoresis and size-exclusion chromatography on Superdex 75 HR10/30 columns (Amersham Biosciences).

Biotinylation of scFv antibodies. Single-chain Fv antibodies were biotinylated using the EZ-Link Sulfo-NHS-SS-Biotinylation kit (Perbio Science). Briefly, purified scFv protein was diluted in 0.5–2 ml phosphate buffered saline (PBS), added to a 20-fold molar excess of 10 m*M* Sulfo-NHS-SS-Biotin, and incubated on ice for 1 hour. Biotinylated proteins were subsequently purified using spin-column chromatography (Perbio Science) according to the manufacturer's instructions.

Iodination of scFv antibodies. Single-chain Fv antibody fragments were radiolabeled with $Na^{125}I$ using the iodogen method (25). Iodination reaction tubes precoated with iodogen were used according to the manufacturer's instructions (Perbio Science). Typically, 25 μg of purified scFv in 150 μl of PBS was radiolabeled to specific activities of 0.15–0.2 MBq/μg. The efficiency of iodination was evaluated by instant thin-layer chromatography and typically found to be >90%. The purity

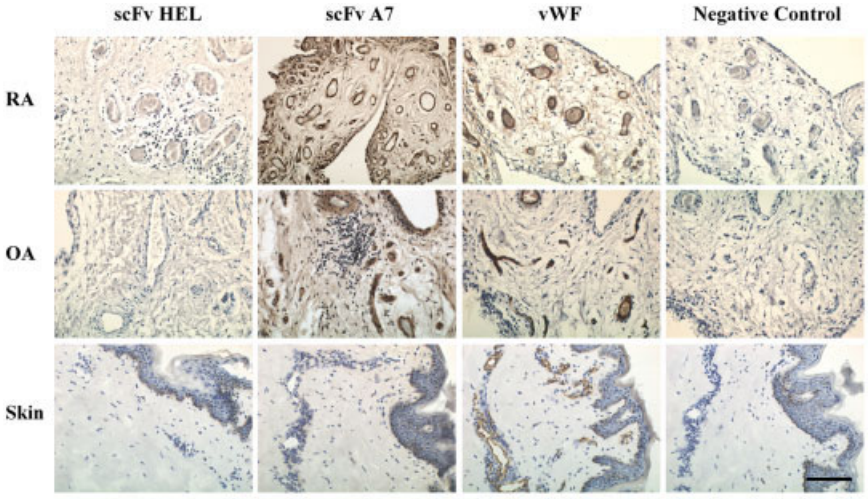

Figure 1. Immunohistochemical analysis of single-chain Fv (scFv) antibody reactivity with human arthritic synovial tissue. The reactivity of scFv antibody (scFv A7) with sections of human arthritic synovial and skin tissue was examined using biotinylated scFv A7. Biotinylated scFv HEL was used as an antibody negative control. The presence of blood vessels in tissue samples was visualized with anti-human von Willebrand factor (vWF) antibody. Biotinylated scFv antibodies were detected with avidin–biotin–horseradish peroxidase (HRP) complex, while anti-vWF antibody reactivity was detected using an HRP-labeled antibody. RA = rheumatoid arthritis; OA = osteoarthritis. Bar = 100 μm.

of the labeled scFv was determined by size-exclusion high-performance liquid chromatography.

In vivo localization of soluble scFv A7 antibody. Two SCID mice bearing double xenografts of human arthritic synovial and skin tissues (2 arthritic synovium and 2 human skin grafts per animal) were injected with 6 μg of biotinylated scFv A7 four weeks after transplantation. Biotinylated anti–hen egg lysozyme antibody, scFv HEL (22), was used as a negative control. The biotinylated antibody fragments were administered via the tail vein in a total volume of 200 μl and were allowed to circulate for 15 minutes, after which time the mice were perfused under terminal anesthesia. The human grafts along with murine tissues were excised and immediately snap-frozen in liquid nitrogen for histologic examination. The tissue-specific localization of soluble scFv A7 was examined by immunohistochemical detection of biotinylated antibody using avidin–biotin–horseradish peroxidase complex (Dako).

In vivo targeting capacity of iodinated scFv A7 antibody. Five double-transplanted SCID mice (2 arthritic synovium and 2 human skin grafts per animal) were injected with iodinated scFv antibody 4 weeks following transplantation. Each animal was administered an injection, via the tail vein, of 200 μl sterile saline containing 1.25 μg labeled scFv with a specific activity of 0.16 MBq/μg. Mice were killed 4 hours or 24 hours after injection, and grafts as well as mouse organs were collected for gamma counting. The results were corrected for tissue weight and background radioactivity in the blood pool and expressed as a percentage of the total injected dose. Iodinated scFv HEL was used as an untargeted scFv control.

Immunohistochemical analysis. Slide-mounted frozen tissue sections were fixed in ice-cold acetone. Paraffin-embedded tissues were dewaxed and subsequently treated with proteinase K (Dako) for 4 minutes at room temperature for antigen retrieval. Slides were stained with 1 μg of biotinylated scFv A7 and visualized with avidin–biotin–horseradish peroxidase complex using 3,3′-diaminobenzidine chromogen. The presence of human blood vessels in tissue sections was visualized using mouse anti-human von Willebrand factor (vWF) (Dako), followed by a horseradish peroxidase–conjugated anti-mouse antibody (Dako). Rabbit anti-mouse CD31 (BD Biosciences) and rabbit anti-mouse CD34 (Cambridge Bioscience) were used to detect mouse endothelial cells in murine tissues. An anti–α-smooth muscle actin antibody (Sigma) was used to visualize the stromal component of the microvasculature. Sections were counterstained with hematoxylin, mounted with Depex mounting medium (Dako), and analyzed using a light microscope (Olympus). Images were acquired with CellP Soft Imaging System version 1.2 (Olympus).

Immunofluorescence analysis. Slide-mounted frozen tissue sections were fixed in ice-cold acetone prior to antibody staining. Biotinylated scFv A7 reactivity was detected with Texas Red–conjugated NeutrAvidin (Invitrogen). Mouse anti-human vWF, mouse anti-human CD31 (Sigma), and rabbit anti-NG2 antibody (Millipore) reactivity was detected using goat anti-mouse and goat anti-rabbit antibodies conjugated to Alexa Fluor 488 or Alexa Fluor 594 (Invitrogen). Sections were subsequently mounted in fluorescent mounting media (Vectashield) with DAPI nuclear counterstain (Vector) and

examined using an Axioskop 2 microscope (Carl Zeiss). Images were captured by an AxioCam digital color camera using KS300 image analysis software (Carl Zeiss).

Pearson's correlation coefficient analysis. Velocity 5.5 imaging software (PerkinElmer) was used to perform thresholded Pearson's correlation coefficient analysis of images in order to accurately quantify and correlate overlap of image pixels from 2 different channels (26). A value of +1 indicates complete pixel-to-pixel overlap of the pixels from the 2 chosen channels. A value of 0 indicates no overlap or correlation of pixels from 2 different channels, and a value of −1 indicates complete disparity/exclusion of pixels from the 2 channels that have been compared.

Statistical analysis. Results are expressed as the mean ± SEM. Parametric analyses were performed by unpaired 2-tailed *t*-test using GraphPad Prism software.

RESULTS

Isolation of an scFv antibody with binding specificity for human arthritic synovial tissue. In order to select scFv fragments targeting the human synovial microvasculature, 4 cycles of in vivo selection using the human scFv libraries I + J (Tomlinson I + J) (21) were conducted using mice with dual xenografts of synovium (target) and skin (control) tissues. The composition of recovered scFv fragments in the final round of in vivo selection was assessed by examining the ability of 100 phage-encoding full-length inserts to transduce bacteria for secreted antibody protein expression. The functionality of these clones was further confirmed by demonstrating secreted scFv binding to protein A and protein L. Of these 100 clones, 24 expressed secreted scFv antibody at high levels and were subsequently shown to encode the same scFv sequence. Notably, this scFv sequence had already been identified in a previous, independent, in vivo screen of the Tomlinson library, using the same synovial xenograft model system (results not shown). Thus, clone A7, an scFv from the group of 24 identical clones from the final screen, which showed robust soluble antibody expression (>1 mg/100 ml bacterial culture), was chosen for further studies.

Soluble scFv A7 protein was purified as a monomeric protein and used in immunohistochemical analysis to assess binding specificity in human RA and OA synovial tissues in comparison to that of skin, the control tissue used in the in vivo selection process. We examined 15 OA and 8 RA synovial tissue samples and 5 skin samples. As shown in Figure 1, scFv A7 exhibited specific and strong reactivity with the microvasculature of OA and RA synovial tissue. Importantly, scFv A7 exhibited no detectable reactivity with control human skin tissue. The control, nontargeted antibody scFv HEL did not exhibit binding to either synovium or control skin tissue samples.

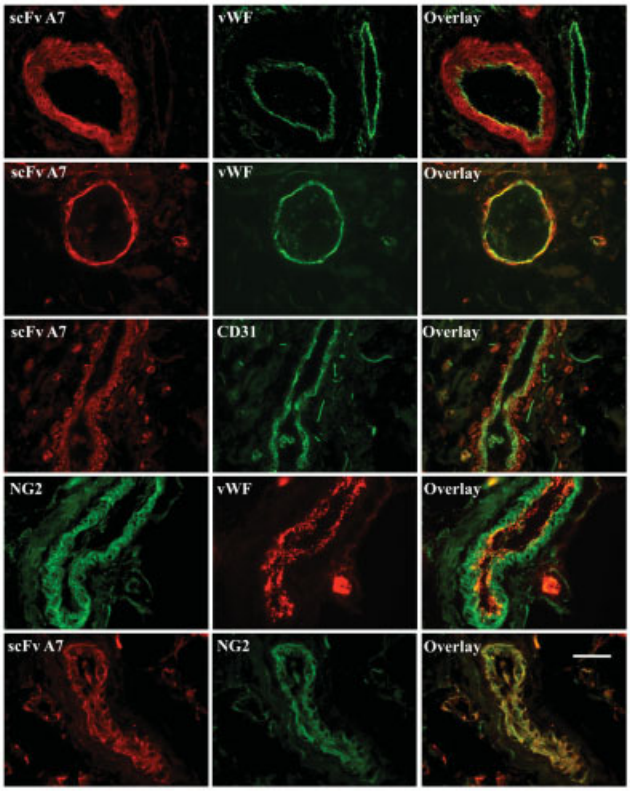

Figure 2. Characterization of cellular reactivity of scFv A7 within synovial microvasculature. The reactivity of biotinylated scFv A7 with cellular components of synovial microvasculature was examined by dual staining of frozen human synovial tissue from RA patients and compared with staining for the endothelial markers vWF and CD31 and the pericyte-specific marker NG2. Bound scFv A7 was detected using Texas Red–avidin conjugate. Binding of vWF, CD31, and NG2 was detected using Alexa Fluor 488– or Alexa Fluor 594–labeled secondary antibodies (green and red, respectively). Bar = 20 μm. See Figure 1 for definitions.

Single-chain Fv A7 antibody specifically binds to arthritic synovial microvasculature. Following the demonstration that scFv A7 exhibits strong reactivity with the microvasculature of arthritic synovial tissue, we sought to determine which cell types within the microvasculature were recognized by this antibody. To do this, costaining of RA synovial tissues was performed using scFv A7 and the 2 endothelial markers vWF and CD31, and the pericyte-specific marker NG2. As shown in Figure 2, there was no overlap in the pattern of staining observed in RA tissue stained with scFv A7 and vWF or CD31. However, costaining with scFv A7 and the pericyte marker NG2 showed complete overlap in the pat-

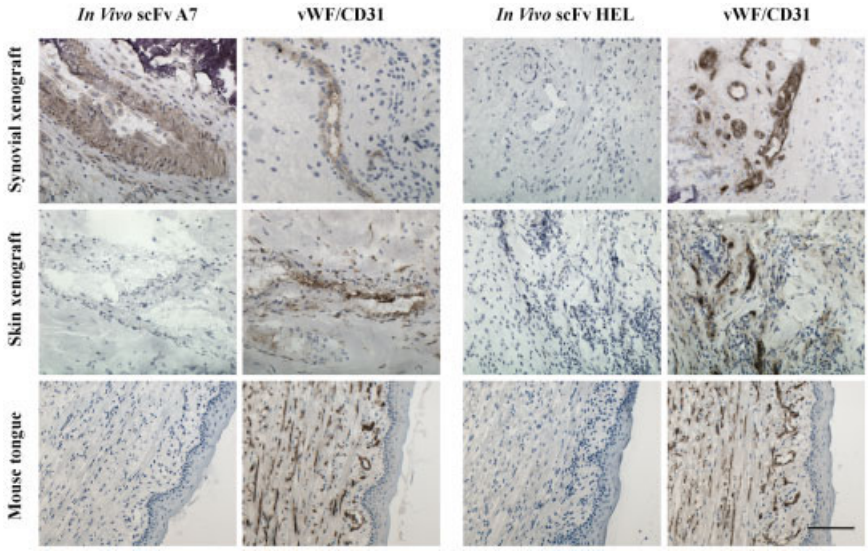

Figure 3. In vivo targeting of scFv A7 to human arthritic synovial microvasculature. The ability of scFv A7 to localize to human arthritic synovial microvasculature in vivo was examined by injecting biotinylated antibody into dual-transplanted SCID mice bearing human arthritic synovial and human skin xenografts. Immunohistochemistry was used to assess the reactivity of scFv A7 with the microvasculature in the recovered xenografts. Biotinylated scFv HEL was used as an antibody negative control. Mouse tongue tissue was used to assess cross-reactivity of scFv A7 antibody. The presence of microvasculature within human tissue was visualized with anti-human vWF antibody, while anti-mouse CD31 was used for mouse tissue. Biotinylated scFv antibodies were detected with avidin–biotin–HRP complex, while anti-vWF and anti-CD31 antibody reactivity was detected using an HRP-labeled antibody. Bar = 100 μm. See Figure 1 for definitions.

tern of cellular staining observed. This demonstrates that scFv A7 recognizes an epitope localized to pericytes and the stromal component of the microvasculature of RA synovium.

In order to increase the accuracy and level of confidence about the degree of colocalization, we used Pearson's correlation coefficient to provide a numeric and nonsubjective analysis (27). The Pearson correlation ranges from +1 to −1, whereby a correlation of +1 indicates complete overlap of pixels from 2 different channels. A value of 0 indicates no overlap, and a correlation of −1 indicates complete pixel disparity/exclusion between the 2 channels being compared. Our Pearson's colocalization analysis of scFv A7 reactivity (red pixels) and CD31 reactivity (green pixels) resulted in a Pearson's correlation of 0.07, demonstrating no colocalization of scFv A7 and CD31 reactivity. Similarly, Pearson's colocalization analysis of NG2 reactivity (green pixels) and vWF reactivity (red pixels) resulted in a Pearson's correlation of 0.01, demonstrating no colocalization of NG2 and vWF reactivity. However, Pearson's colocalization analysis of scFv A7 reactivity (red pixels) and NG2 reactivity (green pixels) resulted in a Pearson's correlation of 0.6, demonstrating significant colocalization of scFv A7 and NG2 reactivity.

Single-chain Fv A7 antibody retains synovial specificity in vivo. In order to examine the specificity of scFv A7 targeting in vivo, SCID mice bearing arthritic synovium (test tissue) and human skin (control tissue) xenografts were injected intravenously with biotinylated scFv A7 or biotinylated scFv HEL (as a negative control). As shown in Figure 3, after in vivo circulation, biotinylated scFv A7 could be detected in the human synovial microvasculature by simply adding avidin–biotin–horseradish peroxidase complex to xenograft sections. In contrast, scFv A7 reactivity was not observed with control human skin tissue xenografts. Additionally, no detectable reactivity was observed with the control scFv HEL antibody (Figure 3). To confirm the vascular reactivity of scFv A7 in the positive grafts and to exclude the possibility that the negative staining observed in human skin grafts and mouse tongue are not due to an

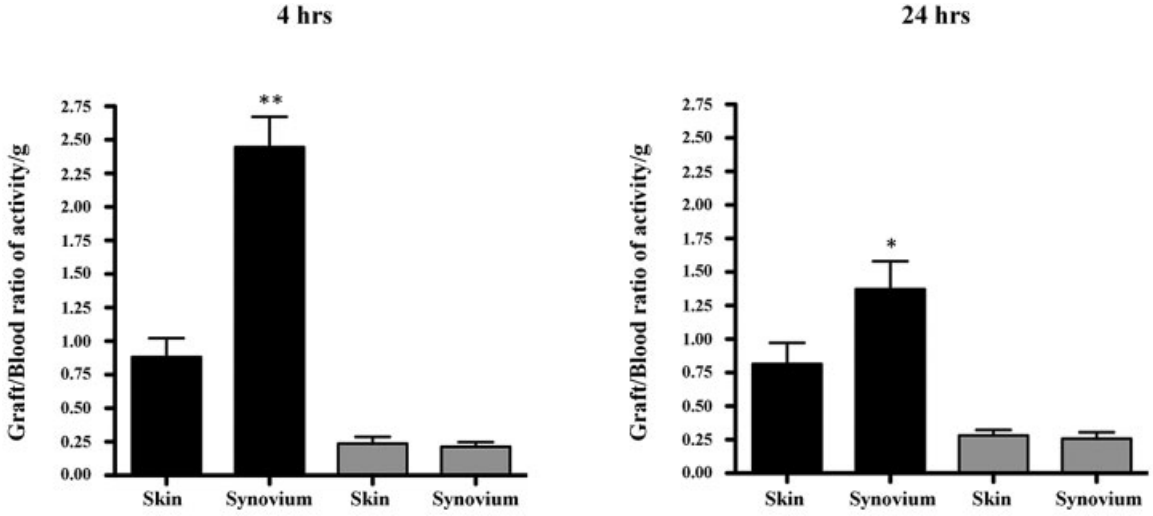

Figure 4. In vivo targeting of human arthritic synovial tissue with ^{125}I-labeled single-chain Fv (scFv) A7 antibody. The ability of scFv A7 to preferentially target the microvasculature of human arthritic synovial xenografts in vivo was examined by injecting iodinated scFv A7 (black) into SCID mice bearing dual synovial and skin xenografts. Graft tissues were examined by gamma counting 4 hours (n = 5) and 24 hours (n = 6) after antibody administration. The results were corrected for tissue weight and background radioactivity in the blood pool and expressed as tissue-to-blood ratios of the percentage of the injected dose. Iodinated scFv HEL (gray) was used as a negative control. Results are expressed as the mean ± SEM. ** = $P = 0.0079$; * = $P = 0.0513$ versus skin graft injected with ^{125}I-labeled scFv A7, by unpaired 2-tailed *t*-test.

absence of vasculature, all tissues were stained for human vWF and/or mouse CD31 (Figure 3). No cross-reactivity with host mouse tissues was observed, as exemplified by examination of mouse tongue tissue, where microvasculature was clearly visible (Figure 3). Taken together, these data further confirm the synovium-specific reactivity of the scFv A7 antibody and its capacity to reach its target in vivo.

In vivo targeting of arthritic synovial tissue by scFv A7. To quantitatively assess antibody tissue specificity in vivo, we examined the ability of iodinated scFv A7 to target human synovial tissue xenografts. Iodinated scFv HEL was used as a nontargeted control antibody, while human skin was used as control xenograft tissue. Figure 4 shows the tissue-to-blood ratio of the percentage of the injected dose localizing in each tissue at 4 hours and 24 hours. These data demonstrate that 4 hours following injection, 3-fold more radiolabeled scFv A7 was localized to the human arthritic synovium xenografts than to the human skin xenografts. Further, despite an apparent fall in overall activity of scFv A7 in the synovium at 24 hours, significant differential reactivity was still observed when compared to skin at this time point. Overall, these data further confirm that the scFv A7 antibody retains the synovial targeting specificity of the parental phage clone in vivo.

Single-chain Fv A7 reactivity in normal and inflamed human tissues. In order to further investigate scFv A7 binding specificity over and above the original targeted tissues, we examined the reactivity of this antibody using an array for a comprehensive range of normal human tissues. As shown in Figure 5A, scFv A7 did not exhibit reactivity with the various cellular components of the tissues represented on this array. In particular, no detectable reactivity was seen with the microvasculature of organs such as the adrenal gland, ovary, heart, ileum, and esophagus, all of which were shown to be positive for vWF staining with evident microvasculature.

Next we examined scFv A7 reactivity with the microvasculature of normal human synovial tissue obtained from subjects undergoing joint arthroscopy for prolonged, unexplained knee pain that did not develop into arthritic conditions during a 5-year followup survey (28). The results presented in Figure 5B are representative of 11 samples and demonstrate that the microvasculature found in normal human synovium, as detected by vWF reactivity, contains a stromal vascular compo-

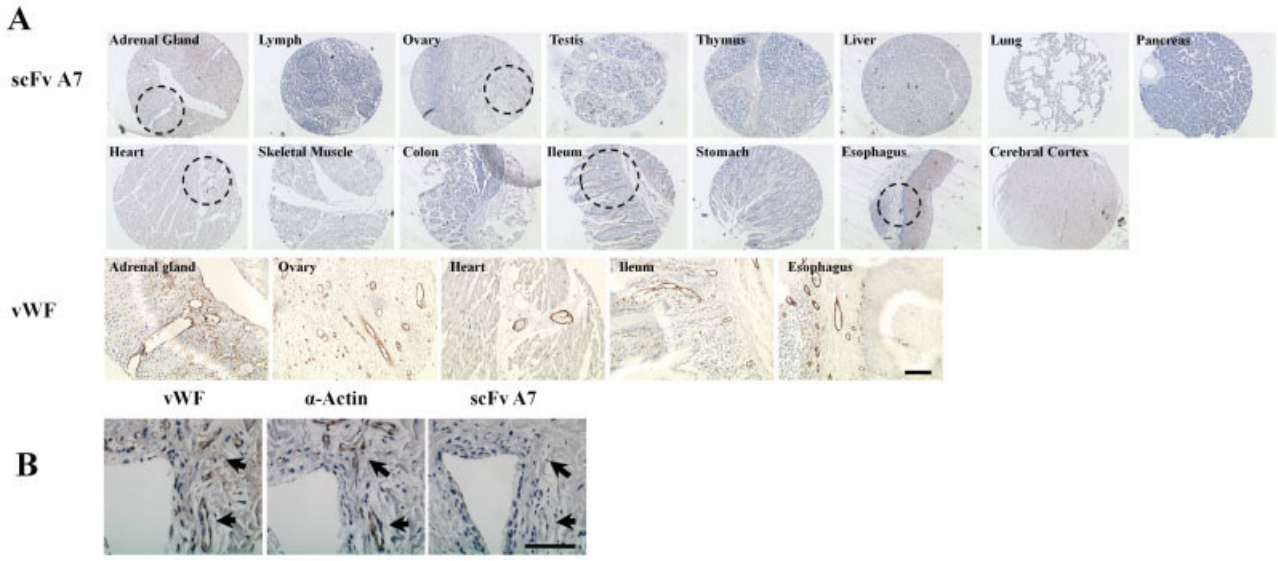

Figure 5. Immunohistochemistry of scFv A7 in normal human tissues. **A,** Assessment of reactivity of scFv A7 antibody with normal human tissues using a paraffin-embedded whole-body survey tissue microarray. Bound biotinylated scFv A7 antibody was detected using avidin–HRP conjugate. The presence of blood vessels in tissue samples was visualized with anti-human vWF antibody and an HRP-labeled secondary antibody. Representative areas in selected samples at top (dashed circles) are presented at higher magnification at bottom. Bar = 100 μm. **B,** Reactivity of scFv A7 with normal human synovial tissue. Sequential sections show blood vessels that stain with vWF and α-actin. No reactivity is observed using scFv A7 antibody. Images shown are representative of 11 independent samples examined. **Arrows** indicate the position of microvessels. Bar = 50 μm. See Figure 1 for definitions.

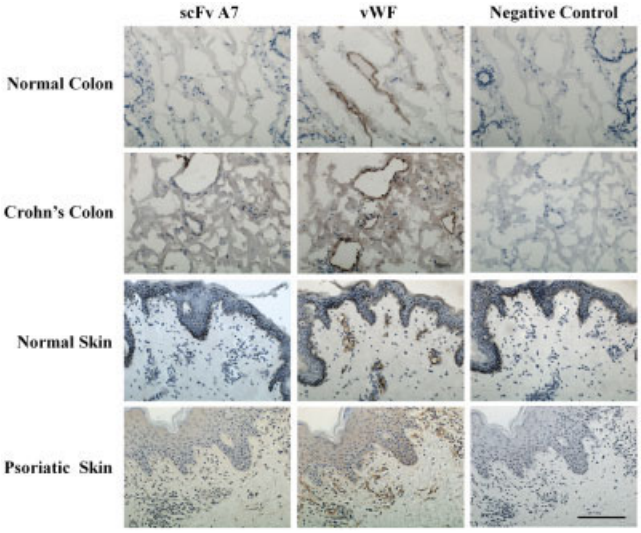

Figure 6. Reactivity of scFv A7 antibody with the microvasculature of inflammatory tissues. The reactivity of scFv A7 with normal colon, colon from patients with Crohn's disease, normal skin, and psoriatic skin was assessed. The presence of microvasculature was visualized using anti-human vWF antibody. Biotinylated scFv A7 was detected with avidin–biotin–HRP complex, while anti-vWF antibody reactivity was detected using an HRP-labeled secondary antibody. Images shown are representative of the 5 normal colon samples, 7 samples of colon from patients with Crohn's disease, 5 psoriatic skin samples, and 3 normal skin samples examined. Bar = 100 μm. See Figure 1 for definitions.

nent as detected by α-smooth muscle actin reactivity. In contrast, scFv A7 showed no reactivity with the microvasculature found in these synovium samples.

Finally, in order to establish whether the reactivity of scFv A7 is specific to the microvasculature of arthritic synovium or a common feature of neovasculogenesis related to the presence of inflammation, we examined scFv A7 staining in tissue samples from patients with Crohn's disease (n = 7) and psoriasis (n = 5), where the presence of microvasculature was detected using anti-human vWF. The results presented in Figure 6 demonstrate that scFv A7 exhibits no detectable reactivity with the microvasculature found in tissues from patients with either Crohn's disease or psoriasis. Thus, these results demonstrate that the target epitope for scFv A7 is absent from normal human tissues and microvasculature and is not expressed in the neovasculogenesis seen in inflammatory conditions. Taken together, these results further support the conclusion that scFv A7 is specific for the microvasculature found in arthritic synovium.

DISCUSSION

Over the past decade, the therapy of RA has been transformed through the application of recombinant

antibodies targeting inflammatory cytokines (24). However, despite the obvious impact of these agents, high-magnitude responses and treatment-free remission remain elusive goals (29,30). Further, many patients remain nonresponders or partial responders (14), and within the responder cohort a loss of efficacy can be seen over time, as can specific adverse effects (31,32).

The development of new therapeutics for RA, with the ability to elicit greater clinical responses and acceptable safety profiles, remains an unmet need. Toward this aim, we have used a human synovial xenograft model established in our laboratory (19,20) to carry out in vivo phage display selection of scFv antibodies with specificity for the human synovial microvasculature. In this model, synovial grafts implanted subcutaneously into SCID mice remain viable and continue to express human tissue–specific markers (17,20). Using this approach we have isolated and characterized scFv A7, a novel human scFv antibody that efficiently and preferentially targets the synovial microvasculature in RA, and we have demonstrated that this antibody specifically recognizes perivascular cells in this tissue. Abnormalities of vascular morphology and angiogenesis in arthritic synovium have been previously described at the macroscopic, histologic, and molecular levels (11,33). It is well established that blood vessels of inflammatory tissue lack the tight endothelial monolayer essential for normal barrier function, resulting in increased endothelial permeability (leakiness) and extravasation of immune cells to the extracellular space (34,35). In this context, given that our in vivo phage screening strategy is against human synovial grafts vascularized by permeable vessels, the selection of an antibody that recognizes a stromal vascular antigen is not surprising.

Our results demonstrate that the reactivity of scFv A7 is specific to the microvasculature of arthritic synovium, since the antibody does not exhibit reactivity with the microvasculature or other cellular components of normal human tissue from a spectrum of organs. Further, expression of the scFv A7 epitope is not a general feature of neovasculogenesis, since we detected no binding to the microvasculature of the tissue from patients with Crohn's disease or psoriasis. These results indicate that the expression of the epitope for scFv A7 is likely to be tissue specific and restricted to the microvasculature found in arthritic synovium rather than a feature of the microvasculature seen in neoangiogenesis or vasculogenesis in inflammatory diseases. The specific reactivity of scFv A7 suggests that the target molecule for scFv A7 may have potential as a biomarker in arthritis and may also have applications as an immunotherapeutic target in the development of new strategies for therapy of this condition.

Angiogenesis is an important and possibly a primary event in the pathogenesis of the chronic inflammatory process of RA (36). Hence, targeting angiogenesis could play a part in a polypharmacy intervention strategy for the treatment of arthritic disease (9,37–39). In the course of angiogenesis, the associated tissue remodeling leads to the expression and/or exposure of molecules on endothelial and perivascular cells, which are inaccessible, much lower in abundance, or undetectable in healthy adult tissues. For example, the oncofetal extra domain B (ED-B) of fibronectin represents one of the best characterized markers of angiogenesis (37) and is abundantly expressed in many diseases including RA (38,40). Moreover, antibody-mediated targeted delivery of proinflammatory cytokines using L19, the human antibody specific for ED-B (41), can result in a significant increase in the therapeutic index of biopharmaceuticals in animal models of cancer (42,43) and has recently been evaluated for interleukin-2 (IL-2) and TNFα delivery in phase I and II clinical trials (39). Further, L19 together with F8, an antibody specific for the ED-A of fibronectin, have been used to deliver IL-10 to inhibit the progression of collagen-induced arthritis (38,44). Most recently, 3 recombinant human antibodies specific for matrix metalloproteinases 1, 2, and 3 have been developed and are currently being evaluated for antibody-based pharmacodelivery applications in arthritis (45).

Taken together, these findings clearly demonstrate the utility of perivascular and stromal targeting for the development of ligand-based strategies for treatment of arthritic disease. In this context, we have shown that in vivo, scFv A7 can target the microvasculature of arthritic synovium efficiently and is preferentially retained on the target tissue for at least 24 hours after systemic administration. These data provide functional evidence for the potential use of scFv A7 as an agent to target therapeutics to the arthritic joint.

Although vascular targeting research has mainly focused on tumor angiogenesis, the development of nononcologic applications has recently gained momentum and is likely to become an important area of pharmaceutical intervention. Over the last decade, a spectrum of innovative bispecific antibody formats has been described, with scFv fragments being extensively used as fundamental building blocks to develop 13 novel antibodies that are currently in clinical phase I and II trials (46), as well as a spectrum of new candidate antibodies with biologic potency (47, 48). As described

here, scFv A7 represents a new building block for the development of vascular targeting of biopharmaceuticals, capable of selective accumulation at neovascular sites in RA.

ACKNOWLEDGMENTS

We are grateful to Professor Thomas MacDonald for providing tissue samples from patients with Crohn's disease and Professor Rino Cerio for providing tissue samples of psoriatic skin. We thank Dr. Vineeth Rajkumar for advice and assistance with image analysis.

AUTHOR CONTRIBUTIONS

All authors were involved in drafting the article or revising it critically for important intellectual content, and all authors approved the final version to be published. Dr. Pitzalis had full access to all of the data in the study and takes responsibility for the integrity of the data and the accuracy of the data analysis.

Study conception and design. Kamperidis, Kamalati, Ferrari, Jones, Garrood, Smith, Diez-Posada, Hughes, Finucane, Mather, Nissim, George, Pitzalis.

Acquisition of data. Kamperidis, Kamalati, Ferrari, Jones, Garrood, Smith, Diez-Posada, Hughes, Finucane, Mather, Nissim.

Analysis and interpretation of data. Kamperidis, Kamalati, Ferrari, Jones, Garrood, Smith, Diez-Posada, Hughes, Finucane, Mather, Nissim, George, Pitzalis.

REFERENCES

1. Callahan LF. Awareness of the prevalence and impact of arthritis: the role of health professionals [editorial]. Arthritis Care Res 1995;8:63–5.
2. Young A, Koduri G, Batley M, Kulinskaya E, Gough A, Norton S, et al. Mortality in rheumatoid arthritis: increased in the early course of disease, in ischaemic heart disease and in pulmonary fibrosis. Rheumatology (Oxford) 2007;46:350–7.
3. Paleolog EM. Angiogenesis in rheumatoid arthritis. Arthritis Res 2002;4:S81–90.
4. Choy EH, Panayi GS. Cytokine pathways and joint inflammation in rheumatoid arthritis. N Engl J Med 2001;344:907–16.
5. Szekanecz Z, Koch AE. Vascular involvement in rheumatic diseases: 'vascular rheumatology.' Arthritis Res Ther 2008;10:224.
6. Paleolog EM. The vasculature in rheumatoid arthritis: cause or consequence? Int J Exp Pathol 2009;90:249–61.
7. Hirohata S, Sakakibara J. Angioneogenesis as a possible elusive triggering factor in rheumatoid arthritis. Lancet 1999;353:1331.
8. Clavel G, Bessis N, Lemeiter D, Fardellone P, Mejjad O, Menard JF, et al. Angiogenesis markers (VEGF, soluble receptor of VEGF and angiopoietin-1) in very early arthritis and their association with inflammation and joint destruction. Clin Immunol 2007;124:158–64.
9. Khong TL, Larsen H, Raatz Y, Paleolog E. Angiogenesis as a therapeutic target in arthritis: learning the lessons of the colorectal cancer experience. Angiogenesis 2007;10:243–58.
10. Lainer-Carr D, Brahn E. Angiogenesis inhibition as a therapeutic approach for inflammatory synovitis. Nat Clin Pract Rheumatol 2007;3:434–42.
11. Szekanecz Z, Besenyei T, Paragh G, Koch AE. New insights in synovial angiogenesis. Joint Bone Spine 2010;77:13–9.
12. Rothe A, Power BE, Hudson PJ. Therapeutic advances in rheumatology with the use of recombinant proteins. Nat Clin Pract Rheumatol 2008;4:605–14.
13. Kremer JM. Rational use of new and existing disease-modifying agents in rheumatoid arthritis. Ann Intern Med 2001;134:695–706.
14. Taylor PC, Feldmann M. Anti-TNF biologic agents: still the therapy of choice for rheumatoid arthritis. Nat Rev Rheumatol 2009;5:578–82.
15. Khraishi M. Comparative overview of safety of the biologics in rheumatoid arthritis. J Rheumatol Suppl 2009;82:25–32.
16. Hansel TT, Kropshofer H, Singer T, Mitchell JA, George AJ. The safety and side effects of monoclonal antibodies. Nat Rev Drug Discov 2010;9:325–38.
17. Garrood T, Blades M, Haskard DO, Mather S, Pitzalis C. A novel model for the pre-clinical imaging of inflamed human synovial vasculature. Rheumatology (Oxford) 2009;48:926–31.
18. Lee L, Buckley C, Blades MC, Panayi G, George AJ, Pitzalis C. Identification of synovium-specific homing peptides by in vivo phage display selection. Arthritis Rheum 2002;46:2109–20.
19. George AJ, Lee L, Pitzalis C. Isolating ligands specific for human vasculature using in vivo phage selection. Trends Biotechnol 2003;21:199–203.
20. Wahid S, Blades MC, De Lord D, Brown I, Blake G, Yanni G, et al. Tumour necrosis factor-alpha (TNF-α) enhances lymphocyte migration into rheumatoid synovial tissue transplanted into severe combined immunodeficient (SCID) mice. Clin Exp Immunol 2000;122:133–42.
21. De Wildt RM, Mundy CR, Gorick BD, Tomlinson IM. Antibody arrays for high-throughput screening of antibody-antigen interactions. Nat Biotechnol 2000;18:989–94.
22. Hughes C, Faurholm B, Dell'Accio F, Manzo A, Seed M, Eltawil N, et al. Human single-chain variable fragment that specifically targets arthritic cartilage. Arthritis Rheum 2010;62:1007–16.
23. Goletz S, Christensen PA, Kristensen P, Blohm D, Tomlinson I, Winter G, et al. Selection of large diversities of antiidiotypic antibody fragments by phage display. J Mol Biol 2002;315:1087–97.
24. Harrison JL, Williams SC, Winter G, Nissim A. Screening of phage antibody libraries. Methods Enzymol 1996;267:83–109.
25. Visser GW, Klok RP, Gebbinck JW, ter Linden T, van Dongen GA, Molthoff CF. Optimal quality ^{131}I-monoclonal antibodies on high-dose labeling in a large reaction volume and temporarily coating the antibody with IODO-GEN. J Nucl Med 2001;42:509–19.
26. Barlow AL, Macleod A, Noppen S, Sanderson J, Guerin CJ. Colocalization analysis in fluorescence micrographs: verification of a more accurate calculation of Pearson's correlation coefficient. Microsc Microanal 2010;16:710–24.
27. Adler J, Parmryd I. Quantifying colocalization by correlation: the Pearson correlation coefficient is superior to the Mander's overlap coefficient. Cytometry A 2010;77:733–42.
28. Smith MD, Barg E, Weedon H, Papengelis V, Smeets T, Tak PP, et al. Microarchitecture and protective mechanisms in synovial tissue from clinically and arthroscopically normal knee joints. Ann Rheum Dis 2003;62:303–7.
29. Emery P, Fleischmann RM, Moreland LW, Hsia EC, Strusberg I, Durez P, et al. Golimumab, a human anti–tumor necrosis factor α monoclonal antibody, injected subcutaneously every four weeks in methotrexate-naive patients with active rheumatoid arthritis: twenty-four–week results of a phase III, multicenter, randomized, double-blind, placebo-controlled study of golimumab before methotrexate as first-line therapy for early-onset rheumatoid arthritis [published erratum appears in Arthritis Rheum 2010;62:3005]. Arthritis Rheum 2009;60:2272–83.
30. Keystone EC, Genovese MC, Klareskog L, Hsia EC, Hall ST, Miranda PC, et al. Golimumab, a human antibody to tumour necrosis factor α given by monthly subcutaneous injections, in

active rheumatoid arthritis despite methotrexate therapy: the GO-FORWARD Study. Ann Rheum Dis 2009;68:789–96.
31. Van Vollenhoven RF. Treatment of rheumatoid arthritis: state of the art 2009. Nat Rev Rheumatol 2009;5:531–41.
32. Lipsky PE. Are new agents needed to treat RA? Nat Rev Rheumatol 2009;5:521–2.
33. Szekanecz Z, Besenyei T, Szentpetery A, Koch AE. Angiogenesis and vasculogenesis in rheumatoid arthritis. Curr Opin Rheumatol 2010;22:299–306.
34. Middleton J, Americh L, Gayon R, Julien D, Aguilar L, Amalric F, et al. Endothelial cell phenotypes in the rheumatoid synovium: activated, angiogenic, apoptotic and leaky. Arthritis Res Ther 2004;6:60–72.
35. Pitzalis C, Garrood T. From ubiquitous antigens to joint-specific inflammation: could local vascular permeability be the missing link? Trends Immunol 2006;27:299–302.
36. Alam C, Colville-Nash P, Seed M. Modelling angiogenesis in inflammation. In: Seed MP, Walsh DA, editors. Angiogenesis in inflammation: mechanisms and clinical correlates. Basel: Birkhauser Verlag; 2008. p. 99–148.
37. Rybak JN, Trachsel E, Scheuermann J, Neri D. Ligand-based vascular targeting of disease. ChemMedChem 2007;2:22–40.
38. Trachsel E, Bootz F, Silacci M, Kaspar M, Kosmehl H, Neri D. Antibody-mediated delivery of IL-10 inhibits the progression of established collagen-induced arthritis. Arthritis Res Ther 2007;9: R9.
39. Schliemann C, Neri D. Antibody-based vascular tumor targeting. Recent Results Cancer Res 2010;180:201–16.
40. Trachsel E, Kaspar M, Bootz F, Detmar M, Neri D. A human mAb specific to oncofetal fibronectin selectively targets chronic skin inflammation in vivo. J Invest Dermatol 2007;127:881–6.
41. Pini A, Viti F, Santucci A, Carnemolla B, Zardi L, Neri P, et al. Design and use of a phage display library: human antibodies with subnanomolar affinity against a marker of angiogenesis eluted from a two-dimensional gel. J Biol Chem 1998;273:21769–76.
42. Menrad A, Menssen HD. ED-B fibronectin as a target for antibody-based cancer treatments. Expert Opin Ther Targets 2005;9:491–500.
43. Dela Cruz JS, Huang TH, Penichet ML, Morrison SL. Antibody-cytokine fusion proteins: innovative weapons in the war against cancer. Clin Exp Med 2004;4:57–64.
44. Schwager K, Kaspar M, Bootz F, Marcolongo R, Paresce E, Neri D, et al. Preclinical characterization of DEKAVIL (F8-IL10), a novel clinical-stage immunocytokine which inhibits the progression of collagen-induced arthritis. Arthritis Res Ther 2009;11: R142.
45. Pfaffen S, Hemmerle T, Weber M, Neri D. Isolation and characterization of human monoclonal antibodies specific to MMP-1A, MMP-2 and MMP-3. Exp Cell Res 2009;316:836–47.
46. Chames P, Baty D. Bispecific antibodies for cancer therapy: the light at the end of the tunnel? MAbs 2009;1:539–47.
47. Michaelson JS, Demarest SJ, Miller B, Amatucci A, Snyder WB, Wu X, et al. Anti-tumor activity of stability-engineered IgG-like bispecific antibodies targeting TRAIL-R2 and LTβR. MAbs 2009; 1:128–41.
48. Mabry R, Lewis KE, Moore M, McKernan PA, Bukowski TR, Bontadelli K, et al. Engineering of stable bispecific antibodies targeting IL-17A and IL-23. Protein Eng Des Sel 2010;23:115–27.

(12) INTERNATIONAL APPLICATION PUBLISHED UNDER THE PATENT COOPERATION TREATY (PCT)

(19) World Intellectual Property Organization
International Bureau

(43) International Publication Date
5 April 2012 (05.04.2012)

PCT

(10) International Publication Number
WO 2012/042270 A1

(51) International Patent Classification:
C07K 16/18 (2006.01)

(21) International Application Number:
PCT/GB201 1/05 1854

(22) International Filing Date:
30 September 201 1 (30.09.201 1)

(25) Filing Language: English

(26) Publication Language: English

(30) Priority Data:
1016494.5 30 September 2010 (30.09.2010) GB

(71) Applicant *(for all designated States except US):* **QUEEN MARY AND WESTFIELD COLLEGE UNIVERSITY OF LONDON** [GB/GB]; Mile End Road, London E1 4NS (GB).

(72) Inventor; and

(75) Inventor/Applicant *(for US only):* **PITZALIS, Costantino** [IT/GB]; Centre for Experimental Medicine & Rheumatology, William Harvey Research Institute, Baits and The London, Queen Mary's School of Medicine and Dentistry, 2nd Floor John Vane Science Building Charterhouse Square London EC1M 6BQ (GB).

(74) Agent: **HOLLIDAY, Louise;** D Young & Co LLP, 120 Holborn, London EC1N 2DY (GB).

(81) Designated States *(unless otherwise indicated, for every kind of national protection available):* AE, AG, AL, AM, AO, AT, AU, AZ, BA, BB, BG, BH, BR, BW, BY, BZ, CA, CH, CL, CN, CO, CR, CU, CZ, DE, DK, DM, DO, DZ, EC, EE, EG, ES, FI, GB, GD, GE, GH, GM, GT, HN, HR, HU, ID, IL, IN, IS, JP, KE, KG, KM, KN, KP, KR, KZ, LA, LC, LK, LR, LS, LT, LU, LY, MA, MD, ME, MG, MK, MN, MW, MX, MY, MZ, NA, NG, NI, NO, NZ, OM, PE, PG, PH, PL, PT, QA, RO, RS, RU, RW, SC, SD, SE, SG, SK, SL, SM, ST, SV, SY, TH, TJ, TM, TN, TR, TT, TZ, UA, UG, US, UZ, VC, VN, ZA, ZM, ZW.

(84) Designated States *(unless otherwise indicated, for every kind of regional protection available):* ARIPO (BW, GH, GM, KE, LR, LS, MW, MZ, NA, RW, SD, SL, SZ, TZ, UG, ZM, ZW), Eurasian (AM, AZ, BY, KG, KZ, MD, RU, TJ, TM), European (AL, AT, BE, BG, CH, CY, CZ, DE, DK, EE, ES, FI, FR, GB, GR, HR, HU, IE, IS, IT, LT, LU, LV, MC, MK, MT, NL, NO, PL, PT, RO, RS, SE, SI, SK, SM, TR), OAPI (BF, BJ, CF, CG, CI, CM, GA, GN, GQ, GW, ML, MR, NE, SN, TD, TG).

Published:

— *with international search report (Art. 21(3))*

— *with sequence listing part of description (Rule 5.2(a))*

(54) Title: ANTIBODY SPECIFICALLY BINDING SYNOVIAL MICROVASCULATURE OF ARTHRITIS PATIENTS

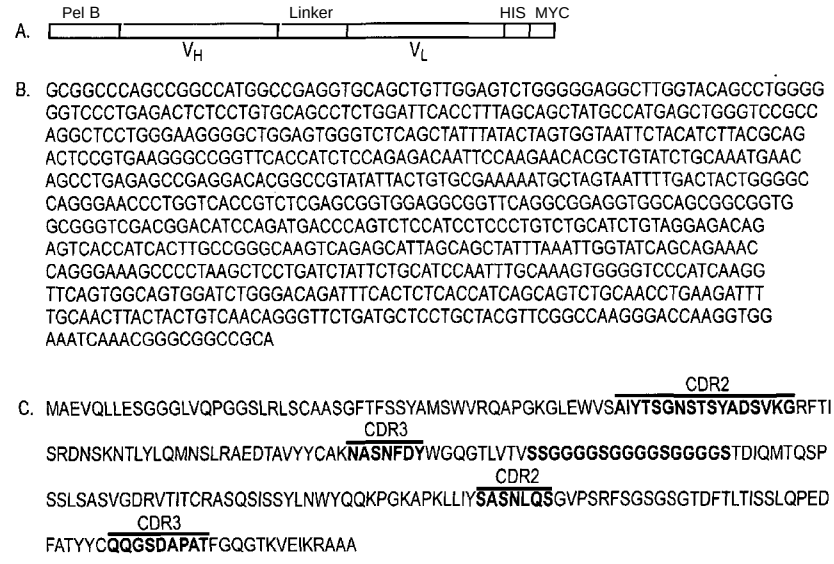

FIG. 7

(57) Abstract: The present invention provides an antigen binding polypeptide which specifically targets the synovial microvasculaturc of arthritis patients and comprises one or more complementarity determining regions (CDRs) selected from the group consisting of SEQ ID NOs 1 to 4. The present invention also relates to the use of such antigen binding polypeptides and conjugates thereof for use in the diagnosis and treatment of arthritis.

WO 2012/042270 A1